Cholesterol and StARD1: a common nexus in Alcoholic Liver Injury and Niemann-Pick Type C disease-associated mitochondrial stress

Estel Solsona i Vilarrasa

Cholesterol and StARD1: a common nexus in Alcoholic Liver Injury and Niemann-Pick Type C disease-associated mitochondrial stress

Estel Solsona i Vilarrasa

Doctoral Thesis

2020

DOCTORAL PROGRAM IN BIOMEDICINE

Cholesterol and StARD1: a common nexus in Alcoholic Liver Injury and Niemann-Pick Type C disease-associated mitochondrial stress

A dissertation submitted by Estel Solsona i Vilarrasa to the Medical School of the University of Barcelona in partial fulfillment of the requirements for the degree of Doctor in Philosophy in Biomedicine.

This doctoral thesis has been conducted under the supervision of Dra. Mª del Carmen García Ruiz and Prof. José Carlos Fernández-Checa Torres at the Department of Cell Death and Proliferation of the Institute of Biomedical Research of Barcelona (IIBB), Spanish National Research Council (CSIC).

Barcelona, 2020

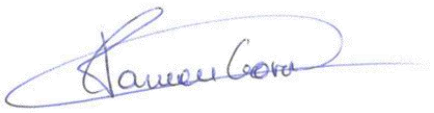

Dra. Mª del Carmen García Ruiz
Thesis Director

Prof. José Carlos Fernández-Checa Torres
Thesis Director

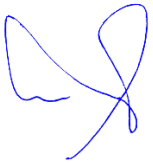

Prof. Carles Enrich Bastús
UB Tutor

Estel Solsona i Vilarrasa
Doctoral Student

INDEX

ABBREVIATIONS

4-HNE: 4-hydroxynonenal

AA: Antimycin A

Ab: Antibody

ACAT1: Acetyl-CoA acetyltransferase

ACDase: Acid ceramidase

ADH: Alcohol dehydrogenase

AKT: Alpha serine/threonine-protein kinase

ALD: Alcoholic liver disease

ALDH: Aldehyde dehydrogenase

ALT: Alanine aminotransferase

AMPK: AMP-activated protein kinase

APC: Adenomatous polyposis coli

APO: Apolipoproteins

ASM: Acid sphingomyelinase

AST: Aspartate aminotransferase

ATP: Adenosine triphosphate

ATPase: ATP synthase

BCA: Bicinchoninic acid

bHLH-Zip: Basic helix-loop-helix leucine zipper

BN-PAGE: Blue native polyacrylamide gel electrophoresis

BSA: Bovine serum albumin

CB: Coomassie blue

CBSAC: Cholesterol-BSA complex

cDNA: Complementary deoxyribonucleic acid

CO_2: Carbon dioxide

$CoCl_2$: Cobalt chloride

CoQ: Coenzyme Q

Ct: Cycle Threshold

CYP11A1: Cytochrome P450 Family 11 Subfamily A Member 1

CYP27: Sterol 27-hydroxylase

CYP2E1: Cytochrome P450 2E1

CYP2F2: Cytochrome P450 2F2

CYP7A1: Cholesterol 7alpha-hydroxylase

CYP8B1: Cytochrome P450 Family 8 Subfamily B Member 1

CYT C: Cytochrome c

DCF: 2',7'-dichlorofluorescein

dH_2O: Distilled water

DHE: Dihydroethdium

DIC: Dicarboxylate

DILI: Drug-induced liver injury

DMSO: Dimethyl sulfoxide

DNA: Deoxyribonucleic acid

DNP: 2,4-dinitrophenol

DNPH: 2,4-dinitrophenylhydrazine

DPH: 1,6-diphenylhexatriene

DRP1: Dynamin-related protein 1

DTNB: 5, 5'-dithio-bis-2-nitrobenzoic acid

EM: Electron microscopy

Ent-CBSAC: Enantiomer cholesterol-BSA complex

ER: Endoplasmic reticulum

ESC: Embryonic stem cells

ETC: Electron transport chain

EtOH: Ethanol

FAD: Flavin adenine dinucleotide

$FADH_2$: Flavin adenine dinucleotide (reduced form)

FBS: Fetal bovine serum

FCCP: Carbonyl cyanide-4-(trifluoromethoxy)phenylhydrazone

FFA-BSA: Fatty acid-free bovine serum albumin

FSH: Follicle-stimulating hormone

GFP: Green fluorescence protein

GI: Gastrointestinal tract

Abbreviations

GLUL: Glutamine synthetase
GR: Glutathione reductase
GS: Glutathione synthetase
GSH: Glutathione
GSHee: Glutathione ethyl ester
GSLs: Glycosphingolipids
GST: glutathione-S-transferase
H&E: Hematoxylin and eosin
H2DCFDA: 2',7'-dichlorodihydrofluorescein diacetate
H_2O_2: Hydrogen peroxide
HC: High cholesterol
HDL: High-density lipoprotein
HHcy: Hyperhomocysteinemia
HMG-CoA: 3-hydroxy-3-methylglutaryl coenzyme A
HMG-CoAR: 3-hydroxy-3-methylglutaryl coenzyme A reductase
HPLC: High performance liquid chromatography
HPβCD: 2-hydroxypropyl-β-cyclodextrin
HRP: Horseradish peroxidase
HSC: Hepatic stellate cells
ICAM-1: Intercellular adhesion molecule-1
ICF: Immunocytofluorescence
IHC: Immunohistochemistry
IHF: Immunohistofluorescence
IL: Interleukin
IMM: Inner mitochondrial membrane
IMS: Intermembrane space
iNOS: Inducible nitric oxide synthase
INSIG: Insulin-induced gene 1 protein
ISH: *In situ* hybridization
LCAT: Lecithin-cholesterol acyltransferase
LD: Lipid droplets
LDC: Lieber DeCarli
LDL: Low-density lipoprotein
LH: Luteinizing hormone
LPS: Lipopolysaccharide
LXRs: Liver X receptors
MAM: Mitochondria-associated ER membranes
mCholesterol: Mitochondrial cholesterol
MDA: Malondialdehyde
MEOS: Microsomal Ethanol-Oxidizing System
MFN: Mitofusin
mGSH: Mitochondrial glutathione
MICOS: Mitochondrial contact site and cristae organizing system
MLN64: Metastatic lymph node 64 protein
mQ-H_2O: Milli-Q water
mRNA: Messenger ribonucleic acid
MS: Methionine synthase
MTT: 3-(4,5-Dimethylthiazol-2-yl)-2,5-Diphenyltetrazolium Bromide
NAC: N-acetylcysteine
NAD: Nicotinamide adenine dinucleotide
NADH: Nicotinamide adenine dinucleotide (reduced form)
NAFLD: Nonalcoholic fatty liver disease
NP: Niemann Pick
NPC: Niemann-Pick Type C
NPC1: NPC Intracellular Cholesterol Transporter 1
NPC2: NPC Intracellular Cholesterol Transporter 2
O_2: Oxygen
OCR: Oxygen consumption rate
OGC: 2-oxoglutarate

OMM: Outer mitochondrial membrane
OPA1: Optic atrophy 1
ORPs: OSBP-related proteins (ORPs)
OSBP: Oxysterol-binding protein
PCR: Polymerase chain reaction
PMH: Primary mouse hepatocytes
PP: Periportal
PPARs: Peroxisome proliferator-activated receptors
Prx: Peroxiredoxins
PV: Perivenous
RCR: Respiratory control ratio
RNA: Ribonucleic acid
ROS: Reactive oxygen species
RT: Room temperature
RT-PCR: Real-time polymerase chain reaction
SAMe: S-adenosyl-L-methionine
SCAP: SREBP cleavage-activating protein
SCP2: Sterol carrier protein 2
SDS-PAGE: Sodium dodecyl sulphate polyacrylamide gel electrophoresis
SEM: Standard error of the mean
smFISH: Single-molecule fluorescence ISH
SOD: Superoxide dismutase
SREBPs: Sterol regulatory element-binding proteins
StARD1: Steroidogenic acute regulatory protein
StART: Steroidogenic acute regulatory lipid transfer (domain)
TBST: Tris Buffered Saline with Tween
TCA: Trichloroacetic acid
TEM: Transmission electron microscopy
TFs: Transcription factors
TGF-β: Transforming growth factor beta
TMRM: Tetrametylrhodamine methyl ester
TNB: 5-thionitrobenzoic acid
TNF: Tumor necrosis factor
Trx: Thioredoxins
TrXR: Thioredoxin reductase
TSPO: Translocator protein
UCR: Uncoupling control ratio
UV: Ultraviolet
VDAC: Voltage-dependent ion channel
VLDL: Very-low-density lipoprotein
WT: Wild type
α-KGDH: α-ketoglutarate dehydrogenase
γ-GCS: γ-glutamylcysteine synthetase

INTRODUCTION

1. CHOLESTEROL

Cholesterol discovery dates back at 1769 when the French physician-chemist François Poulletier isolated pure cholesterol crystals from gallstones. Some years later in 1815 cholesterol was rediscovered by the chemist Michel E. Chevreul, who isolated it from animal fats and named it cholesterine from the Greek chole- (bile) and stereos (solid) in honor at its discovery. The exact molecular formula of cholesterol was accurately established in 1888 by the Austrian botanist Friedrich Reinitzer. Nowadays we know it as cholesterol due to the chemical suffix -ol for the alcohol group that contains (Dam, 1958).

Since its discovery, cholesterol has attracted the attention of many investigators and research areas to the point that more than ten Nobel Prizes have been awarded to scientists who dedicated major parts of their careers to cholesterol research. In 1964 Konrad Bloch and Feodor Lynen received a novel prize for their understanding of cholesterol metabolism and some years later, in 1985, Michael Brown and Joseph Goldstein were awarded for their discovery of LDL-cholesterol receptors (Mesquita et al., 2015). Nowadays, cholesterol metabolism and its implications in many diseases such as cardiac and brain vascular diseases but also dementias, hepatic disorders and cancer, are the focus of many basic research and clinical investigations (Luo et al., 2020).

1.1. CHOLESTEROL STRUCTURE AND PROPERTIES

Cholesterol is one of the most important lipids in the human body. It is part of biological membranes, where it plays an essential role in maintaining cellular integrity and functionality through the interaction with other membrane lipids and proteins. Its unique structure provides special biophysical properties that increase the ordering of neighboring lipids overall influencing membrane fluidity, permeability and curvature. However, too much ordering is detrimental because it can increase membrane rigidity so much that the diffusion of membrane proteins can slow down. To prevent this to happen, cholesterol levels in the cell are subjected to very precise regulation (Hofsäss et al., 2003). Besides this function, cholesterol is also a precursor for steroid hormones, bile acids and vitamin D, and has diverse functions in intracellular signal transduction (Maxfield and Tabas, 2005).

Cholesterol is an organic molecule that belongs to the steroid family of lipid compounds. Its core structure is composed by four fused rings (three cyclohexane rings and one cyclopentane ring). At one end of this main structure there is one aliphatic chain with eight carbon atoms and, at the other end, one hydroxyl group, the only polar component of the molecule. Both hydrophilic and

hydrophobic poles determine cholesterol positioning within the lipid bilayer. This structure is often referred as free cholesterol to be distinguished from cholesteryl esters, which contain long-chain fatty acids linked to the hydroxyl group. Cholesteryl esters are much more hydrophobic than free cholesterol and, although they do not contribute to membrane structures, they appear to be the preferred form for cholesterol transport in plasma and as a biologically inert storage (**Figure I-1**) (Maxfield and Tabas, 2005; Tabas, 2002; Yeagle, 1985).

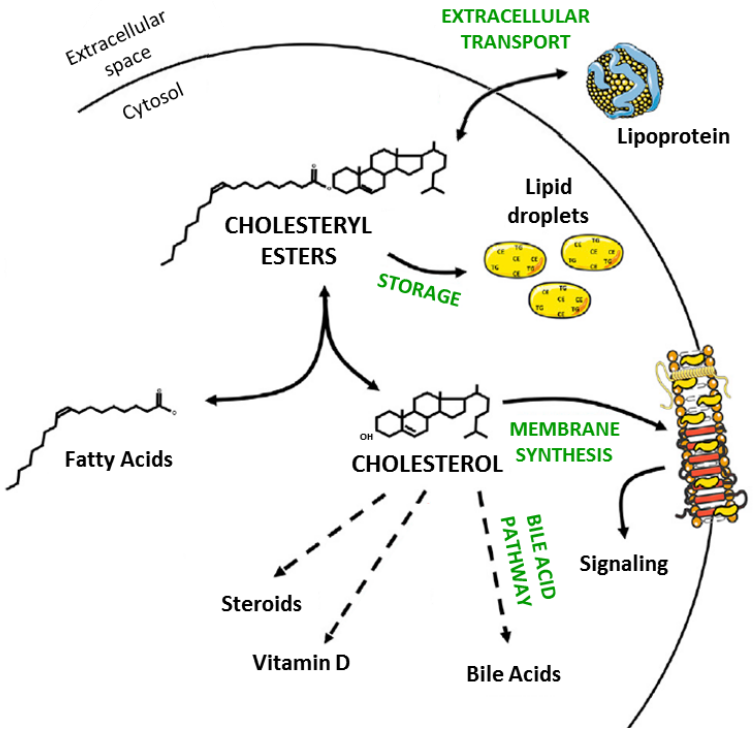

Figure I-1. Structures and functions of (free) cholesterol and cholesteryl esters.
Adapted from (Riscal et al., 2019).

1.2. CHOLESTEROL SOURCES

Cholesterol is either supplied from the diet (exogenous mechanism) or synthesized *de novo* by many cells of the body, especially hepatocytes from the liver (endogenous mechanism). The contribution of these two pathways on total body cholesterol has been estimated as a ratio of ~30:70 respectively (Arnold and Kwiterovich, 2003; Grundy, 1983).

1.2.1. Dietary cholesterol uptake

Long-distance lipid transport, i.e. the transfer of fats between body tissues, is carried out by lipoproteins. These sphered macromolecular complexes enable triglycerides, cholesterol and other lipids to be carried in all extracellular water, as in blood plasma or other extracellular fluids. Different combinations of lipids and proteins give rise to particles of different densities:

chylomicrons, very-low-density lipoprotein (VLDL), low-density lipoprotein (LDL) and high-density lipoprotein (HDL). They are all constituted by one nucleus with apolar lipids (cholesteryl esters and triglycerides) and an external polar layer composed by phospholipids, free cholesterol and apolipoproteins (APO). The latter act as signals to guide lipoproteins to specific tissues and activate the enzymes responsible for degrading them (Siri-Tarino and Krauss, 2016). With all these particles and many tissues involved, the uptake of cholesterol from food follows an intricate pathway (**Figure I-2**) (Feingold and Grunfeld, 2000; Groen et al., 2014; Kapourchali et al., 2016; Lusis and Pajukanta, 2008; Marques et al., 2018).

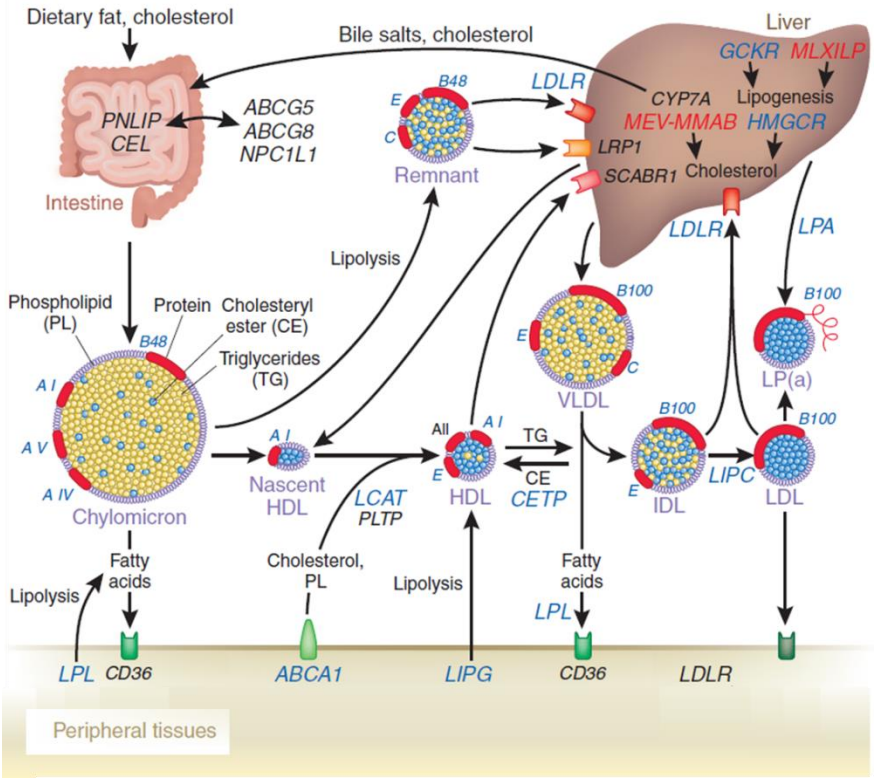

Figure I-2. Overview of lipoprotein mediated cholesterol transport mechanisms. Adapted from (Lusis and Pajukanta, 2008).

Dietary lipids arrive intact in the duodenum, where they are first emulsified by bile and then absorbed by enterocytes, the epithelial cells from the digestive tube. Once inside these cells, cholesterol along with triglycerides is packaged into chylomicrons, a type of lipoproteins composed of 85% triglycerides, 9% phospholipids, 4% cholesterol and 2% protein. The apolipoproteins that constitute chylomicrons are apo E, apo-B48 and apo C-II. Chylomicrons transport dietary lipids to adipose, cardiac and skeletal muscle tissue, where triglycerides are hydrolyzed by the activity of the lipoprotein lipase, allowing the released free fatty acids to be absorbed by these tissues. Apo C-II is the responsible for activating lipoprotein lipases. When a

large portion of the triglyceride core has been hydrolyzed, chylomicron remnants are formed and taken up by the liver. Apo E and apo-B48 are involved in the chylomicron identification by hepatocytes for endocytosis and breakdown. Once in the liver, chylomicrons release their lipid content and are degraded in the lysosomes (Groen et al., 2014; Kapourchali et al., 2016).

In turn, hepatocytes secrete VLDL particles into the circulation. These lipoproteins contain more triglycerides, free cholesterol, cholesteryl esters, other lipids and apolipoproteins such as apo-B100, apo C-I, II, III and apo E. Apo C-II activates lipoprotein lipases in capillaries thus triggering triglycerides hydrolysis and providing fatty acids for cells. After this hydrolysis VLDL become LDL, the main lipoprotein that delivers cholesterol to peripheral cells since it is rich in free cholesterol, cholesteryl esters and apo-B100. These lipoproteins bind and internalize into peripheral cells that contain the apo-B100 receptor. Once inside these cells, LDL fuse with lysosomes, which contain enzymes that hydrolyze cholesteryl esters thus facilitating free cholesterol release to the cytosol (Groen et al., 2014; Kapourchali et al., 2016).

In parallel, liver also synthesizes HDL, which are lipoproteins that contain low cholesterol levels. Their main function is to collect excessive cholesterol from peripheral tissues bringing it back to the liver so it can be metabolized. This process is known as reverse cholesterol transport. Cholesterol from non-hepatic peripheral tissues is transferred to HDL by the transporter ABCA1, acting apo-AI as an acceptor. Following this, the enzyme lecithin-cholesterol acyltransferase (LCAT) esterifies free cholesterol into cholesteryl esters thus resulting in the cholesterol relocation from the HDL membrane to its hydrophobic core and allowing more free cholesterol uptake. Once back in the liver, HDL release cholesterol leftovers, which are excreted into the bile either directly or after its conversion into bile acids. Bile is accumulated in the biliary vesicle until food reaches the duodenum being then released to the intestine. A major part of cholesterol and bile salts are reabsorbed while others are excreted, being this the main pathway of organism cholesterol elimination (Marques et al., 2018).

1.2.2. *De novo* cholesterol synthesis

Cells can synthesize cholesterol *de novo* through the mevalonate pathway. The initial step in this pathway is the conversion of acetyl-CoA and acetoacetyl-CoA into 3-hydroxy-3-methylglutaryl coenzyme A (HMG-CoA). HMG-CoA is then converted into mevalonate via the enzyme HMG-CoA reductase (HMG-CoAR). Subsequent enzymatic reactions lead to the formation of different intermediates being cholesterol one of the final products of the pathway. Enzymes involved in this

pathway are found in cytosol, endoplasmic reticulum (ER) and peroxisomes (**Figure I-3**) (Cerqueira et al., 2016; Riscal et al., 2019).

The reaction catalyzed by HMG-CoAR is the limiting step of the mevalonate pathway. This enzyme is anchored in the ER membrane through its N-terminal side and exposes its catalytic domain towards the cytosol. Due to its leading role in *de novo* cholesterol synthesis, it has become the therapeutic target for the treatment of hypercholesterolemia. In fact, the most common cholesterol-lowering drugs are statins, which act by competitively inhibiting HMG-CoAR. Since statins are structurally similar to HMG-CoA, they fit into the HMG-CoAR's active site and compete with the native substrate overall reducing the amount of cholesterol produced (Istvan, 2002; Istvan and Deisenhofer, 2000; Stancu and Sima, 2001). To further reduce cholesterol levels in the body, some statins such as atorvastatin are commonly used in combination with ezetimibe, which is a cholesterol absorption inhibitor. Thus, these medicines together impair both dietary cholesterol uptake and de novo cholesterol synthesis (Buhaescu and Izzedine, 2007; Sirtori, 2014).

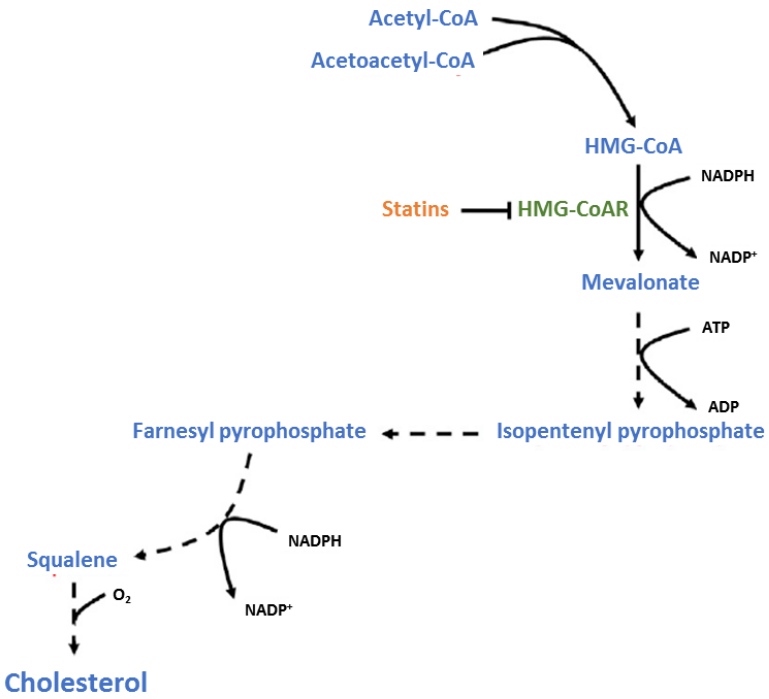

Figure I-3. Simplified scheme of mevalonate pathway. Adapted from (Riscal et al., 2019).

1.3. CHOLESTEROL METABOLISM REGULATION

Sustaining cholesterol homeostasis is essential to maintain proper cellular functioning since either too little or too much body cholesterol can induce tissue damage. There are thus several sophisticated and complex mechanisms that regulate intestinal cholesterol absorption,

cholesterol uptake by cells and *de novo* cholesterol synthesis. We will next summarize some of the most-well known key players in cholesterol metabolism regulation (Afonso et al., 2018; DeBose-Boyd, 2008; Dietschy et al., 1993).

- SREBPs (sterol regulatory element-binding proteins): SREBP is a family of membrane-anchored transcription factors that enhance cholesterol synthesis and uptake by modulating genes encoding LDL receptors and enzymes involved in the mevalonate pathway. Mammalian genomes have two separate SREBP genes leading to a total of three different isoforms of SREBP, each of them responsible for activating transcription of different genes:

  - SREBP-1a: it activates genes involved in cholesterol, fatty acids and triglycerides synthesis.
  - SREBP-1c: it favors the transcription of genes needed for the synthesis of fatty acids (ATP citrate lyase, acetil-CoA carboxylase, fatty acid synthase) and triglycerides (glycerol-3-phosphate acyltransferase).
  - SREBP-2: it regulates transcription of genes involved in cholesterol synthesis (HMG-CoA synthase and reductase, squalene synthase) and its uptake such as the LDL receptors.

  SREBP belong to the basic helix-loop-helix leucine zipper (bHLH-Zip) family. Each SREBP precursor is organized in three domains: the NH2-terminal domain, which contains the region bHLH-Zip that allows DNA binding, the transmembrane domain, and the COOH-terminal domain. SREBP precursors are anchored in the ER membrane and bound through their COOH-terminal domain to the SREBP cleavage-activating protein (SCAP). When steroid levels are low, SCAP guides SREBP to the Golgi apparatus through COPII vesicles. Once in the Golgi, SREBP undergoes proteolytic processing by proteins S1P and S2P, overall resulting in the release of the NH2-terminal domain that travels to the nucleus and promotes gene transcription. Contrary, when levels of steroids are high, SREBP and SCAP are retained in the ER by binding to the Insulin-induced gene 1 protein (INSIG). This binding blocks SREBP2 ER-to-Golgi transport thus inhibiting SREBP-mediated transcription and overall cholesterol synthesis (**Figure I-4**) (Horton et al., 2002; Sun et al., 2007).

- INSIG-mediated ubiquitination of HMG-CoAR: HMG-CoAR is inhibited by one of its own products, lanosterol. When there is an increase of lanosterol levels in the ER, proteins INSIG-1 and INSIG-2 quickly bind to HMG-CoAR. GP78, an ubiquitin kinase that is anchored to ER, then ubiquitins HMG-CoAR so that it is degraded in the proteasomes overall reducing the mevalonate pathway activity and, therefore, new cholesterol synthesis (**Figure I-4**) (Sever et al., 2003).

- Liver X receptors (LXRs): LXR are nuclear transcription factors that control cholesterol, fatty acid and glucose homeostasis. When cellular oxysterols (oxidized derivatives of cholesterol) accumulate as a result of increasing concentrations of cholesterol, LXR induce the transcription of genes that protect cells from cholesterol overload. LXR activation regulates cholesterol biosynthesis/efflux and bile acid metabolism/excretion in the liver. LXR also increase cholesterol efflux in the peripheral tissues and decrease absorption and increase fecal excretion in the intestine (Peet et al., 1998; Töröcsik et al., 2009; Zhao and Dahlman-Wright, 2010).

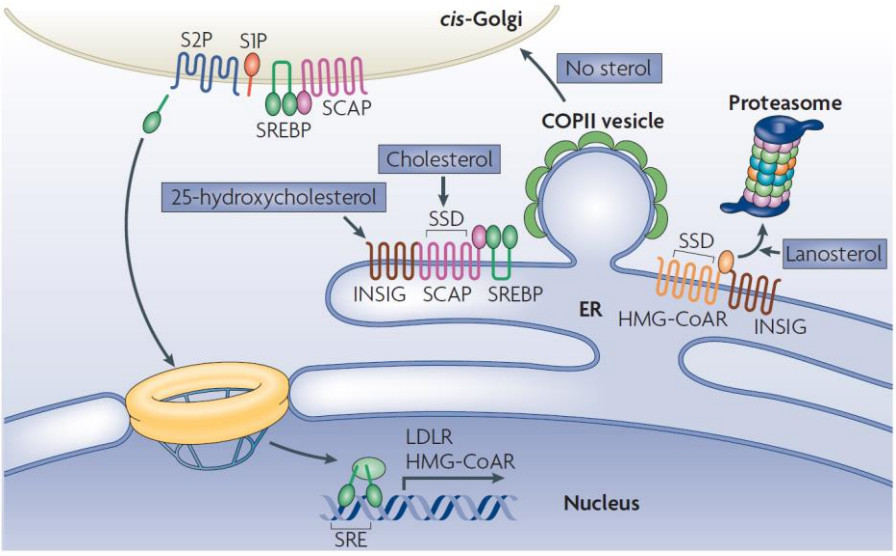

Figure I-4. SREBP and INSIG-mediated cholesterol homeostasis regulation. Taken from (Ikonen, 2008).

There are other factors that can also affect cholesterol homeostasis mainly by targeting HMG-CoAR. Diurnal rhythm, insulin and glucagon, thyroid hormone, glucocorticoids, estrogen and bile acids have been reported to influence cholesterol synthesis. They regulate HMG-CoAR by transcriptional, translational and post-translational mechanisms (Goldstein and Brown, 1990). Oxygen is another regulatory factor since cholesterol synthesis is a highly oxygen-consumptive process. The synthesis of one molecule of cholesterol from acetyl-CoA requires eleven molecules of dioxygen. It has been seen that oxygen deprivation (hypoxia) blocks cholesterol synthesis and stimulates degradation of HMG-CoAR (Nguyen et al., 2007).

1.4. INTRACELLULAR CHOLESTEROL TRAFFICKING AND DISTRIBUTION

Cholesterol is heterogeneously distributed between membranes and subcellular compartments. In the plasma membrane, it makes up about the 20-25% of the lipid bilayer on average. It is also abundant in the endocytic recycling compartment and in the trans-Golgi apparatus. By contrast,

the ER has a low cholesterol content and a large fraction of unsaturated lipids. Cholesterol levels in mitochondria and lysosomes are also low. The distinct cholesterol composition between these organelles is tightly regulated in order to ensure proper organelle functioning (Ikonen, 2008; Lange, 1991; Mukherjee et al., 1998).

Intracellular cholesterol can come from different sites: 1) from the ER, where it is endogenously synthesized, 2) from lipid droplets located in the cytosol, where excess cholesterol is stored as cholesteryl esters, and 3) from endocytic compartments, where cholesterol captured from the extracellular space via receptor is located. Over years, great achievements have been made in the knowledge of cholesterol transport and distribution between subcellular compartments and in and out of the cell. However, there are many fundamental aspects that still remain not well understood for a number of reasons. First, tracking the distribution and movement of cholesterol *in vivo* is challenging. Second, cholesterol is moved between some cellular compartments by a combination of vesicular and non-vesicular pathways, which makes the distinction of all processes involved difficult. Finally, although cholesterol is poorly soluble in water, it can spontaneously move on its own between membranes that are close at an appreciable rate, overall complicating the analysis of cholesterol transport. Although further research in this topic is required, nowadays cholesterol transport within the cell can be explained through two different mechanism: vesicular and non-vesicular transport (Enrich et al., 2015; Ikonen, 2008; Maxfield and Tabas, 2005; Maxfield and Wüstner, 2002; Meng et al., 2020; Soccio Raymond E. and Breslow Jan L., 2004).

1.4.1. Vesicular transport

The intracellular cholesterol vesicular transport is mainly linked to the cholesterol uptake from lipoproteins through receptor-mediated mechanisms. LDL receptors that are found in the plasma membrane have a high affinity for lipoproteins that contain the apolipoproteins apo B and apo E, such as chylomicron remnants, VLDL and mostly LDL. These particles are endocyted by invagination forming, as a result, clathrin-coated vesicles. These vesicles then fuse with early endosomes, from where LDL receptors disassociate and are recycled back to the plasma membrane via the endocytic recycling compartment. Late endosomes and lately, lysosomes, are then in charge of the hydrolysis of cholesteryl esters into free cholesterol by the action of an acid lipase, and the cholesterol release to other subcellular compartments such as the plasma membrane, mitochondria and the ER (Sugii et al., 2003). Cholesterol that reaches the ER is re-esterified via the enzyme Acetyl-CoA acetyltransferase (ACAT1) and, as necessary, stored in cytoplasmic lipid droplets. Although the cholesterol transport within the endosomal-lysosomal system is pretty well understood, the cholesterol efflux from these compartments is poorly

characterized. Some lately studies indicate that contact sites and fusion events between these organelles and other compartments mediate the distribution of cholesterol (**Figure I-5**) (Meng et al., 2020).

NPC Intracellular Cholesterol Transporter 1 (NPC1) and 2 (NPC2) are two proteins that act in concert playing a key role in cholesterol trafficking from the endosomal-lysosomal system to other compartments. Apparently, NPC2 transfers cholesterol to NPC1, which is located in the organelle's external membrane. NPC1 then mediates cholesterol transport to the other compartments (Li et al., 2016; Maxfield and Wüstner, 2002). The absence of these proteins causes an accumulation of cholesterol and other lipids in late endocytic organelles, overall affecting cell function. Specifically, NPC1 absence is related to neurodegenerative diseases such as Niemann-Pick Type C (NPC) disease, which affects not only the brain but also other organs such the pancreas and liver where cholesterol accumulation is also observed.

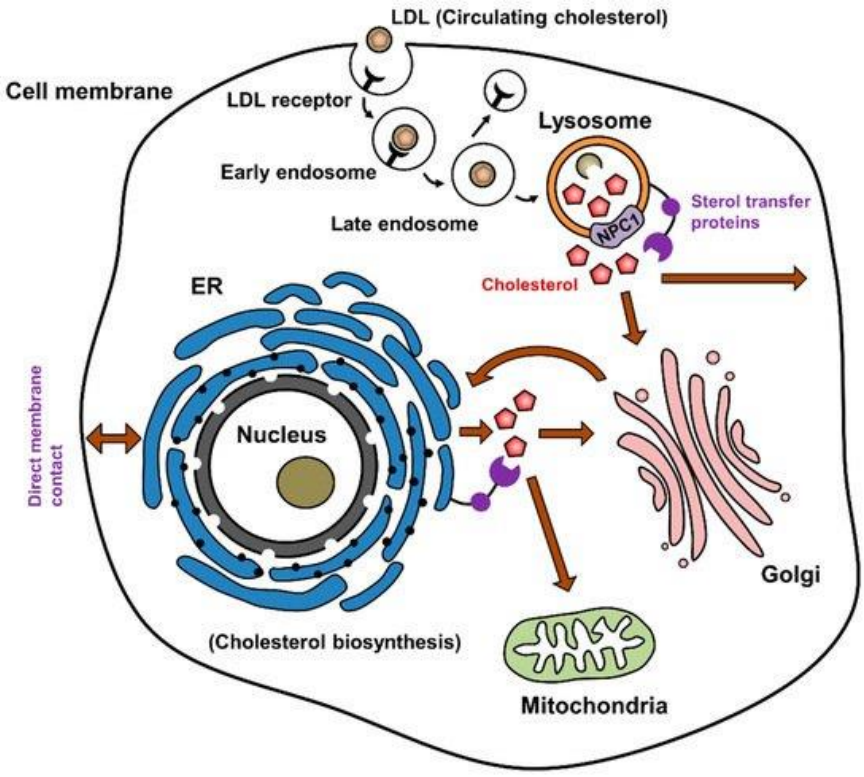

Figure I-5. Intracellular cholesterol transport. Taken from (Lyu et al., 2019).

1.4.2. Non-vesicular transport

It is accepted that cholesterol as well as other lipids can move between many intracellular compartments by non-vesicular mechanisms. For instance, it is known that cholesterol synthesized *de novo* leaves the ER mostly by non-vesicular mechanisms that bypass ER-Golgi

membrane transport. Besides, the movement of cholesteryl esters between ER and lipid droplets as well as the cholesterol mitochondrial import is not mediated by vesicles. However, most of the non-vesicular cholesterol transport mechanisms remain poorly understood. Evidence indicates that this type of transport occurs by both direct membrane contacts and by simple detachment of cholesterol from one membrane, its crossing through the hydrophilic cytoplasm with the help of a Lipid Transfer Protein, and its final adsorption into the target membrane. In the last decades, efforts have been made in deciphering mechanisms of non-vesicular intracellular cholesterol transport although in some cases proof of their role is still lacking (**Figure I-6**) (Luo et al., 2019; Meng et al., 2020; Prinz, 2007):

- Steroidogenic acute regulatory lipid transfer (StART) domain family of proteins: it is the best known example of lipid transfer proteins (Miller, 2007a). All these proteins contain a StART domain that allows their binding to different substances or ligands such as sterols and phosphatidylcholine. Within this family, the steroidogenic acute regulatory protein, commonly referred to as StARD1, stands out by acting on the mitochondrial outer membrane to facilitate cholesterol transfer to the inner membrane (Miller, 2007a; Stocco, 2001, 2000, 1999; Tugaeva and Sluchanko, 2019). Another important component of this family is StARD3, also known as metastatic lymph node 64 protein (MLN64), which mediates cholesterol transport to the outer mitochondrial membrane (Zhang et al., 2002). StARD3 also participates in the cholesterol transport between late endocytic organelles and the ER via interaction with VAPA and VAPB (Wilhelm et al., 2017).

- Translocator protein (TSPO): TSPO, originally described as Peripheral benzodiazepine receptor (PBR), is located in the outer mitochondrial membrane and involved in cholesterol mitochondrial import (Papadopoulos, 2003).

- Sterol carrier protein 2 (SCP2): it is a soluble carrier that traffics cholesterol to cholesterol-rich membrane microstructural domains (Schroeder et al., 2010, 2007).

- Oxysterol-binding protein (OSBP)-related proteins (ORPs): it is a big family of lipid transfer proteins. Among them, ORP1L has recently been implicated in cholesterol transfer from late endosomes to the ER at contacts between these organelles (Dong et al., 2019; Höglinger et al., 2019; Zhao and Dahlman-Wright, 2010).

- NPC1: many studies have reported NPC1 as an important player in cholesterol efflux from the endosomal-lysosomal system via different mechanisms. NPC1 cooperates with one member

of the ORPs family, ORP5, to mediate cholesterol transport to the ER (Du et al., 2011). A recent investigation has reported that NPC1 also regulates ER contact sites with late endocytic organelles by interacting with the ER-localized sterol transport protein Gramd1b (Höglinger et al., 2019).

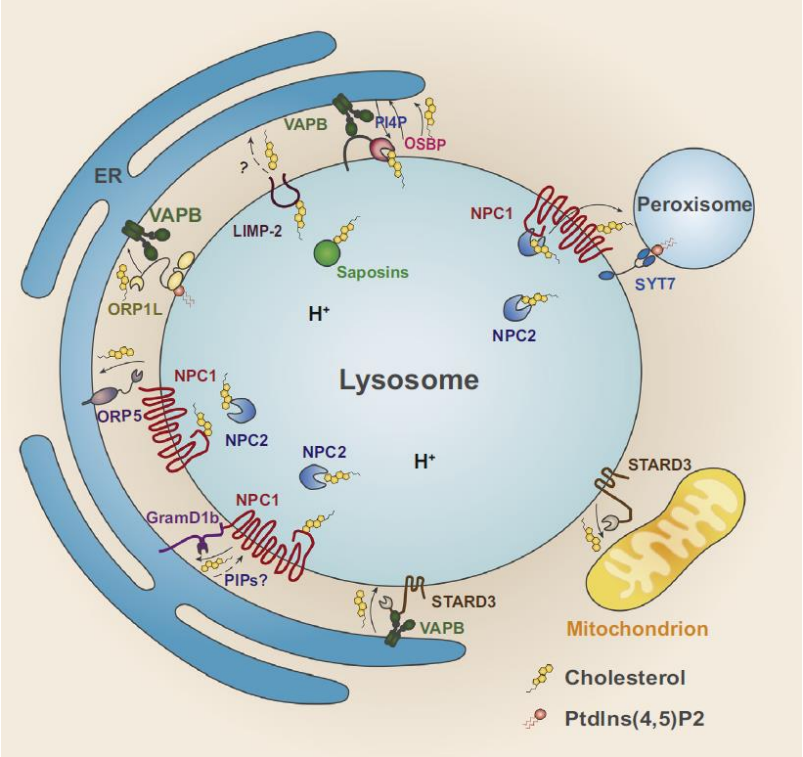

Figure I-6. Non-vesicular intracellular cholesterol transfer between organelles. Taken from (Meng et al., 2020).

1.5. PHYSIOLOGICAL ROLE OF MITOCHONDRIAL CHOLESTEROL

Mitochondria are cholesterol-poor organelles with estimates ranging from 0.5-3% of the content found in other cellular membranes (Van Meer et al., 2008). Cholesterol in mitochondria is required for membrane biogenesis and maintenance as well as for the synthesis of steroids and bile acids. For steroidogenesis, which takes place in specific tissues such as adrenal glands, ovaries, testis, placenta and brain, cholesterol is metabolized at the inner mitochondrial membrane to pregnenolone by the enzyme cytochrome P450 family 11 Subfamily A Member 1 (CYP11A1). Pregnenolone is the immediate precursor for the synthesis of most of the steroid hormones including sex steroids (androgens, estrogens, and progestogens) and corticosteroids (glucocorticoids and mineralocorticoids) as well as neurosteroids (Jefcoate, 2002; Miller and Auchus, 2011; Papadopoulos and Miller, 2012). Bile acids formation from cholesterol takes place in the liver cells via two pathways: the classic pathway, initiated by microsomal cholesterol 7alpha-

hydroxylase (CYP7A1), and the alternative pathway, initiated by sterol 27-hydroxylase (CYP27), an enzyme located in the inner mitochondrial membrane. Cholesterol in liver mitochondria is thus essential for carrying out bile acid synthesis via the alternative pathway (Kiriyama and Nochi, 2019; Pandak and Kakiyama, 2019; Šarenac and Mikov, 2018). Mitochondrial cholesterol (mCholesterol) levels are subjected to a tight regulation, especially in steroidogenic tissues or liver where this cholesterol is used to synthesize steroid hormones or bile acids, respectively. Cholesterol availability in mitochondria is thus the rate-limiting step of steroidogenesis and bile acids synthesis (Elustondo et al., 2017; García-Ruiz et al., 2009).

Increasing evidence shows that mCholesterol levels can influence mitochondrial function independent of its conversion to pregnenolone or bile acids. While in physiological conditions mCholesterol levels are low and firmly controlled, excessive accumulation of this lipid in the organelle has been observed in a wide range of pathophysiological situations including cardiovascular disorders, Alzheimer's disease, cancer, Niemann-Pick Type C (NPC) disease and hepatic injuries such as Alcoholic Liver Disease (ALD). Increased mCholesterol levels induce mitochondrial membrane order alterations as well as function impairment of specific mitochondrial carriers. These changes in mitochondrial membranes subsequently initiate a cascade of events that trigger mitochondrial dysfunction and, lately, cell damage (Arenas et al., 2020; Baggetto et al., 1992; Baggetto and Testa-Parussini, 1990; Ballinger, 2005; Barbero-Camps et al., 2014; Colell et al., 2003; Coll et al., 2003; Crain et al., 1983; Domínguez-Pérez et al., 2019; Feo et al., 1975; Fernández et al., 2009b; Marí et al., 2014, 2006; Mei et al., 2012; Montero et al., 2008; Ribas et al., 2016; Torres et al., 2019, 2017b). Exploring the mechanisms of mCholesterol homeostasis and transport as well as their effects on mitochondrial function may reveal novel information very valuable for the understanding and treatment of this wide variety of pathological conditions.

In the next chapter we describe the main aspects of mitochondrial biology focusing on the currently known mechanisms of mCholesterol import and cholesterol-driven mitochondrial dysfunction and what still remains inconclusive until the date.

2. MITOCHONDRIA

Mitochondria are semiautonomous double-membrane-bound subcellular organelles found in most eukaryotic organisms. They are responsible for the majority of energy metabolism within cells, converting oxygen (O_2) and nutrients into carbon dioxide (CO_2) and water and synthesizing

adenosine triphosphate (ATP) in the process. Thus, mitochondria are often referred as the powerhouses of the cell.

The first observations of intracellular structures that probably represented mitochondria were published in the 1840s. The word mitochondrion comes from the Greek μίτος (mitos, "thread") and χονδρίον (chondrion, "granule") and reflects the way these organelles looked to the first scientists that observed them. From then and with the help of technological advances, many scientists have contributed to expanding the current knowledge on mitochondria and their implications in human diseases (Ernster and Schatz, 1981).

2.1. MITOCHONDRIAL PROPERTIES AND STRUCTURE

The number of mitochondria in a cell differ greatly according to the organism, tissue and cell type. For example, red blood cells do not have mitochondria, while fibroblasts can have a population of dozens to hundreds of them and liver cells may have more than 2000. Another characteristic feature of mitochondria is that they have their own independent genome, which shows substantial similarity to bacterial genomes.

Mitochondria are commonly between 0.75 and 3μm² in area but vary considerably in size. Structurally, they are composed of two membranes and two subcompartments each one carrying out specialized functions (**Figure I-7**) (Giacomello et al., 2020; Lejay et al., 2012):

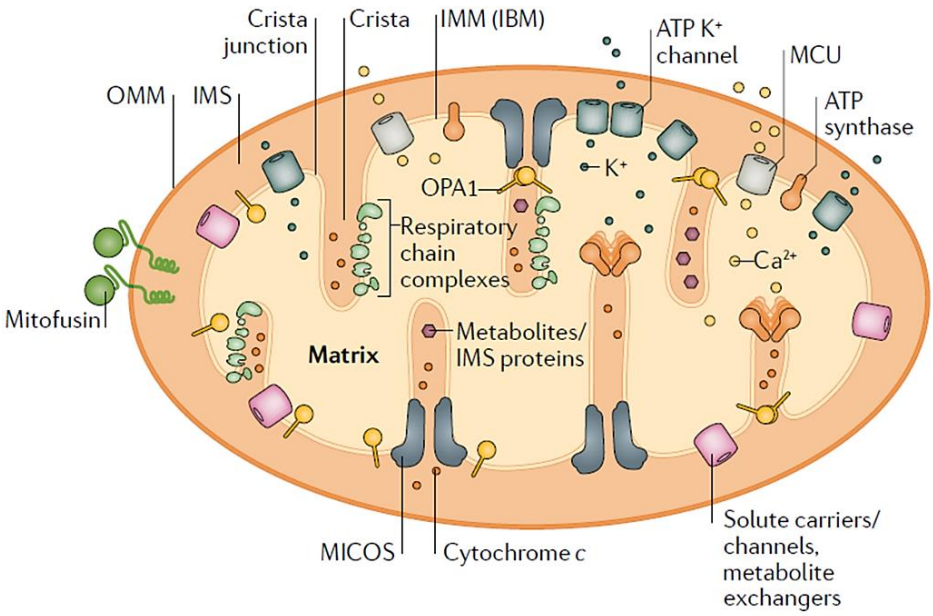

Figure I-7. Structure of mitochondria with some essential mitochondrial components. Taken from (Giacomello et al., 2020).

- Outer mitochondrial membrane (OMM): this membrane encloses the entire organelle separating it from cytosol. It is very similar in lipid composition to the plasma membrane and the ER. It is mainly formed by phospholipids of unsaturated fatty acids such as phosphatidylcholine, phosphatidylethanolamine and phosphatidylinositol, and large numbers of integral membrane proteins called porins. The protein-to-lipid ratio is around 50:50. OMM is quite permeable allowing the freely passage of ions and small molecules. The voltage-dependent ion channel (VDAC) is the primary transporter of these small particles between the cytosol and the intermembrane space. In contrast, larger proteins can enter mitochondria if a signaling sequence at their N-terminus binds to a large multisubunit protein called translocase, which then actively moves them across the outer membrane. OMM also contains enzymes involved in diverse activities such as monoamine oxidase and fatty acid Co-A ligase. Disruption of the OMM permits proteins in the intermembrane space to leak into the cytosol, leading to certain cell death.

- Inner mitochondrial membrane (IMM): it has a protein-to-lipid ratio of 80:20. Its lipid composition is based on low cholesterol levels, 45-50% of phosphatidylcholine, 25-35% phosphatidylethanolamine and 10-20% cardiolipins. Cardiolipin is a kind of diphosphatidylglycerol lipid that is not found in any biological membrane but in the IMM, where it is essential for the optimal function of numerous enzymes that are involved in mitochondrial energy metabolism. IMM is freely permeable to oxygen, carbon dioxide and water but, in contrast to OMM, it is highly impermeable to ions and small molecules. Sophisticated ion transporters thus exist to allow specific molecules to cross this barrier. Apart from being a chemical barrier, IMM is also an electrical insulator since it insulates the membrane potential generated by the action of the enzymes of the electron transport chain. Structurally, IMM is formed by invaginations called crests that penetrate the mitochondrial matrix providing a large amount of surface area for chemical reactions to occur on. A key multiprotein complex regulating cristae biogenesis is the mitochondrial contact site and cristae organizing system (MICOS). Enzymes from the electron transport chain and other protein transporters are located in the IMM.

- Intermembrane space (IMS): it is located between the OMM and IMM. It has a high concentration of protons due to their pumping by the electron transport chain. Because the OMM is freely permeable to small molecules, the concentrations of small molecules such as ions and sugars in the intermembrane space is similar to the cytosol. However, the protein composition of this space is different from the protein composition of the cytosol. Some of

the proteins located in this area are creatine and adenylate synthetase needed for AMP transformation into ADP, and proapoptotic proteins such as cytochrome c and Smac/Diablo.

- Mitochondrial matrix: it is the space enclosed by the IMM. It contains a highly concentrated mixture of hundreds of enzymes, special mitochondrial ribosomes, RNA and several copies of the mitochondrial DNA genome. A wide range of metabolic pathways crucial for mitochondrial functionality such as Krebs cycle, fatty acids β-oxidation, alternative bile acid synthesis and steroid synthesis take place in this compartment.

2.1.1. Mitochondrial dynamics

Mitochondria are commonly illustrated as singular oval-shaped structures. However, it has been known for at least a century that they form a highly dynamic network within most cells. Mitochondrial dynamics is a general term that includes the movement of mitochondria along the cytoskeleton and the regulation of mitochondrial morphology by fusion and fission events. These processes are important not only for maintaining mitochondrial health but also for coordinating metabolism and cell signaling (Giacomello et al., 2020; Liesa et al., 2009).

Mitochondria must be properly distributed within the cell in order to execute their roles. Their mobilization to specific subcellular destinations is accomplished in part by their attachment to the microtubular apparatus. The key players in this process are Miro-anchoring proteins on the OMM and the adaptor protein Milton, which can interact with kinesin and dynein molecular motors attached to microtubules (Dorn, 2019; Melkov and Abdu, 2018). Apart from being transported within the cell, mitochondria can also fuse and divide in response to cell demands and environment. These morphological changes are essential for many cellular processes such as cell cycle, immunity, apoptosis and mitochondrial quality control. An increase in fusion activity leads to mitochondrial elongation while increased fission results in mitochondrial fragmentation. Over years, many proteins that control fusion and fission events have been identified such as mitofusins (MFN) 1 and 2, optic atrophy 1 (OPA1) and dynamin-related protein 1 (DRP1). All these molecules are GTP hydrolyzing proteins that belong to the dynamin family (Liesa et al., 2009).

Mitochondrial fission is a multi-step process that leads the division of one mitochondrion in two daughter mitochondria. This process is mainly regulated by Drp1 with the participation of Dnm2 and FIS1 among other molecules. Mitochondrial fusion is driven by a two-step process with MFN1 and 2 mediating OMM fusion followed by OPA1-mediated IMM fusion (**Figure I-8**). The mechanisms of mitochondrial fusion and fission are regulated by proteolysis and post-

translational modifications of the implicated molecules. In addition, there is increasing evidence that contact sites with other organelles are also involved in the regulation of such processes. Since the overall mechanisms of mitochondrial fusion and fission have not been thoroughly completely established, a number of components which conduct or regulate these activities are likely to remain to be determined (Tilokani et al., 2018).

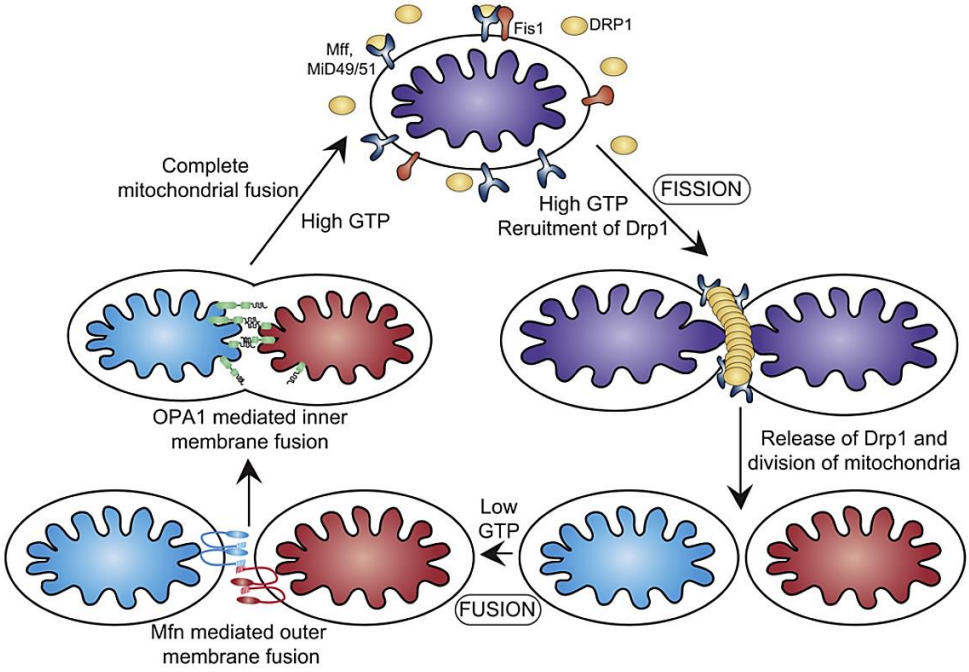

Figure I-8. Mitochondrial dynamics. Taken from (Osellame et al., 2012)

Numerous human disorders such as obesity, diabetes, cancer and non-alcoholic steatohepatitis have been associated with alterations in mitochondrial dynamics and its main machinery components (Bach et al., 2003; Dai and Jiang, 2019; Hernández-Alvarez et al., 2019; Rovira-Llopis et al., 2017). Deficiency in molecules involved in mitochondrial fusion (mainly MFN2 and OPA1) and/or in mitochondrial fusion by itself have been reported to reduce mitochondrial membrane potential and respiration in several cell types. Current evidence indicates that changes in mitochondrial fission proteins have similar impacts on mitochondrial metabolism (Chan, 2020; Youle and Bliek, 2012). However, relatively little is known about the mechanisms by which disruption of mitochondrial fusion or fission alters mitochondrial energy production. Understanding the molecular mechanisms that regulate mitochondrial dynamics is essential not only to decipher the relation between mitochondrial shape and function but also to unravel the molecular basis of diseases associated with mitochondrial morphology defects.

2.2. MITOCHONDRIAL FUNCTIONALITY

Apart from supplying cellular energy, mitochondria are also involved in a wide range of tasks including control of cell cycle, apoptosis, innate immunity, redox signalling and monitoring of cell differentiation, growth and development. Here we focus on one essential aspect: the role of mitochondria in energy production (Osellame et al., 2012).

2.2.1. Energy production

Every cellular action requires energy and this energy is stored in ATP. Found in all forms of life, ATP is often described as the "molecular unit of currency" of intracellular energy transfer. It can be produced by a number of distinct cellular processes. Mitochondria house the major enzymatic systems used to generate ATP from the oxidation of sugars, fats and proteins. Each of these three substrates can be catabolized to acetyl-CoA, which is then used in the Krebs cycle that takes place in the mitochondrial matrix. In addition to acetyl-CoA, the free energy liberated in these oxidative reactions is transferred to NADH and $FADH_2$ and carried to the mitochondrial electron transport chain (**Figure I-9**) (Osellame et al., 2012; Spinelli and Haigis, 2018):

- Sugars: they enter the mitochondria as pyruvate after undergoing glycolysis in the cytosol. Once in the mitochondrial matrix, pyruvate is oxidized and combined with coenzyme A to form CO_2, acetyl-CoA and NADH. Molecules of acetyl-CoA can then participate in the Krebs cycle and NADH is used in the electron transport chain.

- Fats: β-oxidation it is the catabolic process by which fatty acid molecules are broken down in the mitochondria to generate acetyl-CoA, which enters the Krebs cycle, and NADH and FADH2, which are used in the respiratory chain. While short and medium chain fatty acids freely enter the mitochondria, the entry of long chain fatty acids depends on an enzyme located on the outer mitochondrial membrane called carnitine palmitoyltransferase I (CPT-I). Fatty acid oxidation also occurs in peroxisomes when the fatty acid chains are too long to be handled by the mitochondria. Once in the mitochondrial matrix, free fatty acids undergo dehydrogenation, hydration, dehydrogenation and thiolysis, releasing an acetyl-CoA molecule and a shorter fatty acid chain. This cycle is repeated several times until the fatty acid polycarbonate chain is consumed.

- Proteins: mitochondria contain various enzymes that convert specific amino acids into pyruvate, acetyl-CoA or directly into particular Krebs cycle intermediates.

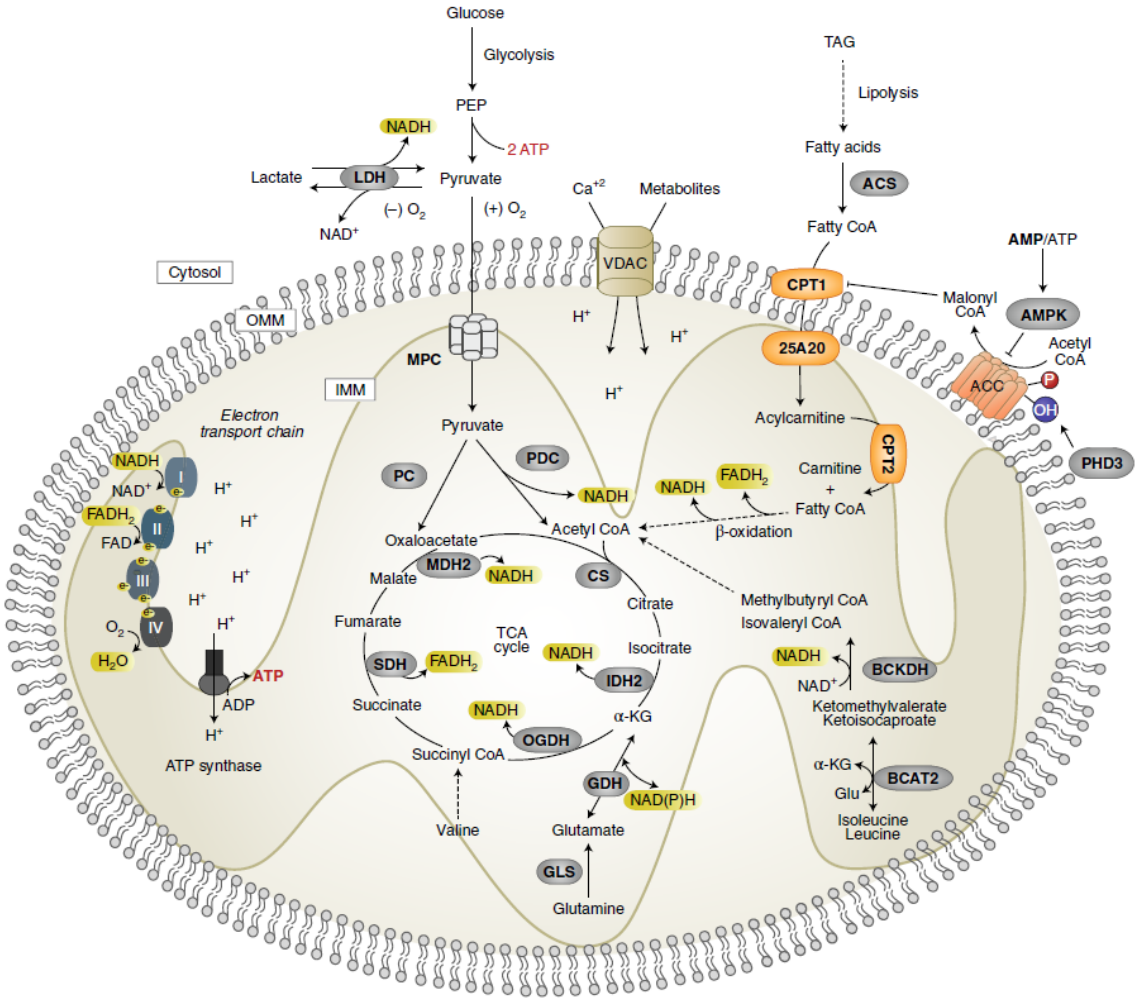

Figure I-9. Enzymatic systems used to generate ATP from the oxidation of sugars, fats and proteins. Taken from (Spinelli and Haigis, 2018).

Acetyl-CoA molecules derived from carbohydrates, fatty acid and protein catabolism are the main fuel for the Krebs cycle. Krebs cycle, also known as the citric acid cycle or tricarboxylic acid cycle, is a series of chemical reactions responsible for most of the energy needs in complex organisms. Besides, the molecules that are produced in these reactions can later be used for the synthesis of fatty acids, steroids, cholesterol, proteins and DNA. Acetyl-CoA enters the Krebs cycle where it is oxidized and ends up generating two CO_2 molecules and four pairs of hydrogen atoms that are transferred to NAD^+ and FAD overall resulting in NADH and $FADH_2$ respectively. This reducing power together with the one generated during sugars and fats oxidation is then used in numerous reactions but mainly in the electron transport chain (**Figure I-10**) (Osellame et al., 2012; Spinelli and Haigis, 2018).

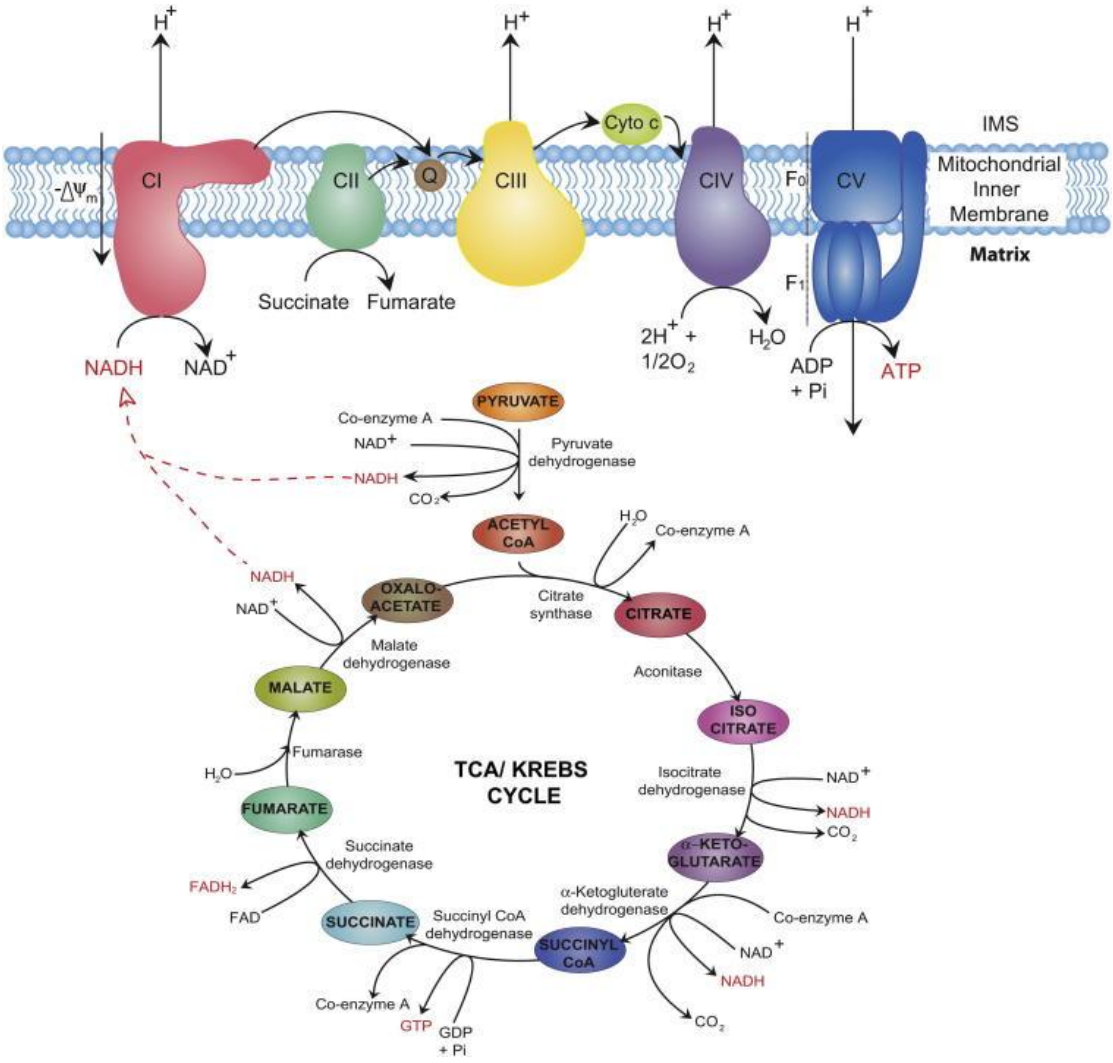

Figure I-10. Bioenergetics of the Krebs cycle and the Electron transport chain. Taken from (Osellame et al., 2012).

Subsequent to Krebs cycle, oxidative phosphorylation is the process where energy is harnessed to create the biggest amount of ATP molecules. This process is coupled to a series of protein complexes known as the electron transport chain (ETC). ETC protein complexes are embedded in the IMM and protrude towards the matrix and the IMS, and coenzymes diffuse through the membrane or bind to its surface. Electrons are passed from one member of the ETC to another in a series of redox reactions. As electrons are passed down the chain, they move from a higher to a lower energy level releasing energy that is used to pump protons ions from the matrix into the IMS. Electron flow in the ETC follows this pathway (**Figure I-10**) (Zhao et al., 2019):

- Complex I (NADH ubiquinone oxireductase): it is the largest complex in the ETC. It catalyzes the transfer of electrons from NADH to the lipid-soluble carrier called Coenzyme Q (CoQ), also known as ubiquinone. As a result of this reaction, Complex I translocates four protons across the IMM, thus producing a proton gradient.

- Complex II (succinate dehydrogenase): it is composed of four peptides. It catalyzes the oxidation of succinate to fumarate in the Krebs cycle and transfers the electrons to the CoQ. Complex I and II do not operate in sequence but accomplish the same goal: the transfer of electrons from reduced substrates to CoQ. However, unlike complex I, no protons are transported to the intermembrane space through complex II.
- Complex III (CoQH2-cytochrome c reductase): it is in charge of transferring the electrons from CoQ to cytochrome c, a water-soluble electron carrier located within the IMS. From this reaction a total of four protons are released to the IMS.
- Complex IV (cytochrome C oxidase): it receives the electrons from cytochrome c molecules and transfers them to oxygen molecules creating H_20. At the same time, eight protons are removed from the mitochondrial matrix (although only four are translocated across the membrane), contributing to the proton gradient.

As described, at the same time that electrons are transported through the chain to reach Complex IV, protons are pumped into the IMS. The accumulation of protons in the IMS creates an electrical potential and a chemical gradient. Due to the extreme impermeability of IMM, protons enter the mitochondrial matrix through the F0 region of the enzyme ATP synthase (ATPase). This proton input generates the energy necessary for the synthesis of ATP from ADP and inorganic phosphorus (Pi) by the F1 region of the ATPase (**Figure I-10**) (R. Guo et al., 2018; Zhao et al., 2019; Zorova et al., 2018). In order for oxidative phosphorylation to take place, the proton electrochemical gradient must be generated and the IMM must be intact so that the protons that return to the matrix do so through the process coupled to ATP synthesis.

The total energy gained from the complete breakdown of one molecule of glucose (six-carbon) by glycolysis, the formation of two acetyl-CoA molecules, their catabolism in the Krebs cycle and oxidative phosphorylation is a minimum of 30 ATP molecules in eukaryotes. The number of ATP molecules derived from the β-oxidation of a 6 carbon segment of a fatty acid chain and the subsequent oxidation of the resulting 3 molecules of acetyl-CoA is equal about 40 ATP molecules.

2.2.1.1. Respiratory SuperComplexes

Over years it has been thought that complexes from the ETC work as independent entities dispersed in the IMM with CoQ and cytochrome c acting as mobile carriers. This idea is known as fluid model. However, modern biological research has revealed strong evidence that these enzymatic complexes can also assemble into larger supramolecular structures called respiratory supercomplexes, what is established as the plasticity model (Acín-Perez and Enriquez, 2014).

Biologists Chance and Williams were the first to propose in 1955 the idea that respiratory enzymes assemble into larger complexes (Chance and Williams, 1955). However, it was not until 1985 when researchers began isolating Complex III/Complex IV supercomplexes from bacteria and yeast. Finally, in 2000 Schägger and Pfeiffer accomplished to isolate bovine mitochondrial membrane proteins showing Complex I, III and IV arranged in supercomplexes (Schägger and Pfeiffer, 2000; Wu et al., 2020). From then, scientific efforts combined with technological developments such as advances in super-resolution light microscopy have allowed the expansion of supercomplexes knowledge.

The most common supercomplexes observed are Complex I/III, Complex I/III/IV and Complex III/IV, while most of Complex II is found in a free-floating form (**Figure I-11**). Complex V can be found between the other supercomplexes but hardly as part of the supercomplex unit. The assembly of supercomplexes appears to be dynamic because respiratory enzymes can vary between participating in large supercomplexes and being in a free state. It is not yet fully understood what induces changes in complex assembly but it seems to depend on the lipid composition of the mitochondrial membrane (Chaban et al., 2014; Letts et al., 2016; Vartak et al., 2013; Vonck and Schäfer, 2009).

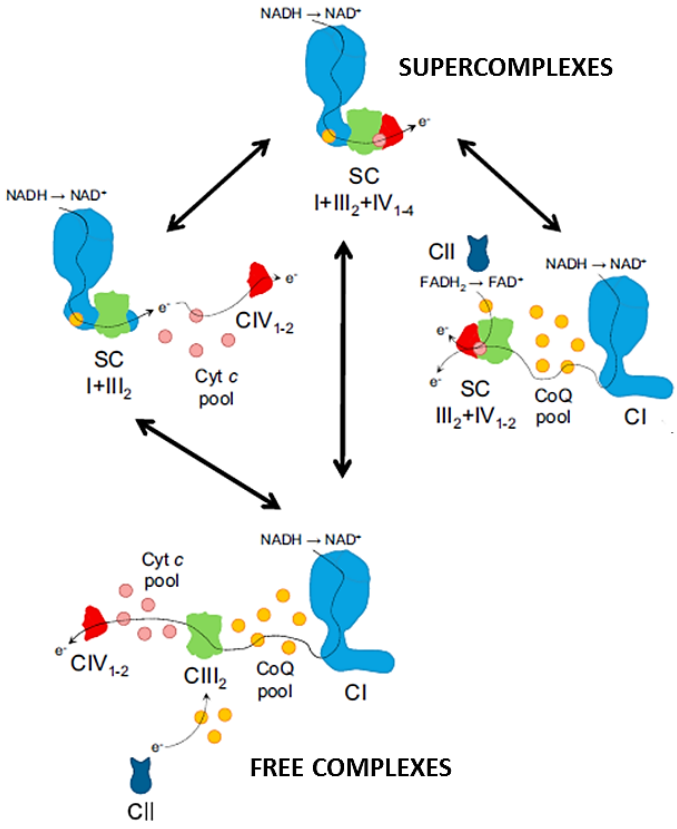

Figure I-11. Schematic representation of the dynamic rearrangements of respiratory chain complexes. Taken from (Barrientos and Ugalde, 2013).

The functional purpose of supercomplexes is not completely clear, but more recent work is starting to decipher some of their roles. It has been hypothesized that the organization of respiratory enzymes into supercomplexes enhances metabolism efficiency and the catalytic activity of the ETC (Acín-Pérez et al., 2008; Cogliati et al., 2013). Incorporating the individual complexes into supercomplexes has also been suggested to reduce reactive oxygen species (ROS) production (Maranzana et al., 2013). Another consideration is that supercomplexes represent a physical adaptation of the respiratory system to its environment. As the IMM is an extremely protein-dense environment, the packed structure of supercomplexes provides a convenient way to allow more complexes to be jammed into the membrane while preventing unfavorable and irreversible interactions that can lead to aggregation or degradation of proteins (Genova and Lenaz, 2014; Hirst, 2018; Lapuente-Brun et al., 2013).

In a significant number of human mitochondrial diseases the structure and mechanism of the mitochondrial electron transport chain is impaired. At present, one of the subjects undergoing intense study in the mitochondrial research field are the mechanisms that regulate the function and biogenesis of respiratory supercomplexes. Increased understanding in this area is clearly of great significance for understanding the roles of oxidative phosphorylation deficiencies in mitochondrial diseases (Milenkovic et al., 2017).

2.3. MITOCHONDRIAL OXIDATIVE STRESS

Many diverse pro-oxidant and antioxidant processes are ongoing in mitochondria. Under physiological conditions these organelles generate small amounts of ROS, which are perfectly acceptable by the organism and beneficial by playing an important role in cell signaling. However, pathological situations that induce an imbalance, either by an increase in mitochondrial ROS production or by a defective eliminating capacity, can cause mitochondrial oxidative stress, the organelle dysfunction and lately, cell death. This alteration in the balance between mitochondrial pro-oxidant molecules and antioxidant systems plays a fundamental role in the development of numerous diseases (García-Ruiz and Fernández-Checa, 2018; Kurutas, 2016; Schieber and Chandel, 2014).

2.3.1. Mitochondrial Reactive Oxygen Species

ROS are formed as a natural byproduct of the normal metabolism of oxygen. The term includes diverse species that have unpaired electrons in the last orbital of its molecular structure, such as superoxide anion ($O_2^{\cdot -}$) and radicals hydroxyl (·OH), peroxyl ($RO_2\cdot$), hydroperoxy ($HO_2\cdot$) and alkoxyl

(RO·). Also included in this group are non-radical O_2-derived species such as hydrogen peroxide (H_2O_2). Among them, superoxide is a free radical with moderate reactivity, but its generation can lead to more reactive or secondary ROS derivatives. Indeed, superoxide can undergo dismutation to hydrogen peroxide, which can then be converted to the highly reactive hydroxyl radical in the presence of transition metals (Fe^{2+}, Cu^{+}) by means of the Fenton reaction (Phaniendra et al., 2015; Ribas et al., 2014).

Most ROS are generated in mitochondria as by-products during the electron transport chain. The reduction of O_2 to H_2O in the ETC is incomplete, since between 0.2-2% of the electrons passing through the chain are lost giving rise to ROS. This loss mainly occurs in complex I and especially in complex III (Zhao et al., 2019). Other enzymes within these organelles not directly tied to the ETC are also sources of mitochondrial ROS such as the cytochrome CYP450 and the α-ketoglutarate dehydrogenase (α-KGDH), an important component of the Krebs cycle that contributes to ROS formation in a way that is dependent on the $NADH/NAD^{+}$ ratio. Apart from mitochondria, ROS are also generated in other intracellular sites including cytosol, peroxisomes, plasma membrane and ER. Additional sources of ROS include exogenous agents such as pollutants, tobacco, xenobiotics or radiation.

While small amounts of ROS are beneficial, excessive ROS levels can be harmful by inducing excessive oxidative stress that results in protein carboxylation, lipids peroxidation and DNA damage. Lipid peroxidation occurs in the presence of oxidizable fats and generates aldehyde groups such as 4-hydroxynonenal (4-HNE) and malondialdehyde (MDA). ROS alone and lipid peroxidation-derived aldehydes can then damage mitochondrial components such as mDNA and components of the ETC overall inducing mitochondrial and cellular dysfunction (Zhao et al., 2019).

2.3.2. Mitochondrial antioxidant systems: Mn-SOD, Prx3/Trx2 and mGSH

Despite the constant generation of ROS, evolution has allowed living aerobic organisms to adapt to the presence of these toxic species and to survive in oxygen-rich environments. This requires an effective defense system against them. ROS are neutralized by enzymatic systems such as superoxide dismutase, catalase and glutathione peroxidase, elements including copper, zinc, iron and selenium, as well as antioxidants such as vitamins A, C and E. Here we concentrate on the main mitochondrial ROS clearing systems: Mn-SOD, Prx3/Trx2 and mitochondrial glutathione (mGSH) (**Figure I-12**) (Ighodaro and Akinloye, 2018; Kurutas, 2016; Mailloux, 2018).

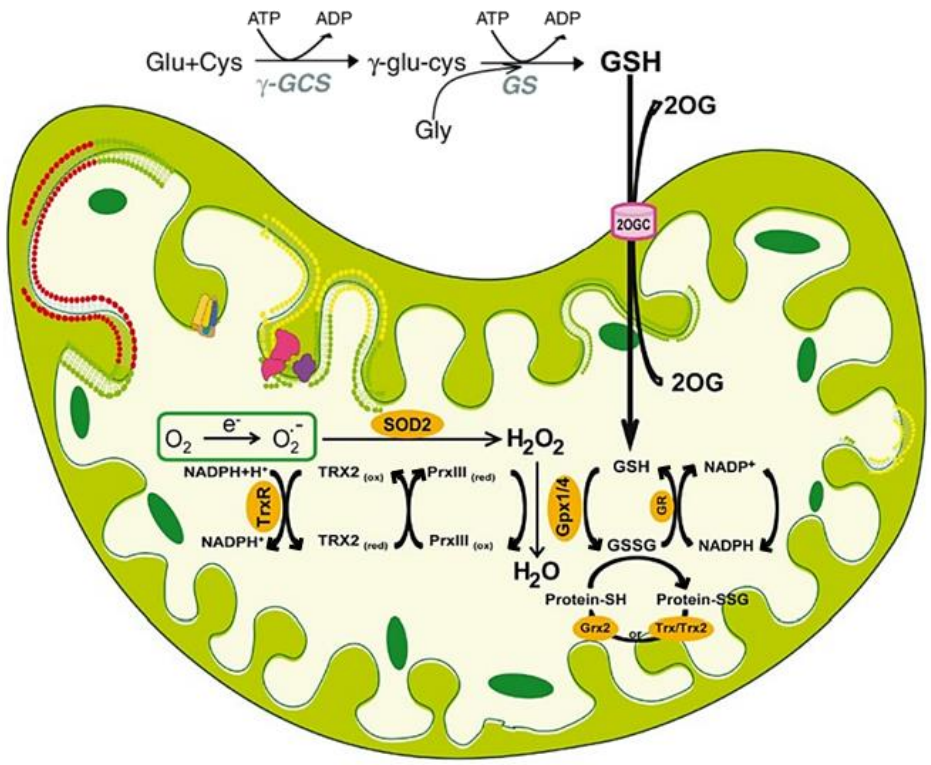

Figure I-12. Mitochondrial antioxidant strategies. Adapted from (García-Ruiz and Fernández-Checa, 2018).

- Mn-SOD

Superoxide dismutase (SOD) is an enzyme that transforms toxic superoxide into hydrogen peroxide and diatomic oxygen. It is considered the cell's most powerful enzymatic defense system against ROS since, to date, it is the only known class of enzyme able to autonomously eliminate superoxide anion in a biological system. Three families of SOD are currently known in mammals, each one defined by the metals utilized for stability and catalysis as well as the overall structure of the enzymes. The most primitive of the families is the Fe- or Mn-containing SODs. Fe-SOD is present in bacteria, archaea, protists and eukaryotic plants, while Mn-SOD is also found in all species ranging from archaea to eukarya. The second family of SODs possesses both Cu and Zn (CuZn-SOD). The CuZn-SOD's are ubiquitous among plant and animal species, and are localized in the nucleus, cytoplasm, mitochondrial IMS, chloroplast and even the extracellular matrix. The last family is the Ni-containing SODs (NiSOD) and are mainly contained to marine bacteria and algae (Case, 2017).

Among all SODs, Mn-SOD (or SOD2) is located in the mitochondrial matrix and is the first line of defense against mitochondrial superoxide (**Figure I-12**). Genetic modifications have been made in animals for many SOD enzymes by homologous recombination, but only the inactivation of SOD2

has had severe consequences on the phenotype causing neonatal death. SOD2-deficient mice have been reported to show primary effects such as the inactivation of some enzymes containing Fe-S centers such as mitochondrial complexes I and II, a high production of ROS and an inhibition of the ability to produce ATP (Melov et al., 1999). In fact, mutations in SOD2 have been associated with idiopathic cardiomyopathy, premature aging and cancer (Holley et al., 2011).

- Prx3/Trx2

Peroxiredoxins (Prx) are a ubiquitous family of antioxidant enzymes that play dominant roles in regulating peroxide levels. Prx catalytic mechanism is based on the oxidation of a redox-sensitive cysteine located in their active site to a sulfenic acid by the peroxide substrate. The recycling of the sulfenic acid back to a thiol is then performed by thioredoxins (Trx), which are kept in the reduced state by the enzyme thioredoxin reductase (TrxR) in a NADPH-dependent reaction (**Figure I-12**) (Perkins et al., 2015).

Prx3 is the Prx isoform exclusively located in mitochondria and plays an essential role in mitochondrial H_2O_2 clearance. Prx5 is also present in these organelles but also in other subcellular compartments. Regarding to Trx family, Trx2 and TrxR2 are the isoforms present in mitochondria that work in combination with Prx3 (Chang et al., 2004; Cox et al., 2010).

- mGSH

Glutathione (GSH) was discovered in 1888 by De Rey-Pailhade and, over years of study, it is currently considered one of the cell's greatest antioxidant defense. GSH is a tripeptide that is synthesized in the cytosol from the amino acids glutamate, cysteine and glycine. Its chemical structure provides stability and gives it certain specific biological functions. The synthesis of GSH is carried out through two ATP-dependent stages (**Figure I-12**) (Meister, 1988a, 1988b):

  - 1st stage: it is the limiting stage of GSH synthesis and consists on the transformation of glutamate and cysteine into γ-Glu-Cys by the enzyme γ-glutamylcysteine synthetase (γ-GCS) that is dependent on Mg^{2+} and Mn^{2+}. This enzyme is physiologically regulated by two important factors: 1) competitive feedback inhibition, since GSH is capable of binding to the γ-GCS site through which glutamate binds, and 2) the intracellular availability of cysteine.

  - 2nd stage: the second step of GSH synthesis is controlled by the enzyme glutathione synthetase (GS) that catalyzes the condensation of γ-Glu-Cys and glycine to form GSH.

In contrast to synthesis, which occurs at the intracellular level, GSH degradation occurs in the extracellular space and only in cells that express the enzyme γ-glutamyltranspeptidase (γ-GGT) on their membrane surface.

Glutathione exists in reduced (GSH) and oxidized (GSSG) states. In the reduced state, the thiol group of cysteine in GSH is able to donate a reduction equivalent to unstable molecules such as free radicals in order to neutralize them. Furthermore, GSH can reduce peroxides including H_2O_2 by the action of glutathione peroxidase (GPXs) (**Figure I-12**). Apart from neutralizing ROS, GSH is also responsible for the detoxification of xenobiotics or their metabolites. These electrophilic compounds are conjugated with GSH either spontaneously or with the help of the glutathione-S-transferase (GST) giving rise to mercapturates that will be subsequently eliminated. The result of all these reactions is GSSG, which in the presence of NADPH is reduced again by the GSH reductase (GR) (Traverso et al., 2013). The ratio of GSH to GSSG within cells is a measure of cellular oxidative stress. In healthy cells and tissues, up to 98% of the total glutathione pool is in the reduced form, with the remainder in the disulfide form. Thus, an increased GSSG-to-GSH ratio is indicative of oxidative stress. GSH levels, and therefore the redox status of the cell, is a dynamic process that depends on the balance between the rate of synthesis of GSH, the flow of GSH and GSSG, the use of GSH by various enzymes and the levels of NADPH (Owen and Butterfield, 2010).

GSH is synthesized in all mammalian cells but the major organs that regulate GSH and cysteine homeostasis are the liver, lungs and kidneys. The liver releases GSH into the blood plasma and bile, while the kidney releases it into the tubules. GSH is distributed in intracellular organelles, including the ER and the mitochondria. Apart from these organelles, GSH can also be found in the nucleus. GSH transport from the cytosol to the mitochondria occurs by transporters located on the IMM and it is an essential process for ensuring a proper antioxidant defense in the organelle. The dicarboxylate (DIC) and 2-oxoglutarate (OGC) carriers have been established as mGSH transporters in liver and kidney. Their activity has been reported to be impaired by changes in mitochondrial membrane physical properties, such as the increase of cholesterol content (more details are given in section 2.4.2) (Barbero-Camps et al., 2014, 2013; Bosch et al., 2011; Caballero et al., 2009; Colell et al., 1997; Fernández et al., 2013, 2009b; Llacuna et al., 2011; Lluis et al., 2003; Marí et al., 2006).

In mitochondria the GSH is mainly in its reduced form and represents a minor portion of the total cellular glutathione (10%-15%). Accumulation of mitochondrial ROS due to a decrease in mGSH leads to not only mitochondrial damage but also the oxidization of cytoplasmic components overall affecting cell function. mGSH is also crucial in the regulation of the mitochondrial

permeability transition, which is usually important in the processes of necrosis and apoptosis (Fernández-Checa et al., 1998; Ribas et al., 2014).

2.4. CHOLESTEROL IN MITOCHONDRIA

2.4.1. mCholesterol transporter StARD1

As exposed in section 1.5, the mitochondrial membrane accommodates a low fraction of the total cholesterol content of the cell. This small pool of cholesterol in the mitochondria plays a fundamental physiological role both in the synthesis of bile acids in hepatocytes and in the synthesis of steroidogenic hormones in specialized tissues. The activity of these pathways mainly depends on the cholesterol availability and in the mCholesterol import machinery.

There are several routes responsible for cholesterol transport from different sources to mitochondria. This lipid is primarily transported to mitochondria through lipid transfer proteins at membrane contact sites or by diffusible lipid transfer proteins acting in the cytosol (Elustondo et al., 2017; Scharwey et al., 2013). The transfer of cholesterol across membrane contact sites between mitochondria and other subcellular compartments is supported by several lines of evidences, but still requires direct experimental proof in many cases. For instance, the presence of acetyl-CoA acyltransferase and HMG-CoA reductase in the mitochondria-associated ER membranes (MAM) suggests a role for these membranes in mCholesterol import (Rusiñol et al., 1994; Vance, 2014). StART family of proteins are the best known example of molecules involved in the trafficking of cholesterol to mitochondria (Alpy and Tomasetto, 2005; Miller, 2007a; Tugaeva and Sluchanko, 2019). Among their members, the major role of supplying mitochondria with cholesterol belongs to the steroidogenic acute regulatory protein (StARD1), named due to its role in the active phase of steroidogenesis.

StARD1 is a highly conserved protein that contains a C-terminal functional StART domain responsible for lipid binding, and an N-terminal leader sequence targeting it to mitochondria. The resulting structure creates a hydrophobic cavity that can bind and accommodate one molecule of cholesterol at a time (Tsujishita and Hurley, 2000) (**Figure I-13**). The cholesterol orientation in the protein cavity has been long discussed with recent studies showing that even within the same StART family of proteins the position of cholesterol in the pocket differs (Kumar et al., 2018; Sluchanko et al., 2017).

StARD1 is synthesized *de novo* as needed and all stages of its biosynthesis are under strict control to ensure precise amounts of the active protein in the cell (**Figure I-13**). Its transcription is

regulated by a wide-range of transcription factors (TFs) that are predominantly activated by regulators of steroidogenesis through cAMP-PKA signaling pathway. Hormones such as luteinizing hormone (LH) and follicle-stimulating hormone (FSH) are among these TFs activators (Lavoie and King, 2009). After transcription, some of the synthesized StARD1's mRNAs are degraded after binding with the ncRNA let-7. Remaining mRNAs are transported from the nucleus to the cytoplasm, where the full-size protein of 285 amino acids and 37 kDa is synthesized (Tugaeva et al., 2020). StARD1 is then subjected to some post-translational modifications such as phosphorylation. Phosphorylation at Ser57 and Ser195 by PKA seem to regulate mitochondrial import and protein activity, respectively. ERK1/2 phosphorylation at Ser233 enhances protein association with the OMM and protects StARD1 from too early degradation in the matrix. StARD1 then moves towards mitochondria, where it interacts with other proteins forming a multi-protein complex named transduceosome in the OMM. This complex includes StARD1, the Translocator protein (TSPO), the voltage dependent anion channel 1 (VDAC1), the TSPO-associated protein 7 (PAP7, also known as ACBD3), the protein kinase A regulatory subunit 1α (PKAR1α) and the the ATPase family AAA domain-containing 3A (ATAD3a) protein (**Figure I-13**) (Issop et al., 2013; Li and Rousseau, 2012; Miller, 2013; Rone et al., 2012). Although the role of every individual protein has been more or less defined, the working mechanism of the whole complex has not yet been identified.

TSPO stands out among these proteins. With its 5 transmembrane helices inserted in the OMM, TSPO forms a pore-like arrangement that contains a cholesterol binding motif (Jamin et al., 2005). TSPO ligands have been shown to alter steroidogenesis and mCholesterol distribution in different animal and cellular models (Lacapère and Papadopoulos, 2003; Papadopoulos, 2003). Interestingly, depletion of TSPO decreases steroidogenesis even in the presence of StARD1, suggesting that both StARD1 and TSPO proteins are indispensable molecules for mCholesterol import (Hauet et al., 2005). The importance of TSPO has been further reported by studies using TSPO mutant mice models in which this protein is crucial for murine development as well as for hormone-driven steroidogenesis (Fan et al., 2015). Although all these findings have considered TSPO essential for mitochondrial steroidogenesis, recent investigations have disassociated it from this process, remaining its steroidogenic role currently unclear (Hadjiivanova, 2009; Morohaku et al., 2014; Selvaraj et al., 2015; Stocco, 2014).

Apart from being located in the OMM as part of the transduceosome, StARD1 can also enter the mitochondrial matrix, where the N-terminal sequence of 63 amino acids is cleaved resulting in the mature protein form of 30 kDa that is involved in steroidogenesis. Ultimately, it undergoes

degradation by a wide range of proteases including ATP-dependent Lon protease and AFG3L2 among others (Artemenko et al., 2001; Tugaeva et al., 2020).

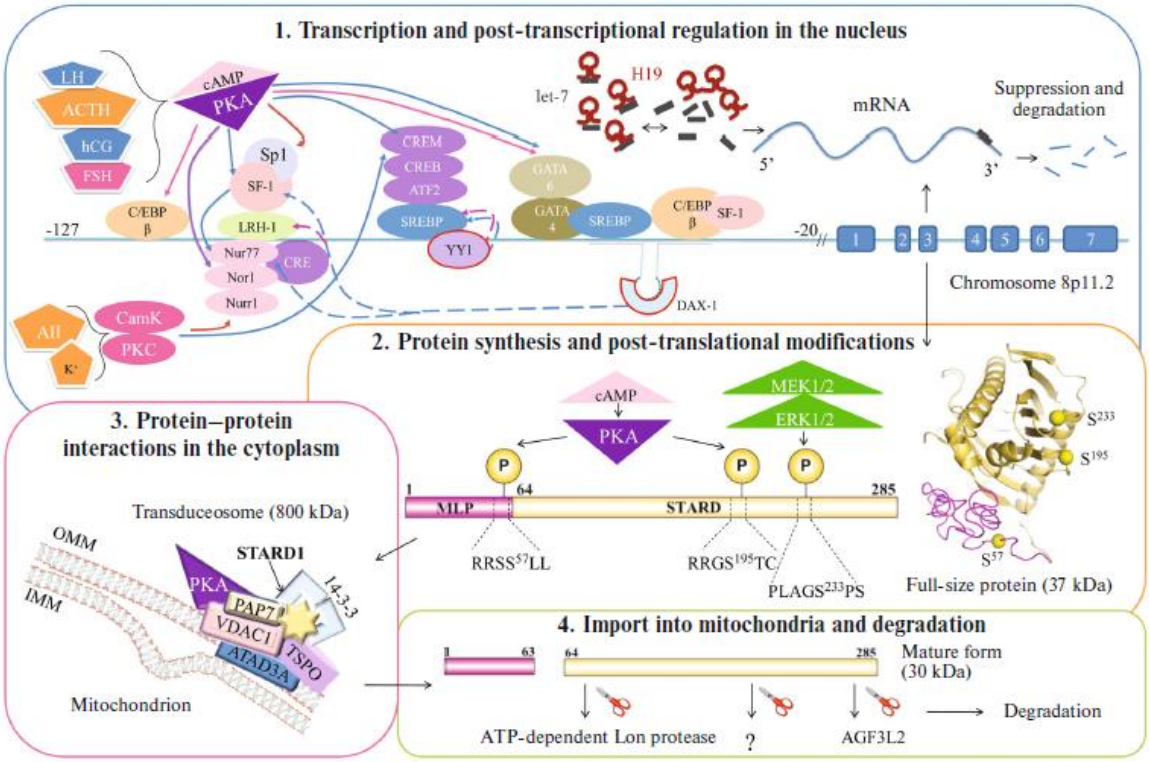

Figure I-13. StARD1 regulation in humans. Taken from (Tugaeva and Sluchanko, 2019). LH: Luteinizing hormone, ACTH: adrenocorticotropic hormone, hCG: human chorionic gonadotropin, FSH: follicle-stimulating hormone, AII: angiotensin II, SF-1: steroidogenic factor 1, LRH-1: liver receptor homolog 1, NGFIB=Nur77: nerve growth factor IB, Nurr1: nur-related protein 1, Nor1: neuron-derived orphan receptor 1, GATA 4: GATA Binding Protein 4, GATA 6: GATA Binding Protein 6, C/EBPβ: CCAAT/enhancer binding protein β; CREB: cAMP response element binding proteins, CREM: cAMP response element modulator, SREBP: sterol regulatory element binding protein, DAX1: dosage-sensitive sex reversal (DAX 1) and Yin Yang 1 (YY1). Solid lines, TF activation; dashed lines, TF inhibition.

StARD1 loss-of-function mutations lead to congenital lipoid adrenal hyperplasia, an illness characterized by impaired synthesis of steroid hormones. In addition, modifications in StARD1 expression have been shown to cause alterations in cellular sterol metabolism since StARD1 overexpression in hepatocytes increases bile acid production as opposed to StARD3 (Pandak et al., 2002; Ren et al., 2004). StARD1 has also been related to different diseases characterized by mCholesterol accumulation such as neurologic disorders including Alzheimer's disease and Down syndrome and hepatic diseases like acetaminophen-induced acute liver failure and nonalcoholic steatohepatitis (Arenas et al., 2020; Caballero et al., 2009; Torres et al., 2019).

2.4.2. Effects of mCholesterol accumulation on mitochondrial functionality

Alterations in mCholesterol levels by either deficient cholesterol clearance or excessive import can lead to accumulation of this lipid in mitochondrial membranes. This event can compromise cell function and viability as it triggers mitochondrial dysfunction at several levels. Many model systems of mCholesterol enrichment *in vitro* and mitochondria isolated from cells with (patho)physiological mCholesterol accumulation clearly establish that the accumulation of this lipid in mitochondria affects the organelle function (**Figure I-14**) (García-Ruiz et al., 2009; Martin et al., 2016):

- Biophysical changes in mitochondrial membranes: it is known that cholesterol regulates the organization of the membrane giving rise to the coexistence of ordered and disordered lipid phases that regulate the permeability of the membrane and the function of the resident proteins. It has been observed in different animal models that elevated mCholesterol levels lead to a decrease of the membrane fluidity (Baggetto et al., 1992; Colell et al., 2003; Montero et al., 2008; Paradis et al., 2013). This increase in membrane rigidity correlates with the degree of cholesterol enrichment and can be reversed by cholesterol extraction using methyl-β-cyclodextrin (Bosch et al., 2011; Montero et al., 2008; Ziolkowski et al., 2010). Another biophysical consequence of mCholesterol accumulation is a decrease in the IMM passive proton permeability (Baggetto et al., 1992).

- Impaired mGSH import: an increase in mCholesterol levels leads to reduced α-ketoglutarate transport and impaired GSH import into mitochondria (Barbero-Camps et al., 2014, 2013; Bosch et al., 2011; Caballero et al., 2009; Colell et al., 1997; Fernández et al., 2013, 2009b; Llacuna et al., 2011; Lluis et al., 2003; Marí et al., 2006). This fact is linked to the increased mitochondrial membrane rigidity by cholesterol accumulation since fluidization of mitochondrial membranes restores the transport capacity of GSH into the mitochondria (Coll et al., 2003; Lluis et al., 2003). mCholesterol-induced GSH depletion is a molecular mechanism underlying many different pathologies as various studies using nutritional and genetic experimental models have linked this pathway to a wide-range of diseases such as Alzheimer's disease, NPC disease, hepatic diseases and obesity. In some of these diseases, GSH depletion by mCholesterol enrichment sensitizes cells to inputs such as LPS or inflammatory cytokines leading to further mitochondrial damage and cell death (Colell et al., 1997; Coll et al., 2003; Fernández et al., 2009b; Fernández-Checa et al., 1991; Marí et al., 2006). Treatment with a membrane-permeable glutathione ethyl ester prevents mitochondrial dysfunction and cell death in several cell models with increased mCholesterol levels, indicating that the depletion

of mGSH is a key factor in the pathological consequences of mCholesterol accumulation (Ha et al., 2012; Murphy, 2011; Ribas et al., 2014; Torres et al., 2017b).

- Alterations in mitochondrial permeability transition and apoptosis: it has also been seen in isolated mitochondria that variations in cholesterol levels are capable of modulating the mitochondrial response against apoptotic stimuli. Increased mCholesterol levels have been reported to inhibit permeability transition pore opening after exposure to the ANT ligand atractyloside, ROS or high calcium levels (Colell et al., 2003; Montero et al., 2010, 2008).

- Potential modification of mitochondrial bioenergetics: several studies have reported consequences of mCholesterol accumulation on bioenergetics. However, the underlying mechanisms vary among model systems and are not yet fully understood. While some investigations have found decreases in ATP synthesis, ATP hydrolysis or respiration in mitochondria enriched with cholesterol (Baggetto et al., 1992; Campbell and Chan, 2007; Echegoyen et al., 1993; Yu et al., 2005), other studies have found no effects of increased mCholesterol levels on respiration (Colell et al., 2003; Dietzen and Davis, 1994). This controversy may in part be due to different experimental conditions and different mechanisms of mitochondrial import as mCholesterol increase in the OMM or in both mitochondrial membranes can have different functional implications.

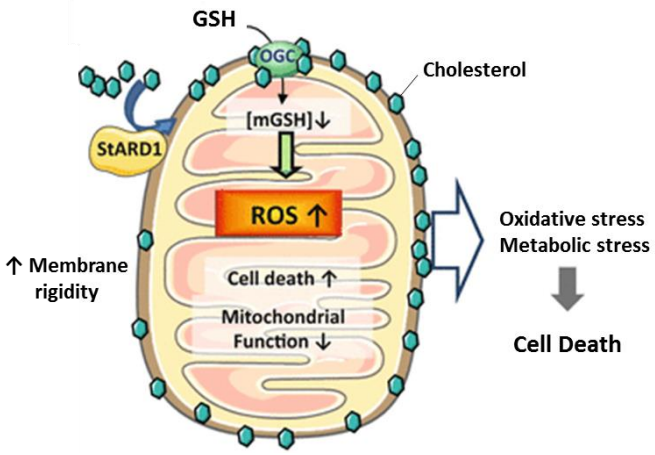

Figure I-14. Effects of mCholesterol accumulation on mitochondrial functionality. Adapted from (García-Ruiz et al., 2017).

Although many mechanisms regarding cholesterol-mediated mitochondrial dysfunction have been deciphered in the last years, some aspects still require further clarification. For instance, the specific effects of mCholesterol accumulation on mitochondrial bioenergetics still remain inconclusive as it is still not clear whether mCholesterol levels impact on mitochondrial respiration

and how. The organization of functional respiratory complexes in relation to mCholesterol accumulation has also been never approached. In addition, many of these studies regarding mCholesterol in disease have characterized mitochondrial function in a (patho)physiological model with elevated mCholesterol levels, which makes it difficult to distinguish between functional effects caused by mCholesterol or also by other pathological factors. Models specifically involving targeted manipulations of mCholesterol import and content will thus allow better conclusions about the functional consequences of altered mCholesterol levels.

2.4.3. mCholesterol in disease

As previously stated, mCholesterol enrichment and the above mentioned causative effects underlie the pathogenesis of many chronic diseases such as cardiovascular disorders, cancer and Alzheimer's disease. In addition, other studies have shown an association between increased mCholesterol levels and liver injury (Arenas et al., 2020; Baggetto et al., 1992; Baggetto and Testa-Parussini, 1990; Ballinger, 2005; Barbero-Camps et al., 2014; Colell et al., 2003; Coll et al., 2003; Crain et al., 1983; Domínguez-Pérez et al., 2019; Feo et al., 1975; Fernández et al., 2009b; Marí et al., 2014, 2006; Mei et al., 2012; Montero et al., 2008; Ribas et al., 2016; Torres et al., 2019, 2017b). While the participation of cholesterol in the pathogenesis of certain vascular and cardiac diseases is well studied, the specific contribution of this molecule on other disorders in which cholesterol, and especially its mitochondrial fraction play a critical role, remains not fully understood. This is the case of hepatic diseases such as ALD as well as NPC disease, in which not only the liver but also the brain and the spleen are affected. Thus, further investigation of the cholesterol-driven pathological mechanisms involved in these two diseases is relevant for the diseases understanding and future potential treatment.

3. THE LIVER

The liver is the largest gland in the body and the second biggest organ after skin weighing about 1.5Kg in adult humans. In terms of function, it is one of the most important organs since it performs a wide range of metabolic activities required for homeostasis, nutrition and immunity. It stands out for being the body’s master detoxifier of drugs and other foreign substances and an essential metabolizer of fat, carbohydrates and proteins. Terms related to liver usually carry the prefix hepa-, from the Ancient Greek ἡπατικός (hēpatikós, “of the liver”).

3.1. LIVER ANATOMY

3.1.1. Hepatic vascular system and biliary tract

The main function of the liver is to remove waste and toxic products and process nutrients and medicines carried by the blood so that the latter can reach other tissues. There are two distinct sources that supply blood to the liver (**Figure I-15**):

- Hepatic portal vein: all the blood that passes through the gastrointestinal tract, gallbladder, pancreas and spleen is delivered to the liver by the hepatic portal vein. This portal blood carries not only nutrients but also drugs and toxins or byproducts of blood-cell recycling that have been absorbed in the intestine or produced in the spleen.

- Hepatic artery: the liver also receives blood carrying oxygen by the hepatic artery that comes from the aorta and the latter from the heart.

Immediately before entering the liver and in order to reach all the hepatic tissue, both portal vein and hepatic artery ramify into smaller vessels. Portal venules and hepatic arterioles are the final result of such ramifications. Blood carried by these vessels ultimately mixes together in the hepatic sinusoids, which are hepatic vascular spaces lined by a fenestrated endothelium. Hepatocytes, the chief functional units of liver, are tightly packed around this endothelium, having thus easy access to the oxygen, nutrients, toxins and waste materials carried by the blood. After processing the blood borne nutrients and removing toxins, hepatocytes release nutrients needed by other cells back into the sinusoids. Clean blood then drains into the central veins ending up in the hepatic veins and, finally, the inferior cava vein (**Figure I-15**). The inferior cava vein collects deoxygenated blood from not only the liver but also the abdomen, pelvis and lower limbs and carries it to the right atrium of the heart. The heart energetically pumps the nutrient-rich blood first to the lungs to take up some oxygen and then to all other cells in the body (Lautt, 2009).

Aside from the hepatic vascular system, another important structure present in the liver is the biliary tract, a series of channels and ducts that carry bile from the liver to the intestine. Along the sinusoid, hepatocytes are welded together by junctional complexes to form bile canaliculi, the first channel in the biliary system. These small tubes accumulate the bile produced by hepatocytes. From here, bile flows in the opposite direction to blood flow, first into bile ductules, and finally into the bile duct (**Figure I-15**). This duct then joins with the cystic duct from the gallbladder, forming the common bile duct through which bile flows into the small intestine.

Portal triads are distinctive arrangements in the hepatic tissue that consist of one terminal portal venule, one hepatic arteriole and one or two small bile ductules as well as other structures such as lymphatic vessels and branches of the vagus nerve (Arias et al., 2011) (**Figure I-15**).

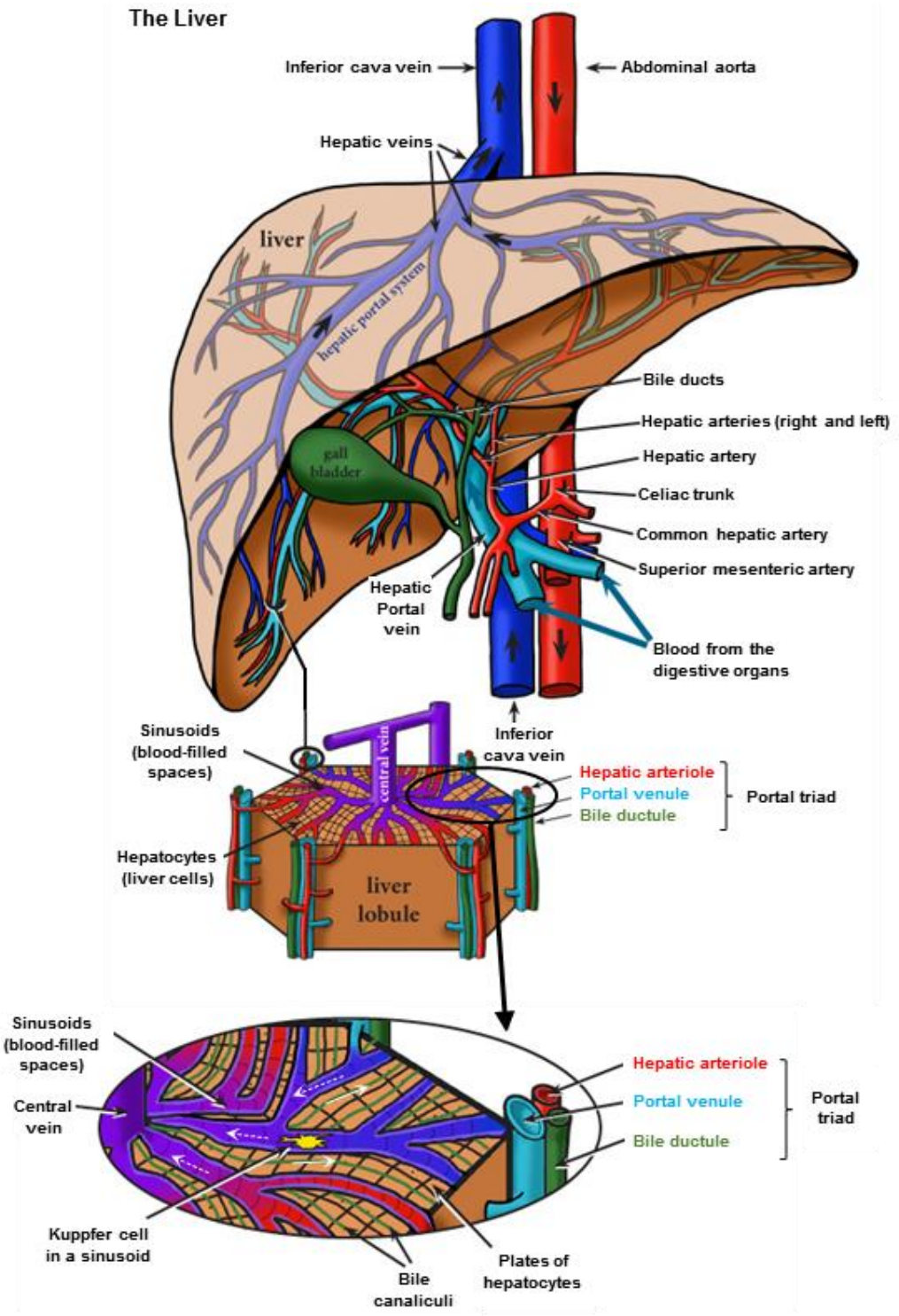

Figure I-15. Microscopic anatomy of the liver showing the hepatic vascular system and the biliary tract. Vessels in red and blue carry oxygenated and deoxygenated blood, respectively. At the bottom part of the figure: normal white arrows highlight bile flow from hepatocytes next to central vein to portal triad; dashed white arrows highlight the blood flow from the portal to the central zone. Adapted from (Amsel, 2005).

3.1.2. Liver tissue organization

There are different ways of dividing the hepatic parenchyma into units. Among them, three classifications can be distinguished (**Figure I-16**) (Fu et al., 2018; "Junqueira's Basic Histology: Text and Atlas, 15e | AccessMedicine | McGraw-Hill Medical," 2013).

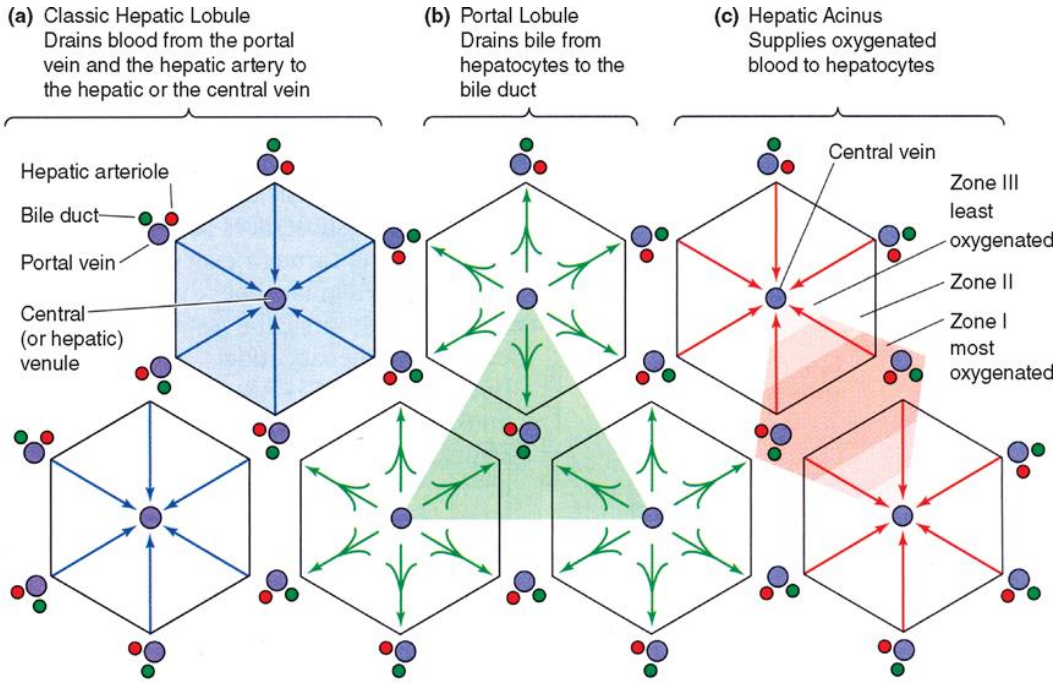

Figure I-16. Structural and functional units of the hepatic parenchyma: (a) classic liver lobule, (b) portal lobule and (c) hepatic acinus. Taken from ("Junqueira's Basic Histology: Text and Atlas, 15e | AccessMedicine | McGraw-Hill Medical," 2013).

a) Classic hepatic lobule: It is the traditional and most common description of the hepatic parenchyma. The liver is organized into hexagonal lobules, which are delimited by six portal triads and have one central vein in the middle. Sinusoids are radially distributed from portal triads to the central vein surrounding the hepatocytes. In these hepatic lobules the blood flow is centripetal, while the biliary flow is centrifugal. This lobular organization of the human liver is not immediately evident under the microscope since lobules do not have distinct boundaries (**Figure I-16a**).

b) Portal lobule: In this classification the lobule has a triangular shape. One portal triad is located in the middle of the lobule and it is limited by the three closest central veins. This model emphasizes hepatic exocrine functions since it shows the biliary flow from the hepatocytes next to the central vein to the bile duct at the portal triad (**Figure I-16b**).

c) Hepatic acinus: The hepatic parenchyma adopts a rhomboidal shape where the shortest axis would go from one portal triad to another, and the long one would go from one central vein to another one. This functional unit that correlates the blood perfusion in the parenchyma is known as hepatic acinus and reveals three different metabolic zones in the liver: zone I or periportal, zone II and zone III or perivenous (**Figure I-16c**). The metabolic differences between these three zones leads to a particular phenomenon known as hepatic zonation.

3.2. HEPATIC ZONATION

The liver is not a uniform mass of cells that performs all functions equally. Blood flow from the portal triad to the central vein creates gradients of oxygen, nutrients and hormones along the hepatic acinus, which give rise to a highly variable microenvironment. Aside from this spatial variability, most liver tasks are heterogeneously carried out by different subsets of hepatocytes, a division of function that is linked to the anatomical structure of the liver. This separation of metabolic pathways along the hepatic acinus is known as liver zonation (Ben-Moshe and Itzkovitz, 2019).

Hepatic zonation breaks the hepatic acinus into three distinct zones. Each zone possesses hepatocytes that receive different gradients of oxygen and nutrients, and that have differential metabolic gene expression and functionality (Kusminski and Scherer, 2018). Thus, depending on their location, hepatocytes within the liver assume distinct biochemical programs (Ben-Moshe and Itzkovitz, 2019). Zone 1, or periportal (PP) region, is the first to receive the blood coming from the portal vein and the hepatic artery. With oxygen and nutrient rich conditions prevailing, there is a subset of oxygen demanding pathways that are preferentially located in the PP region. Mitochondrial β-oxidation, gluconeogenesis and glycogen synthesis predominantly occur in this zone. Hepatocytes next to the portal triad are also mainly involved in ureagenesis, amino acid breakdown and cholesterol biosynthesis. Zone 3, or perivenous (PV) region, is composed by the hepatocytes close to the central vein. This subset of cells mostly takes care of glycolysis, lipogenesis, ketogenesis and triglycerides synthesis as well as alcohol detoxification. Zone 2, although it does not have any specific limitation in terms of oxygen and nutrients, it has intermediate characteristics between the other two zones (**Figure I-17**). Experts in the field have provided a panel of landmark genes that can be considered for distinguishing PP and PV areas when studying liver zonation: the PV zonated genes Glul and Cyp2e1 and the PP zonated genes Ass1, Asl, Alb and Cyp2f2 (Ben-Moshe and Itzkovitz, 2019; Halpern et al., 2017). This heterogeneity along the hepatic acinus appears to be a prerequisite for the effective functioning of the whole

liver in nutrient metabolism and in a multitude of other roles (Gebhardt and Matz-Soja, 2014; Jungermann and Keitzmann, 1996).

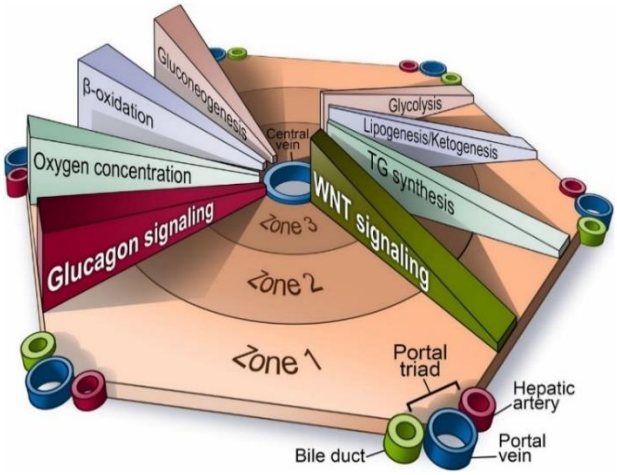

Figure I-17. Zonation of different biochemical pathways in the liver. Taken from (Kusminski and Scherer, 2018).

The fact that each zone performs different functions is driven by substrate availability. However, there is a higher order imposed by specific regulatory factors that also contributes to establishing this differential metabolic structure in the liver. One of the best well-known mechanisms is the Wnt/β-catenin pathway, which is involved in cell development, differentiation and cellular homeostasis. The Wnt pathway is most active in the PV region where it triggers the expression of PV genes (**Figure I-17**). The adenomatous polyposis coli (APC) is one of the key negative regulators of Wnt signaling and, as such, governs the activity of the pathway along the hepatic acinus. Another mechanism involved in hepatic zonation is the Ras/MAPK/ERK signaling pathway, which is the PP equivalent of the Wnt pathway. Thus, it directly induces components of pathways that predominate in the PP region. Another driver for PP gene expression is the hepatocyte nuclear factor 4 alpha (HNF4α), which also suppresses PV genes by acting as a modulator of β-catenin (Colletti et al., 2009; Gougelet et al., 2014; Kusminski and Scherer, 2018; Stanulović et al., 2007).

In the last decades, hepatic zonation of gene expression and biochemical pathways together with its regulatory mechanisms have been profoundly studied and established. However, its physiological significance is emerging at a lower speed. Nowadays, liver zonation is an underestimated phenomenon that should be more often considered when studying hepatic metabolism since performing gene expression and metabolomics on the entire hepatic extract instead of focusing on specific liver areas can completely obscure existing differences in the organ.

3.2.1. Methods for studying hepatocyte heterogeneity

Liver zonation can be nowadays studied via different techniques. Conclusions drawn from the different zonal hepatic studies largely depend on the methodology used, since each method approaches liver heterogeneity in its own specific way. It is thus important to know all the available techniques as well as their strengths and weaknesses.

3.2.1.1. Histochemistry, immunohistochemistry and *in situ* hybridization

The earliest studies on liver zonation date back as early as 1856. These first investigations used histochemistry, immunohistochemistry and *in situ* hybridization techniques (Beale, 1856; Chiquoine, 1953; Deane, 1944; Kater, 1933). Histochemistry combines the techniques of biochemistry and histology for visualization of biological structures in tissue sections allowing, under certain circumstances, quantitative description of their distribution. However, in some cases these methods suffer from inadequate fixation, limited specificity of the reactions and zonal differences in substrate affinities. Technique specificity can be greatly enhanced by using immunohistochemistry. However, this method also needs to be carefully evaluated in order to avoid artifacts due to fixation and antibody penetration. A good complement of immunohistochemistry is *in situ* hybridization (ISH), which reveals mRNA distribution in the tissue with even higher specificity. Recently developed single-molecule fluorescence ISH (smFISH) is an alternative to traditional ISH that enables measuring the absolute numbers of mRNA molecules in cells *in situ*. This approach has lately enabled the generation of a global expression map of liver zonation with high spatial resolution (Ben-Moshe and Itzkovitz, 2019; Gebhardt, 1992; Halpern et al., 2017; Jungermann and Katz, 1982).

3.2.1.2. Microdissection and microbiochemistry

Liver microdissection followed by microbiochemical determination of enzyme activities or metabolite concentrations to investigate hepatic zonation emerged almost in parallel with immunohistochemistry techniques and has evolved over time. Microdissection allows the investigator to visually select the hepatic areas of interest and to separate them cleanly from the background tissue (Hunt and Finkelstein, 2004). The first method used was manual microdissection, which involves the use of a standard or inverted microscope. The main disadvantage of this method is that it cannot discriminate between parenchymal and non-parencymal cells. Another method related to microdissection that have been used to study liver zonation is the micropunch plug technique, which consists on collecting cylindrical plugs of PP and PV areas of a liver. Despite being very efficient, this technique requires previous animal feeding

with sodium phenobarbital, which enhances the color contrast between PP and PV regions allowing their posterior distinction (Gebhardt, 1992; Jungermann and Katz, 1982; Misra et al., 1988). Collection of intact tissue from PP and PV zones has also been recently performed by laser-capture microdissection. This method avoids tissue damage and extracted RNA can be directly used for microarray studies. However, like manual microdissection, it cannot discriminate between different contributions of hepatocytes and non-parenchymal cells (Gebhardt and Matz-Soja, 2014; Saito et al., 2013).

3.2.1.3. Separation of periportal and perivenous hepatocytes by liver perfusion

Liver perfusion is one of the most powerful methods for studying liver functional heterogeneity. Separation of isolated hepatocytes into PP and PV fractions was first attempted by separating the cells according to density by equilibrium density centrifugation, density and shape by sedimentation velocity centrifugation, and by specific adsorption chromatography. However, only partial separations of PP and PV hepatocytes were achieved, which were not sufficient for the desired metabolic characterization of the cell populations (Jungermann and Katz, 1982). Later, the digitonin-collagenase perfusion method emerged as an outstanding approach that enabled the isolation of massive amounts of cells enriched for PP or PV hepatocytes (Lindros and Penttilä, 1985; Quistorff et al., 1985; Quistorff and Grunnet, 1987). In this method, the detergent digitonin is perfused to the liver in either an orthograde or a retrograde direction to selectively damage PP or PV hepatocytes, respectively. This process ensures the enrichment of undamaged cells in the desired zone of interest, which can then be dissociated using collagenase. The method efficiency and the quality of hepatocytes separation needs to be later checked based on different enzymatic expression between both cell types. Despite being a powerful technique, it also has some drawbacks: it is technically challenging, it suffers from the more or less severe damage of the cells during the isolation procedure, and each enriched PP and PV subfraction has to be prepared from different livers thus increasing the amount of animals that need to be used.

3.2.1.4. Light and electron microscopy

Hepatic zonation can also be studied by using light and electron microscopy as these approaches allow the visualization of hepatocyte structure and ultrastructure from the different hepatic regions. However, despite being very visual and informative tools, they require from a certain expertise in order to recognize the different hepatic zones. Selecting the areas containing central veins, portal tracts or both is an essential step to ensure proper analysis. Some studies have used this technique to analyze the effect of fasting or liver regeneration after partial hepatectomy on

ultrastructural zonal heterogeneity of hepatocytes and their organelles within the hepatic acinus (Elsayed et al., 2019; Ferri et al., 2005).

3.3. LIVER CYTOLOGY

The liver is composed by several cell types of different embryological origin that interact between each other and with the extracellular matrix. The diverse liver functions are mostly performed by hepatocytes. Liver non-parenchymal cells, i.e., liver endothelial cells, kupffer cells, hepatic stellate cells, biliary epithelial cells (cholangiocytes) and additional immune cell populations, support hepatocyte function (**Figure I-18**) (Jungermann and Keitzmann, 1996; Kmiec, 2001; Trefts et al., 2017).

- Hepatocytes: these cells constitute 80% of the liver mass and 60% of its cell composition (Godoy et al., 2013). They are the primary epithelial cell population of the liver. Hepatocytes are highly metabolically active thus their cytoplasm is enriched in organelles such as mitochondria, lysosomes, rough and smooth endoplasmic reticulum and Golgi apparatus. It also contains glycogen inclusions and lipid vesicles. These cells play a role in a wide variety of secretory, metabolic and endocrine functions. Hepatocytes are polarized: they face the sinusoids with their basolateral surface and form the bile canaliculi with their apical membrane. The sinusoidal domain contains microvillus, which allow the exchange of nutrients/metabolites and O_2/CO_2 with the blood (**Figure I-18**).

- Endothelial cells: this cell type forms the fenestrated sinusoidal walls. Their organization is critical for maintaining certain barrier functions while allowing the exchange of proteins and particles between the sinusoidal lumen and the other hepatic cell types (**Figure I-18**). Besides, these cells have a high pinocytic activity that allows the removal of most of the residues that are in the plasma. They are also capable of producing endothelin-1, a vasoconstrictor factor.

- Kupffer cells: they are specialized macrophages that reside between endothelial cells in the sinusoids. Together with endothelial cells, they are the first barrier against cellular and molecular residues introduced through the portal circulation (**Figure I-18**). They phagocyte aged erythrocytes, dead hepatocytes and other antigens such as bacteria. Kupffer cells can also act as antigen-presenting cells and secrete chemokines and cytokines such as TNFα and IL1β to coordinate an inflammatory response against a parenchymal damage. Due to their role in inflammation, they are key players of different liver disorders such as steatohepatitis and ischemia-reperfusion injury.

- Hepatic stellate cells: they constitute the 10-15% of hepatic population. They are located in the Disse space, the area between hepatocytes and the sinusoids (**Figure I-18**). They represent a dynamic cell population that can exist in a quiescent or activated state. In physiologic conditions, their main function is the accumulation of Vitamin A in lipid droplets. These cells are also involved in the production, secretion and degradation of collagen and other components from the extracellular matrix. Following hepatic injury, they get activated and converted into myofibroblasts. In this state, they lose all vitamin A stores and increase extracellular matrix and collagen synthesis leading to hepatic fibrosis and, lately, cirrhosis.

- Cholangiocytes: these cells represent around the 3-5% of all hepatic cells. They compose the biliary conducts (**Figure I-18**). Their main function is to depurate and modify the hepatocytes biliary secretion.

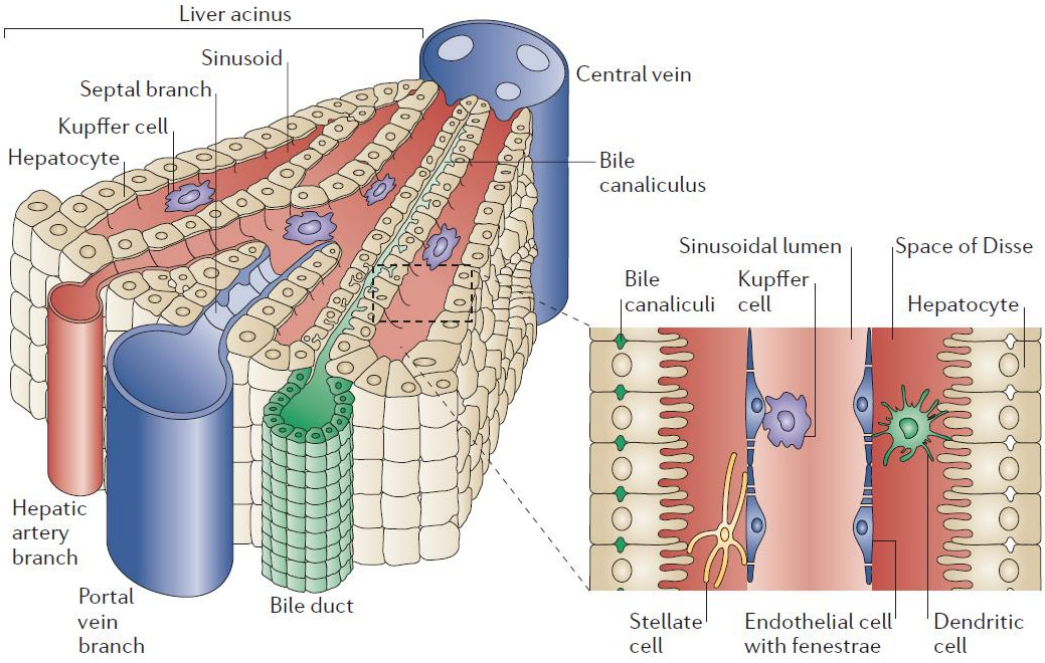

Figure I-18. Hepatic cells and their location in a liver lobule. Taken from (Adams and Eksteen, 2006).

3.4. LIVER PHYSIOLOGY

The liver is a multi-tasking organ that performs diverse functions critical for maintaining physiological homeostasis. It dynamically controls the metabolite content of the body by storing nutrients and releasing them in a regulated manner when there is an energetic demand by other extra-hepatic organs. Besides, the liver performs elaborate detoxification processes, forming a crucial line of defense against pathogens and xenobiotics. It also has exocrine and endocrine functions by producing bile acid and hormones respectively. The liver is also one of the main

protein synthesis sites in the body (Ben-Moshe and Itzkovitz, 2019; Chiang, 2014; Kalra and Tuma, 2020; Michalopoulos, 2007; Trefts et al., 2017).

3.4.1. Metabolic functions

- Proteins: protein metabolism in the liver is essential for the individual. The oxidative deamination of amino acids to use them as a source of energy or to synthesize lipids and carbohydrates is a specific hepatic function. The toxic ammonia generated in this process is then neutralized into urea via the urea cycle and released to the plasma so that kidneys can uptake it and eliminated through the urine. 90% of plasmatic proteins such as albumin and other coagulation factors are synthesized in the liver. Besides, the liver can produce all non-essential amino acids and other compounds derived from them (Chiang, 2014; Trefts et al., 2017).

- Lipids: in the liver, fatty acids are stored as triglycerides, which are composed by glycerol and free fatty acids. The latest will go to mitochondria in order to be catalyzed via β-oxidation and become acetyl-CoA, which will then undergo Krebs cycle resulting in a high amount of energy production. This process is not liver specific since it also takes place in other organs. However, the liver is the only capable of converting acetyl-CoA into acetoacetate, beta-hydroxybutyrate or acetone, overall known as ketone bodies. This process allows the subsequently distribution of ketone bodies into other organs where they can be re-converted into acetyl-CoA and be used as a source of energy for the tissue. This unique liver function is essential during periods of low food intake, carbohydrate restrictive diets, starvation or prolonged intense exercise in order to feed other organs and satisfy their energy demand. Besides, the liver synthesizes phospholipids and cholesterol. Phospholipids and around 20% of cholesterol are transported in lipoproteins to other tissues in order to create cellular membranes and other structures and compounds. The other 80% of cholesterol will become part of biliary salts. Liver can also synthesize fatty acids from proteins and carbohydrates, which are transported to the adipose tissue (Chiang, 2014; Trefts et al., 2017).

- Carbohydrates: the liver plays a central role in maintaining blood glucose levels since it can store and release glucose when the body needs it. This organ can also synthesize glucose from amino acids, lactate, pyruvate and glycerol via gluconeogenesis (**Figure I-19**) (Chiang, 2014; Trefts et al., 2017).

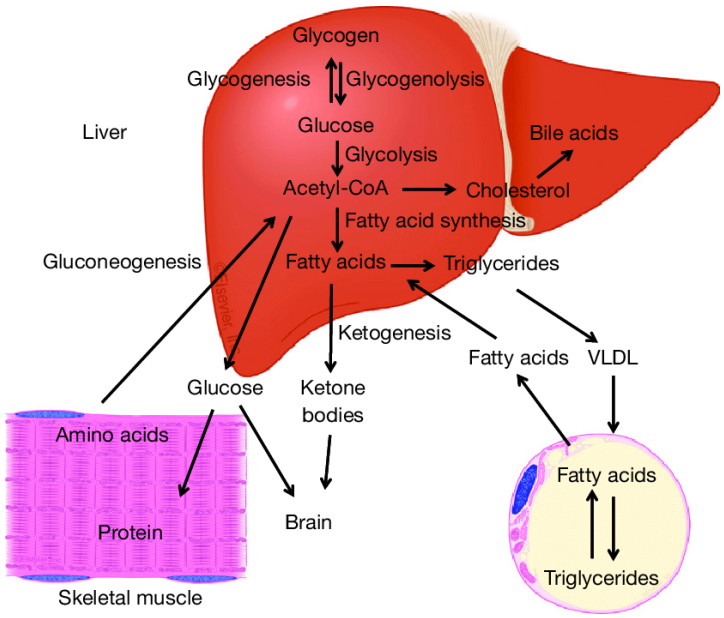

Figure I-19. Major hepatic metabolic functions. Taken from (Chiang, 2014).

3.4.2. Storage functions

- Glycogen: glycogen is a multibranched polysaccharide of glucose that represents the main storage form of glucose in the body. Both glycogenesis and glycogenolysis, so the synthesis and destruction of glycogen respectively, take place in the liver. Thus, as a response to insulin signaling, the liver stores the excessive amounts of circulating glucose into glycogen. Contrary, if glucose levels are low, epinephrine and glucagon will promote hepatic glycogenolysis and the release of resulting glucose into the blood.

- Vitamins: liver stores mainly vitamins A, D, E and B12. It also contains vitamin K, needed for the synthesis of some coagulation factors.

- Iron and copper: iron is mainly stored in the liver as ferritin. Copper is also stored in this organ and used for some proteins during cellular respiration and enzymes during hemoglobin production.

- Blood: the liver can store large volumes of blood. In physiologic conditions, it contains around 10% of whole body's blood. In pathologic circumstances such as heart failure, the liver can accumulate up to one liter of additional blood.

3.4.3. Detoxifying functions

The liver helps to detoxify the blood getting rid of harmful substances. It uses lysosomes to eliminate certain compounds, but the major route of metabolism and detoxification is through

biotransformation, which consists on converting xenobiotics from a lipophilic form to a hydrophilic form. Many metabolites, hormones and xenobiotic will subsequently be excreted to the bile. Formation of urea in the liver is also a detoxifying function since it eliminates toxic ammonia (Kalra and Tuma, 2020).

3.4.4. Production and excretion of bile

Liver is the responsible for bile production, a substance that is mainly composed of water, biliary salts, biliary pigments, some lipids and bicarbonate. Bile emulsions lipids and facilitates their digestion in the duodenum, the first part of the small intestine. Bile is also used in order to excrete residues to the blood such as the bilirubin that results from hemoglobin destruction, cholesterol or calcium. All these residues will end up in the feces (Kalra and Tuma, 2020).

3.4.5. Immunologic function

Blood that comes from the portal vein usually carries bacteria coming from the intestine. Some hepatic cells with immunologic functions, such as Kupffer cells, react towards these bacteria in order to eliminate them before they enter to the circulating blood (Kalra and Tuma, 2020).

3.4.6. Regenerative capacity

Liver is the only organ capable of regenerating itself after a significant loss of tissue due to a specific damage or a hepatectomy. During its regeneration, their hepatocytes divide and allow the recuperation of the original organ size. Livers regenerative capacity is exceptional: within a week after removing two-thirds of the liver, the liver can return to the same weight it was before surgery (Michalopoulos, 2007).

3.5. HEPATIC DISEASES

There are many types of diseases that can affect the liver. Considering the unique and essential functions of this organ in homeostasis, metabolism and detoxification, hepatic diseases can be devastating and, in some cases, life-threatening (Chiang, 2014; Kalra and Tuma, 2020). In fact, liver diseases account for approximately 2 million deaths per year worldwide, being cirrhosis the 11th most common cause of death globally (Asrani et al., 2019). Some of the most common hepatic diseases are:

- Hepatitis: it refers to an inflammatory condition of the liver that is commonly caused by a viral infection. There are five main hepatitis viruses, referred to as types A, B, C, D and E. HAV infection can take place by eating or drinking something that is tainted by fecal matter. It is

thus more common in developing countries that lack clean drinking water and have poor sanitation systems. Although some patients can suffer liver failure, HAV usually goes away on its own in almost all cases with no serious complications. HBV and HCV are more commonly spread through unprotected sexual contact, through sharing needles or by accidentally injection with a contaminated needle. About 95% of adults who are exposed to HBV fully recover within 6 months without medication. If it lasts longer than 6 months, it makes the patient more likely to get liver cancer or other diseases. There is a vaccination against the disease to prevent it. In the case of HCV, the virus can produce both acute and chronic hepatitis, ranging in severity from a mild illness lasting a few weeks to a serious lifelong illness. Symptoms may not show up for many years.

- Autoimmune hepatitis: in this disease the immune system itself attacks the liver and triggers its inflammation. It is a chronic disease that can last many years. If untreated, it can lead to cirrhosis and liver failure.

- Primary biliary cholangitis: it results from progressive destruction of the hepatic bile ducts. When the ducts are injured, the bile backs up inside the liver and scars it eventually leading to cirrhosis.

- Primary sclerosing cholangitis: in this disease bile ducts become blocked. This causes bile to accumulate in the liver, where it gradually damages liver cells and causes hepatic fibrosis or cirrhosis. It can also lead to liver cancer, needing in some cases a liver transplant. This disease progresses slowly. Many patients may have the disease for years before symptoms develop.

- Liver cancer: it is the growth and spread of proliferative cells in the liver. Two types of liver cancers can be distinguished: primary liver cancer that originates in the liver such as hepatocellular carcinoma, and metastatic liver cancer, the cancer that spreads from another organ to the liver.

- Hemochromatosis: this inherited condition causes an excess of iron absorption and storage in the body, which can damage the liver, heart and other organs. Without treatment, the disease can cause these organs to fail.

- Wilson's disease: this inherited disease is characterized by body excessive retention of copper. Copper accumulation in the liver begins to damage the organ. After enough damage, the liver releases the copper directly into the bloodstream reaching and damaging other organs such as kidneys, brain and eyes. If not treated, Wilson Disease can cause nerve and psychiatric problems, liver failure and death.

- Drug-induced liver injury (DILI): it is the hepatic damage produced by drug overdoses such as acetaminophen overconsumption among others. While most cases of DILI are benign and improve after drug withdrawal, others can be life-threatening.
- Alcoholic liver disease (ALD): it is caused by alcohol abuse, which damages the liver leading to a buildup of fats, inflammation and scarring. More characteristics of alcoholic liver disease will be further discussed in Section 4.
- Nonalcoholic fatty liver disease (NAFLD): it is the buildup of extra fat in liver cells not caused by alcohol consumption. It is normal for the liver to contain some fat. However, if more than 5-10% percent of the liver's weight is fat, then it is called a fatty liver. The more severe form of NAFLD is called nonalcoholic steatohepatitis (NASH), which courses with inflammation and fibrosis challenging proper liver function. NASH causes the liver to swell and become damaged.

Symptoms of liver diseases vary depending on the underlying cause. However, there are some general symptoms that are shared among hepatic disorders: swelling of the abdomen and legs, changes in color of the stool and urine, bruising easily and jaundice (yellowing of the skin and eyes). Analysis such as imaging and liver function tests can check for liver damage and help to diagnose liver diseases. The main diagnostic indicators of liver disorders and injury include increasing levels of aspartate aminotransferase (AST) and alanine aminotransferase (ALT) in serum, jaundice, increasing clotting times, edema and hepatic encephalopathy. In the last decades increased progress has been made in understanding liver development, physiology and repair. However, hepatic diseases are still one of the main causes of death worldwide. This drives the need to further study these diseases and their underlying pathological mechanisms, which will certainly help in ensuring early diagnose and promoting better disease outcome (Marcellin and Kutala, 2018). In the next two sections we will focus on ALD and NPC, a lysosomal lipid storage disorder that it is nowadays recognized as a relatively common cause of liver disease in early life.

4. ALCOHOLIC LIVER DISEASE

Alcohol has been part of the human culture for thousands of years and has become the most socially-accepted addictive drug worldwide. Although excessive alcohol consumption is known to be the oldest form of liver injury, it was not until the 20th century when it was studied with a scientific perspective. In 1965, Lieber and colleagues identified for the first time the hepatotoxic function of alcohol, instead of the malnutrition effect, previously assumed (Lieber et al., 1965).

Nowadays, the term alcoholic liver disease (ALD) is worldwide recognized as a complex disease induced by alcohol excessive consumption with a broad spectrum of hepatic disorders.

According to the World Health Organization, 3 million people die every year worldwide as a result of the harmful use of alcohol, which represent about 5.3% of all annual deaths (World Health Organization, 2018). Besides liver injury, excess of alcohol consumption is a causal factor of other diseases and injury conditions. Many people, their families and communities daily suffer the consequences of alcohol overconsumption due to not only health problems such as mental disorders, cancer and strokes but also injuries resulting from domestic violence and traffic accidents. Beyond health consequences, the damaging use of alcohol also brings significant social and economic losses to individuals and society at large.

4.1. RISK FACTORS FOR ALD

The impact of alcohol consumption in populations is mostly determined by the total volume of alcohol consumed and the pattern of drinking. Besides these two elements, also individual and societal vulnerability factors need to be taken into account.

Individual vulnerability refers to factors that make some people more susceptible to consuming more alcohol and more sensitive to the harms caused by this toxic. Individual risk factors include age, gender, diet and smoking as well as genetic differences among individuals or ethnic groups. In relation to diet, evidence shows that obese individuals tend to be more susceptible to alcohol-induced liver injury at lower doses than healthy-weight counterparts (Loomba et al., 2009). Regarding to ethnic groups, it has been seen that East Asians are more vulnerable to alcohol compared to people from Western Nations. This fact is mainly due to the presence in 40% of East Asians of an inactive variant of the Aldehyde dehydrogenase 2 (ALDH2), the enzyme that degrades the toxic acetaldehyde resulting from alcohol metabolism (Jin et al., 2015).

Environmental factors including economic development, culture, alcohol availability and national alcohol policies also play an important role in ALD. All these societal factors have an effect on drinking habits and harms caused by alcohol. The level of development of one country is also a significant risk factor. For instance, although residents of less developed countries tend to drink less alcohol, they also have fewer health services available to reduce its damaging effects. Alcohol regulation is another important point. The quality of alcoholic drinks should be analyzed more systematically since their composition can directly contribute to the disease burden (Rehm et al., 2010).

Thus, it is of a great importance to consider these wide-range of interrelated individual and societal factors to understand the variety in ALD manifestations among alcoholic patients.

4.2. CLINICAL CHARACTERISTICS OF ALD

4.2.1. Stages

ALD comprises a range of stages including simple steatosis, steatohepatitis, cirrhosis and end-stage hepatocellular carcinoma. There are three main stages of ALD, although there is often an overlap between each stage (**Figure I-20**) (Gao and Bataller, 2011; Lamas-Paz et al., 2018; Louvet and Mathurin, 2015).

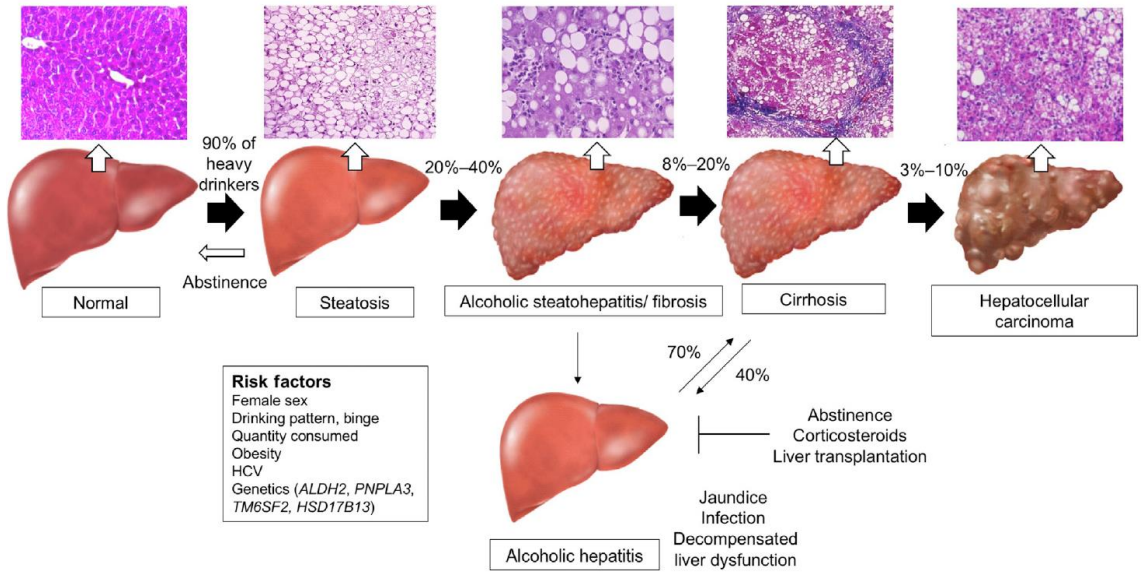

Figure I-20. Stages and progression of ALD. Taken from (Ohashi et al., 2018).

- Alcoholic fatty liver disease (hepatic steatosis)

Just a few days of drinking a large volume of alcohol can lead to the accumulation of fats in the liver, stage that is known as alcoholic fatty liver disease or hepatic steatosis. Alcohol induces hepatic fatty acid uptake, impairment of fatty acid oxidation, promotion of *de novo* lipid synthesis and neutral lipid storage as well as inhibition of lipid export and lipid droplet catabolism. All these pathways converge impacting on cellular lipid homeostasis and triggering hepatic fat accumulation. This first stage of ALD rarely causes any symptoms but it is an important warning sign that the individual is drinking at a harmful level. Alcoholic fatty liver disease is often reversible if the affected person abstains from alcohol from this point onward (Jeon and Carr, 2020).

- Alcoholic steatohepatitis

Alcoholic steatohepatitis is a potentially serious condition that can be caused by alcohol misuse after many years of heavy drinking. Less commonly, alcoholic hepatitis can also occur if the individual drinks a large amount of alcohol in a short period of time, what is known as binge drinking. Hepatitis is a general term of swelling and inflammation of the liver. Excessive alcohol consumption causes intestinal bacterial overgrowth, endotoxins accumulation and increased intestinal permeability by disrupting the intestinal barrier function. This disruption facilitates the translocation of bacterial products from the intestine to the liver leading to the activation and recruitment of inflammatory cells to this organ. These changes are also associated with hepatic fibrosis, which is mainly coordinated by hepatic stellate cells. This second ALD stage is usually reversible if the individual stops alcohol drinking on a long-term basis. Severe alcoholic hepatitis, however, is a serious and life-threatening illness. When hepatitis develops, it may be the first time a person is aware that the liver is being damaged through alcohol (Ohashi et al., 2018; Purohit and Russo, 2002).

- Cirrhosis

Cirrhosis occurs when the liver has been inflamed for a long time, leading to scarring and loss of function. Excessive and long-term alcohol oxidation destroys hepatocytes structure, causing microtubule dysfunction and further affecting the transportation of nutrients. Besides, collagen synthesis is stimulated and there is an accumulation of extracellular matrix proteins that form liver cirrhosis. As the liver no longer processes toxins properly, it will be more sensitive to medications and alcohol, which can be a life-threatening condition. Cirrhosis damage is irreversible, but the patient can prevent further damage and significantly increase life expectancy by stopping alcohol consumption. However, although life-long abstinence can improve liver function, the permanent and severe damage from cirrhosis might mean that the patient needs a liver transplant to survive (Kong et al., 2019)

4.2.2. Hepatic zonal pattern in ALD

Liver pathologies often exhibit zonated patterns that can be attributed to the functional zonation of hepatocytes (Ben-Moshe and Itzkovitz, 2019). ALD is known to progress in a zonated manner starting from the PV area and spreading into the PP zone as the disease evolves (Keegan et al., 1995; MacSween and Burt, 1986; Nakano et al., 1982). The course of ALD begins with the accumulation of lipid droplets, causing hepatic steatosis. The increased expression of lipogenesis genes and reduced expression of fatty acid β-oxidation genes in PV hepatocytes already suggest

that alcohol-induced lipid accumulation might be faster in this zone than in PP regions. Indeed, in rat models of ethanol intoxication, the accumulation of lipid droplets is first observed in the PV zone compared to the PP (Iseri et al., 1966). Similar PV zonation patterns have been observed in human patients with alcoholic fatty liver disease (Chalasani et al., 2008). In addition to lipid homeostasis, the different zonal expression of the key alcohol metabolizing enzymes alcohol dehydrogenase (ADH) and cytochrome P450 2E1 (CYP2E1) also plays an important role. A major activity of these enzymes has been described in the PV zone of the liver lobule not only in basal conditions but also after long-term alcohol intake (Bühler et al., 1992). Thus, alcohol detoxification mainly takes place in the PV area being the most affected one by this toxic compound in early stages of the disease (**Figure I-21**). It is consequently of a great relevance to take liver zonation into account when studying specific liver diseases such as ALD.

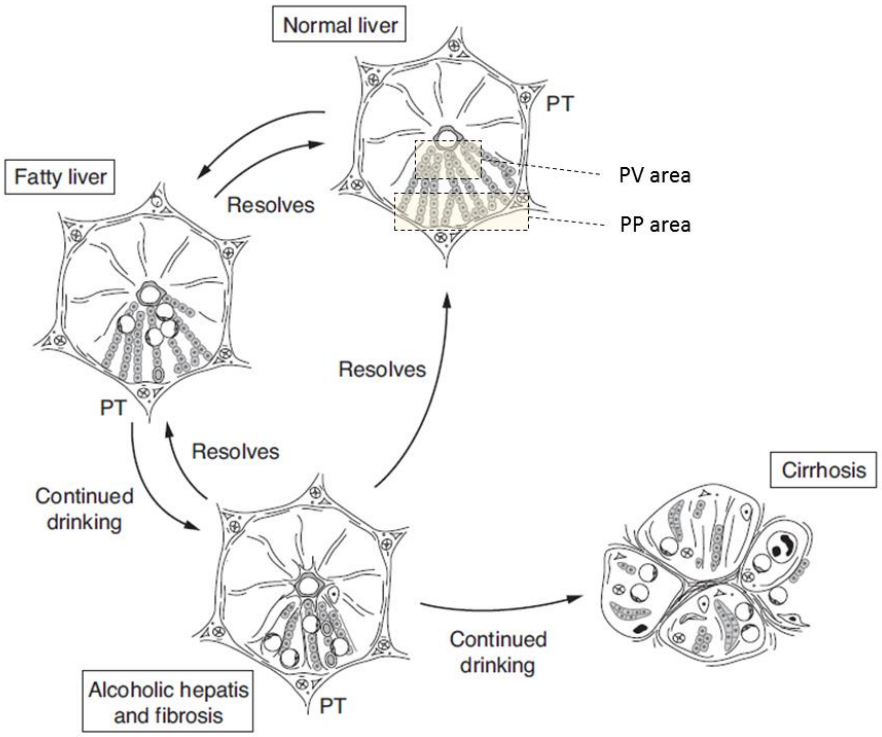

Figure I-21. Zonal progression amongst the various histologic stages of ALD. Adapted from (Schiff et al., 2011). PT: portal tract, PV: perivenous, PP: periportal.

4.2.3. Treatment

There is currently no specific medical treatment for ALD. Stop drinking not always reverses alcohol-induced liver damage, being liver transplantation the treatment choice for patients with liver failure in end-stage liver disease. Aside from liver transplantation, there are other available therapies and promising approaches to treat ALD patients such as corticosteroids and N-acetylcysteine (NAC). Corticosteroids downregulate TNFα production and upregulate IL-10

expression (an anti-inflammatory cytokine) overall reducing short-term mortality. However, this medication does not improve long-term survival. NAC is a GSH precursor antioxidant. Treatment of ALD with NAC alone does not improve short-term survival. However, the combination of NAC with corticosteroids significantly improves patient survival. Anti-TNFα therapy such as infliximab also improves disease severity and survival despite having some-side effects when combined with corticosteroids. Work with animal models have also revealed S-adenosyl-L-methionine (SAMe) as a potential treatment for ALD (García-Ruiz et al., 1995; McClain et al., 2002). However, although some randomized clinical trials have been made with patients suffering ALD, the benefits of SAMe treatment are still not clear (Rambaldi and Gluud, 2006). There is thus a therapeutic need for ALD that it is neither completely covered nor optimal. The study of the physiologic and molecular mechanisms associated to this pathology is of a great importance to better understand the disease and to find new treatments that would benefit ALD patients (Kong et al., 2019; Ohashi et al., 2018).

4.3. ALD EXPERIMENTAL MODELS

Effective treatment options for ALD are very limited due to the lack of suitable *in vivo* models that recapitulate the full spectrum of human ALD. The ideal experimental model should present all aspects of the ALD process, including significant steatosis, hepatic inflammatory cells infiltration and liver injury (Lamas-Paz et al., 2018). Among the different experimental model organisms used nowadays in laboratories, mammalian rodents (rats and mice) are the most frequently used to study ALD. They are highly-resistant to successive in-breeding with low genetic variability between individual animals, they have a short lifespan and a fast rate of reproduction, they are small in size and easy to handle, and costs per animal in terms of initial purchase, housing and maintenance are considerable low compared to other organisms. In addition, rodents are an excellent organism for the generation of transgenic and knockout models. However, although rodents are reasonably similar to humans in terms of liver physiology, there is still some disparity in liver injury between these two species after ethanol exposure. The main differences are the natural aversion of rodents to alcohol and the rate of alcohol oxidation since it is five times faster in rodents than in humans (Holmes et al., 1986). In addition, the difference in the innate immune systems between these two species must be carefully considered as immune responses play an essential role in ALD pathology (Mestas and Hughes, 2004).

Numerous models employing rodent animals have been established to investigate the effects of acute and chronic alcohol exposure on the initiation and progression of ALD (**Table I-1**). Administration of ethanol in these animal models ranges from voluntary oral intake via drinking water or a liquid diet (Lieber-De Carli model) to direct alcohol gastric administration (Tsukamoto-French model) (Altamirano and Bataller, 2011).

Models	Animal model	Characteristics	Advantages and disadvantages
Lieber-DeCarli liquid diet[27,28]	Rat/mice	Chronic ethanol feeding (4-12 wk)	Easy to perform Marked elevation of ALT Short term feeding with no mortality rate No liver fibrosis
	Rat/mice	Chronic ethanol feeding + single/multiple binges (4-6 wk)	Easy to perform Marked elevation of ALT and marked steatosis Long term feeding + multiple binges with a high mortality rate No liver fibrosis
	Rat/mice	+ Second hit: DEN, LPS, CCl_4, APAP (4-12 wk)	Easy to perform Marked elevation of ALT and marked steatosis Long term feeding + multiple binges + injection with a high mortality rate Liver fibrosis
Ethanol *ad libitum* feeding[27,28]	Mice	Oral alcohol in drinking water (10 d/1-2 wk)	Easy to perform Minimal elevation of ALT and mild steatosis Short-or long-term feeding with no mortality rate No liver fibrosis
The Tsukamoto-French model[27,28]	Rat/mice	Intragastric infusion (2-3 mo)	Difficult to perform Requirement for intensive medical care Marked elevation of ALT and steatosis Long-term feeding with a high mortality rate Mild liver fibrosis
The NIAA model[47]	Mice	LDE + single ethanol binge	Cost and time efficient High blood alcohol levels Liver injury Inflammation Fatty liver
	Rat /mice	LDE + 3 ethanol binges	Cost and time efficient Increased blood alcohol levels Augmented liver injury Increases in ERK1/2
Ethanol + CCl_4 treatment[106]	Mice	4% ethanol liquid diet + 2 times IP CCl_4 injection per week (8 wk)	Easy to perform Toxic components Elevated acetaldehyde levels Liver fibrosis

Table I-1. Comparison of ALD experimental models. Taken from (Lamas-Paz et al., 2018). ALT: Alanine aminotransferase, DEN: diethylnitrosamine, LPS: lipopolysaccharide, CCl_4: carbon tetrachloride, APAP: acetaminophen, LDE: Lieber-DeCarli ethanol diet, IP: intraperitoneal.

4.3.1. Lieber-De Carli Liquid Diet

For many years the main ALD experimental model was based on the use of alcohol in drinking water together with solid food. However, the aversion of rodents to alcohol in some cases prevented them from significant liver damage. To overcome this problem, a new model was invented: animals had access only to an ethanol-containing liquid diet formula but with no other food or drink. In this case, the daily intake of ethanol increased two to three times more than that achieved from drinking the ethanol-only solution. Significant liver steatosis was observed using this approach. These findings first introduced by Lieber et al in 1963 opened a new era for ALD research. This diet later became known as the Lieber-DeCarli liquid diet and is nowadays a standard experimental model for the study of ALD (F. Guo et al., 2018; Lamas-Paz et al., 2018; Lieber et al., 1963).

The Lieber-DeCarli diet is an isocalorically-controlled liquid diet in that the total caloric content (0.6-1.0 cal/mL) in the diet remains unchanged, while specific components vary to serve different

groups and experimental objectives. The control diet, often used for pair-fed control groups, is formulated from several key parts of nutrition: Casein (consisting of methionine and cystine), contributes 18% of total calories; fat, derived from olive and corn oils, makes up 35% of total calories; fat-soluble vitamins (A, D, E, K) and water-soluble vitamin B12, minerals and fiber; the remaining formula (dextrin and maltose mixture) provided the majority of energy (47% of the total calories). In the ethanol-containing formula, an amount equal to 36% of total calories of the dextrin and maltose mixture is removed and replaced by isocalorically measured alcohol (DeCarli and Lieber, 1967; Lieber and DeCarli, 1989, 1982).

The feeding period using Lieber-DeCarli diet model should start with gradually increased amounts of ethanol during approximate five days to allow the animal adaptation to the ethanol. Then, feeding usually varies between four and twelve weeks in mouse and one and nine months in rats. Lieber-DeCarli ethanol feeding causes marked elevation of serum alanine aminotransaminase (ALT) and aspartate aminotransferase (AST) as well as varying degrees of hepatic steatosis but it does not induce other major hepatic pathological changes. Many attempts have since been made to elevate the effect of this diet and induce more sever forms of liver injury (eg. the chronic-binge ethanol feeding rodents model, which combines a chronic feeding period using Lieber-DeCarli diet and one or multiple binges) (Altamirano and Bataller, 2011; Lamas-Paz et al., 2018).

4.4. PHYSIOLOGIC AND MOLECULAR MECHANISMS OF ALD

4.4.1. Alcohol metabolism

Alcohol is a polar molecular substance that is soluble in both water and lipid. After being consumed, it is absorbed into the blood circulation through the gastrointestinal tract (GI). Following absorption in the GI, only 2% to 10% of total ingested alcohol is directly eliminated through the lungs, kidneys and sweat in an unchanged form. Most alcohol will thus undergo metabolic processing in the liver (**Figure I-22**).

Ethanol (C_2H_6O) is first oxidized and transformed into acetaldehyde (C_2H_4O) in hepatocytes. There are three metabolic systems which participate in the oxidative metabolism of alcohol into acetaldehyde (Kong et al., 2019; Lamas-Paz et al., 2018; Lieber, 2005):

- Alcohol dehydrogenase (ADH) system: Alcohol is mainly metabolized by the hepatocyte cytoplasmic ADH system, which oxidizes ethanol into acetaldehyde using nicotinamide adenine dinucleotide (NAD^+) as a co-factor (**Figure I-22**). ADH1, amongst the other isoenzymes of ADH, plays a main role in ethanol metabolism in the liver.

- Microsomal Ethanol-Oxidizing System (MEOS): The second alternative pathway is the microsomal ethanol oxidation system (MEOS), which depends on cytochrome P450 (CYP450) enzymes, particularly on CYP2E1 (**Figure I-22**). Under normal physiological conditions, CYP2E1 only catalyzes the oxidization of a small amount of ethanol, such as 10%. However, CYP2E1 is upregulated in chronic alcohol abuse conditions and leads to converting more alcohol to acetaldehyde.

- Catalase: The third pathway involves an enzyme called catalase, which is located in peroxisomes. Catalase usually catalyzes hydrogen peroxide removal but is also capable of catalyzing the oxidation of alcohol to acetaldehyde (**Figure I-22**). However, quantitatively this is considered a minor pathway of ethanol oxidation.

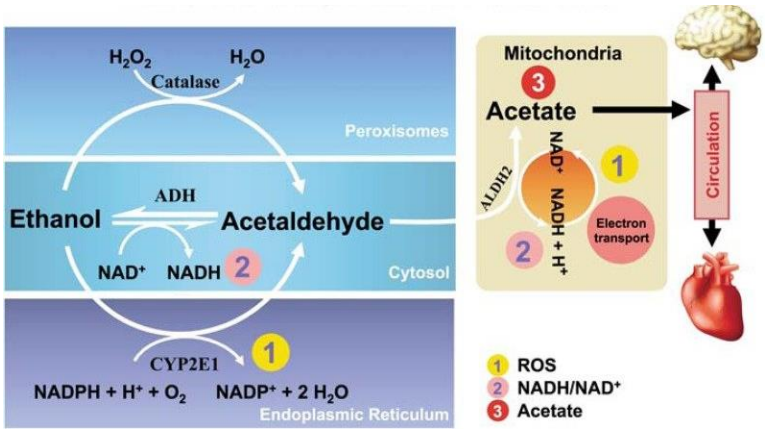

Figure I-22. Oxidative pathways of alcohol metabolism in the liver. Taken from (Zakhari, 2013).

Once acetaldehyde is formed by any of these three pathways, successive oxidation reactions take place. Acetaldehyde is metabolized further in the mitochondria by the mitochondrial aldehyde dehydrogenase (ALDH) to form acetate and NADH. Most of the acetate resulting from ethanol metabolism escapes the liver into the blood (**Figure I-22**). Cells from heart, skeletal muscle and brain have mitochondria that contain enzymes capable of transforming acetate to acetyl CoA. These cells readily take up acetate and convert it into acetyl CoA, which is further oxidized in the Krebs cycle generating CO_2 and water as the end-products of ethanol oxidation (Cederbaum, 2012; Ceni et al., 2014; Manzo-Avalos and Saavedra-Molina, 2010; Zakhari, 2013).

When the concentration of ethanol in blood and tissue fluid is low, ethanol is mainly metabolized by the ADH pathway and almost all acetaldehyde is rapidly converted into acetate, which in turn is metabolized by extra-hepatic tissues. In contrast, excessive alcohol consumption leads to the upregulation of the other two enzymatic systems, resulting in biochemical changes in hepatocytes. The increase in alcohol oxidation specifically through CYP2E1 induces ROS formation. ROS accumulation contributes to increased oxidative stress and triggers many

pathological effects such as damage in proteins, lipids and DNA (Cederbaum, 2012, 2006). Increased alcohol oxidation also results in elevated NADH levels. This change in NAD^+/NADH ratio has been considered to play a major role in the initial pathogenesis of alcohol-induced fatty liver. Besides, the re-oxidation of NADH via the electron transport chain in the mitochondria results in the formation of even more ROS that will further contribute to oxidative stress (Baraona and Lieber, 1979; Crabb and Liangpunsakul, 2006; Lieber, 2005). Overall, while low alcohol intake is not significantly damaging, alcohol overconsumption promotes the accumulation of the cytotoxic metabolites acetaldehyde and acetate, excessive formation of ROS and lipid homeostasis changes. These factors subsequently converge into determining an inflammatory status in the liver and, in a long term, the loss of hepatic function.

4.4.2. Pathological effects of alcohol oxidation

There are many molecules and signaling pathways involved in ALD that contribute to the disease burden. The study of the pathogenic mechanisms in ALD highlights three main pathways: lipid metabolism, hepatotoxicity and immune system. Although these pathways seem to be quite diverse, they are connected by an intricate network of tight interactions overall leading to hepatic injury (**Figure I-23**) (Boccuto and Abenavoli, 2017; Kong et al., 2019; Lamas-Paz et al., 2018).

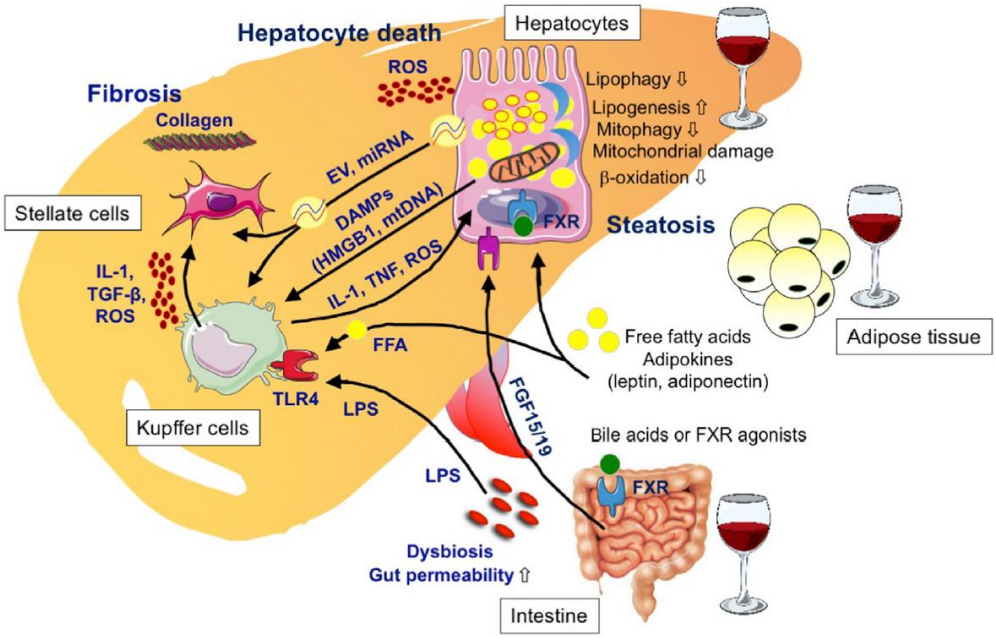

Figure I-23. Pathological effects of alcohol oxidation. Taken from (Ohashi et al., 2018). LPS: lipopolysaccharide, DAMPs: damaged-associated molecular patterns, EVs: extracellular vesicles, FGF; fibroblast growth factor, FXR: farnesoid X receptor, HMGB1: high mobility group box 1, IL: interleukin, miRNA: microRNA, mtDNA: mitochondrial DNA, FFA: free fatty acid, ROS: reactive oxygen species, TGF: transforming growth factor, TLR: toll-like receptor, TNF: tumor necrosis factor, DNA: deoxyribonucleic acid.

4.4.2.1. Lipid accumulation in ALD

The mechanisms of lipid accumulation in the liver during alcohol consumption involve the alteration of molecules and pathways that control lipid synthesis and oxidation (Ceni et al., 2014). Some of the best well-known key players in lipid alteration by alcohol abuse are:

- Decreased NAD^+/NADH ratio: Major reactions in alcohol oxidation require the coenzyme NAD^+ for transferring hydrogen. As a result of increased ethanol oxidation, the amount of reducing equivalents (NADH) is increased. This change in NAD^+/NADH ratio promotes hepatic triglyceride accumulation and fatty acid synthesis since many of the enzymes of fatty acid oxidation are pyridine nucleotide dependent, thus, their activities are inhibited by NADH, resulting in reduced ability to oxidize fatty acids (Baraona and Lieber, 1979; Crabb and Liangpunsakul, 2006).

- Inhibition of Peroxisome proliferator-activated receptors (PPARs): PPARs regulate the transcription of genes involved in the esterification and export of fatty acids to oxidize them in the mitochondria, peroxisomes and microsomes. Ethanol metabolism interferes with the transcriptional activity of PPARα, inhibits PPARα-DNA binding activity and decreases PPARα target genes, overall leading to the accumulation of fatty acids (Fischer et al., 2003; Lu et al., 2008; Nanji et al., 2004).

- Induction of SREBPs: SREBPs are a family of transcription factors strictly correlated with PPARs and that control a set of enzymes involved in the synthesis of fatty acids and triglycerides as well as cholesterol (see section 1.3. for more details). Acetaldehyde produced from ethanol metabolism enhances the levels of SREBP-1 to promote the synthesis of fatty acids which results in fatty acid accumulation in hepatocytes (Ji and Kaplowitz, 2003; You et al., 2002).

- AMP-activated protein kinase (AMPK) downregulation: AMPK is a metabolic sensor by phosphorylation of enzymes involved in lipid metabolism. Chronic ethanol exposure inhibits AMPK activity through the inhibition of protein kinase (PK)Cζ and liver kinase (LK)B1 phosphorylation. This inhibition plays a key role in the development of steatosis by the activation of hepatic lipogenesis, cholesterol synthesis, and glucose production in parallel with the decrease in fatty acid oxidation (García-Villafranca et al., 2008; Tomita et al., 2005; You et al., 2004).

- Reduction of Autophagy: Autophagy is upregulated by increased AMPK. Ethanol exposure decreases AMPK, thereby reducing autophagy activity which can enhance lipid accumulation through impaired lipophagy (Chao et al., 2018).

4.4.2.2. Ethanol Hepatotoxicity

Chronic alcohol consumption promotes biochemical changes in hepatocytes that can finally lead to hepatocyte death. Different molecules, pathways and subcellular compartments are implicated in the hepatotoxic function of alcohol:

- Acetaldehyde: The first product of alcohol metabolization has a central role in the pathogenesis of ALD by causing damage to hepatocytes. This toxic impairs cellular functions and gene expression by forming adducts with proteins and DNA. Regarding to proteins, it can bind to albumin, tubulin, collagen and microsomal enzymes overall resulting in protein dysfunction. Defects in assembly of microtubules, protein excretion and enzymatic activity have all been attributed to acetaldehyde. The formation of these protein-acetaldehyde adducts also results in the production of immunodominant antigenic determinants that activate the adaptive immune system and contribute to the disease progression (Setshedi et al., 2010; Stewart et al., 2004). Aside from protein and DNA adducts formation, acetaldehyde can also bind to GSH inhibiting its antioxidant function, induce ER stress and increase hepatocyte sensitivity to TNF-α (Lluis et al., 2003).

- Oxidative stress and antioxidant systems: Under physiological conditions, fluctuations in ROS levels are involved in different signaling pathways and cellular functions are properly maintained through proper redox balance. However, extreme alcohol oxidation induces the excessive formation and accumulation of ROS in the hepatocyte. As acetaldehyde does, this increased amount of alcohol-induced free radicals can also react with proteins, lipids and DNA forming adducts that result in cell damage. Alcohol-induced ROS, such as hydrogen peroxide and superoxide ions, are also associated with the pro-inflammatory profile of alcohol-mediated liver damage via recruiting immune cells and inducing pro-inflammatory cytokines circulation that will finally cause hepatocyte damage (Kong et al., 2019). In addition to increasing ROS, ethanol consumption results in the dynamic imbalance of endogenous antioxidant systems mainly by targeting the nuclear factor erythroid 2-related factor 2 (Nrf-2), which regulates the expression of antioxidant proteins (Zhao et al., 2018). Alcohol also damages other antioxidant genes that have important roles in ROS scavenging such as SOD, GSH, catalase, peroxidase-1, metallothionein and heme oxygenase (Han et al., 2016; Kong et al., 2019; McClain et al., 2017).

- Methionine cycle: methionine is an essential amino acid that is mainly metabolized by the liver into SAMe, which is needed for methylation of a large variety of substrates (DNA, proteins, lipids) and polyamine synthesis. Changes in SAMe concentration impact on the

normal hepatic function (Mato and Lu, 2007). Ethanol causes abnormal methionine metabolism by inhibiting the enzyme methionine synthase (MS) that regenerates methionine from homocysteine, causing as a result hyperhomocysteinemia (HHcy). HHcy has been implicated in the pathogenesis of ALD through activation of ER stress. Ethanol-induced HHcy promotes cell injury via apoptosis, fat accumulation and inflammation (Ji, 2008; Kaplowitz and Ji, 2006).

- ER Stress: The ER is the intracellular organelle responsible for synthesis, folding, trafficking and maturation of membrane and secretory proteins. Physiologic stresses can lead to an imbalance between the demand and the capacity of the ER for protein folding, thereby causing ER stress that can lead to lipid accumulation, inflammation and cell death. As previously stated, alcohol intake induces ER stress by different mechanisms such as acetaldehyde-protein adduct formation, oxidative stress and alcohol-induced HHcy.
- Mitochondrial damage: Among the different subcellular compartments, mitochondria is one of the most damaged by alcohol overconsumption. Alcohol oxidation induces a wide-range of mitochondrial alterations starting from mitochondrial DNA and protein damage and leading to the activation of mitochondria-dependent apoptosis. More mechanisms of alcohol-induced mitochondrial dysfunction will be further discussed in Section 4.5.

4.4.2.3. Hepatic inflammation in ALD

Innate immunity has a central role in the pathogenesis of ALD. In recent decades significant progress has been made in understanding the molecular mechanism contributing to the alcohol-dependent activation of innate immunity and inflammation (Ceni et al., 2014).

Chronic drinking causes imbalance of intestinal flora by triggering excessive proliferation of gram negative bacteria in the intestine. This in turn causes intestinal accumulation of lipopolysaccharides (LPS), also known as lipoglycans or endotoxins. Aside from this, alcohol also triggers increased permeability of the intestine. On one hand, the metabolism of alcohol by gram negative bacteria and intestinal epithelial cells results in acetaldehyde accumulation, which damages the intestinal barrier. On the other hand, alcohol also stimulates the production of a large number of nuclear transcription factors NF-B and inducible nitric oxide synthase (iNOS), which increase the intestine intercellular permeability by damaging the microtubule cytoskeleton and inducing cell conformational changes. Disruption of the intestinal barrier allows the transference of the accumulated endotoxins from the intestine to the liver overall causing inflammatory changes in this organ (Purohit et al., 2008).

Once in the liver, endotoxins can activate Kupffer and inflammatory cells, which inhibit macrophage phagocytosis and stimulate the proliferation of hepatic stellate cells (HSC) by releasing cytokines such as TNF-α, interleukin IL-1, IL-17, CXC chemokines, osteopontin and inflammatory factors and free radicals (Gao and Bataller, 2011). Additionally, the secretion of specific chemokines produced by Kupffer cells and HSC promote neutrophils migration and infiltration to damaged liver tissues. This neutrophil recruitment is also triggered by the alcohol-induced upregulation of intercellular adhesion molecule-1 (ICAM-1) expression on the surface of neutrophils and E-selectin expression on sinusoidal endothelial cells. The activated Kupffer cells and recruited neutrophils release fibrosis-related factors, such as the transforming growth factor beta (TGF-β) and the platelet-derived growth factor, as well as IL-1β and TNFα overall promoting hepatocyte apoptosis and local inflammation and, consequently, liver damage (Kong et al., 2019; Ma et al., 2016; Ohashi et al., 2018).

4.5. ROLE OF MITOCHONDRIA IN ALD

Mitochondria contribute to alcohol metabolism via acetaldehyde oxidation through ALDH and NAD^+ replenishment by NADH oxidation in the respiratory mitochondrial chain. However, these organelles are also target of the deleterious effects of alcohol. Over the years, increased evidence has pointed towards mitochondrial abnormalities at the morphological and functional levels caused by alcohol abuse. Due to mitochondrial importance in energy production, metabolism and cell fate decisions, changes in mitochondria caused by alcohol are considered a relevant contributory factor in ALD (García-Ruiz et al., 2013; Rubin et al., 1970; Song et al., 2014). The mechanisms by which alcohol injures mitochondria are diverse:

- DNA and protein damage: Chronic alcohol intake damages mitochondrial DNA as well as decreases mitochondrial protein synthesis by impairing mitochondrial ribosomes (Bailey et al., 2006; Cahill and Cunningham, 2000; Venkatraman et al., 2004a). Aside from this, intramitochondrial proteins can be irreversibly oxidized by ROS as well as reactive lipid species such as 4-HNE generated in response to alcohol intake. This contributes to the dysregulation of fatty acid metabolism and increased activation of the mitochondrial permeability transition pore (Baraona et al., 2002; King et al., 2010; Lee et al., 2003; Pastorino et al., 1999). Some studies have also reported that alcohol can trigger mitochondrial protein hyperacetylation, an important regulatory post-translational mechanism of protein function that relies on acetyl-CoA as the acetyl group donor and that is controlled by deacetylation enzymes, mainly sirtuins (Fritz et al., 2011; Picklo, 2008). The inactivation of proteins critical for mitochondrial function may contribute to alcohol-induced liver injury.

- Changes in mitochondrial membrane composition and fluidity: Alcohol intake can modify lipid composition of mitochondrial membranes as many studies have reported changes in phospholipid distribution, cardiolipin levels and increased cholesterol accumulation (Cunningham et al., 1983; Ellingson et al., 1988; Marí et al., 2014; Taraschi and Rubin, 1985). These alterations result in increased mitochondrial membrane rigidity and impact on the proper functioning of mitochondrial membrane proteins (Colell et al., 2001, 1997).

- Excessive mitochondrial ROS production: Disproportionate alcohol oxidation via ADH and ALDH produces abundant levels of NADH that enter the mitochondrial respiratory chain for oxidation and result in increased mitochondrial ROS production (Bailey and Cunningham, 2002; Wu and Cederbaum, 2009). Besides this mechanism, the inducible CYP2E1 also contributes to mitochondrial superoxide anion generation in response to alcohol. Although it is mainly targeted to the ER by a signal recognition mechanism, alcohol feeding has been shown to induce the expression of CYP2E1 also in liver mitochondria (Knockaert et al., 2011; Robin et al., 2005). The main mitochondrial free radical is superoxide anion, which can then be the source of additional ROS and oxidants, including peroxynitrite and hydrogen peroxide.

- Altered mitochondrial antioxidant system: From all the antioxidant mechanisms present in mitochondria (see chapter 2.3.2.), mGSH has been shown to be depleted by alcohol feeding in a wide variety of animal models (Colell et al., 1997; García-Ruiz et al., 1994; García-Ruiz et al., 1995; Hirano et al., 1992). This decrease in mGSH is caused by the defect in the transport of GSH from the cytosol to the mitochondrial matrix, which in turn is caused by alcohol-mediated mCholesterol accumulation (Coll et al., 2003; Fernández et al., 2013). The impact of mCholesterol loading in the depletion of mGSH is not an exclusive feature of alcohol intake but it has also been reported in other contexts such as nonalcoholic steatohepatitis and anthrax-induced cell death (Ha et al., 2012; Josekutty et al., 2013).

- Altered mitochondrial respiration: Alcohol consumption has been reported to alter mitochondrial oxidative phosphorylation although this impairment seems to be species-dependent. While alcohol decreases mitochondrial respiration in rats by downregulating the synthesis of subunits of the main respiratory complexes such as NADH dehydrogenase, cytochrome b-c1 (Complex III) and the ATP synthase complex (Complex V) (Bernstein and Penniall, 1978; Cunningham et al., 1990; Venkatraman et al., 2004a), it has been reported to stimulate mitochondrial respiration in mice (Han et al., 2012; Venkatraman et al., 2004b; Zhang et al., 2010). Considering these findings, the mechanisms that determine the species

dependent alteration of mitochondrial respiration caused by alcohol intake are not fully understood yet.

- Alteration in mitochondrial morphology and dynamics: The role of mitochondrial dynamics in alcohol-induced mitochondrial function and liver injury has been poorly studied. Some studies have shown that hepatic mitochondria from alcohol fed individuals exhibit a heterogeneous morphological appearance manifested predominantly in the formation of longer tubular and thinner mitochondria compared with round or oval morphology of mitochondria from healthy counterparts (Bruguera et al., 1977; Das et al., 2012; Han et al., 2012; Matsuhashi et al., 1998). However, whether these changes reflect alterations in mitochondrial fusion or fission remains to be better established.

- Activation of mitochondria-dependent apoptosis: Accumulated ROS due to alcohol metabolism also plays an important role in mitochondria-dependent apoptosis. One of the pathways involved is the inhibition of the phosphorylation of alpha serine/threonine-protein kinase (AKT), which causes the down-regulation of cyclin D1 and cell cycle arrest in G0/G1. This in turn activates mitochondria-dependent apoptosis overall leading to mitochondrial damage (Abdelmegeed et al., 2013; Kong et al., 2019).

In view of the critical status of mitochondria during alcohol consumption and the importance of these organelles in many cellular functions, further characterization of key players contributing to alcohol-induced mitochondrial dysfunction are relevant to better understand ALD pathogenesis. This knowledge will certainly advance the design and testing of novel mitochondria-specific therapeutics that will hopefully help in the development of more effective and earlier diagnostic test strategies and in disease treatment.

4.5.1. Alcohol and mCholesterol

As exposed in chapter 2.4.3, mCholesterol accumulation is a hallmark of different pathologies such as Alzheimer's disease, NPC disease, hepatic diseases and obesity. In relation to ALD, it has been reported that alcohol feeding induces mCholesterol accumulation, which causes mitochondrial membrane rigidity and impairs transport of GSH from cytosol to the mitochondria. Decreased levels of mGSH cannot protect from ethanol-induced mitochondrial oxidative stress overall causing mitochondrial damage. In addition to this, mGSH depletion via mCholesterol accumulation is one of the factors that sensitize hepatocytes to the damage caused by inflammatory cytokines involved in ALD such as TNFα (Coll et al., 2003; Fernández-Checa et al., 1997; Fernández-Checa and Kaplowitz, 2005; Lluis et al., 2003). Regarding to liver zonation and as

previously described, ALD is known to progress from PV to PP hepatic areas. Indeed, the depletion of mGSH caused by chronic alcohol feeding has been observed to preferentially occur in PV hepatocytes (García-Ruiz et al., 1994; García-Ruiz et al., 1995). The fact that mGSH is mostly decreased in hepatic zone III suggests a higher mCholesterol accumulation in this zone. However, the distribution of alcohol-induced mCholesterol accumulation along the hepatic acinus as well as its zonal deleterious effects have never been determined.

All these findings suggest cholesterol accumulation in mitochondria as a key mechanism in ALD onset and progression. Modulation of mCholesterol levels could thus influence ALD progression, and therapies to decrease mCholesterol levels could be of medical relevance in the disease treatment. Although the knowledge of alcohol-induced mCholesterol accumulation consequences has increased substantially in recent years, further characterization of this mechanism as well as its regulatory system is needed to better understand ALD pathogenesis. Among the different mCholesterol transporters, StARD1 emerges as a leading regulator since it has already been related to ALD but never been fully characterized (Fernández et al., 2013; Marí et al., 2014).

5. NIEMANN-PICK TYPE C DISEASE

Niemann Pick's (NP) disease was described for the first time in the early 20th century by the German physicians Albert Niemann and Ludwick Pick. It is an inherited autosomal recessive disease that results in neurodegeneration, liver disease and premature death. There are four recognized forms of Niemann-Pick disease: types A and B (NPA and NPB), type C (NPC) and type D (NPD). The underlying defect in types A and B involves mutations in the SMPD1 gene and deficiency of the enzyme acid sphingomyelinase (ASM). If ASM is missing or does not act correctly, the lipid sphingomyelin cannot be properly metabolized and is accumulated within the cell, ultimately causing cell death and significant organ system failure. Type A is rare and occurs mainly in infants, who show severe and progressive brain disease. Children with NPA do not live beyond their first few years. In contrast, type B patients are neurologically normal and they usually have longer life expectancy. NP type C is caused by mutations in the NPC1 (NPC type 1C) or the NPC2 genes (NPC type 2C). Deficiency in NPC1 and NPC2 function results in the accumulation of cholesterol, gangliosides and other lipids in cells, specifically in endosomal vesicles. NPC patients present marked neurological impairment that begins in the thalamus and Purkinje cells in the cerebellum, causing cerebellar ataxia, cataplexy, epilepsy and other neurological disorders. Type D is very similar to type C in its manifestations, being considered a variant of it (Bajwa and Azhar, 2020; Torres et al., 2017a).

5.1. CLINICAL CHARACTERISTICS OF NPC DISEASE

NPC is referred to as a lipid storage disease since it is characterized by the body's inability to transport cholesterol and other lipids inside of cells resulting in the accumulation of these substances within various tissues. Because of the damaging accumulation of lipids throughout the body, especially in the liver, spleen and brain, NPC individuals present physical, neurological, emotional and cognitive alterations. The prevalence of NPC disease has been estimated at 1:150,000 in Western Europe with variations between ethnic groups (Geberhiwot et al., 2018).

5.1.1. Symptoms

NPC disease affects neurologic and psychiatric functions, as well as various internal organs. It is a highly variable disorder as individuals with the disease can have onset of symptoms at different ages and follow independent progression. While visceral symptoms are more typically seen in individuals presenting at a younger age, neurologic and psychiatric symptoms often occur slowly over time in individuals presenting in the later age groups (**Figure I-24**) (Patterson, 1993; Seker Yilmaz et al., 2020; Vanier, 2010).

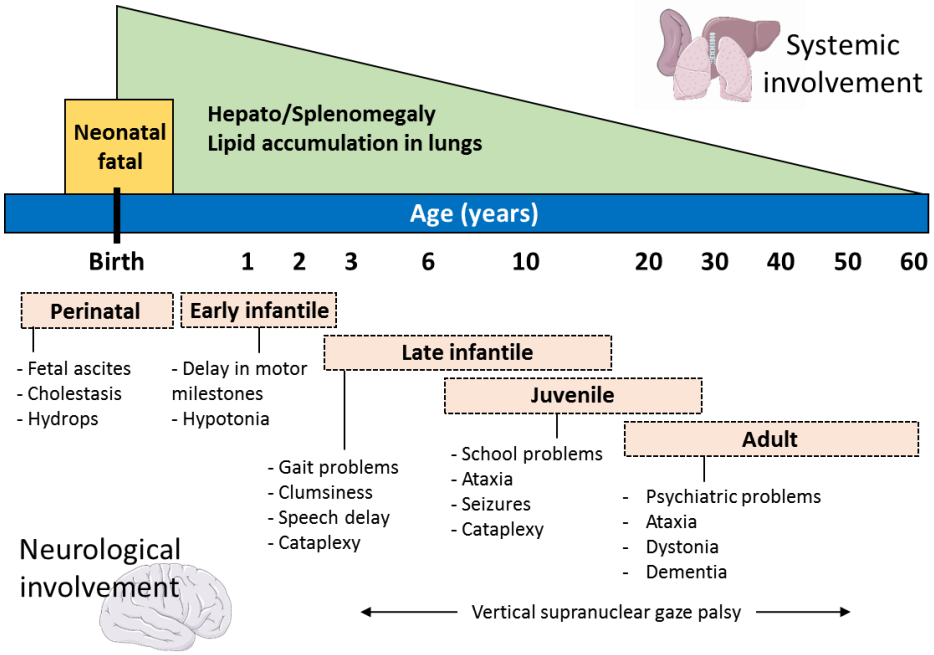

Figure I-24. Schematic representation of the main forms and clinical symptoms of NPC disease.
Adapted from (Vanier, 2010).

Perinatal NPC (shortly before and after birth) is characterized by fetal ascites, cholestasis associated with jaundice and growth deficiency, hepatomegaly, splenomegaly and accumulation of lipids in lungs. All these symptoms can progress to cause life-threatening complications during

this period. In the early infantile period (2 months to < 2 years), affected individuals may present with abnormal liver and spleen enlargement and, in some cases, may develop lack of muscle tone and delays in psychomotor development. The classic presentation of NPC occurs during middle to late childhood (late infantile, 2 to 15 years). It is characterized by difficulty in drawing, writing, speaking and swallowing, lack of muscle coordination and cognitive impairment. Other neurologic findings can include epileptic seizures and vertical supranuclear gaze palsy, the inability to look in a vertical direction as a result of cerebral impairment. Juvenile and adult onset of NPC (6-25 years and >15 years, respectively) are associated with a similar neurological presentation although the rate of progression is often much slower. Following a long-term gradual neurological decline, death often results from respiratory failure.

5.1.2. Treatment

Treatment options for NPC disease are quite limited. Most of the drugs used are aimed at controlling some of its symptoms such as seizures, abnormal posturing of limbs and tremors. Physical, speech and occupational therapy are also used to help with daily functioning. In combination with such treatments, other medications designed to reduce the synthesis of precursor metabolites or products that are known to accumulate in this disease are used (Aerts et al., 2006; Rosenbaum and Maxfield, 2011).

Butyldeoxynojirimycin, also known as miglustat, is an inhibitor of glycosphingolipid biosynthesis licensed as a NPC modifying medicine in the European Union (Geberhiwot et al., 2018; Pineda et al., 2019). It was reported that its daily administration in $NPC^{-/-}$ mice reduces glycosphingolipid accumulation, delays the clinical signs of the disease and markedly prolongs survival (Stein et al., 2012). It also stabilizes and ameliorates the course of human NPC disease (Patterson et al., 2015). However, while miglustat is significantly successful in delaying NPC disease progression, it does not mobilize the accumulation of intracellular cholesterol associated with this disorder. Another drug that has been tried is 2-hydroxypropyl-β-cyclodextrin (HPβCD), a cholesterol binding agent. HPβCD administration in $NPC^{-/-}$ mice delays clinical onset, increases lifespan, and decreases deposition of cholesterol and glycolipids in the central nervous system and other organs (Davidson et al., 2009; Liu et al., 2008; Matsuo et al., 2013). A wide range of other cholesterol-lowering agents including nicotinic acid, lovastatin, cholestyramine and their combinations has also been tested but has not reported improved neurological outcomes (Patterson et al., 1993). Low cholesterol diets are also often used but there is no evidence of their efficacy. Other treatments such as antioxidants like NAC, vitamin E or vitamin C have had little effect in modifying NPC pathology (Fu et al., 2013; Marín et al., 2014). Enzyme replacement to correct secondary enzyme

defects (Devlin et al., 2010) and future genetic interventions may hopefully represent promising therapies for NPC in the near future (Santos-Lozano et al., 2015).

5.2. NPC EXPERIMENTAL MODELS

NPC is an extremely complex disease in both clinical and physiological aspects. To date no single experimental model is capable of reproducing the complete pathology of the disease. It is thus essential to know all the available NPC disease models in order to properly choose the most appropriate one for the study's objectives.

NPC disease is caused predominantly by mutations in NPC1 (95% of cases) or NPC2 genes. Both genes are highly conserved among eukaryotes, which allows the generation of NPC models ranging from mammals to fungi, including mouse, zebrafish, fruit fly and yeast among others (Fog and Kirkegaard, 2019; Lopez and Scott, 2013). Mice are the most used model in the field, specifically the Npc1-null mice model known as *Npc1*^{nih} (or *Npc1*^{m1n}), which arose as a result of insertional mutagenesis in the BALB/c strain resulting in a Npc1 null allele (Loftus et al., 1997; Pentchev et al., 1980). These mice present accumulation of free cholesterol and glycosphingolipids and recapitulate the clinical phenotype of human NPC disease with loss of motor coordination, cognitive problems in learning and recall assays as well as profound inflammation in liver and brain among other aspects (Bhuvaneswaran et al., 1982; Morris et al., 1982; Shio et al., 1982). However, although the Npc1-null mouse resembles the human disease progression, it is not the most translational model since very few NPC patients are homozygous for truncating mutations but present point mutations in NPC1 or NPC2 genes leading to misfolded NPC proteins. Consequently, other murine models with NPC1 point mutations have been generated and used in many studies. Among them, the *Npc1*$^{pf/pf}$ mouse model is characterized by producing a non-functional NPC protein due to a mutation in the cholesterol binding cavity (Xie et al., 2011). Another model is the *Npc*^{1I1061T} mouse model, which harbors the I1061T missense substitution that leads to a misfolded NPC1 protein that is prematurely degraded (Praggastis et al., 2015). While the clinical features of the *Npc1*$^{pf/pf}$ mouse model are similar to *Npc1*^{nih} mice, the disease in *Npc1*^{I1061T} mice is less severe. Additionally, apart from genetically modified models, antisense oligonucleotide knockdown methods have been used *in vivo* to downregulate Npc1 expression in livers of wild type mice. Such approaches result in hepatomegaly, lipid accumulation, cell death and liver damage (Rimkunas et al., 2008).

In addition to the whole-organism models of NPC, other tools such as neuronal cells differentiated from stem cells and patient-derived cell lines are used to study NPC molecular mechanisms and

effects of potential therapies. The most common used cell lines are fibroblasts derived from human skin biopsies which facilitate the investigation of fundamental aspects of human NPC disease (Platt, 2018; Torres et al., 2017a).

5.3. MOLECULAR MECHANISMS OF NPC DISEASE

NPC disease is a multi-faceted pathology as it progresses via multiple pathways to affect numerous intracellular events that ultimately result in cell death. The involvement of many different events explains the difficulty of finding a unique and specific treatment for the disease and challenges NPC research to deeply characterize all the molecular mechanisms involved (Wheeler and Sillence, 2020).

5.3.1. Altered cellular lipid content

NPC1 is an integral membrane protein of 1278 amino acids with three luminal and thirteen transmembrane domains, as well as a lysosomal signal region. As stated in the section 1.4, NPC1 plays an important role in cholesterol trafficking, in particular in late endosome exit and distribution to other organelles (Infante et al., 2008). In contrast, NPC2 is a soluble protein made up of 151 amino acids and four highly conserved domains responsible for cholesterol-binding and release. It resides in the lysosomal lumen and transfers cholesterol to NPC1 (Kwon et al., 2009). Mutations in NPC1 or NPC2 genes give rise to non-functional proteins overall leading to the lysosomal accumulation of cholesterol specifically in tissues such as the liver, spleen and brain (**Figure I-25**) (Kobayashi et al., 1999; Sokol et al., 1988).

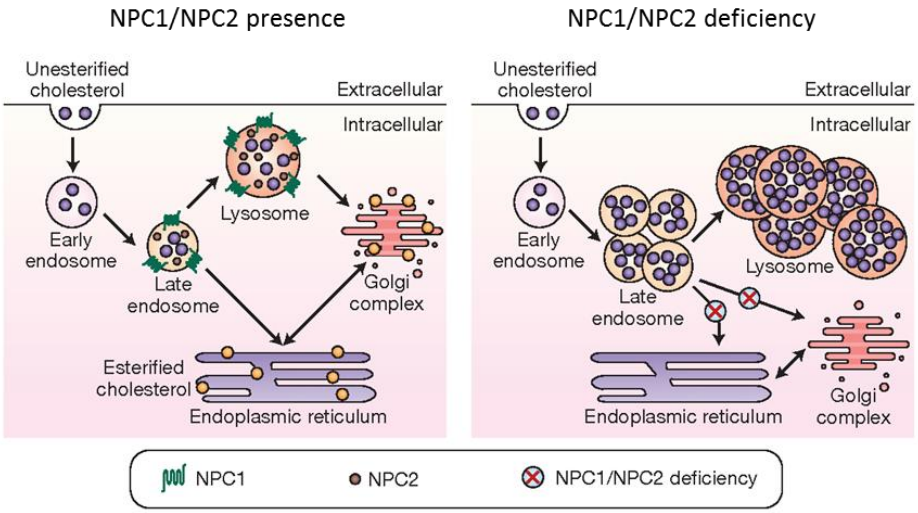

Figure I-25. Lipid-trafficking defects in NPC disease. Adapted from (Pacheco and Lieberman, 2008).

The truncated efflux of cholesterol out of lysosomes generates two main problems for the cell: there is an excessive amount of cholesterol-rich vesicles in the cytosol, and there is a relative deficiency of cholesterol in the organelles to which these compounds where originally destined, e.g. ER and Golgi (Du et al., 2011; Frolov et al., 2003; Garver and Heidenreich, 2002). Besides, the defect in lysosomal export tricks the cell into thinking that a cholesterol deficiency is currently present and that more cholesterol is needed. This results in increased *de novo* cholesterol synthesis and, consequently, elevated cellular cholesterol content (Liscum et al., 1989).

Apart from cholesterol, other kinds of lipids also accumulate in NPC disease and have been associated to a variety of NPC-related pathologies. The most well-known are sphingomyelin and glycosphingolipids (GSLs), including complex gangliosides such as GM2 and GM3 (Davidson et al., 2009; Newton et al., 2017). A particular consequence of GSLs accumulation is a defective intracellular calcium signaling, as has been demonstrated in several gangliosidoses (Lloyd-Evans et al., 2010). Defective intracellular calcium is damaging for the cell because calcium plays essential roles in regulating a variety of cellular events such as autophagy and cellular stress.

5.3.2. Impaired autophagy

Autophagy is a conserved and regulated cellular mechanism that mediates the removal of unnecessary or damaged macromolecules and organelles. Firstly, a portion of cytoplasm containing molecules or organelles is enclosed by a phagophore resulting in the formation of an autophagosome. Then, the outer membrane of the autophagosome fuses with a late endosome to form an amphisome, which subsequently will fuse with a lysosome forming an autolysosome where the cargos are finally degraded by lysosomal hydrolases (Dikic and Elazar, 2018).

The formation of autophagosomes is clearly enhanced in NPC disease as reported in different NPC models (Ko et al., 2005; Liao et al., 2007; Pacheco et al., 2007). However, the fusion of autophagosomes with late endosome is incomplete, translating in an accumulation of ubiquitinated proteins and dysfunctional organelles in the cell (Liao et al., 2007; Osellame and Duchen, 2014). The impairment of amphisome formation is mainly attributed to the inability of NPC1-deficient late endosomes to recruit components of the SNARE machinery involved in autophagosome-late endosome fusion (**Figure I-26**) (Sarkar et al., 2013). Overall, unbalance of autophagy induction and flux leads to autophagic stress, a critical cellular situation that precedes cell death (Elrick and Lieberman, 2013).

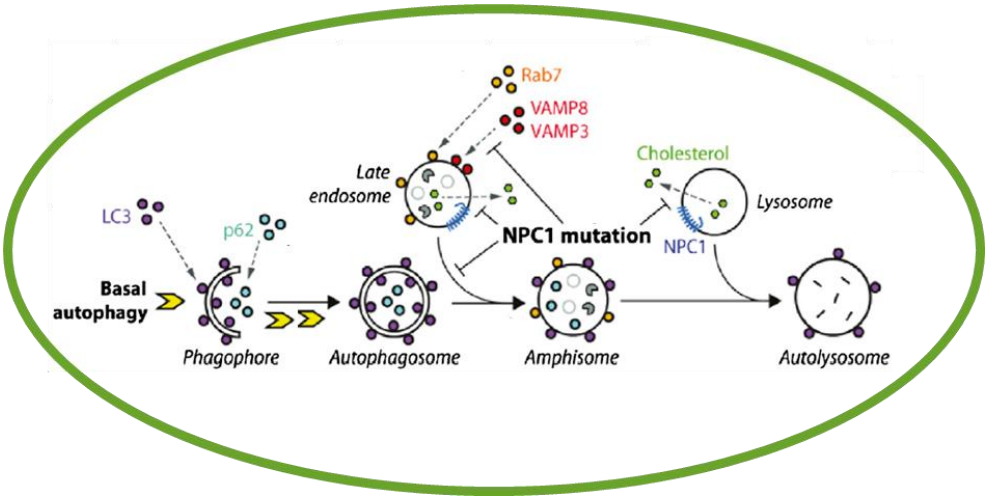

Figure I-26. Schematic representation of defective autophagy in NPC disease. Adapted from (Sarkar et al., 2013).

5.3.3. Unbalanced oxidative stress and antioxidant defense

Oxidative damage has been observed in animal and cellular NPC models as well as in NPC patients (Vázquez et al., 2012). Human NPC fibroblasts show upregulation of genes related to oxidative stress (De Windt et al., 2007; Reddy et al., 2006) in addition to increased concentrations of ROS and lipid peroxidation (Zampieri et al., 2009). Same features have been observed in tissues from NPC mutant mice (Smith et al., 2009; Torres et al., 2017b; Vázquez et al., 2011). Regarding to NPC patients, evaluation of plasma of NPC patients showed increased cholesterol oxidation products among other oxidative stress markers (Fu et al., 2010; Porter et al., 2010).

Decreased antioxidant capacity is a key event associated with increase oxidative stress in NPC disease. Different studies have reported reduced GSH content in various NPC models, with a specific decrease in mitochondria (Marí et al., 2006; Torres et al., 2017b; Vázquez et al., 2011). Depletion of mGSH is critical for NPC disease as its replenishment by GSH ethyl ester (GSHee) restores the mGSH pool, protects from oxidative stress and rescues other parameters such as oxidative phosphorylation in tissues from $Npc1^{-/-}$ mice and Npc1 fibroblasts (Torres et al., 2017b). In contrast, replenishment of cytosolic GSH by NAC fails to restore the mGSH pool and shows little impact in improving NPC pathology (Fu et al., 2013; Torres et al., 2017b).

5.3.4. Mitochondrial dysfunction

Crosstalk between the late endocytic compartment and other organelles such as mitochondria or ER is nowadays one of the most studied topics in neurodegenerative disease research including NPC disease. Regarding mitochondria, it has been observed in NPC models that essential mitochondrial parameters such as ATP synthesis, mitochondrial morphology and the input of GSH

to the mitochondrial matrix are altered, and together result in a reduction in energy production, increased ROS generation and increased energy demand in NPC cells (Torres et al., 2017b; Visentin et al., 2013; Yu et al., 2005).

One cause of mitochondrial damage is the release of lysosomal molecules to the cytosol due to lysosomal membrane permeabilization by excessive lipid content (Kosicek et al., 2018). Cathepsins are among these lysosomal released proteins. They act on mitochondria by triggering mitochondrial release of cytochrome c, which activates the intrinsic apoptotic pathway and, consequently, cell death (Amritraj et al., 2013; Cirman et al., 2004).

5.4. REGULATION OF mCHOLESTEROL IN NPC DISEASE

Mitochondrial dysfunction in NPC disease is also caused by the accumulation of cholesterol in the organelle. Interestingly, many studies have reported increased mCholesterol content in neurons and hepatocytes from $Npc1^{-/-}$ mice, event that may contribute to the reported increased mitochondrial membrane rigidity and decreased mGSH import (Charman et al., 2010; Fernández et al., 2009b; Marí et al., 2006; Yu et al., 2005). Although mCholesterol accumulation has emerged as a key player in NPC pathogenesis, the underlying mechanisms that lead to excess endolysosomal cholesterol shuttling to mitochondria instead of ER or Golgi are not fully understood.

To the date, MLN64 has emerged as one of the potential key players in the transport of cholesterol from lysosomes to mitochondria in NPC disease. This contribution is based on the observed increased expression of MLN64 in fibroblasts from NPC patients, fact that correlates with elevated mCholesterol content and decreased mitochondrial membrane potential (Balboa et al., 2017). However, targeted mutation of the MLN64 STAR domain results in modest alterations in cellular sterol metabolism (Kishida et al., 2004). Another transporter that could be involved in the regulation of mCholesterol in NPC disease is StARD1. Although this protein is key in the intramitochondrial trafficking of cholesterol, the regulation of StARD1 in NPC disease has not been explored yet. It is thus important to further unravel the sophisticated connection between lysosomes and mitochondria in order to understand the impact of mitochondrial dysfunction in the progression of NPC disease.

OBJECTIVES

Accumulation of cholesterol in mitochondrial membranes is a hallmark of chronic diseases, including cardiovascular disorders, cancer and Alzheimer's disease. In addition, previous studies have shown an association between increased mCholesterol levels and liver injury of different etiology including alcoholic and nonalcoholic liver diseases. mCholesterol increase influences the physical properties of mitochondrial membranes and negatively impacts on the organelle function. Besides, this event initiates a cascade of pathological processes that also result in cell and tissue damage.

The overall goal of the present doctoral thesis is to study the effects of mCholesterol accumulation on hepatic function. We aim to further characterize mCholesterol-related pathological mechanisms underlying two specific liver diseases: alcoholic liver disease and Niemann-Pick Type C disease. These studies will not only provide a better understanding of the molecular mechanisms associated to these two disorders, but they will also uncover cellular vulnerabilities that could be explored for development of potential therapeutics for these pathologies.

In order to address this overall aim, the following studies and their respective objectives are proposed:

STUDY I. CHARACTERIZATION OF THE EFFECTS OF mCHOLESTEROL ACCUMULATION ON THE FUNCTION OF LIVER MITOCHONDRIA

Cholesterol accumulation in mitochondrial membranes impacts on the organelle function as it triggers mitochondrial dysfunction at several levels such as changes in membrane biophysical properties and impaired mGSH import. Although many mechanisms regarding cholesterol-mediated mitochondrial dysfunction have been deciphered in the last years, some aspects still require further clarification. The objectives of this first study are:

- To examine the impact of mCholesterol accumulation on mitochondrial structure and function through *in vivo* and *in vitro* models specifically involving targeted manipulations of mCholesterol import and content.

- To study the impact of mCholesterol accumulation on mitochondrial oxygen consumption rates and the assembly of mitochondrial respiratory supercomplexes.

STUDY II. EXAMINATION OF THE ZONAL-DEPENDENT ALCOHOL-INDUCED LIVER INJURY FOCUSING ON mCHOLESTEROL ACCUMULATION AND ITS REGULATION BY STARD1

Many molecules and signaling pathways have been described on the pathological process of ALD during the past decades. Among them, mCholesterol accumulation has been described to induce mGSH depletion and increase oxidative stress overall resulting in liver damage. Among its regulators, the mCholesterol transporter StARD1 emerges as a potential key player in ALD. Many studies have described the contribution of StARD1 in a wide-range of disorders such as Alzehimer's disease and drug-induced liver injury. However, the role of StARD1 in ALD remains to be understood. The objectives of this study are:

- To analyze the distribution of StARD1 and the mCholesterol induced by alcohol intake along the hepatic acinus (periportal and perivenous zones).

- To study the role of StARD1 and alcohol-induced mCholesterol accumulation on mitochondrial morphology and function in PP and PV hepatocytes.

STUDY III. INVESTIGATION OF THE MOLECULAR MECHANISMS THAT LEAD TO mCHOLESTEROL ACCUMULATION IN NPC DISEASE

In addition to lysosomes, cholesterol accumulation in mitochondria is a hallmark of NPC disease, which causes mitochondrial dysfunction and depletion of antioxidant defenses. However, the mechanism of mCholesterol accumulation in NPC disease remains unknown. StARD1 stands out for its role in intramitochondrial cholesterol trafficking and could be a potential regulator of mCholesterol levels in NPC disease. Thus, the objectives of this third study are:

- To analyze StARD1 levels in different NPC models as a potential mechanism for mCholesterol accumulation.

- To explore novel molecular pathways involved in StARD1 regulation and mCholesterol accumulation in NPC disease.

MATERIALS AND METHODS

1. MOUSE MODELS

All mice were raised under specific pathogen free conditions with controlled temperature and humidity on a 12h light-dark cycle in the animal care facility of the Medical School of Universitat de Barcelona. Animals had free access to water and food with the exception of the Lieber-DeCarli liquid diet model where mice were pair-fed. All studies were performed in male mice to avoid hormonal fluctuations of female estrouscycle.

1.1. WILD TYPE MICE

All wild type (WT) mice (C57BL/6 strain) were purchased from Charles River, USA, with the exception of $NPC^{-/-}$ studies where wild type littermates were used as controls. Prior to their use in a study, purchased mice rested for one week in order to get acquainted to the new environment.

1.2. LIVER-SPECIFIC CONDITIONAL STARD1 KNOCKOUT MICE

As mice with global StARD1 deletion die soon after birth due to adrenal lipoid hyperplasia, we generated mice with liver-specific StARD1 deletion ($StARD1^{\Delta Hep}$) by means of the Cre-lox technology and the knockout-first allele strategy. To this end, a plasmid for targeted conditional deletion of StARD1 gene (Star tm1a(eucomm)Hmgu) was obtained from the Eucomm (International Mouse Phenotyping Consortium, IMPC) and used to transfect 129/C57bl6 embryonic stem cells (ESC). The construct disrupts StARD1 gene by placing a LacZ reporter cassette (LacZ) 5' of a loxP-flanked neomycin-resistance selection cassette (NEO), which lies immediately upstream of StARD1 exon 2. NEO facilitates *in vitro* selection of targeted ESC, while the LacZ cassette can be used in the generation of reporter-tagged animals, i.e., animals expressing LacZ in the tissues that express StARD1. A third loxP site is inserted immediately after StARD1 exon 5. In addition, two FRT (flippase recognition target) sites are inserted in the allele, one upstream of LacZ and one between NEO and the loxP site immediately before exon 2. This allele is referred to as "targeted mutation 1a" (tm1a), and is designated "knockout-first," because the insertion of the LacZ trapping allele is itself expected to disrupt splicing of StARD1. Positive specific targeted ESC clones were then selected, amplified and microinjected in blastocysts. After implantation in pseudopregnant mice, we obtained chimeras that transmitted the targeted gene to their progeny. To then allow simultaneous removal of both the LacZ and NEO cassettes and restoration of StARD1 gene, StARD1tm1a mice were crossed with transgenic C57BL/6J mice expressing FLP1 recombinase that mediated the Frt sites recombination and resulted in two LoxP sites flanking exons 2 to 5 of StARD1 gene (Tm1b construction, floxed StARD1, $StARD1^{f/f}$).

Homozygous StARD1 floxed animals were then crossed with albumin-Cre mice (C57BL/6-TgN[AlbCre]21Mgn; Jackson Laboratories) to obtain StARD1$^{f/f\text{-}AlbCre}$ (construction tm1c, StARD1 Liver-specific knockout, StARD1$^{\Delta Hep}$). With the presence of the albumin promoter, these mice exhibit specific deletion of StARD1 in the liver with unchanged expression in steroidogenic tissues and white adipose tissue (**Figure M-1**).

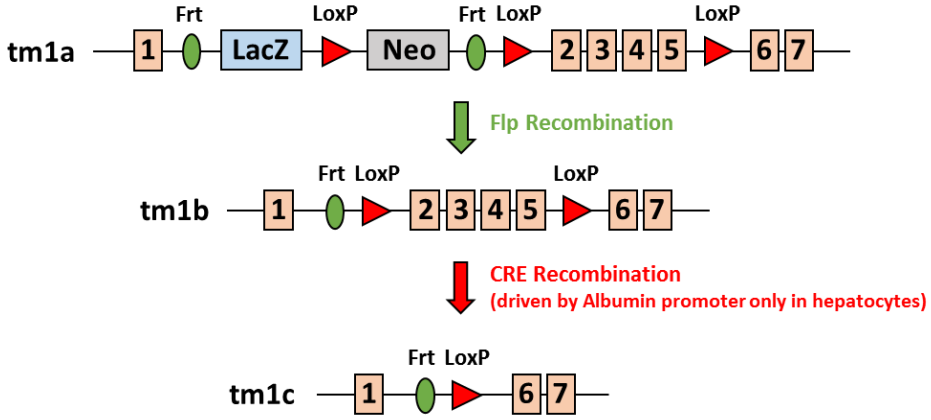

Figure M-1. Schematic of the EUCOMM vector design illustrating the targeting and recombination process for StARD1 gene.

1.2.1. Breeding

Liver-specific conditional StARD1 knockout mice were backcrossed to C57BL/6J strain for 9 generations. 8-weeks-old StARD1$^{f/f}$ littermates and StARD1$^{\Delta Hep}$ mice were fed a Liver DeCarli diet as described as follows.

1.2.2. DNA extraction

StARD1$^{f/f}$ and StARD1$^{\Delta Hep}$ mice were genotyped by polymerase chain reaction (PCR) using ear-clipped DNA. Genomic DNA was extracted from ear clipped tissue at weaning time (21 days) with QuickExtract DNA kit (Epicentre, QE09050).

Protocol:

- Add 50µl of QuickExtract solution to each tube containing the tissue.
- Vortex the mix for 30sec.
- Incubate 6min at 65°C.
- Vortex the mix for 30sec.
- Incubate 2min at 98°C.
- Vortex the mix for 30sec and place the tube on ice.

- Centrifuge the tube at 14000rpms for 2min at 4°C.
- Use 1µl of the extracted DNA (200ng of DNA approximately) for each PCR reaction.
- Store DNA at -20°C.

1.2.3. Genotyping

Genotyping for StARD1 and Cre was performed using the following primers (**Table M-1**):

Primer	Sequence 5' --> 3'	Primer Type
Seq 5 arm 1F N9881	AAGGCCCTAGTTGTTCTGGA	$StARD1^{f/f}$
StKO_frt_Rev	TCCAGCCACATCTCTAACTCTCAAG	$StARD1^{f/f}$
Cre_II_Forward	AAATGGTTTCCCGCAGAAC	$StARD1^{\Delta Hep}$
CRE_II_Reverse	ATTGCTGTCACTTGGTCGTG	$StARD1^{\Delta Hep}$

Table M-1. $StARD1^{f/f}$ and $StARD1^{\Delta Hep}$ genotyping primers.

PCR mix (**Table M-2**):

	[Stock]	[Final]	x1 reaction (µl)
NH_4 buffer	10X	1X	2
$MgCl_2$	50mM	3mM	1.2
dNTP mix	10mM	0.2mM	0.4
Primer mix (fw+rv)	10µM	300nM	0.6
Biotaq (Bioline)	5u/µl	0.1u/µl	0.4
DNA (sample)	~200ng/µl	~200ng	1
H_2O molecular biology grade	-	Up to 20µl	14.4

Table M-2. Genotyping PCR mix.

1.3. NPC1 KNOCKOUT MICE

$Npc1^{-/-}$ mice ($NPC1^{NIH}$, BALB/cJ strain) were obtained from The Jackson Laboratories. The mutant allele consists of 824bp of MaLR retroposon-like DNA that replaced 703bp of wild-type genomic sequence.

1.3.1. Breeding

NPC1 knockout mice were propagated using heterozygous breeding pairs. $Npc1^{-/-}$ phenotype is inherited as an autosomal recessive trait so heterozygous breeding pairs yield 25% WT mice ($NPC^{+/+}$), 25% $NPC1^{-/-}$ mice and 50% of heterozygous mice. WT littermates were used as controls.

1.3.2. DNA extraction

Followed the step 1.2.2.

1.3.3. Genotyping

WT primers were used to amplify a 173-base pair (bp) product that is specific for the WT NPC1 gene. To amplify the mutant gene, the same forward primer as wild type was used and a reverse antisense primer was used to amplify a 475-bp product that was specific for the mutant gene of the NPC1 gene (**Table M-3**):

Primer	Sequence 5' --> 3'	Primer Type
oIMR0927	TGAGCCCAAGCATAACTTCC	Mutant
oIMR0928	CTGTAGCTCATCTGCCATCG	WT
oIMR0929	TCTCACAGCCACAAGCTTCC	WT
oIMR4125	GGTGCTGGACAGCCAAGTA	

Table M-3. $NPC^{+/+}$ and $NPC^{-/-}$ genotyping primers.

For PCR mix we used the same conditions as with liver-specific conditional StARD1 knockout mice (**Table M-2**).

2. *IN VIVO* EXPERIMENTAL MODELS

All procedures involving animals and their care were approved by the Ethics Committee of the University of Barcelona and were conducted in accordance with institutional guidelines in compliance with national and international laws and policies.

2.1. HIGH CHOLESTEROL DIET ADMINISTRATION

8 weeks WT mice were randomly separated in two groups that were fed with a regular chow diet (CTRL) or a high cholesterol diet (HC, 2% cholesterol and 0.5% sodium cholate, custom made Research Diets, Brogaarden Denmark, C18021901) for up to two days. In some cases, mice were fed with a diet enriched in 0.5% sodium cholate (Research Diet) alone.

2.2. LIEBER DECARLI LIQUID DIET ADMINISTRATION

8 weeks WT, $StARD1^{f/f}$ or $StARD1^{\Delta Hep}$ mice were randomly separated in two groups that were fed with a Lieber DeCarli (LDC) liquid diet with maltodextrin (CTRL) or ethanol (EtOH) (Research Diets, Brogaarden, L10016A). The feeding period using LDC diet model started with gradually increased amounts of ethanol during five days to allow animals of EtOH group to ethanol adaptation followed by feeding with either CTRL or 5% EtOH diet for 10 days more.

LDC diet feeding protocol:

- Day 1: feed CTRL LDC liquid diet to all animals.
- Day 2: feed CTRL LDC diet to CTRL group and 1% EtOH LDC diet to EtOH group.
- Day 3: feed CTRL LDC diet to CTRL group and 2% EtOH LDC diet to EtOH group.
- Day 4: feed CTRL LDC diet to CTRL group and 3% EtOH LDC diet to EtOH group.
- Day 5: feed CTRL LDC diet to CTRL group and 4% EtOH LDC diet to EtOH group.
- Day 6-15: feed CTRL LDC diet to CTRL group and 5% EtOH LDC diet to EtOH group.

Diet preparation:

- Control LDC diet (CTRL): to prepare 1 liter of diet mix 778.22ml of tap water, 132.18g of L10016A diet and 89.6g of Maltodextrin. Mix with a blender and keep at 4°C.
- Ethanol-containing LDC diet (EtOH): to prepare 1 liter of diet mix 817.82ml of tap water, 132.18g of L10016A diet and 50ml of absolute ethanol. Mix with a blender and keep at 4°C.

Diets were prepared fresh daily and were administered in feeding tubes. CTRL and EtOH diets were pair fed taking into account that each animal eats approximately 20ml of liquid diet per day. Control and treated mice body weight was measured weekly and survival was registered.

2.3. GSH ETHYL ESTER ADMINISTRATION

8 weeks WT mice submitted to CTRL or HC diet were treated with GSH ethyl ester (GSHee) (Sigma, St. Louis, MO) intraperitoneally at 1.25mmol/kg every 12 hours for a total of 2 days.

3. SERUM ANALYSIS

At the time of sacrifice, mice were anesthetized with a lethal dose of 100mg/kg of sodium pentobarbital intraperitoneally. Blood was harvested from the mouse tail or the lower cava vein depending on the experiment and centrifuged for 15min at 10000rpm at 4°C. Serum was subsequently collected from the top phase avoiding bottom phase contamination and diluted four times with saline.

Serum cholesterol, bile acids and aminotransferases (alanine aminotransferase (ALT) and aspartate aminotransferase (AST)) were analyzed by the Clinical Core Laboratories at the *Hospital Clinic i Provincial de Barcelona* on an ADVIA 2400 Chemistry System (Siemens Medical Solutions,

Erlangen, Germany) using commercial available kits, ADVIA Chemistry System 1650 (Bayer-Siemens) and CHOD-PAP (Roche Diagnostics).

4. HEPATIC LIPID ANALYSIS

Triglycerides, free fatty acids and total cholesterol content in liver were measured with a biochemical analyzer by the Clinical Core Laboratories at the *Hospital Clinic i Provincial de Barcelona*. Data was normalized by protein content, determined by Bradford protein assay.

5. HISTOLOGY

5.1. TISSUE HARVESTING AND PRESERVATION

5.1.1. Frozen tissue

Tissues were quickly harvested after blood collection, flash frozen in liquid nitrogen and stored at -80°C. Flash frozen tissues were cut in a cryostat (Leica, CM-1950) at 8-12µm at an approximate temperature of -20°C. Sections were placed in superfrost slides (Menzel-Gläser, J18000AMNZ).

5.1.2. Formalin-fixed paraffin-embedded tissue

Tissues were quickly harvested after blood collection, placed in histology cassettes, fixed in 10% formalin (Sigma, HT501128) for 48h and embedded in paraffin. Inclusion in paraffin was performed in an automated paraffin inclusor (Citadel 1000, Shandon) following this protocol:

- 1h in H_2O two times.
- 1h in 70% ethanol two times.
- 1h in 90% ethanol two times.
- 1h in 100% ethanol two times.
- 1h in xylol two times
- 2h in paraffin two times.

Once tissues were embedded in paraffin, paraffin blocks were made to improve the cutting process in the microtome (Leica, RM2155). Sections at 7µm were used for hematoxylin and eosin staining and cuts at 5µm were used for immunohistochemistry. Sections were placed in histogrip-treated slides (VWR, 631-1553).

5.2. TISSUE STAININGS

5.2.1. Hematoxylin and eosin staining

Hematoxylin and eosin (H&E) staining is the most widely used stain in histology. It has the ability to demonstrate a wide range of normal and abnormal cell and tissue components and it is a relatively simple stain to carry out on paraffin or frozen sections. Hematoxylin has a basic pH and it has affinity for acid structures such as the nuclei, which are referred as basophilic structures. Eosin acts as an acid dye staining basic structures, which are referred as acidophilic structures (e.g. cytoplasm). H&E staining was performed in 7µm formalin-fixed paraffin-embedded tissue liver sections.

Protocol:

- Melt the paraffin in a stove at 100°C.
- Wash out the paraffin 10min in xylol.
- Sample hydration: rehydrate the sample with dilution series of ethanol (100% - 90% - 70% - 30%) till distilled water (dH_2O). Hydrated sections will allow aqueous reagents to penetrate into the tissue.
- Hematoxylin staining: 4min in Hematoxylin Solution, Harris Modified (Sigma, HHS32). Nuclei and acidic structures will appear reddish-purple stained.
- Wash out the extra hematoxylin with abundant running tap water.
- Differentiation: removes hematoxylin background staining and improves contrast. Rinse in alcoholic-HCl 96% (480ml absolute alcohol + 20ml HCl 12N) until a reddish stain appears.
- Rinse in ammoniacal water (dH_2O with 3-4 drops of 25% ammoniac solution) until the staining turns blue again.
- Wash with running tap water for 2min.
- Rinse with dH_2O for 2min.
- Eosin staining: rinse the sections in alcoholic eosin (Sigma, HT110132) for 1.5min. This step will stain many non-nuclear elements in different shades of pink.
- Sample dehydration: rinse samples through alcohol to remove all traces of water (70% - 90% - 100% alcohol). Eosin staining washes out with water so the more we maintain the samples in 70% ethanol the less eosin staining will remain. Rinse in xylol for 5min after that.
- Mount sections: use the DPX mounting media for histology (Fluka, 44581). Add a small drop of DPX to the specimen. Carefully place a cover slip onto the drop, avoiding air bubbles.
- Remove any excess of mounting media with a paper towel.

- Samples can be observed with transmitted light microscopy (equipment used: Olympus BX41 Microscope equipped with a Zeiss Axiocam 305 color digital camera).

5.2.2. Oil Red staining

Oil Red O is a fat-soluble dye used for staining of neutral triglycerides and lipids on frozen sections. This staining must not be performed in paraffin-embedded tissue since paraffin embedding or alcohol based fixation removes most neutral lipids.

Solutions:

- Oil Red Stock Solution: 0.5g Oil Red O (Sigma, O0625) in 100ml of isopropanol. Stir the solution overnight in a capped container to avoid isopropanol evaporation.
- Oil Red Working Solution: 60ml of stock solution with 40ml of dH_2O. Stir and let it sit for several days so oil red is completely dissolved. Always paper filter before using it.

Protocol:

- Let 8µm frozen sections to cool down at room temperature (RT) for 10min.
- Rinse in dH_2O for 5 min, three times.
- Dip in 60% isopropanol 10sec.
- Rinse in Oil Red working solution 30min.
- Remove Oil Red excess by rinsing in 60% isopropanol 5 min, two times.
- Wash with dH_2O for 5 min, 4 times.
- Counterstain with hematoxylin 5 min.
- Wash with dH_2O for 5 min, 3 times.
- Mount sections: use an aqueous mounting media (Aquatex, Merck, 108562). Carefully place a cover slip on the mounting media, avoiding air bubbles.
- Allow samples to dry.
- Samples can be observed with transmitted light microscopy (equipment used: Olympus BX41 Microscope equipped with a Zeiss Axiocam 305 color digital camera).

5.3. IMMUNOHISTOCHEMISTRY

Immunohistochemistry (IHC) refers to the process of detecting antigens (e.g. proteins) in tissue sections by exploiting the principle of antibodies binding specifically to antigens in biological tissues. This method encompasses a broad range of chemical reactions used to produce a microscopically visible signal where the antigen-antibody interaction is produced, usually by

generating a stain or sometimes emitting photons. In the studies carried out in this thesis we used this method to detect StARD1 in 5µm formalin-fixed paraffin-embedded tissue liver sections.

Protocol:

- Melt the paraffin in a stove at 100°C.
- Wash out the paraffin 10min in xylol.
- Sample hydration: rehydrate tissue sections with dilution series of ethanol (100% - 90% - 70% - 30%) till dH_2O. Hydrated sections will allow aqueous reagents to penetrate into the tissue.
- Antigen unmasking: this treatment undoes the bounds made by the action of formalin during the fixation revealing antigens for optimum immunostaining.
    - Put the slides in a container compatible with the microwave.
    - Cover the slides with citrate buffer (2% sodium citrate, pH 6.0).
    - Heat 9min in the microwave at 800W until it boils and then count 4min.
    - Let it cool down for 20min.
- Wash the sections with PBS 3 times for 3min.
- Endogenous peroxidase blocking: endogenous peroxidase activity is any activity that results in the degradation of H_2O_2. Such activity is a property of catalases in the liver. Since this protocol has a horseradish peroxidase (HRP)-based detection method it is necessary to block the endogenous peroxidase activity to reduce background staining.
    - Apply peroxidase-blocking solution on top of the liver sections for 10min.
    - Wash with PBS 3 times for 5min.
- Block with only antibody diluent for 20min (abcam, ab64211).
- Block with Avidin/Biotin blocking kit (10min for each) (Vector, SP2001).
- Primary antibody incubation: dilute StARD1 primary antibody (Santa Cruz, sc23524) in antibody diluent and incubate overnight at 4°C in a humidity chamber.
- Wash with PBS, 3 times for 3min.
- Incubate with a biotinylated secondary antibody for 45min in a wet chamber.
- Wash with PBS, 3 times for 3min.
- Incubate for 30min at RT with Avidin-Biotin complex (ABC) (Vector Laboratories, Vectastain kit PK6100D) reconstituted 30min before use.
- Wash with PBS, 3 times for 3min.
- Develop with DAB (diluted 1/10 with peroxidase buffer). Colour brown. Time is variable.
- Rinse with tap water.
- Counterstain with hematoxylin (Dako, S2020).

- Rinse with tap water.
- Mounting: Use an aqueous mounting media (Aquatex, Merck, 108562) to mount the coverslips. Let dry for a few hours protected from the light.
- Samples can be observed with transmitted light microscopy (equipment used: Olympus BX41 Microscope equipped with a Zeiss Axiocam 305 color digital camera).

5.4. IMMUNOHISTOFLUORESCENCE

Immunohistofluorescence (IHF) is a specialized type of IHC that uses fluorescent dyes to visualize antibody-antigen binding under a fluorescent microscope. Direct IF uses a single antibody directed against the target of interest that is directly conjugated to a fluorophore. Indirect ICF uses two antibodies: the primary antibody is unconjugated and the secondary antibody is fluorophore-conjugated and directed against the primary antibody.

Protocol:

- Let 12µm frozen sections to cool down at RT for 10min.
- Wash the sections with PBS 2 times for 5min.
- Fix sections in 10% formalin for 1h at RT.
- Wash with PBS 3 times for 5min.
- Block with antibody diluyent (Abcam, ab64211) and 10% Normal Goat Serum ready-to-use (Life technologies, #5000627) at RT for 20 and 10 minutes, respectively.
- Wash with PBS.
- Primary antibody incubation: dilute primary antibody in antibody diluyent (Abcam, ab64211) and incubate overnight at 4°C.
- Wash with PBS.
- Secondary antibody incubation: incubate sections with the appropriate fluorochrome-conjugated secondary antibody for 45 minutes at RT.
- (Optional in case of cholesterol detection) Stain sections with 0.2mg/ml Filipin in PBS for 3 hours at RT.
- Wash with PBS.
- Mounting: use fluorescent mounting medium (Dako, #S3023) or ProLong™ Diamond Antifade Mountant with DAPI (Invitrogen, P36962) to mount the coverslips.
- Samples can be observed with a fluorescence microscope (equipment used: Leica TCS-SPE DM2500).

6. ELECTRON MICROSCOPY

Electron microscopy (EM) is a technique for obtaining high resolution images of biological and non-biological specimens. It is mainly used to investigate the detailed structure of tissues, cells, organelles and macromolecular complexes. The high resolution of EM images results from the use of electrons instead of photons (light) as the source of illuminating radiation.

In the present thesis we have carried out transmission electron microscopy (TEM) in order to perform liver ultrastructure examinations. We have used a transmission electron microscope JEOL JEM-1010 fitted with a Gatan Orius SC1000 (model 832) digital camera from the Electron microscopy unit at the *Facultat de Medicina, Universitat de Barcelona*.

Buffers (**Table M-4**):

HANKS 10X	
Compound	Concentration
NaCl	1.4M
KCl	53.6mM
$MgSO_4 \cdot 7H_2O$	8.1mM
$Na_2HPO_4 \cdot 2H_2O$	6.7mM
KH_2HPO_4	8.8mM
mQ-H_2O	-

HANKS 1X (freshly prepared)	
Compound	Concentration
HANKS 10X	10%
Hepes	12.6mM
$NaHCO_3$	25mM
mQ-H_2O	-

Table M-4. Buffers HANKS10X and HANKS1X used for electron microscopy protocol.

Saturate HANKS 1X buffer with 95% CO_2 and 5% O_2 for 20min to stabilize the pH, and then add the rest of the compounds to HANKS1X to complete HANKS I (**Table M-5**):

HANKS I (cleaning buffer)	
Compound	Concentration
BSA	0.5%
EGTA	0.9mM

Table M-5. Buffer HANKS I used for electron microscopy protocol.

Fixative: 3% glutaraldehyde solution in phosphate buffer.

Protocol:

- Allow HANKS I buffer to reach 37°C in a water bath.
- Aliquot around 30ml of 3% glutaraldehyde solution per mouse and leave it at RT (keep the rest of solution on ice).
- Clean the peristaltic pump tubes with 70% EtOH, dH_2O and then fill the circuit with warm HANKS I buffer at a speed of 6-8ml/min.

- Anesthetize the mouse with a dose of 100mg/kg of sodium pentobarbital intraperitoneally.
- Prepare one surgical suture about 12cm long (Lab. Aragó S.A., Seda trenada 2/0).
- Open the mouse with a laparotomy.
- Place one suture under the portal vein.
- Insert the catheter (BD, 381212) into the portal vein and immobilize it with the suture around it. If the catheter does not fill with blood, fill it with warm HANKS I buffer avoiding bubble formation.
- Stop the peristaltic pump (Cole-Parmer, MasterFlex L/S, #7553-79) and connect it to the catheter. Avoid bubble formation.
- Start the pump and cut the inferior cava vein so the blood can exit the system.
- Clean the liver with HANKS I buffer. This will prepare the liver for fixation. Make pressure above the cut part of the inferior cava vein with the tweezers during 10sec to allow the buffer penetrate in the liver.
- Once the liver is clean, change to 3% glutaraldehyde at RT.
- Perfuse the liver with the fixative until the liver turns pale and becomes stiff (it can take around 5min).
- After fixation, carefully remove the liver and place it in a petri dish with cold 3% glutaraldehyde covering it.
- Cut 3-4 cubes of 1-2mm^3 with a blade. Determine which lobe will be used for this analysis and always cut cubes from the same lobe (cubes are usually obtained from the big lobe).
- Place cubes in a 2ml tube containing 1.5ml of cold 3% glutaraldehyde (1.5ml).
- Keep cubes at 4°C and bring them to the TEM unit in order to be processed as follows:
    - Liver tissue fragments are post-fixed in 1% osmium tetroxide, dehydrated, and embedded in epoxy resin. Semithin sections are then cut and stained with methylene blue for light microscopy. After determining the hepatic zone of interest under an optical microscope, the selected sections are piramidized to perform ultrathin sections that are stained with 2% uranyl acetate for 10min and with a lead-staining solution for 5min. Ultrathin sections are then placed into a 100 mesh grid and observed using the transmission electron microscope JEOL JEM-1010 fitted with a Gatan Orius SC1000 (model 832) digital camera (**Figure M-2**). Images from stained ultrathin sections are acquired by moving at random across the EM grid (two grids per animal) and then analyzed using the iTEM analysis program (Soft Imaging System, Muenster, Germany).

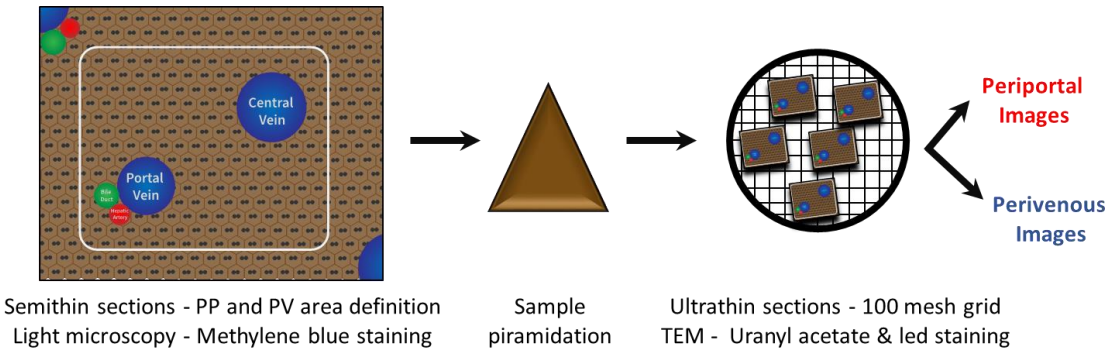

Figure M-2. TEM strategy to locate PP and PV areas in a same section for TEM visualization.

ImageJ software has been used to quantify mitochondrial size and number. Analyses of hepatocytes lipid droplet and glycogen content have been performed with the trainable Weka Segmentation plug-in from ImageJ in collaboration with the advanced optical microscopy unit at the *Facultat de Medicina, Universitat de Barcelona*.

7. IMMUNOCYTOFLUORESCENCE AND LASER CONFOCAL IMAGING

Immunocytofluorescence (ICF) is a method used to detect a target (e.g. protein) in cells using an antibody and subsequent visualization using a fluorophore. The fluorophore is then detected by fluorescence microscopy, always involving excitation of fluorescence with a defined wavelength band of light and detection of the longer-wave emission from the fluorophore.

Confocal microscopy is an optical imaging technique that can be used in ICF since it increases optical resolution and contrast of a sample by using point illumination and a spatial pinhole eliminating the out-of-focus light in specimens that are thicker than the focal plane.

Protocol:

- Seed cells in 6 or 12-wells plates containing coverslips.
- Fix cells with 4% paraformaldehyde for 15min at RT.
- Wash three times with PBS.
- Permeabilization and blocking: incubate coverslips with 0.2% saponin and 1% FFA-BSA in PBS for 15min at RT.
- Wash three times with PBS.
- Incubate coverslips with primary antibody diluted in 1% FFA-BSA/PBS overnight at 4°C (**Table M-6**).
- Wash twice with PBS.

- Incubate with secondary antibody diluted in 0.1% FFA-BSA/PBS for 1h at RT and protected from light (**Table M-7**).
- Wash three times with PBS.
- (Optional in case of cholesterol detection) Incubate with Filipin at 0.33mg/ml for 15min at RT at dark.
- Wash three times with PBS.
- Mount the coverslips on glass slides with mounting medium.
- Allow mounting medium to dry out at least 2h.
- Visualize the samples in a confocal fluorescence microscope (equipment used: Leica TCS-SPE DM2500).
    - Filipin: λ_{ex} 340-380nm / λ_{em} 385-470nm
    - Alexa 488: λ_{ex} 495nm / λ_{em} 519nm

Antibody	Host	Dilution	Buffer	Reference	Company
ACDase	Rb	1:200	1% FFA-BSA/PBS	SAB3500293	Sigma Aldrich
Cyt C	Mo	1:200	1% FFA-BSA/PBS	556432	BD Pharmingen
TOM20	Rb	1:200	1% FFA-BSA/PBS	sc11415	SCBT

Table M-6. Primary antibodies used in ICF. Rb, rabbit. Mo, mouse. SCBT, Santa Cruz Biotechnology.

Antibody	Host	Dilution	Buffer	Reference	Company
Anti-mouse IgG antibody conjugated with Alexa Fluor 488	Chicken	1:1000	0.1 FFA-BSA/PBS	A-21200	ThermoFisher
Anti-rabbit IgG antibody conjugated with Alexa Fluor 488	Chicken	1:1000	0.1 FFA-BSA/PBS	A-21441	ThermoFisher

Table M-7. Secondary antibodies used in ICF. Rb, rabbit. Mo, mouse. SCBT, Santa Cruz Biotechnology.

8. CELL CULTURE

8.1. PRIMARY MOUSE HEPATOCYTES

Hepatocytes located in the periportal and perivenous zones of the liver lobule show remarkable differences in the levels and activities of various enzymes and other proteins. Depending on the purpose of the experiment, two different types of primary mouse hepatocytes (PMH) isolations were performed:

- Total PMH isolation: results in a mixed suspension of PP and PV hepatocytes.
- PP/PV PMH isolation: allows the obtaining of enriched populations of the two cell types separately.

8.1.1. Total PMH

8.1.1.1. Isolation

Total PMH were isolated by collagenase perfusion through portal vein followed by a differential centrifugation.

Buffers (**Table M-8**):

HANKS 10X	
Compound	Concentration
NaCl	1.4M
KCl	53.6mM
$MgSO_4 \cdot 7H_2O$	8.1mM
$Na_2HPO_4 \cdot 2H_2O$	6.7mM
KH_2HPO_4	8.8mM
mQ-H_2O	-

HANKS 1X (freshly prepared)	
Compound	Concentration
HANKS 10X	10%
Hepes	12.6mM
$NaHCO_3$	25mM
mQ-H_2O	-

Table M-8. Buffers HANKS10X and HANKS1X used for PMH isolation.

Saturate HANKS 1X buffer with 95% CO_2 and 5% O_2 for 20min to stabilize the pH, and then add the rest of the compounds to HANKS1X to complete HANKS I and II (**Table M-9**):

HANKS I (cleaning buffer)	
Compound	Concentration
BSA	0.5%
EGTA	0.9mM

HANKS II (digestion buffer)	
Compound	Concentration
Collagenase (fraction V) (Sigma, C5138)	160U/ml
$CaCl_2 \cdot 2H_2O$	4mM

Table M-9. Buffers HANKS I and HANKS II used for PMH isolation. BSA, Bovine serum albumin.

EGTA is crucial in the cleaning buffer to avoid coagulation and calcium is necessary for the digestion buffer as a cofactor of the collagenase. Filter buffers through a 0.45µm bottle filter. All the compounds were purchased from Sigma Aldrich.

Protocol:

- Allow HANKS I and II buffers to reach 37°C in a water bath.
- Clean the peristaltic pump tubes with 70% EtOH, dH_2O and then fill the circuit with warm HANKS I buffer at a speed of 6-8ml/min.
- Anesthetize the mouse with a dose of 100mg/kg of sodium pentobarbital intraperitoneally.
- Prepare one surgical suture about 12cm long (Suturas Aragó, Seda trenzada negra 2/0).
- Open the mouse with a laparotomy.
- Place one suture under the portal vein.

- Insert the catheter (BD Insyte, 381212) into the portal vein and immobilize it with the suture around it. If the catheter does not fill with blood, fill it with warm HANKS I buffer avoiding bubble formation.
- Stop the peristaltic pump (Cole-Parmer, MasterFlex L/S, #7553-79) and connect it to the catheter. Avoid bubble formation.
- Start the pump and cut the inferior cava vein so the blood can exit the system.
- Clean the liver with HANKS I buffer. This will prepare the liver for digestion. Make pressure above the cut part of the inferior cava vein with the tweezers during 10sec to allow the buffer penetrate in the liver.
- Once the liver is clean, change to HANKS II buffer to start the digestion. It will take 3-6min to digest. Make pressure in the inferior cava vein with the tweezers during 10sec to better perfuse in the liver. The liver will turn slightly white/brown while it starts swelling. It is crucial to reach an optimal digestion point since too much or insufficient digestion will result in poor hepatocyte viability and content. The liver is digested when it does not increase its volume when applying the pressure at the cut part of the inferior cava vein.
- Pour some HANKS II buffer in a petri dish and prepare a small Erlenmeyer with a funnel and a sterile maze to filter the non-digested parts of the liver.
- Take the liver out and disaggregate the tissue in a petri dish with HANKS II buffer using a pair of tweezers to liberate the hepatocytes from the digested liver.
- Filter hepatocytes through the maze and adjust to a final volume of 50ml with HANKS II buffer.
- Centrifuge at 60xg for 3min at 4°C.
- Discard the supernatant containing Kupffer, hepatic stellate and sinusoidal endothelial cells and resuspend the pellet containing the hepatocytes with warm isolation medium (twice the volume of the pellet).
- After hepatocytes resuspension, use Trypan Blue staining to determine hepatocytes viability rate and cellular concentration. Isolations with a viability rate below a 70% were discarded:
    - Dissolve 50µl of the resuspended hepatocytes in 950µl of 0.2% Trypan Blue (Sigma, T8154).
    - Wait a minute and start to count for alive (white) and dead (blue) cells using a Neubauer Chamber.
    - Multiply the number of cells by the Trypan Blue dilution factor (1/20) and by the volume of the Neubauer Chamber (10^4 cells/ml). The sum of alive and dead cells will give us the total number of cells that we will use to calculate the % of viability: alive cells/total number of cells x100.

8.1.1.2. Culture

After isolation, PMH were seeded on culture vessels at different densities depending on the vessel type and the purpose of the experiment. Culture vessels were precoated with collagen in order to ensure hepatocyte adhesion.

Protocol for plates' collagen coating:

- Prepare 0.02M Acetic Acid in mQ-H_2O (114µl Acetic Acid + 100ml mQ-H_2O) and filter it with a 0.2µm filter to sterilize it.
- Prepare a 50µg/ml collagen solution in 0.02M Acetic Acid (commercial Collagen I, rat tail, Gibco A10483-01). The volume of collagen solution to prepare depends on the number and type of culture vessels to be coated.
- Cover the desired vessels with the collagen solution.
- Incubate for 20-30min at RT.
- Aspirate collagen.
- Let vessels air dry in the cell culture hood for minimum 30min.
- Cover vessels with tin foil and keep them at 4°C until needed.
- Prior to use, wash them once or twice with PBS to remove residual acetic acid.

Once seeded, PMH were kept in an incubator at 37°C with 5% CO_2. Two different culture media were used: isolation medium, which is supplemented with fetal bovine serum (FBS) and used for the first 3h post isolation, and maintenance media, a non-FBS supplemented medium used for the rest of the culture and during the treatments (**Table M-10**).

Isolation Medium (with FBS)	
Compound	Concentration
DMEM:F12 (Gibco, 21331-020)	
Penicilin/Streptomycin (Gibco, 15140-122)	100U/ml
L-Glutamine (Gibco, 25030-024)	200mM
Hepes pH 7,4 (Sigma, H4034)	150mM
FBS (Gibco, 26140079)	10%

Maintenance Medium (without FBS)	
Compound	Concentration
DMEM:F12 (Gibco, 21331-020)	
Penicilin/Streptomycin (Gibco, 15140-122)	100U/ml
L-Glutamine (Gibco, 25030-024)	200mM
Hepes pH 7,4 (Sigma, H4034)	150mM

Table M-10. Mediums used for PMH culture.

8.1.1.3. Treatments

PMH keep their phenotype for 36-48h after isolation, so treatments should be done during this time to avoid artifacts.

8.1.1.3.1. $CoCl_2$ and EtOH treatment

To assess the effects of hypoxia and ethanol in PMH, cultured PMH were treated for 24 hours with 100µM cobalt chloride ($CoCl_2$) (Sigma, C8661) and/or 100mM absolute ethanol (EtOH) (Merck, 100983).

8.1.1.3.2. U18666A treatment

Cultured PMH were treated with 2µg/ml U18666A (Calbiochem, 662015) for 16 hours.

8.1.2. PP/PV PMH

PP/PV PMH isolation shares the same culture and treatment conditions with total PMH isolation but differs in the isolation procedure.

8.1.2.1. Isolation

PP and PV PMH were obtained through perfusion of portal and superior cava veins followed by a dual digitonin-collagenase digestion and differential centrifugation. This technique is based on the destruction of unwanted cells by using digitonin, which is a non-ionic detergent that permeabilizes cell membranes. Only one cell population type is obtained per mouse.

Buffers:

- HANKS 10X, HANKS 1X and HANKS I are the same as the ones used for Total PMH isolation (see **Tables M8 and M9**).
- HANKS II differs in the Collagenase content since for PP/PV PMH isolation only a 1/3 of Collagenase is added (53.3U/ml).
- Digitonin buffer: 2.5mM Digitonin (Sigma, D5628) in HANKS 1X + 0.5% BSA. Heat in a microwave 40ml of 2.5mM Digitonin HANKS 1X until it boils. Stir and heat again until it completely dissolves. It may take a while. Be careful because boiling can make the solution rise and pour out of the vase. When completely dissolved, place the solution in a water bath

at 55°C for 10 min. When it reaches 55ªC, add 0.5% of BSA and stir with a magnetic bar to dissolve properly.

Protocol:

- Allow HANKS I and II buffers to reach 37°C in a water bath.
- Allow digitonin buffer to reach 55°C in a water bath.
- Clean the peristaltic pump tubes with 70% EtOH, dH_2O and then fill the circuit with warm HANKS I buffer at a speed of 3ml/min.
- Anesthetize the mouse with a dose of 100mg/kg sodium pentobarbital intraperitoneally.
- Prepare two surgical sutures about 12cm long (Suturas Aragó, Seda trenzada negra 2/0).
- Open the mouse with a laparotomy.
- Place one suture under the portal vein.
- Insert the catheter (BD Insyte, 381212) into the portal vein and immobilize it with the suture around it (**Figure M-3**). If the catheter does not fill with blood, fill it with warm HANKS I buffer avoiding bubble formation.
- Place a cap onto the catheter end to avoid blood loss.
- Open the mouse chest cavity carefully.
- Put one suture under the superior cava vein.
- Insert a catheter into the superior cava vein from the heart connection towards the liver and immobilize it with the suture around it (**Figure M-3**). If the catheter does not fill with blood, fill it with warm HANKS I buffer avoiding bubble formation.
- Stop the peristaltic pump (Cole-Parmer, MasterFlex L/S) and connect it to the appropriate catheter avoiding bubble formation. HANKS I solution perfusion at 3ml/min is done through the vein closest to the hepatocyte population that we want to isolate:
  - If PP PMH isolation: connect the pump through portal vein.
  - If PV PMH isolation: connect the pump through superior cava vein.
- Start the pump and check that the blood exits the system through the opposite vein cleaning the liver with HANKS I buffer.
- Once the liver is clean, proceed to hepatocyte digitonin destruction. Digitonin perfusion is done at 0.5ml/min in the opposite flow of wash and digestion, i.e., perfuse through the vein closest to the hepatocyte population we want to destroy:
  - If PP PMH isolation: add digitonin buffer through superior cava vein.
  - If PV PMH isolation: add digitonin buffer through portal vein.

  Digitonin perfusion is fast, it will take around 10-30sec. Wait until a pattern is observed.

- Disconnect the pump and perfuse again with HANKS I through the opposite direction of digitonin flow in order to remove all digitonin remains.
- Change to HANKS II buffer to start the digestion. It will take 3-6min to digest.
- Pour some HANKS II buffer in a petri dish and prepare a small Erlenmeyer with a funnel and a sterile maze to filter the non-digested parts of the liver.
- Take the liver out and disaggregate the tissue in a petri dish with HANKS II buffer using a pair of tweezers to liberate the hepatocytes from the digested liver.
- Filter hepatocytes through the maze and adjust to a final volume of 50ml with HANKS II buffer.
- Centrifuge at 60xg for 4min at 4°C.
- Discard the supernatant and resuspend the pellet containing PP or PV PMH with warm isolation medium (twice the volume of the pellet).
- After hepatocytes resuspension, use Trypan Blue staining to determine hepatocytes viability rate and cellular concentration as explained in chapter 6.1.1.1. Isolations with a viability rate below a 70% were discarded.

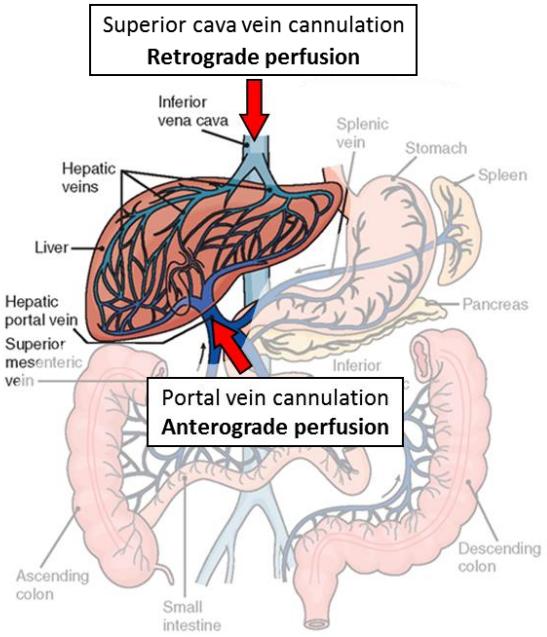

Figure M-3. Schematic view of portal and superior cava veins cannulation performed during the protocol to obtain PP or PV hepatocytes. Adapted from ("Systemic Veins. Structure of the Veins. Functions of the Veins," n.d.).

8.2. HUMAN SKIN FIBROBLASTS

Control human skin fibroblasts ($NPC^{+/+}$) were obtained from control individuals: GM5659D from Coriell Institute for Medical Research, NJ, USA. NPC1 knock-out human fibroblasts ($NPC^{-/-}$) were

obtained from patients with NPC disease: AK2 from the *Laboratoire de Biochimie Metabolique, Institut Federatif de Biologie* (CHU Toulouse, France) and GM03123 from Coriell Institute for Medical Research, NJ, USA.

8.2.1. Culture

$NPC^{+/+}$ and $NPC^{-/-}$ fibroblasts were cultured in DMEM (Invitrogen, 41966-052) with 10% FBS and 10000U/ml Penicillin-Streptomycin at 37°C in an atmosphere of 95% air and 5% CO_2. Aliquots of low passages should be frozen down in order to always have a source of cells in early passages.

Passaging protocol:

- Remove and discard culture medium.
- Wash with warm PBS to remove all traces of serum that could inhibit trypsin action.
- Add Trypsin-EDTA (Invitrogen, 25200-056) to the culture vessel (the volume to add depends on the vessel type).
- Place the vessel in the incubator at 37°C for 2min maximum.
- Observe vessel under an inverted microscope to verify that cells have been detached.
- Add complete growth medium and collect cells by gently pipetting.
- Transfer the appropriate volume of cell suspension to new culture vessels. The suggested subcultivation ratio is 1:2. It is also recommended to renew medium twice per week.

Freezing protocol:

- Prepare 5% dimethyl sulfoxide (DMSO) growing media.
- Add around 2 million cells per cryotube and progressively freeze them down by first placing the tube on dry ice for 1hour, then to -80°C for a week and then to liquid nitrogen for definitive storage.

Thawing protocol:

- Thaw the cells quickly and seed them in a small culture vessel.
- Switch the media after 4h when cells are attached in order to remove the toxic DMSO of the freezing media.

8.2.2. Treatments

8.2.2.1. U18666A treatment

Cultured human skin fibroblasts were treated with 2µg/ml U18666A (Calbiochem, 662015) for 16 hours.

8.2.2.2. ACDase overexpression

Fibroblasts from NPC patients were transfected with cDNA to overexpress ACDase (ASAH1) (MGC Human ASAH1 Sequence-Verified cDNA, Accession: BC016481, Clone ID: 3923451) commercially purchased from GE Dharmacon. Scrambled control GFP vector was used as a control. Transfection was performed using Lipofectamine 2000 Transfection Reagent (Invitrogen, 11668019).

Protocol:

- Seed cells to be 70-90% confluent at transfection.
- Dilute Lipofectamine 2000 Transfection Reagent in Opti-MEM™ Medium (Gibco, 31985070).
- Dilute DNA in Opti-MEM™ Medium.
- Add diluted DNA to diluted Lipofectamine (1:1 ratio).
- Incubate for 20min at RT.
- Add DNA-lipid complex to cells.
- Incubate cells at 37°C for 4-6h.
- Change media to standard fibroblasts culture media (DMEM + 10% FBS + P/S).
- Perform cell analyses 48h after transfection.

8.2.2.3. Hydrogen peroxide treatment

Human skin fibroblasts were treated with 1mM hydrogen peroxide (H_2O_2) (Sigma, H1009) for 24h to evaluate ROS and cell viability.

9. MITOCHONDRIAL ANALYSIS

9.1. MITOCHONDRIAL ISOLATION

Mitochondrial isolation is a necessary procedure to be able to analyze different components such as cholesterol and GSH specifically in mitochondria. We isolated mitochondria from total liver homogenate and from cell extracts.

9.1.1. Liver mitochondria isolation

Buffers (**Table M-11**):

Buffer A (pH 7.4)	
Compound	Concentration
Mannitol	225mM
Sucrose	75mM
EGTA	0.1mM
FFA-BSA	1mg/ml
Hepes-KOH	10mM
mQ-H_2O	-

Buffer B (pH 7.4)	
Compound	Concentration
Sucrose	395mM
EGTA	0.1mM
Hepes-KOH	10mM
mQ-H_2O	-

Table M-11. Buffers for liver mitochondria isolation. Keep them at 4˚C. Buffer B is used to prepare Percoll gradients. FFA-BSA, Fatty acid-free bovine serum albumin. All the reagents were purchased from Sigma Aldrich.

Protocol:

- Add 4.5ml of Buffer A for each gram of liver.
- Cut the liver in pieces and homogenate it using a drill-driven Teflon dounce homogenizer at 1200rpms (4 times up and down).
- Add twice the volume of buffer A (V_{final}= 9ml).
- Take and aliquot of 600-700µl for liver homogenate measurements.
- Centrifuge the rest of liver homogenate at 700g for 15min at 4˚C.
- Discard the pellet and collect the supernatant.
- Centrifuge the supernatant at 10000g, 15min at 4˚C.
- Discard the supernatant and re-suspend the pellet containing mitochondria in 0.5ml of Buffer B (the final volume will be 1ml approximately). This fraction contains mitochondria together with leftovers of other organelles (crude mitochondria).
- For each sample, prepare an ultracentrifuge tube with 7ml of 26% Percoll (Sigma, P1644) and 3ml of 60% Percoll in Buffer B.
- Add the entire sample volume on top of the 26% Percoll top layer.
- Equilibrate the tubes to the same weight with Buffer B.
- Ultra centrifuge samples at 15500rpms, 35min at 4°C. In this step, mitochondria will pass through the 26% Percoll gradient and will stop at the beginning of the 60% Percoll.
- Discard the layers above the mitochondria's band with a plastic Pasteur pipette.
- Gently collect the mitochondria's band with a glass Pasteur pipette and put it in a new tube.
- Add a big volume of Buffer B to the mitochondrial fraction and centrifuge it at 10000g, 15min at 4˚C to wash it. Repeat this step twice.
- Discard the supernatant and resuspend the pellet containing mitochondria with 350µl of Buffer A (so the final volume of mitochondria is around 500µl due to the remaining volume of buffer B after discarding the supernatant). This fraction contains pure mitochondria.

9.1.2. Cellular mitochondria isolation

PMH and fibroblasts were fractionated into cytosol and mitochondria by digitonin permeabilization.

Buffers (**Table M-12**):

Krebs buffer (pH 7.4)	
Compounds	Concentration
Krebs-Henseleit	1%
Hepes	16.8mM
$NaHCO_3$,	24mM
$CaCl_2 \cdot 2H_2O$	2.7mM
mQ-H_2O	-

Mannitol Buffer - Digitonin (MBD) (pH 7.4)	
Compounds	Concentration
Mannitol	250mM
EDTA	19.8mM
Hepes	17mM
Digitonin	0.15%
mQ-H_2O	-

Table M-12. Buffers used for cellular mitochondria isolation. All reagents were purchased from Sigma.

Protocol:

- PMH preparation

- Immediately after PMH isolation and cell counting, pellet $1 \cdot 10^6$ PMH and resuspend them with 600µl of Krebs buffer (cell homogenate).

- Fibroblasts preparation

- Wash cultured fibroblasts with PBS solution to remove all traces of serum that could inhibit trypsin action.
- Add Trypsin-EDTA (Invitrogen, 25200-056) to the cell culture dish and tripsinize cells normally.
- Add culture medium with FBS to stop trypsinisation and centrifuge to obtain a cell pellet.
- Resuspend the cell pellet with Krebs buffer and determine cell concentration by Trypan Blue.
- Aliquot and pellet $2 \cdot 10^6$ fibroblasts and finally resuspend them with 600µl of Krebs Buffer (cell homogenate).

- Cell Fractioning

- From the cell homogenate, separate:
    - 50µl for total protein determination
    - 50µl for total GSH measurement
    - 500µl for cytosolic-mitochondrial fractioning

- Prepare 1.5ml centrifuge tubes containing from the bottom to the top: 100µl of 10% trichloroacetic acid (TCA) (Sigma, T6399), 500µl of a 6:1 (v/v) mixture of silicone (Sigma, 175633) and paraffin oil (Sigma, 18512), and a 100µl top layer of MBD at 37°C.
- Rapidly, add 500µl of cell homogenate inside the 100µl MBD top layer and wait for 30sec at RT (in this short incubation, digitonin makes holes in the cell membrane but it does not damage mitochondria).
- Subsequently, centrifuge tubes for 1min at 13000rpm at RT to separate cytosolic and mitochondrial fractions.
- 3 layers appear:
    - Bottom layer: contains the mitochondrial fraction in 10% TCA.
    - Middle layer: contains the Silicon:Paraffin oil.
    - Top layer: contains the cytosolic fraction.

To analyze cytosolic GSH levels, take a known volume of the cytosolic fraction, dilute with 10% TCA (1:1 ratio) and follow Protocol 9. mGSH levels can be read directly since the fractioning has been performed with 10% TCA in the lower phase. To analyze total GSH levels, the separated 50µl aliquot of cell homogenate (first steps of the protocol) should be diluted with 10% TCA (1:1 ratio).

9.2. MITOPLASTS PREPARATION

A mitoplast is a mitochondrion that has been stripped of its outer membrane leaving the inner membrane intact. In the present doctoral thesis, mitoplasts were prepared by selective solubilization of the outer mitochondrial membrane using digitonin.

Protocol:

- Isolate pure mitochondria from liver following the protocol described on 7.1.1.
- Prepare a pure mitochondrial protein suspension at 8µg/µl in Buffer B (395mM sucrose, 0.1mM EGTA and 10mM HEPES; pH 7.4).
- Prepare a solution of Digitonin 0.768% in Buffer B (7.68µg digitonin/µl). Warm the solution up until digitonin is completely dissolved and then cool it down.
- Mix the 8µg/µl mitochondrial protein suspension with an equal volume of the 7.68µg/µl digitonin solution (the final ratio between digitonin and mitochondria must be 960µg digitonin/mg mitochondria).
- Incubate the mix for 30min in a tube rotator at 4°C (during this step, digitonin makes holes in the outer mitochondrial membrane but it does not affect the inner membrane).

- Centrifuge the sample for 10min at 10000xg at 4°C.
- After centrifugation:
    - Supernatant = Outer mitochondrial membrane. Transfer supernatant to new tubes.
    - Pellet = Mitoplasts. Resuspend the pellet containing mitoplasts in Buffer B and centrifuge again to wash.
- Assess mitoplasts purity through protein expression analysis by checking the absence of markers from the outer mitochondrial membrane (e.g. VDAC1) and the enrichment of markers from the inner mitochondrial membrane (e.g. COXIV).

9.3. MITOCHONDRIAL MEMBRANE POTENTIAL DETERMINATION

Tetrametylrhodamine methyl ester (TMRM) is a dye used to analyze mitochondrial membrane potential in living cells. The lipophilic structure of TMRM allows it to easily penetrate the cellular and mitochondrial lipid membranes. If cells are healthy and have functioning mitochondria, TMRM signal is bright. In contrast, upon loss of mitochondrial membrane potential, TMRM accumulation ceases and the signal dims or disappears. TMRM signal can be detected by fluorescence analysis method.

Protocol:

- Prepare a 10mM TMRM (ThermoFisher Scientific, T668) stock solution in DMSO.
- Prepare a 500nM TMRM solution in culture medium.
- Incubate cultured PMH in 500nM TMRM solution for 30min at 37°C in dark.
- Wash cells with PBS twice.
- Evaluate TMRM fluorescence by fluorescence spectroscopy using the Tecan Fluorescence Microplate Reader (548nm for excitation and 574nm for emission).
- Normalize fluorescence by protein content determined by Bradford or BCA protein assay.

9.4. MEASUREMENT OF MITOCHONDRIAL MEMBRANE RIGIDITY

Fluorescence anisotropy is the phenomenon where the light emitted by a fluorophore has unequal intensities along different axes of polarization. Measurement of fluorescence anisotropy of membranes labelled with fluorescent probes, e.g. 1,6-diphenylhexatriene (DPH), has been widely used to monitor membrane physical changes that correspond to the transition of membranes from gel to liquid crystalline state and vice versa. A linearly polarized beam generated by a vertical polarizer preferentially excites DPH with transition moments aligned parallel to the

incident polarization vector. The resulting fluorescence is directed into two channels through a moving polarizer that measure the intensity of the fluorescence polarized both parallel (I(0-0)) and perpendicular (I(0-90)) to that of the polarized excitation light. With these two measurements, the fluorescence anisotropy (r) can be calculated. When the membrane is fluid (less rigid), DPH molecules move quickly and have depolarized emission, thus displaying low anisotropy values (I(0-0) ~ I(0-90)). However, insertion of compounds into the lipid bilayer diminishes the movement of DPH during the excitation state resulting in increased DPH anisotropy (I(0-0) > I(0-90)) (**Figure M-4**) (Zhao and Lappalainen, 2012).

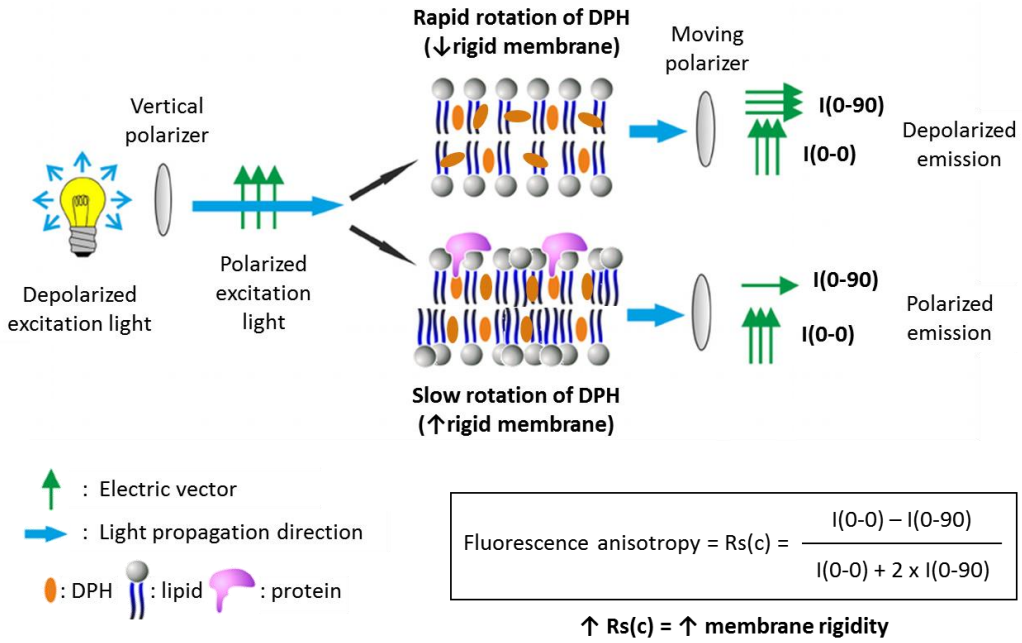

Figure M-4. System used to determine fluorescence anisotropy using DPH probe. Adapted from (Zhao and Lappalainen, 2012).

In this thesis, fluidity of mitochondrial membranes was evaluated by fluorescence anisotropy of mitochondria-bound dye DPH. Mitochondrial membranes are labeled with DPH and the degree of fluorescence anisotropy is determined in a fluorescence spectrophotometer at 37°C with 366nm excitation and 425nm emission wavelength by using polarizing filters in both excitation and emission planes.

Buffer (**Table M-13**):

Buffer MF (pH 7.4)	
Compound	Concentration
Tris-HCl	10mM
KCl	150mM
EDTA	1mM
mQ-H_2O	-

Table M-13. Buffer used for measurement of mitochondrial membrane rigidity. Keep it at 4˚C. All the reagents were purchased from Sigma Aldrich.

Protocol:

- Prepare a 100mM DPH stock (it can be aliquoted and stored at -20°C):
    - Prepare a 20mM DPH solution in tetrahydrofuran.
    - Dilute the previous solution with buffer MF to a final concentration of 100mM.
    - Stir the mix in the dark until a stable dispersion is obtained.
- Prepare a fresh 200µM DPH solution in buffer MF. Cover the solution to protect it from light and put it in a shaker at 37°C for minimum 1h.
- Isolate mitochondria from mouse liver following the protocol described on 7.1.1. Do not purify mitochondria with Percoll gradient since the purification can compromise mitochondrial membranes and thus their physical properties. Use crude mitochondria, i.e. the mitochondrial fraction obtained before the ultracentrifugation step.
- Prepare mitochondrial samples for the assay:
    - Labeled sample: 500µg of mitochondria + 0.5ml of DPH 200µM + MF buffer up to 1.5ml (final DPH concentration in sample: 50µM).
    - Unlabeled sample: 500µg of mitochondria + MF buffer up to 2ml.
- Incubate all samples in a water bath at 37°C shaking for 1h.
- Measure fluorescence polarization in a Hitachi F-4500 fluorescence spectrofluorometer at wavelengths of 366nm for excitation and 425nm for emission.

The results are expressed as anisotropy units (r), where r=(I0/I90)/(I0+2xI90). I0 and I90 represent the intensities of light when polarizers were in parallel or perpendicular orientation, respectively. Light scattering and intrinsic fluorescence were routinely corrected by subtracting the signal obtained from unlabeled samples and the fluorescence of the buffer plus label alone.

9.5. *IN VITRO* CHOLESTEROL LOADING IN MOUSE LIVER MITOCHONDRIA

Mitochondrial membranes *in vitro* cholesterol enrichment was performed by incubation of mitochondria with a cholesterol-BSA complex (CBSAC) or enantiomer cholesterol-BSA complex

(Ent-CBSAC). Enantiomer cholesterol was generously provided by Scott Rychnovsky (Department of Chemistry, University of California Irvine, USA).

Buffer (**Table M-14**):

Buffer CHS (pH 7.4)	
Compound	Concentration
Sucrose	0.25M
EDTA	1mM
mQ-H_2O	-

Buffer B (pH 7.4)	
Compound	Concentration
Sucrose	395mM
EGTA	0.1mM
Hepes-KOH	10mM
mQ-H_2O	-

Table M-14. Buffers used for *in vitro* cholesterol increase in mouse liver mitochondria.
Keep them at 4˚C. All the reagents were purchased from Sigma Aldrich.

Protocol:

Previous to the assay

- Prepare a 10mg/ml cholesterol solution in absolute ethanol (dissolve 50mg of cholesterol or enantiomer cholesterol in 5ml of absolute ethanol).
- Once dissolved, add 5ml of mQ-H_2O to the solution.
- Mix for at least 20min at RT.
- Centrifuge the resulting milk-like solution at 2000xg for 10min.
- Discard supernatant and resuspend the pellet in 5ml of Buffer CHS.
- Gently stir the solution while slowly adding 2g of FFA-BSA at RT.
    - Additionally, prepare the BSA-only control in parallel: dissolve 2g of FAF-BSA in 5ml of buffer CHS.
- Once BSA is completely dissolved, adjust pH to 7.4 and then centrifuge the solutions at 12000xg for 10min at 4°C.
- Collect the supernatants, aliquot them in new tubes and store them at -20°C as CBSAC or Ent-CBSAC stocks (10mg cholesterol/ml) or BSA-only stock (0mg cholesterol/ml).

Day of the assay

- Isolate mitochondria from mouse liver following the protocol described on 7.1.1. Do not purify mitochondria with Percoll gradient since the purification can compromise mitochondrial membranes. Use crude mitochondria, i.e. the mitochondrial fraction obtained before the ultracentrifugation step.

- Add CBSAC, Ent-CBSAC or BSA-only to mouse liver mitochondria at the proportion of 0.2mg complex/mg mitochondria and incubate for 1min at 4°C.
- Dilute mitochondria about 20 times with cold buffer CHS and spin down immediately at 12000xg for 10min at 4°C to eliminate the unbound cholesterol.
- Repeat the washing step twice.
- Resuspend mitochondrial pellet with buffer B and proceed to the desired analysis.

9.6. MITOCHONDRIAL RESPIRATORY SUPERCOMPLEXES BY BLUE NATIVE PAGE

Blue native polyacrylamide gel electrophoresis (BN-PAGE) technique was developed to resolve protein complexes by molecular weight while retaining their native structure. BN-PAGE acts by using Coomassie Blue-G250 dye to coat proteins with the necessary negative charge for migration to the anode. Protein complexes migrate across the acrylamide gel according to their specific pore size until they reach their specific pore size limit. BN-PAGE can separate protein complexes ranging between 100kDa to 10MDa. We performed this technique with isolated mitochondria samples using the NativePAGE™ Sample Prep Kit (Novex by Life Technologies, BN2008).

Buffer (**Table M-15**):

Solubilization buffer A (pH 7.0)	
Compound	Concentration
Sodium Chloride	50mM
Imidazole	50mM
6-aminohexanoic acid (= 6-Aminocaproic acid)	2mM
EDTA	1mM
mQ-H_2O	-

Table M-15. Buffer used for BN-PAGE. Keep it at 4˚C.
All the reagents were purchased from Sigma Aldrich.

Protocol:

<u>Prior to the assay</u>

- Isolate mitochondria from mouse liver following the protocol described on 7.1.1. Do not purify mitochondria with Percoll gradient since the purification can compromise mitochondrial membranes and thus mitochondrial membrane proteins. Use crude mitochondria, i.e. the mitochondrial fraction obtained before the ultracentrifugation step.
- Pellet a fraction of 600-800µg of mitochondria and store it at -80°C.

Day of the assay

- Thaw the mitochondrial pellet from -80°C and resuspend it with 30µl of the solubilization buffer A.
- Quantify protein content by BCA protein assay.
- Prepare 20µl of mitochondrial sample at 10µg/µl in solubilization buffer A (200µg of mitochondria in total).
- Prepare a 10% digitonin stock solution in solubilization buffer A (warm the solution up until digitonin is completely dissolved and then cool it down).
- Add 12µl of 10% digitonin stock to the mitochondrial suspension (final digitonin concentration in 32µl solution: 3.75%) (6mg digitonin/mg mitochondria).
- Incubate sample on ice for 5 minutes.
- Centrifuge lysate at 20000xg for 30 minutes at 4°C.
- Transfer supernatant into new tubes.
- Add 6µl of 5% Coomassie blue (CB) stock (NativePAGE™ 5% G-250 Sample Additive) (final CB concentration in 38µl solution: 0.79%) (final digitonin concentration in 38µl solution: 3.15%).
- Vortex and spin the sample down.
- Do not heat the samples for native electrophoresis.
- Load samples in a Criterion™ TGX™ Precast 4-15% gel (Biorad, #5671083) and run electrophoresis using a running buffer 10x Tris/Gly (Biorad, #1610734) for 60-90min at 200V in a cold chamber to avoid band's broadening.
- Transfer proteins to a PVDF membrane using the Trans-Blot Turbo™ Transfer System (Bio-Rad). Nitrocellulose membrane is not compatible for blotting NativePAGE gels since the nitrocellulose binds the Coomassie G-250 dye very tightly and is not compatible with alcohol-containing solutions used to destain the membrane and fix the proteins.
- Block membrane with 5% Milk (BD, 232100) in TBST for 1h at RT.
- Incubate membrane with primary antibody (**Table M-16**) overnight at 4°C.
- Wash at least 3 times for 10min with TBST.
- Incubate with HRP-conjugated secondary antibody for 1h at RT (**Table M-17**).
- Develop the antibody protein detection using Pierce™ ECL Western Blotting Substrate and the instrument LAS4000 (GE Healtcare).
- Analyze optical density of bans with ImageJ software.
- Use CB staining as the loading control.

Antibody	Host	Dilution	Buffer	Reference	Company
UQCRC2 (G-10)	Mo	1:500	1% BSA-TBST	sc-390378	SCBT
NDUFA9	Mo	1:1000	1% BSA-TBST	459100	Invitrogen
MitoProfile® Total OXPHOS Rodent WB Antibody Cocktail	Mo	1:750	1% BSA-TBST	ab110413	Abcam

Table M-16. Primary antibodies used in BN-PAGE. Rb, rabbit. Mo, mouse. SCBT, Santa Cruz Biotechnology.

Antibody	Host	Dilution	Buffer	Reference	Company
anti-mouse-HRP	Rb	1:20000	TBST	A9044	Sigma Aldrich

Table M-17. Secondary antibodies used in BN-PAGE. HRP, horseradish peroxidase conjugated. Mo, mouse.

9.7. MITOCHONDRIAL RESPIRATION

Mitochondrial respiration is the set of metabolic reactions requiring oxygen that takes place in mitochondria to convert the energy stored in macronutrients to ATP. Measurement of the oxygen consumption rate (OCR) of mitochondria is very valuable since it is an indicator of not only mitochondrial but also cellular metabolism and fitness status. Agilent Seahorse XF analyzers allow measuring OCR in living cells or isolated mitochondria overall estimating key parameters of mitochondrial respiration in real-time mode (Seahorse XF Cell Mito stress test). In this thesis the Seahorse XFe24 Analyzer has been used to measure mitochondrial respiration in cultured human fibroblasts and isolated liver mitochondria.

9.7.1. OCR measurements in cultured cells

OCR measurements in cells using Seahorse technology allow the measuring of different mitochondrial respiration parameters: basal respiration, ATP-linked respiration, H^+ (proton) leak, maximal respiration, spare respiratory capacity and non-mitochondrial respiration (**Figure M-5**).

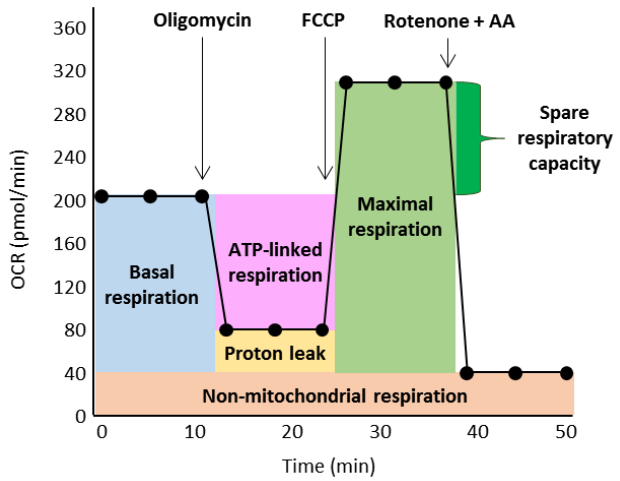

Figure M-5. OCR profile when performing standard Seahorse XF Cell Mito stress test with cultured cells.

The approach requires application of the following cellular respiration modulators (**Figure M-6**):

- Oligomycin, to block ATP synthase.
- Carbonyl cyanide-4-(trifluoromethoxy)phenylhydrazone (FCCP), to make the inner mitochondrial membrane permeable for protons and allow maximum electron flux through the electron transport chain.
- Rotenone, to inhibit complex I.
- Antimycin A (AA), to inhibit complex III.

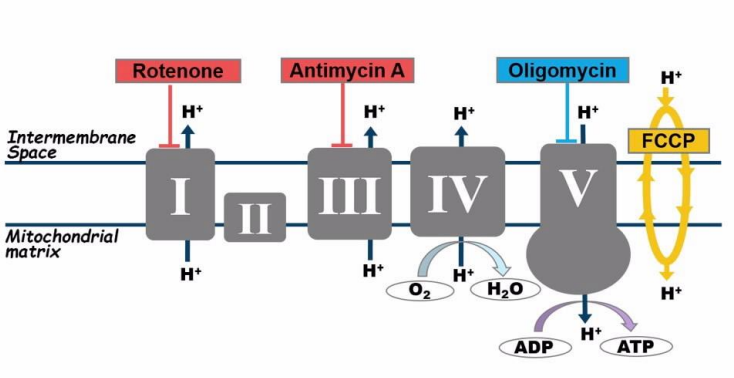

Figure M-6. Modulators of ETC used in OCR measurement by Seahorse technology.

Protocol:

<u>Day Prior to the assay</u>

- Plate 20000 fibroblasts per well of a 96-wells Seahorse cell plate in a final volume of 250µl/well. Do not seed cells in background correction wells: A1, B4, C3 and D6. Keep plate in an incubator at 37°C and 5% CO_2.
- Turn on the Seahorse XFe24 Analyzer and let it warm up to 37°C overnight (or a minimum of 5h).
- Hydrate a sensor cartridge with Seahorse XF Calibrant (Agilent, 100840-000) at 37°C in a non-CO_2 incubator overnight.
- Prepare the Seahorse template/features of the assay in the Wave program. See the instrument user manual for additional details.
- Make sure there are stocks of all the Seahorse reagents prepared at -20°C (see **Table M-18** for preparation).

Compound	Stock concentration	Company
Glucose	1M	Agilent, 103577
Sodium pyruvate	100mM	Agilent, 103578
L-glutamine	200mM	Agilent, 103579
Oligomycin A	6.32mM	Cayman Chemical, 11342
FCCP	10mM	Cayman Chemical, 15218
Rotenone	20mM	Sigma, R8875
AA	20mM	Sigma, A8674

Table M-18. Stock compounds for Seahorse assay.

Day of the assay

- Thaw 1 aliquot of each Seahorse reagent stock (glucose, L-glutamine, oligomycin, FCCP and AA).
- Prepare the assay media by supplementing the Seahorse XF Base Media pH 7.4 (Agilent, 103575-100) as follows:

For fibroblasts:	XF Base Media	(up to 50mL)	48.75mL
	10mM Glucose	(stock: 1M --> 1/250 dilution)	0.5mL
	1mM Sodium Pyruvate	(stock: 100mM --> 1/50 dilution)	0.5mL
	1mM L-Glutamine	(stock: 200mM --> 1/100 dilution)	0.25mL

- Warm assay media at 37°C. pH is already adjusted at 7.4.No filtering is needed.
- Take the Seahorse cell plate from the incubator and perform cell washes:
  - Remove 200µl of media leaving 50µl left on the well.
  - Manually, wash twice the cells by adding and removing 200µl of XF media.
  - On the last wash, aspirate the remaining 50µl of media and gently add the final 500µl of Seahorse assay medium to all wells including Background wells.
  - Incubate cells for 30min at 37°C in an incubator without CO_2.
- Prepare the compounds for loading in sensor cartridge:
  - Port A: 2µM Oligomycin A Volume: 56µl/port

    [stock] $\xrightarrow{1/316}$ [Port] $\xrightarrow{1/10}$ [Well]

    6.32mM → 20µM → 2µM

    Prepare 2ml: 2ml x 20µM = X x 6.32mM

    X= 6.33µl Oligomycin A in 2ml of Seahorse assay media

- Port B: 1µM FCCP Volume: 62µl/port

  [stock] $_{1/400}$ [Port] $_{1/10}$ [Well]

  10mM → 10µM → 1µM

  Prepare 4ml: 2ml x 10µM = X x 10mM

  X= 2µl FCCP in 2ml of Seahorse assay media

- Port C: 1µM Rotenone & A A Volume: 69µl/port

  [stock] $_{1/2000}$ [Port] $_{1/10}$ [Well]

  20mM → 10µM → 1µM

  Prepare 2ml: 2ml x 10µM = X x 20mM

  X= 1µl Rotenone & AA in 2ml of Seahorse assay media

- Load the compounds in the sensor cartridge and perform calibration in the Seahorse analyzer. Ports order:

A	B
C	D

- Load the cell culture plate and start the assay.
- Once the running is finished, measure the protein concentration of each well by BCA protein assay to normalize respiration values.

9.7.2. OCR measurements in isolated mitochondria

Respiratory function tests in isolated mitochondria have the advantages to detect specific defects in the mitochondrial protein function and evaluate the direct mitochondrial effects of pharmacological agents. The same inhibitors FCCP, oligomycin A, rotenone and AA as with cells are used. However, since in this case mitochondria are not in the cellular environment but isolated, fuels for the ETC need to be provided such as ADP and substrates as pyruvate or succinate.

In this assay mitochondria begin in a coupled state with substrate present (State 2). Depending on the purpose of the experiment, substrates can be pyruvate plus malate to study ETC function starting from complex I, or succinate plus rotenone to prevent any complex I driven respiration and study ETC function from complex II. Then, by adding ADP the phosphorylating respiration is initiated (State 3). State 4o is subsequently induced with the addition of oligomycin, which blocks complex V. FCCP-induced maximal uncoupler-stimulated respiration (State 3u) is then measured,

allowing respiratory control ratios (RCR: State 3/State 4o, and UCR: State 3u/State 4o) to be assessed. Finally, AA inhibits complex III and determines the residual respiration (non-mitochondrial respiration) (**Figure M-7**).

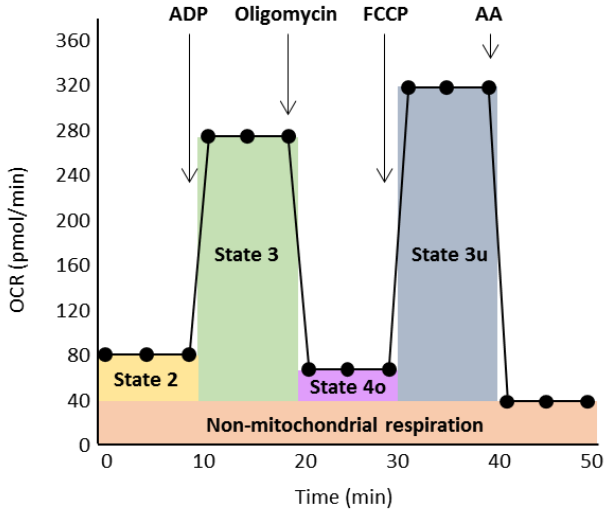

Figure M-7. OCR profile when performing standard Seahorse XF Cell Mito stress test with isolated mitochondria.

Protocol:

Day Prior to the assay

- Turn on the Seahorse XFe24 Analyzer and let it warm up to 37°C overnight (or a minimum of 5h).
- Hydrate a sensor cartridge with Seahorse XF Calibrant (Agilent, 100840-000) at 37°C in a non-CO_2 incubator overnight.
- Prepare the Seahorse template/features of the assay in the Wave program. See the instrument user manual for additional details.
- Make sure there are stocks of all the Seahorse reagents prepared at -20°C (see **Table M-19** for preparation).

Compound	Stock concentration	Company
Pyruvate	0.5M	Sigma, P5280
Malate	0.5M	Sigma, M6413
Succinate	0.5M	Sigma, S9512
ADP	Powder	Sigma, A2754
Oligomycin A	6.32mM	Cayman Chemical, 11342
FCCP	10mM	Cayman Chemical, 15218
Rotenone	20mM	Sigma, R8875
AA	20mM	Sigma, A8674

Table M-19. Stock compounds for Seahorse assay.

- Make sure there are aliquots of 2XMAS Buffer prepared at -20°C (see **Table M-20** for preparation).

2XMAS Buffer (pH 7.2)	
Compound	Stock concentration
Sucrose	140mM
Mannitol	440mM
KH_2PO_4	20mM
$MgCl_2 \cdot 6H$	10mM
HEPES	4mM
EGTA	2mM
FFA-BSA	0.4%
mQ-H_2O	-

Table M-20. 2XMAS buffer used in Seahorse assay.

Day of the assay

- Buffers and cartridge preparation

- Thaw 1 aliquot of each Seahorse reagent stock and 2XMAS Buffer.
- Prepare the assay buffers:

  If pyruvate and malate as substrates:
  - Prepare 1XMAS: Mix 20ml of 2XMAS Buffer + 18.4ml of mQ-H_2O (Vf=38.4ml)
  - Prepare 1XMAS + Substrates: Add 800µl of pyruvate 0.5M and 800µl of malate 0.5M (final 10mM both) to 1XMAS (Vf=40ml). Adjust pH 7.2.
    - Transfer 10ml of 1XMAS+Substrates to a new falcon and leave it on ice (Cold 1XMAS+Subs).
    - Leave the remaining 30ml of 1XMAS+Substrates on a bath at 37°C (Warm 1XMAS+Subs).

  If succinate as substrate plus rotenone:
  - Prepare 1XMAS: Mix 20ml of 2XMAS Buffer + 19.2ml of mQ-H_2O (Vf=39.2ml)
  - Prepare 1XMAS + Substrates: Add 800µl of succinate 0.5M (final 10mM). Adjust pH 7.2.
    - Transfer 10ml of 1XMAS+Substrates to a new falcon and leave it on ice (Cold 1XMAS+Subs).
    - Add 3µl of rotenone 20mM to the remaining 30ml of 1XMAS+Substrates (final 2µM). Adjust pH 7.2 again. Leave it on a bath at 37°C (Warm 1XMAS+Subs).
- Prepare the respiration reagent compounds for loading in sensor cartridge:

  - Port A: ADP 40mM --> 39mg ADP + 1ml mQ-H_2O. Dissolve it properly and then add 1.14ml of warm 1XMAS+Subs. Adjust pH 7.2 with KOH 11% and finally add mQ-H_2O to have a final volume of 2.28ml (ADP has to be freshly prepared and its proper preparation is crucial for the respiration assay).
  - Port B: Oligomycin 25µg/ml --> 10µl stock 6.32mM + 2ml of warm 1XMAS+Subs.
  - Port C: FCCP 40µM --> 8µl stock 10mM + 2ml warm 1XMAS+Subs.
  - Port D: AA 40µM --> 4µl stock 20mM + 2ml warm 1XMAS+Subs.
- Load the compounds in the Sensor Cartridge:
  - Port A = 56µl ADP 40mM ($Conc_{well}$=4mM)
  - Port B = 62µl Oligomycin 25µg/ml ($Conc_{well}$=2.5µg/ml)
  - Port C = 69µl FCCP 40µM ($Conc_{well}$=4µM)
  - Port D = 75µl AA 40µM ($Conc_{well}$=4µM)

  Ports order:

A	B
C	D

- Calibrate the sensor cartridge in the Seahorse analyzer.

- Mitochondrial samples and Seahorse culture plate preparation

- Isolate mitochondria from mouse liver following the protocol described on 7.1.1. Do not purify mitochondria with Percoll gradient since the purification can compromise mitochondrial membranes and thus respiration. Use crude mitochondria, i.e. the mitochondrial fraction obtained before the ultracentrifugation step.
- Prepare a mitochondrial solution at 0.2µg/µl in cold 1XMAS+Subs. The volume of solution to prepare depends on the number of wells to be plated.
- Place 50µl of mitochondrial solution per well of a Seahorse culture plate (10µg mitochondria/well). Do not plate mitochondria but only 50µl of cold 1XMAS+Subs on the background correction wells: A1, B4, C3 and D6.
- Transfer the plate to a centrifuge equipped with a swinging bucket microplate adaptor and spun at 2000g for 15min at 4°C (this step allows mitochondria to remain at the bottom of the plate).
- After centrifugation, add 450µl of warm 1XMAS+Subs per well (Vf=500µl).
- Incubate the plate for 8-10min in the incubator at 37°C without CO_2.

- Once the cartridge is calibrated, replace the utility plate by the Seahorse culture plate containing mitochondria and start the assay.
- Once the running is finished, measure the protein concentration of each well by BCA protein assay to normalize respiration values.

3-5 mitochondrial preparations per experimental group were analyzed always in triplicates in each plate. Measurement protocol for standard liver mitochondria: 2 cycles of 1min mix and 3min measure per state. Measurement protocol for liver mitochondria after incubation with CBSAC: 2 cycles of 1min mix and 4min measure (State 2); 1 cycle of 1min mix and 4min measure (other states).

10. CHOLESTEROL ANALYSIS

10.1. FREE AND TOTAL CHOLESTEROL QUANTIFICATION BY HPLC

The amount of free and total cholesterol incorporated in liver, mitochondria or mitoplasts was measured by high performance liquid chromatography (HPLC). For total cholesterol determination, samples undergo saponification to free all the esterified cholesterol. Thus, the reading of saponified samples will represent total cholesterol levels (the sum of free and esterified cholesterol).

Protocol for cholesterol extraction:

- Cholesterol standards:
    - Prepare a 1mg/ml cholesterol (Sigma, C8867) stock solution in isopropanol.
    - Prepare 7 cholesterol standard solutions containing 0, 5, 10, 20, 40, 80 or 100µg of cholesterol in 200µl with PBS (prepare two sets, one for the FC and the other for the total cholesterol samples).
    - These standards will be carried along with the samples.
- Use about 0.5mg of protein in a final volume of 200µl (adjust the volume with PBS). Use two tubes per sample, for total and for FC quantification.
- Add 200µl of ethanol-33% KOH per tube.
- Vortex 1min and wait 1min. Repeat three times.
- For:
    - Total cholesterol extraction: incubate at 60°C for 30min (saponification). Let it cool down for 5 minutes afterwards.

    - FC extraction: incubate at RT for 30min.
- Add 200µl of mQ-H_2O.
- Add 400µl of Hexane HPLC proof (always maintain the extraction relation of sample:ethanol-KOH:H_2O:Hexane (1:1:1:2)).
- Vortex 1min and wait 1min. Repeat three times.
- Spin down for 2min at 10000 rpms at RT.
- Collect 200µl from the hexane top layer containing the cholesterol and transfer them into a new tube.
- Dry the hexane in a speed vacuum for minimum 45min.
- Store samples at -20°C if HPLC is immediately performed, or at -80°C if HPLC will be ran later the same day or another day.

Protocol for cholesterol levels determination:

- HPLC Conditions:
    - Column --> µBondapak C18 Column, 125Å, 10 µm, 3.9 mm X 300 mm, 1/pk, Waters
    - Mobile phase composition:
        - A pump --> Acetonitrile
        - B pump --> Isopropanol (2-propanol):Acetonitrile:mQ-H_2O (60:30:10)
    - Absorbance --> 200nm
    - Flow rate --> 1ml/min
    - Running time --> 15 minutes per sample
    - Methanol 80% to clean the needle

- Samples processing:
    - Take samples from -20°C/-80°C.
    - Add 200µl of isopropanol to each sample.
    - Vortex for 5 minutes.
    - Spin down at 10000rpm for 2 min at RT.
    - Transfer the maximum possible volume of supernatant (±170µl) to HPLC tubes (avoid touching the bottom of the tube).
    - Prepare extra HPLC tubes to do the blanks: only put 200µl of isopropanol.
    - Place the tubes into the HPLC machine and run the protocol.

The amount of cholesterol of each sample was calculated according to a calibration line derived from the known cholesterol standards concentrations.

10.2. FREE CHOLESTEROL LABELING BY FILIPIN STAINING

10.2.1. In tissues

Filipin is a mixture of chemical compounds isolated by chemists in 1955 from Streptomyces filipinensis. This actinomycete was discovered in a soil sample collected in the Philippine Islands, hence the name Filipin. Filipin has been widely used as a probe for sterol location in biological membranes. Its interaction with cholesterol alters its absorption and fluorescence spectra allowing visualization with a fluorescence microscope capable of excitation at 340-380nm and emission at 385-470nm. It is a tool for histochemical identification of unesterified cholesterol both *in vivo* and *in vitro*.

Protocol:

- Let 8µm frozen sections to cool down at RT for 10min.
- Wash the sections with PBS 2 times for 5min.
- Fix sections with 4% paraformaldehyde for 30min at RT.
- Wash with PBS 3 times for 5min.
- Filipin staining: prepare 50ml of PBS containing 25µg/mL Filipin (Sigma, F-9765) and incubate overnight at 4°C protected from the light (for a 50ml solution, weigh 1.25mg of filipin and dissolve it in 200µl of methanol. Once dissolved, add it to the 50ml of PBS).
- Wash with PBS, 3 times for 5min.
- Mounting: use fluorescent mounting medium without DAPI (Dako, #3023). Add a small drop of mounting media to the specimen and carefully place a cover slip onto the drop, avoiding air bubbles.
- Microscope: use ultraviolet (UV) light to visualize the staining (equipment used: Olympus BX41 Microscope equipped with a Zeiss Axiocam 305 color digital camera).

10.2.2. In cells

In order to study free cholesterol levels in mitochondria from cells, we performed immunocytofluorescence with cytochrome c as a mitochondrial marker and filipin as a cholesterol marker (see section 7 for ICF).

Cholesterol-mitochondria colocalization was analyzed in the ImageJ Software using the Colocalization nBits nimages plug-in created by the advanced optical miscroscopy Unit from the *Facultat de Medicina, Universitat de Barcelona*. This plug-in software highlights the colocalized points of two images of 32-bits (one in green and one in red), and returns the integrated densities of total green (higher than the threshold) and the green from colocalized points, and total red (higher than the threshold) and the red from colocalized points. Two points are considered as colocalized if their respective intensities are strictly higher than the threshold of their channels and if their ratio of intensity is strictly higher than the ratio setting value, which have been defined at 50%. Percentage of green colocalization with red or red colocalization with green is calculated as the ratio of green colocalized points divided by total green multiplied per 100 or as the ratio of red colocalized points divided by total red multiplied per 100, respectively.

11. GSH QUANTIFICATION

Total GSH (GSH and oxidized GSH (GSSG)) levels in liver homogenate and isolated mitochondria from mice and in cellular extracts from isolated PMH or cell lines were analyzed using the enzymatic recycling method.

In this assay, the sulfhydryl group of GSH reacts with DTNB (5, 5'-dithio-bis-2-nitrobenzoic acid, Sigma, D8130) and produces a detectable yellow-colored TNB (5-thionitrobenzoic acid). The GSTNB (GSH linked to TNB) that is concomitantly produced, is reduced by GR to recycle the GSH and produce more TNB. The rate of TNB production is directly proportional to this recycling reaction, which in turn is directly proportional to the concentration of GSH in the sample. Thus, measurement of the absorbance of TNB at 412nm provides an accurate estimation of total GSH in the sample (**Figure M-8**).

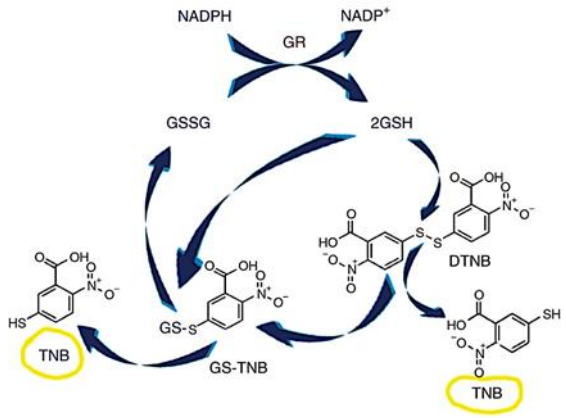

Figure M-8. Recycling assay mechanism. GSSG, oxidized GSH; GR, GSH reductase; DTNB, Ellman's reagent; TNB, 5-thionitrobenzoic acid; GSTNB, mixed disulfide GSH-TNB. Taken from (Giustarini et al., 2013).

- Samples preparation and harvesting

In order to be able to determine GSH levels, all samples need to be previously diluted 1:1 with TCA 10%-PBS, vortexed and spun down at 12000rpm for 5min at 4°C. This step allows cellular membranes disruption and release of GSH to the supernatant.

- Ellman assay

Ellman buffer (pH 8.0)	
Compound	Concentration
KH_2PO_4	0.5M
mQ-H_2O	-

Ellman reagent (pH 7.4)	
Compound	Concentration
DTNB	10mM
$Na_2HPO_4 \cdot 2H_2O$	0.1M
$NaHCO_3$	11.9mM
mQ-H_2O	-

Table M-21. Buffers for the Ellman assay. Ellman buffer can be stored at 4°C. Ellman reagent can be aliquoted and stored at -20°C. All the reagents were purchased from Sigma Aldrich.

- Prepare a 1mM GSH (Sigma, G6529) stock in PBS.
- Prepare 7 GSH standard solutions 0, 10, 20, 30, 40, 50 or 60µM in a final volume of 4ml with PBS.
- Mix in a tube: 2ml of Ellman buffer, 1ml of standard and 30µl of Ellman reagent.
- Mix thoroughly and wait 3min before reading it.
- Read in a spectrophotometer (Beckman Coulter, DU800) at an absorbance of 412nm.

The values obtained will be multiplied by 198 (coefficient of extinction of the spectrophotometer) and will represent the real concentration of the GSH standards prepared that we will use in the recycling assay as well. We will use these data to normalize the absorbance obtained in the recycling assay for the GSH standards.

- Recycling assay

0.5M $NaPO_4$ (pH 7.4)	
Compound	Concentration
$NaH_2PO_4 \cdot H_2O$	95ml, 1N
$Na_2HPO_4 \cdot 2H_2O$	405ml, 1N
mQ-H_2O	500ml

Recycling buffer (pH 7.4)	
Compound	Concentration
EDTA	1mM
DTNB	0.1mM
NADPH	0.15mM
$NaPO_4$	50mM
mQ-H_2O	-

Table M-22. Buffers for the recycling assay. Recycling buffer should be freshly prepared And it has to be protected from light. All the reagents were purchased from Sigma Aldrich.

- Prepare the Recycling buffer, protect it from the light and warm it at 37°C.
- Prepare the GR at a concentration of 10U/ml in mQ-H_2O. It will be stable a few weeks at 4°C.
- Mix in a tube: 2.5ml of recycling buffer at 37°C, 100µl of sample/standard and 100µl of GR.
- Mix by inversion.
- Read during 40sec in the spectrophotometer at an absorbance of 412 nm.

GSH concentrations will be determined referring the samples to the standard curve normalized by the Ellman assay and by protein concentration.

12. MEASUREMENT OF ROS PRODUCTION AND OXIDATIVE STRESS

12.1. DIHYDROETHIDIUM

The superoxide indicator dihydroethdium (DHE) exhibits blue-fluorescence in the cytosol. However, once this probe is oxidized to ethidium, it intercalates within DNA, staining the cell nucleus a bright fluorescent red.

Protocol:

- Prepare a 20mM DHE (ThermoFisher, D1168) stock solution in DMSO (it can be aliquoted and stored at -20°C).
- Prepare a 10µM DHE solution in Hanks balanced salt solution (HBSS) without phenol red (Invitrogen, #14025092).
- Incubate 8µm frozen liver tissue sections with 10µM DHE for 30min at RT protected from light.
- Wash slides with PBS 3 times for 2min each.
- Mount slides with Prolong gold mounting media and let them dry.
- Observe them in a fluorescence microscope (equipment used: Olympus BX41 Microscope equipped with a Zeiss Axiocam 305 color digital camera) at excitation and emission wavelengths of 518 and 606nm, respectively.

12.2. DICHLOROFLUORESCEIN

The cell-permeant 2',7'-dichlorodihydrofluorescein diacetate (H2DCFDA) is a chemically reduced form of fluorescein used as an indicator for general ROS in cells. Upon cleavage of the acetate groups by intracellular esterases and oxidation, the nonfluorescent H2DCFDA is converted to the highly fluorescent 2',7'-dichlorofluorescein (DCF). Fluorescence can then be detected by fluorescence microscopy or spectroscopy.

Protocol:

- Prepare a fresh 10mM DCF (ThermoFisher, D399) stock solution in DMSO.
- Prepare a 10µM DCF solution in culture medium.
- Incubate cultured cells with 10µM DCF solution for 30min at 37°C protected from light.
- Wash cells with PBS twice.
- Evaluate DCF fluorescence by fluorescence spectroscopy using the Tecan Fluorescence Microplate Reader (485nm for excitation and 528nm for emission).
- Normalize fluorescence by protein content determined by Bradford or BCA protein assay.

12.3. CELLROX DEEP RED REAGENT

The cell-permeable CellROX Deep Red reagent is non-fluorescent or very weakly fluorescent while in a reduced state. In contrast, its exhibits strong fluorogenic signal upon oxidation. It reliably measures ROS in live cells and the resulting fluorescence can be measured using traditional fluorescence microscopy, high-content imaging and analysis, microplate fluorometry or flow cytometry.

Protocol:

- Prepare a fresh 5µM CellROX Deep Red (Molecular Probes, C10422) solution in culture medium.
- Incubate cultured cells with 5µM CellROX Deep Red solution for 30min at 37°C protected from light.
- Wash cells with PBS twice.
- Evaluate CellROX Deep Red fluorescence by fluorescence spectroscopy using the Tecan Fluorescence Microplate Reader (640nm for excitation and 665nm for emission).
- Normalize fluorescence by protein content determined by Bradford or BCA protein assay.

12.4. PROTEIN CARBONYLATION

Protein carbonylation is a type of protein oxidation that can be promoted by ROS. Metal catalyzed oxidation of proteins introduces carbonyl groups (aldehydes and ketones) into protein side chains by a site-specific mechanism. This oxidative modification of proteins can modulate their biochemical characteristics such as enzymatic activity and the susceptibility to proteolytic degradation.

In this thesis, protein carbonylation was assessed by measuring the levels of carbonyl groups using the OxyBlot™ Protein Oxidation Detection Kit (Merck Millipore, S7150). With this method, carbonyl groups in the protein side chains are derivatized to 2,4-dinitrophenylhydrazone (DNP-hydrazone) by reaction with 2,4-dinitrophenylhydrazine (DNPH). The DNP-derivatized protein samples are then separated by polyacrylamide gel electrophoresis. After transferring proteins to a membrane filter, the membrane is incubated with primary antibody specific to the DNP moiety of the proteins. This step is followed by incubation with a HRP-antibody conjugate directed against the primary antibody, which allows detecting the amount of carbonylated proteins in the original sample.

Protocol:

- In a tube, place X µl of sample containing 15-20µg of protein.
- Denature proteins by adding X µl of a 12% SDS solution.
- Derivatize the sample by adding 2X µl of 1X DNPH Solution.
    - Additionally prepare a negative control sample by adding 2X µl of 1X Derivatization-Control Solution instead of the DNPH solution.
- Shake well and incubate the mixes for 15min at RT.
- Add 3/2X µl of Neutralization Solution to stop the reaction.
- Load derivatized samples on a 4-12% SDS-polyacrylamide gel (Bio-Rad, XT-Criterion) and perform a one-dimensional SDS-PAGE.
- Transfer proteins to a nitrocellulose membranse using the Trans-Blot Turbo™ Transfer System (Bio-Rad).
- Block membrane for 1h with 1% BSA in TBST at RT.
- Incubate membrane with the primary antibody solution anti-DNP for 1h at RT.
- Wash membrane at least 3 times for 10min with TBST to wash out unspecific binding.
- Incubate membrane with secondary antibody solution anti-Rabbit for 1h at RT.
- Wash membrane with TBST.
- Develop the antibody protein detection using Pierce™ ECL Western Blotting Substrate and the instrument LAS4000 (GE Healtcare).
- Analyze optical density of bans with ImageJ software.

13. MTT ASSAY

For cell viability analysis, cells were incubated with 1.2mM Thiazolyl Blue Tetrazolium Bromide (MTT) (Sigma, M2128) solution for 30 minutes at 37°C in dark. Medium was subsequently

aspirated and cells were resuspended in 1-propanol and evaluated by fluorescence spectroscopy (570nm for formazan and 630nm as background). Viability was finally calculated as absorbance (570-630) x 100 / absorbance control (570-630).

14. PROTEIN EXPRESSION ANALYSIS

14.1. HOMOGENIZATION AND LYSIS

Buffers:

RIPA lysis buffer (pH 8.0)	
Compound	Concentration
NaCl	150mM
IGEPAL	1%
Sodium deoxycholate	0.5%
SDS	0.1%
Tris-HCl	50mM
Protease inhibitor (cOmplete™ Mini, Roche)	
Phosphatase inhibitor (PhosSTOP™, Roche)	

Table M-23. RIPA lysis buffer.

Protocol:

- Dilute the total liver homogenate and mouse liver isolated mitochondria 4 times with RIPA lysis buffer.
- Incubate the samples for 15 min at 4°C vortexing them from time to time.
- Spin down for 5 min at 10000 rpms at 4°C.
- Collect the supernatant avoiding contamination from pellet and upper lipidic phase.

14.2. PROTEIN QUANTIFICATION

Lysates were quantified for protein concentration using Bradford or bicinchoninic acid (BCA) protein assays. Bradford assay is a protein determination method that involves the binding of Coomassie Brilliant Blue G-250 dye to proteins that is detectable at an absorbance of 595nm. There are certain chemical-protein or chemical-dye interactions that may interfere with Bradford assay. In our case, it is important to always dilute the RIPA buffer at least 4 times to dilute the IGEPAL below 0.25%. The BCA Protein Assay combines the well-known reduction of Cu^{2+} to Cu^{1+} by protein in an alkaline medium with the highly sensitive and selective colorimetric detection of the cuprous cation (Cu^{1+}) by bicinchoninic acid.

Bradford assay protocol:

- Prepare BSA standard points to build a standard curve (e.g. 0, 0.1, 0.2, 0.3, 0.4 and 0.5mg/ml) in PBS.
- Dilute lysates in PBS to fit in the standard curve.
- Perform the assay in a 96-well plate in triplicates.
- Add 4µl of the diluted sample or BSA standard per well.
- Using a multichannel pipette add 200µl of Quick Start Bradford Protein Assay (Bio-rad, 500-0201).
- Incubate at RT for at least 20min. Samples should not be incubated longer than 1h at RT.
- Set the spectrophotometer plate reader to 595nm. Measure the absorbance of the standards, blanks, and unknown samples.
- Samples will be referred to the BSA standard curve and they will be assigned a protein concentration.

BCA assay protocol:

- Prepare BSA standard points to build a standard curve (e.g. 0, 0.1, 0.2, 0.3, 0.4 and 0.5mg/ml) in PBS.
- Dilute lysates in PBS to fit in the standard curve.
- Perform the assay in a 96-well plate in triplicates.
- Add 8µl of the diluted sample or BSA standard per well.
- Using a multichannel pipette add 80µl of BCA working reagent (50 parts of BCA Reagent A with 1 part of BCA Reagent B (50:1, Reagent A:B)) (ThermoFisher Scientific, 23225).
- Incubate at 37°C for at least 30min.
- Set the spectrophotometer plate reader to 562nm. Measure the absorbance of the standards, blanks, and unknown samples.
- Samples will be referred to the BSA standard curve and they will be assigned a protein concentration.

14.3. SAMPLE PREPARATION FOR ELECTROPHORESIS

To be able to separate the proteins in a polyacrylamide gel, samples are mixed with a loading buffer to ensure protein stability and weight when loading them into the wells.

Protocol:

- Bring all samples to the same protein concentration so we can load 20-50µg of protein per well in a volume of 15-40µl. Adjust the volumes with mQ-H_2O.
- Add 1/4 of the volume of loading buffer XT Sample Buffer 4x (Bio-Rad, 161-0791) with 0.05% of β-mercaptoethanol and vortex.
- Boil the samples for 5min at 95°C.
- Allow samples to cool down.
- Vortex and spin down.

As a protein standard marker for protein electrophoresis we used Novex Sharp Prestained Protein Standard (Invitrogen, LC5800).

14.4. WESTERN BLOTTING

In this thesis we used sodium dodecyl sulphate polyacrylamide gel electrophoresis (SDS-PAGE) to separate proteins from samples. This technique allows separation of proteins according to their electrophoretic mobility, a function of the length of the polypeptide chain and its charge. SDS is an anionic detergent that linearizes proteins and confers them a negative charge. The binding of SDS to the polypeptide chain imparts an even distribution of charge per unit mass, thereby resulting in a fractionation by approximate size during electrophoresis. After the SDS-PAGE, separated proteins in the gel are electrotransfered into a nitrocellulose membrane and specifically detected on the surface of the membrane with antibodies.

Buffers:

- Running buffer: depending on the size of the protein to be detected we used:
    - 20x XT MES Running Buffer (Bio-rad, 161-0789), to resolve low molecular weight proteins. Diluted in dH_2O.
    - 20x XT MOPS Running Buffer (Bio-rad, 161-0788), to resolve high molecular weight proteins. Diluted in dH_2O.
- Electrotransfer buffer: prepare the buffer and cool it down to 4°C. For 1 liter: 200ml of Trans-Blot® Turbo™ 5X Transfer Buffer, 200ml of absolute ethanol and 600ml of dH_2O.
- TBST: Tris Buffered Saline with Tween® 20, pH 8.0 (T9039, Sigma). Contents of one pouch when dissolved in 1 liter of dH_2O will yield 0.05M Tris buffered saline (NaCl 0.138M; KCl 0.0027M), Tween® 20 0.05%, pH 8.0, at 25°C. We complement it with 5ml of 10% Tween® 20

solution (Bio-Rad) per liter to reach a final concentration of 0.1%. The buffer is used to wash, block and incubate the membranes with the antibodies.

Protocol electrophoresis:

- Load 20-50µg of protein into the 4-12% SDS-polyacrylamide gel (Bio-Rad).
- Electrophoresis system: Criterion Cell (Bio-Rad) vertical midi format electrophoresis cell and Power Pac Basic Power Supply (Bio-Rad).
- Start the electrophoresis at 50V until the samples are together in a front line and then increase the voltage up to 100V until the protein of interest is well resolved (check protein standard for an approximate molecular weight).

Protocol transfer:

- Stack in the following order forming a sandwich, making sure that no bubbles remain between layers: Whatman paper - Gel - Nitrocellulose membrane - Whatman paper.
- Perform the transfer in a Trans-Blot Turbo™ Transfer System (Bio-Rad).

Blocking: to avoid unspecific binding of antibodies, empty membrane areas were blocked for 1h with 5% BSA (Sigma Aldrich) TBST or 5% milk at RT in a small container on an orbital shaker.

14.5. IMMUNODETECTION

Membranes were incubated with primary antibodies overnight at 4°C and shaking. Different buffers and antibodies were used (**Table M-24**).

After the overnight incubation:

- Wash at least 3 times for 10min with TBST to wash out unspecific binding.
- Incubate membranes with the corresponding HRP-conjugated secondary antibodies in TBST (**Table M-25**).
- Wash at least 3 times for 10min with TBST.

Antibody	Host	Dilution	Buffer	Reference	Company
ACDase	Rb	1:1000	1% BSA-TBST	SAB3500293	Sigma Aldrich
β-Actin-HRP	Mo	1:10000	TBST	A3854	Sigma Aldrich
BIP	Rb	1:1000	1% BSA-TBST	SPA826	Stressgen
CHOP	Mo	1:1000	1% BSA-TBST	2895S	Cell Signaling
COXIV	Rb	1:1000	1% BSA-TBST	4844S	Cell Signaling
CYP2E1	Rb	1:1000	5% BSA-TBST	ab28146	Abcam
CYP2F2	Mo	1:1000	1% BSA-TBST	sc374540	SCBT
DIC	Rb	1:1000	1% BSA-TBST	ab32632	Abcam
E-Cadherin	Rat	1:500	1% BSA-TBST	sc59778	SCBT
EIF2α	Rb	1:1000	1% BSA-TBST	9722S	Cell Signaling
p-EIF2α	Rb	1:1000	1% BSA-TBST	9721S	Cell Signaling
FIS1	Rb	1:1000	1% BSA-TBST	ab71498	Abcam
GLUL	Rb	1:1000	5% BSA-TBST	ab73593	Abcam
HIF2α	Rb	1:1000	1% BSA-TBST	ab109616	Abcam
4HNE	Rb	1:1000	5% Milk+0,5% BSA-TBST	ab46545	Abcam
MitoProfile® Total OXPHOS Rodent WB Antibody Cocktail	Mo	1:500	1% BSA-TBST	ab110413	Abcam
MLN64	Rb	1:1000	1% BSA-TBST	sc292868	SCBT
OPA1	Rb	1:1000	1% BSA-TBST	ab42364	Abcam
PDI	Rb	1:1000	1% BSA-TBST	2446S	Cell Signaling
Porin	Mo	1:1000	1% BSA-TBST	MABN504	Merck Millipore
StARD1	Rb	1:1000	1% BSA-TBST	8449S	Cell Signaling
StARD1	Mo	1:1000	1% BSA-TBST	ab58013	Abcam
TOM20	Rb	1:1000	1% BSA-TBST	sc11415	SCBT
XBP1	Mo	1:1000	1% BSA-TBST	SC-8015	SCBT

Table M-24. Primary antibodies used. HRP, horseradish peroxidase conjugated. P, phospho. Rb, rabbit. Mo, mouse. SCBT, Santa Cruz Biotechnology.

Antibody	Host	Dilution	Buffer	Reference	Company
anti-rabbit-HRP	Goat	1:20000	TBST	A0545	Sigma Aldrich
anti-mouse-HRP	Rb	1:20000	TBST	A9044	Sigma Aldrich
anti-rat-HRP	Goat	1:20000	TBST	629520	Invitrogen

Table M-25. Secondary antibodies used. HRP, horseradish peroxidase conjugated. Rb, rabbit.

14.6. DEVELOPMENT, IMAGE CAPTURING AND ANALYSIS

Some primary and all secondary antibodies used are conjugated with HRP. To develop the antibody protein detection we used a peroxidase substrate for enhanced chemiluminescence (ECL Western Blotting Substrate, Thermo Scientific, 32106).

Protocol:

- Reagent 1 (Luminol) and reagent 2 (peroxide) must be at RT.
- Mix in a falcon tube, 1:1 volume of both reagents.
- Apply the on top of the membrane and make sure it is evenly spread.
- Incubate for 2min at RT.
- Remove excess liquid.
- Digitally capture images with the image capturing instrument LAS4000 (GE Healthcare).
- Analyze images with ImageJ software to quantify pixels density of the bands.

15. GENE EXPRESSION ANALYSIS

15.1. mRNA ISOLATION AND QUANTIFICATION

To isolate messenger RNA (mRNA) we used a TRIzol-chloroform extraction (Invitrogen). TRIzol Reagent is a monophasic solution of phenol, guanidine isothiocyanate and other proprietary components, which facilitate the isolation of a variety of RNA species of large or small molecular size. It maintains the integrity of the RNA due to highly effective inhibition of RNase activity while disrupting cells and dissolving cell components during sample homogenization. After homogenizing the sample with TRIzol, chloroform is added, and the homogenate is allowed to separate into a clear upper aqueous layer containing RNA, an interphase, and a red lower organic layer containing the DNA and proteins. Finally, RNA is precipitated from the aqueous layer with isopropanol.

RNA is very sensitive to nucleases. Thus, all material must be autoclaved and all the solutions and organic solvents need to be molecular biology graded, free of DNases and RNase.

Sample homogenization:

- Liver tissue: use 1ml of TRIzol per every 25-50mg of tissue and homogenate with a manual pestle.
- Cultured cells: add approximately 0.5ml of TRIzol per vessel with 500000 cultured cells. Collect cells using a cell scraper and transfer the cellular suspension to an autoclaved tube.

RNA isolation:

- Incubate the homogenized sample for 5min at RT to allow complete dissociation of the nucleoprotein complex.
- Add 0.2ml of chloroform per 1ml of TRIzol used for homogenization.
- Shake tube vigorously by hand for 15sec.

- Incubate for 2-3min at RT.
- Centrifuge the sample at 12000xg for 15min at 4°C. The mixture separates into a lower red phenol-chloroform phase, an interphase, and a colorless upper aqueous phase. RNA remains exclusively in the upper aqueous phase, which is around 50% of the total volume.
- Remove the aqueous phase of the sample by angling the tube 45° and pipetting the solution out. Avoid drawing any of the interphase or organic layer into the pipette when removing the aqueous phase.
- Place the aqueous phase into a new autoclaved tube and proceed to the RNA Isolation Procedure.

RNA precipitation:

- Add 0.5ml of 100% isopropanol to the collected aqueous phase, per each 1ml of TRIzol used for homogenization and mix by inversion.
- Incubate for 10min at RT.
- Centrifuge at 12000xg for 10min at 4°C.

RNA wash:

- Remove supernatant from the tube, leaving only the RNA pellet.
- Wash the pellet with 1ml of 75% ethanol in RNase free water at -20°C per each 1ml of TRIzol Reagent used in the initial homogenization. From this point, the RNA can be stored in 75% ethanol at least 1 year at -20°C, or at least 1 week at 4°C.
- Vortex the sample briefly and then centrifuge the tube at 7500xg for 5min at 4°C.
- Discard the wash.
- Air-dry the RNA pellet for 5-10min. Do not allow the RNA to dry completely, because the pellet can lose solubility. Partially dissolved RNA samples have an A260/280 ratio <1.6.

RNA resuspension:

- Resuspend the RNA pellet in RNase-free water by passing the solution up and down several times through a pipette tip.
- Incubate samples at least 30min at 4°C to allow complete RNA resuspension.

RNA quantification:

- Load 2µl of resuspended mRNA onto the NanoDrop spectrophotometer (Thermo Scientific, NanoDrop 1000).
- Measure the sample absorbance at 260nm and 280nm to calculate nucleic acid concentration (260nm) and the purity of the sample (260/280 ratio between 1.7-2.0).

15.2. cDNA SYNTHESIS

Complementary DNA (cDNA) synthesis transforms the isolated mRNA into cDNA, which is a more stable product. This conversion is carried out by a reverse transcriptase (RT) and random primers that bind to non-specific points along the RNA template. The resulting cDNA can be used as a template for a standard PCR.

Protocol:

- Prepare the RNA samples at a concentration of 0.125µg/µl with RNase-free water.
- Prepare the cDNA synthesis reaction mix (SensiFAST™ cDNA Synthesis Kit, BIO-65054). See **Table M-26** below for one reaction.

	X1 (µl)
5X TransAmp Buffer	4
Reverse Transcriptase	1
0.125µg/µl RNA	8
RNase-free water	7
Vf	20µl

Table M-26. cDNA synthesis reaction mix.

- Mix gently by pipetting.
- Run the following protocol in a thermal cycler (ECOGEN, G-Storm): 10min at 25°C, 15min at 42°C, 15min at 48°C, 5min at 85°C, hold 4°C.

15.3. REAL-TIME PCR

Real-time polymerase chain reaction (RT-PCR) technique is a refinement of the original PCR, which is used to amplify nucleic acids in a cyclic process to generate a large number of identical copies. In RT-PCR, the amount of product formed is monitored during the course of the reaction by recording the fluorescence of dyes or probes introduced into the reaction, which is proportional to the amount of product formed, and the number of amplification cycles required to obtain a particular amount of DNA molecules is registered. Assuming a certain amplification efficiency, which typically is close to a doubling of the number of molecules per amplification cycle, it is possible to calculate the number of DNA molecules of the amplified sequence that were initially present in the sample (Kubista et al., 2006).

One important step in relative quantization is the selection of an endogenous control (housekeeping gene) since normalization to the housekeeping gene allows correcting results that

can be skewed by differing amounts of input nucleic acid template. Any gene expressed at the same level in all study samples can potentially be used as an endogenous control. We used β-Actin and β-2-microglobulin (B2M) as endogenous controls.

In this doctoral thesis RT-PCR was performed using the SensiFAST™ SYBR® No-ROX Kit (Bioline, BIO-98020) following the manufacturer's instructions.

Protocol:

- Dilute cDNA synthesis reaction product 1/2 in RNase-free water ($Conc_{final}$ = 25ng cDNA/µl).
- From the 25ng cDNA/µl solution, make a 1/5 dilution to perform the RT-PCR ($Conc_{final}$ = 5ng cDNA/µl).
- Prepare as many RT-PCR mixes as number of genes to check (**Table M-27**). The volume of mix to prepare depends on the number of samples and replicates to be analyzed.

	X1 (µl)
FW Primer 50µM	0.25
RV Primer 50µM	0.25
Sensifast SYBR 2X Bioline	6.25
5ng/µl cDNA	2
RNase-free water	3.75
Vf	12.5µl

Table M-27. RT-PCR mix.

- Load the RT-PCR plate, cover the plate with film and seal it properly.
- Spin the plate down.
- Perform the PCR run following the indicated PCR protocol in a CFX384 Real-Time PCR Detection System (Bio-Rad) (**Table M-28**):

	Time	Temperature	Repetitions
Step 1	2min	95°C	-
Step 2	5sec	95°C	x40 cycles
	10sec	60°C	
	20sec	72°C	
Step 3	1min	95°C	-
Step 4	10sec	10°C	x81 cycles

Table M-28. RT-PCR protocol.

Results were analyzed using the relative quantification method ΔΔCt. The Cycle Threshold (Ct) is defined as the number of cycles required for the fluorescent signal to cross the threshold (e.g.

exceeds background level). Ct levels are inversely proportional to the amount of target nucleic acid in the sample so, the lower the Ct level, the greater the amount of target nucleic acid in the sample. The ΔΔCT method uses arithmetic formulas to achieve the result for relative quantization. The amount of target, normalized to the housekeeping gene and relative to a calibrator (or control experimental group), is given by:

$$\text{Gene expression} = 2^{-(\Delta\Delta Ct)}$$

Where ΔΔCt stands for: $\Delta\Delta Ct = \Delta Ct_{experiment} - \Delta Ct_{control}$

and ΔCt stands for: $\Delta Ct = Ct_{gene\ "X"} - Ct_{Housekeeping\ gene}$

15.4. RT-PCR PRIMERS

The primer sequences (Invitrogen) used to determine the expression of different genes are described in **Table M-29**.

Gene	Accession #	Forward primer (5'-3')	Reverse primer (5'-3')
Srebp2	NM_033218	TGAAGGACTTAGTCATGGGGAC	CGCAGCTTGTGATTGACCT
Hmgcr	NM_008255	GAAGAAGTAGGCCCCCAATC	CACCTCTCCGTGGGTTAAAA
Stard1	NM_011485	ATGTTCCTCGCTACGTTCAAG	CCCAGTGCTCTCCAGTTGAG
Mln64	NM_021547	CTCCAAGTCACAGGCCAGAT	GCTGAGGCAGGAAGAGTGG
Cyp27a1	NM_024264	ACTTGCCCTCCTGTCTCATC	CTATGTGCTGCACTTGCCC
Cyp7a1	NM_007824	GCTGTCCGGATATTCAAGGA	AGCTCAGCTCTGGAGGGAAT
Cyp7b1	NM_007825	CATGCCAAGATAAGGAAGCC	TCCTAGGCCTTCTCTTTGCC
Cyp8b1	NM_010012	CGGAACTTCCTGAACAGCTC	TGGCCTCTTTCACTTCTGCT
GFP	L29345	CAGGAGCGCACCATCTTCTT	CTTGTGCCCCAGGATGTTG
ASAH1 (ACDase)	NM_177924.5	AGTTGCGTCGCCTTAGTCCT	TGCACCTCTGTACGTTGGTC
ACTB	NM_001101.5	TTGCCGACAGGATGCAGAA	GCCGATCCACACGGAGTACT
B2M	NM_009735	TTCAGTATGTTCGGCTTCCC	CCTGGTCTTTCTGGTGCTTG

Table M-29. Primers used in RT-PCR.

16. STATISTICS

Statistical analyses has been performed using GraphPad Prism 6 (Graphpad Software Inc). Unpaired Student's t-test (two tailed) has been performed between two groups, and one or two-way ANOVA followed by Tukey's Multiple Comparison test for statistical comparisons between three or more groups. $P<0.05$ has been considered statistically significant. Results are expressed as mean ± standard error of the mean (SEM). The corresponding number of experiments are indicated in the figure legends.

RESULTS

1. STUDY I. CHOLESTEROL ENRICHMENT IN LIVER MITOCHONDRIA ALTERS MITOCHONDRIAL MORPHOLOGY, IMPAIRS OXIDATIVE PHOSPHORYLATION AND DISRUPTS THE ASSEMBLY OF RESPIRATORY SUPERCOMPLEXES.

1.1. HC DIET ALTERS HEPATIC CHOLESTEROL HOMEOSTASIS WHILE SODIUM CHOLATE FEEDING REPRESSES BILE ACID SYNTHESIS

Although feeding a HC diet supplemented with sodium cholate has been previously used as a nutritional approach to gradually increase liver cholesterol content (Domínguez-Pérez et al., 2019; Marí et al., 2006), the contribution of sodium cholate in the regulation of cholesterol homeostasis in relationship with bile acid synthesis has not been previously examined. Thus, we first characterized the regulation of hepatic cholesterol homeostasis and whether dietary cholesterol feeding in the presence of sodium cholate was channeled for bile acids generation.

8 week old male WT C57BL/6J mice fed 2 days with HC diet presented increased cholesterol levels in serum (**Figure R-1A**) and in liver (**Figure R-1B,C)**, as determined by HPLC analyses or upon staining of liver sections with filipin to detect free cholesterol levels. However, feeding sodium cholate (0.5%) for two days did not significantly increase serum or liver cholesterol levels (**Figure R-1A-C**). Moreover, the increase of liver cholesterol levels following HC feeding translated in decreased expression of key steps involved in *de novo* cholesterol biosynthesis, such as Srebp2 (**Figure R-1D**), a transcription factor that regulates cholesterol biosynthesis, and its target gene Hmgcr (**Figure R-1E**), which catalyzes the rate-limiting step in the mevalonate pathway.

As cholesterol is a precursor for bile acids synthesis, we next examined the expression of enzymes involved in the classical (Cyp7a1, Cyp8b1) and the alternative pathway of bile acid synthesis in mitochondria (Cyp27a1, Cyp7b1) (**Figure R-2A**). While HC feeding markedly decreased the expression of *Cyp7a1* as well as *Cyp8b1*, this effect was primarily due to the presence of sodium cholate in the diet (**Figure R-2B**). HC or sodium cholate feeding, however, exerted a modest effect in the expression of *Cyp27a1* and *Cyp7b1*, indicating a minor impact in the alternate pathway of mitochondrial bile acid synthesis. Consistent with these findings, HC feeding did not stimulate the net increase in the total bile acid pool in the liver, likely reflecting the repression by sodium cholate of the enzymes involved in bile acid synthesis (**Figure R-2C**). Thus, these findings indicate that the presence of sodium cholate in the HC diet contributes to the maintenance of free cholesterol levels, in part, by suppressing its metabolism into bile acid.

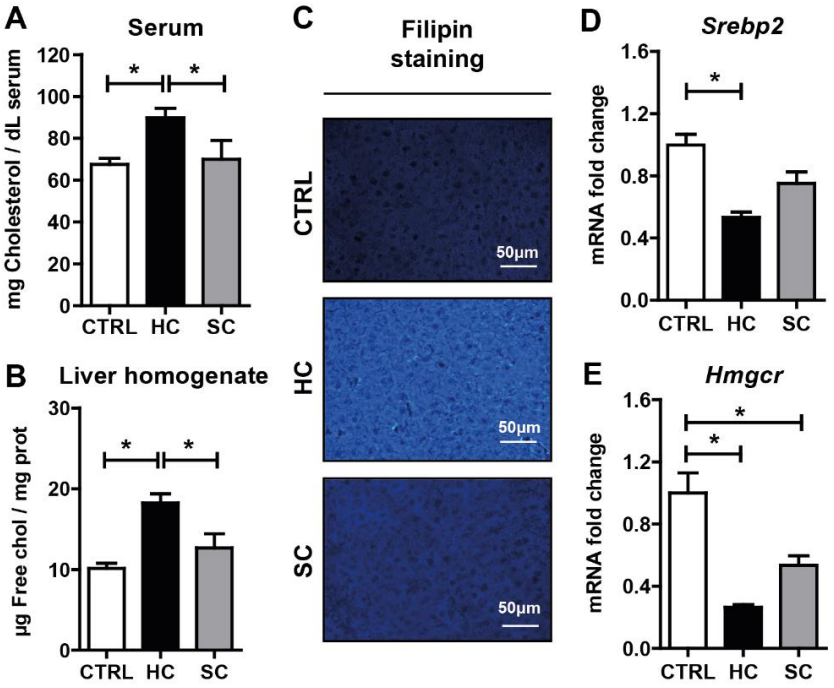

Figure R-1. Alteration of hepatic cholesterol homeostasis by HC feeding. Cholesterol levels in (A) Serum and (B) Liver of WT C57BL/6J mice fed a CTRL, HC or SC (sodium cholate) diet for 2 days. Data are presented as mean ± SEM (N>10, *P<0.05, One-way ANOVA followed by Tukey's Multiple Comparison test). (C) Cholesterol content in liver by Filipin staining in liver cryosections. Representative images obtained by fluorescence microscopy. (D,E) mRNA levels of Srebp2 and Hmgcr in liver. Values are the mean ± SEM of >10 animals per group. *P<0.05.

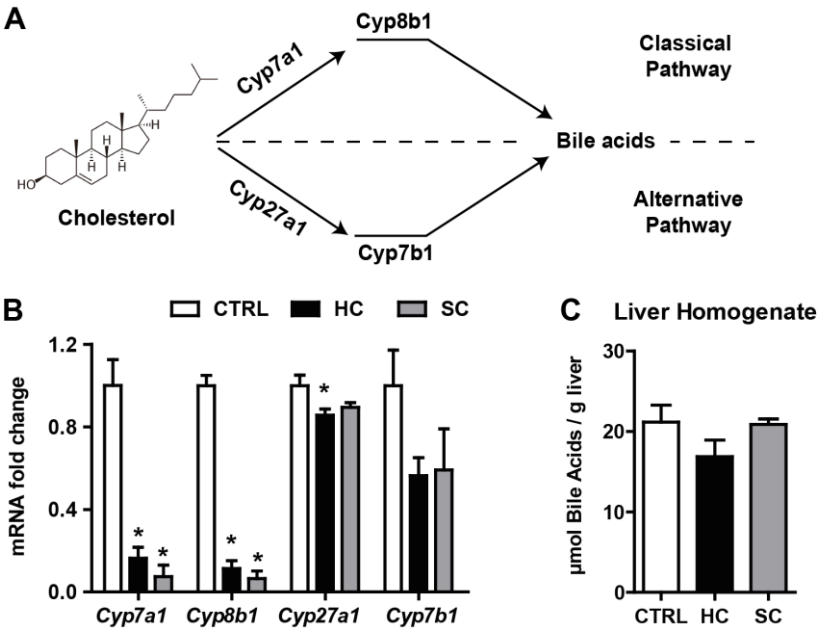

Figure R-2. Alteration of hepatic bile acid synthesis by HC feeding. (A) Diagram of classical and alternative pathways of bile acid synthesis in liver. (B) mRNA levels of Cyp7a1, Cyp8b1, Cyp27a1 and Cyp7b1 in liver. Values are the mean ± SEM of >10 animals per group. *P<0.05 vs. CTRL samples. (C) Bile acids levels in liver. Data are presented as means ± SEM (N>5, *P<0.05, One-way ANOVA followed by Tukey's Multiple Comparison test).

1.2. HC-INDUCED mCHOLESTEROL LOADING DISTRIBUTES IN BOTH MITOCHONDRIAL MEMBRANES AND DISRUPTS MITOCHONDRIAL MORPHOLOGY

Since HC feeding has been shown to increase mCholesterol content (Domínguez-Pérez et al., 2019; Marí et al., 2006), we next examined the expression of putative mCholesterol carriers and the distribution of cholesterol between the outer and inner mitochondrial membranes. Confirming previous findings in rat liver mitochondria (Marí et al., 2006), isolated mitochondria from WT HC-fed mice exhibited a significant increase in free cholesterol levels (>2-fold) determined by HPLC analyses compared to mitochondria from control mice (**Figure R-3A**). Feeding a 0.5% sodium cholate without cholesterol failed to significantly increase mCholesterol levels (5.7 ± 0.7µg free cholesterol/mg protein). The increase in mCholesterol was also observed by confocal imaging of primary mouse hepatocytes (PMH) isolated from HC-fed mice upon staining with filipin (free-cholesterol marker) and Tom20 (mitochondrial marker). As seen, HC feeding resulted in increased filipin staining, which colocalized with Tom20 indicating increased trafficking of free cholesterol into mitochondria (**Figure R-3B,C**). Since StARD1 and MLN64 are known to regulate mCholesterol trafficking (Balboa et al., 2017; Caron et al., 1997; Elustondo et al., 2017; Miller, 2007b), we examined their gene expression in mice fed the HC diet. As shown, StARD1 and MLN64 expression increased after HC feeding (**Figure R-3D**).

We next assessed the relative distribution of cholesterol enrichment within mitochondrial membranes. Mitoplasts were isolated from intact mitochondria after permeabilization of the outer membrane upon digitonin treatment. Mitoplasts purity was confirmed by the de-enrichment of porin and the increase in COX IV, compared to intact mitochondria that were enriched in both markers (**Figure R-4A**). While cholesterol levels in mitoplasts were lower than in intact mitochondria, the cholesterol content of mitoplasts from cholesterol-enriched mitochondria was higher than in mitoplasts from control mitochondria, indicating the enrichment of cholesterol in both outer and inner mitochondrial membranes (**Figure R-4B**).

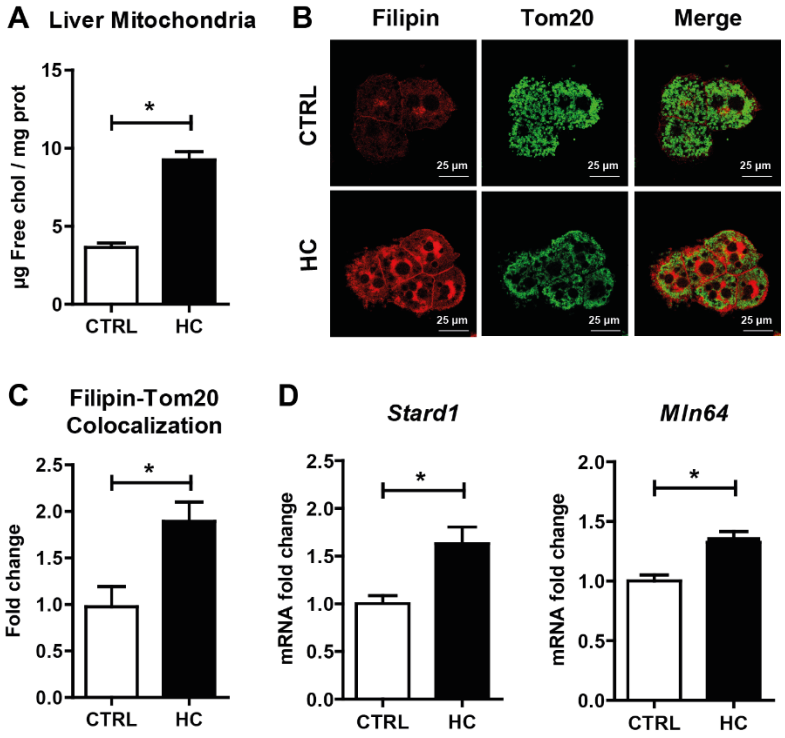

Figure R-3. Effects of HC feeding on liver mCholesterol levels. WT C57BL/6J mice were fed a CTRL or HC diet for 2 days. Cholesterol levels in mitochondria by (A) HPLC and (B) Immunocytochemistry using Tom20 and Filipin. (C) Staining markers colocalization analyzed using ImageJ software. Data are presented as means ± SEM (N>10, *P<0.05, Unpaired Student's t-test (two tailed)). (D) mRNA levels of StARD1 and MLN64 in liver. Values are the mean ± SEM of >10 animals per group. *P<0.05.

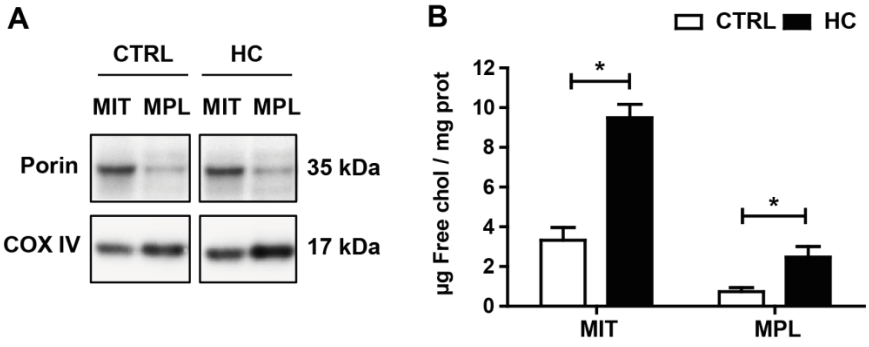

Figure R-4. Distribution of cholesterol enrichment by HC feeding within mitochondrial membranes. WT C57BL/6J mice were fed a CTRL or HC diet for 2 days. (A) Purity of mitoplasts from CTRL and cholesterol-enriched mitochondria (MIT: Mitochondria, MPL:Mitoplast). (B) Levels of cholesterol in mitochondria and mitoplasts by HPLC. Data are presented as means ± SEM (N>3, *P<0.05, Unpaired Student's t-test (two tailed)).

The increase of cholesterol in mitochondrial membranes is known to change membrane physical properties (Fernández et al., 2009a; Marí et al., 2006; Maxfield and Tabas, 2005). Thus, we next confirmed whether the presence of cholesterol in mitochondrial membrane inserted into the lipid bilayers and altered membrane fluidity. Fluorescence anisotropy analysis of mitochondria labeled with the fluorescent probe DPH revealed an increase in membrane order of mitochondria from HC-fed animals compared to control mice (**Figure R-5A**). Moreover, we next addressed whether the loss of mitochondrial fluidity by cholesterol enrichment altered mitochondrial morphology. Electron microscopy analyses revealed that mitochondria from HC-fed mice appeared rounded and with abnormal cristae compared to mitochondria from control animals (**Figure R-5B**). Although mitochondrial number was not altered by cholesterol accumulation, a significant decrease in mitochondrial length was observed (**Figure R-5C**). These findings indicate that nutritional cholesterol feeding traffics to mitochondria and alters mitochondrial membrane fluidity and morphology.

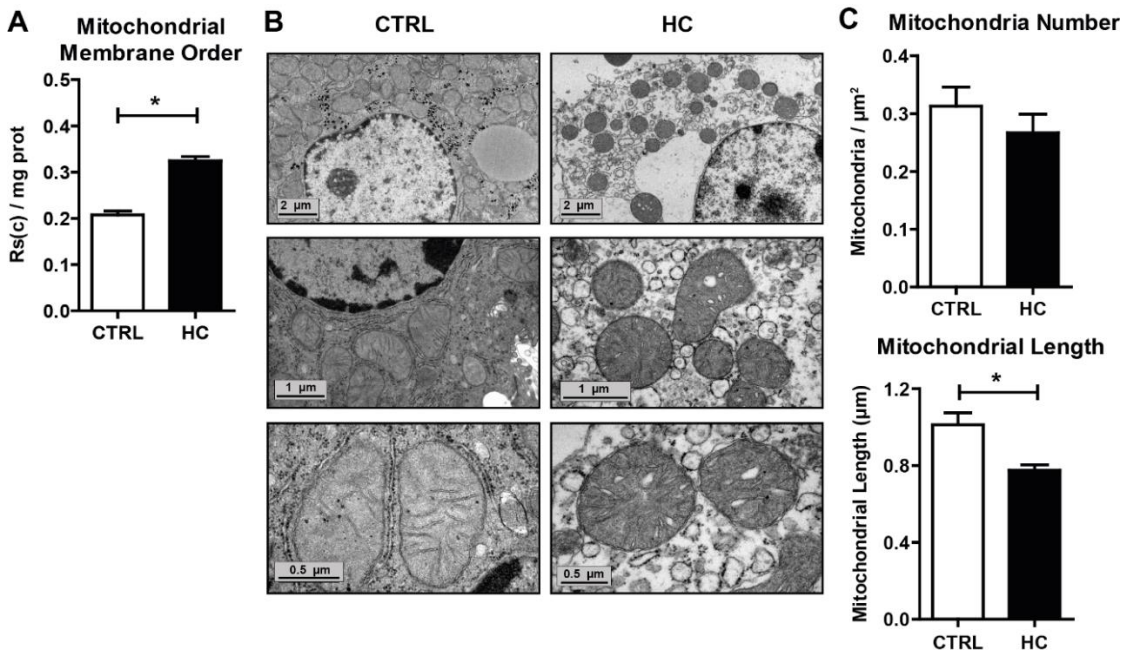

Figure R-5. Effects of HC feeding on liver mitochondrial membrane order and morphology. WT C57BL/6J mice were fed a CTRL or HC diet for 2 days. (A) Mitochondrial membrane order measured by DPH fluorescence anisotropy. (B) Electron microscopy analyses of livers from mice fed a CTRL or HC diet for 2 days. Images were acquired with a Gatan Orius digital camera by moving randomly across the EM grid and are representative of 3 replicates per group. (C) Mitochondrial number and length of liver samples quantified from images of ultrathin sections (B) and analyzed using ImageJ software. Data are presented as means ± SEM (N=3, *P<0.05, Unpaired Student's t-test (two tailed)).

1.3. mCHOLESTEROL ENRICHMENT IMPAIRS COMPLEX I AND COMPLEX II-DRIVEN STATE 3 RESPIRATION

In view of the preceding findings indicating increased cholesterol in mitochondrial membranes, we next examined the impact of this event in mitochondrial respiration, determining real-time OCR by a Seahorse flux analyzer. Using pyruvate and malate as substrates of complex I, mitochondria from HC-fed mice showed a significant reduction in mitochondrial performance and respiratory states compared to mitochondria from mice-fed CTRL diet (**Figure R-6A**). In particular, HC feeding impaired ADP-stimulated state 3 respiration as well as the FCCP-induced maximal uncoupler-stimulated respiration (state 3u) without significant change in state 4o respiration (**Figure R-6B**). These alterations were reflected in the respiratory control ratio (RCR) (state 3/state 4o) and uncoupling control ratio (UCR) (state 3u/state 4o), decreasing both in mitochondria from HC-fed mice (**Figure R-6C**).

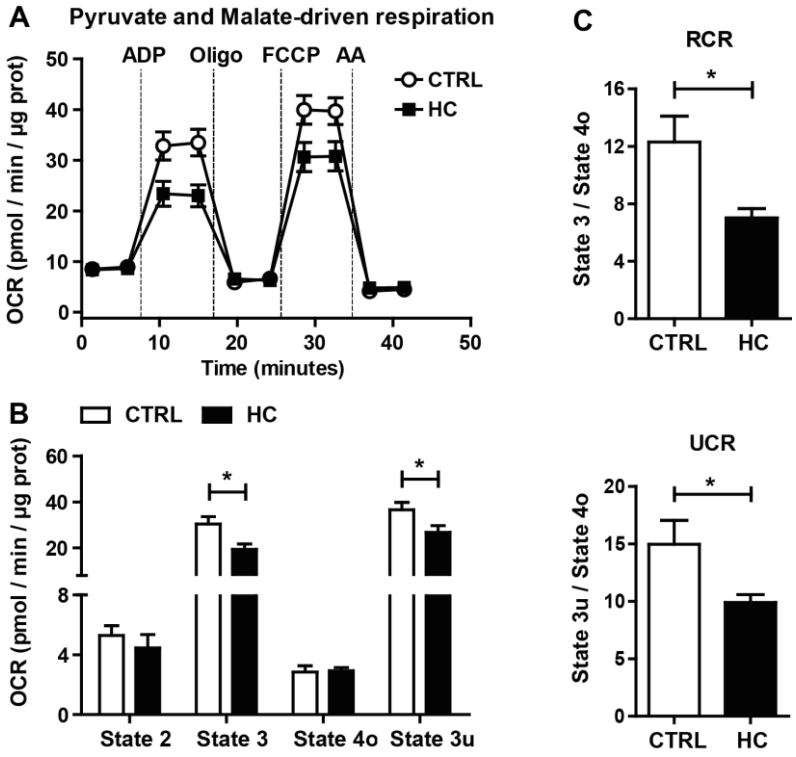

Figure R-6. Effect of cholesterol in mitochondrial OCR using pyruvate and malate as substrates. WT C57BL/6J mice were fed a CTRL or HC diet for 2 days. (A,B) Respiration of CTRL and cholesterol-enriched mitochondria using XFe24 Seahorse Analyzer. Mitochondria began in a coupled state with pyruvate and malate (10mM) present (state 2). State 3 initiated with ADP (4mM) addition, state 4 was induced with the injection of oligomycin (2.5µg/ml) (state 4o), and FCCP (4µM) induced maximal uncoupler-stimulated respiration (state 3u). Non-mitochondrial respiration was assessed by OCR measurement in the presence of AA (4µM). (C) Respiratory control ratios (RCR: state 3/state 4o, and UCR: state 3u/state 4o). Data are presented as means ± SEM (N>10, *P<0.05, Unpaired Student's t-test (two tailed)).

Similar analysis was performed using succinate plus rotenone to examine respiration through complex II. HC feeding impaired OCR from succinate plus rotenone with decreased state 3 and state 3u (**Figure R-7A,B**). In addition, HC feeding decreased succinate plus rotenone-driven state 4o respiration (**Figure R-7B**), which translated in unchanged RCR and UCR ratios (**Figure R-7C**). Thus, these findings indicate that *in vivo* mCholesterol loading significantly impairs mitochondrial complex I and complex II-driven state 3 respiration.

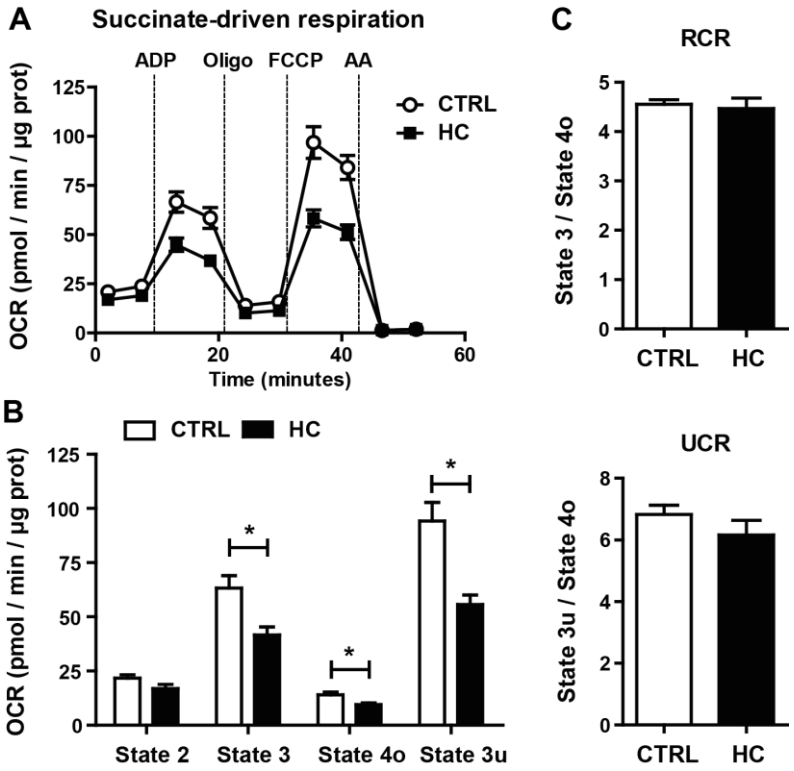

Figure R-7. Effect of cholesterol in mitochondrial respiration from succinate and rotenone. WT C57BL/6J mice were fed a CTRL or HC diet for 2 days. (A,B) Respiration of CTRL and cholesterol-enriched mitochondria using XFe24 Seahorse Analyzer. Mitochondria began in a coupled state with succinate (10mM) and rotenone (2µM) present (state 2). State 3: ADP (4mM), State 4o: Oligomycin (2.5µg/ml), State 3u: FCCP (4µM), Non-mitochondrial respiration: AA (4µM). (C) Respiratory control ratios (RCR: state 3/state 4o, and UCR: state 3u/state 4o). Data are presented as means ± SEM (N>10, *P<0.05, Unpaired Student's t-test (two tailed)).

Since the proton-motive force generated from coupled respiration determines the mitochondrial membrane potential, we next assessed the impact of mCholesterol loading in membrane potential. Incubation of PMH from HC-fed mice stained with TMRM revealed a decrease in mitochondrial membrane potential (**Figure R-8**). Overall, these findings demonstrate the deleterious effects of cholesterol enrichment on mitochondrial respiration.

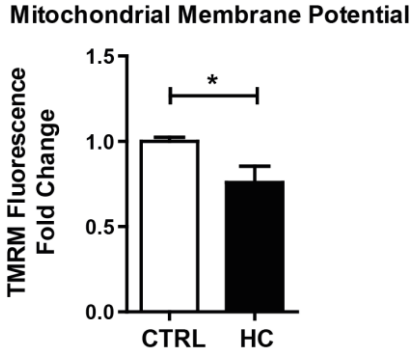

Figure R-8. Effect of cholesterol in mitochondrial membrane potential. Mitochondrial membrane potential measured by TMRM Fluorescence in a fluorescence spectroscope. Data are presented as means ± SEM (N>3, *P<0.05, Unpaired Student's t-test (two tailed)).

1.4. CHOLESTEROL-LIPID INTERACTIONS CONTRIBUTE TO DECREASED COMPLEX I-DRIVEN STATE 3 RESPIRATION

To determine whether the impairment of mitochondrial respiration by HC-induced mCholesterol loading is a direct consequence of cholesterol enrichment in mitochondrial membranes, we used an *in situ* approach in which cholesterol complexed with BSA (CBSAC) results in the enrichment of cholesterol content in both membranes (Colell et al., 2003). Compared to incubation with BSA alone, CBSAC resulted in the increase in cholesterol levels with a 4-fold increase. Real-time OCR driven by pyruvate plus malate revealed that cholesterol did not affect state 3 or state 3u respiration, although it uncoupled mitochondrial respiration as revealed by the increased state 4o respiration (**Figure R-9A**), which translated in decreased RCR and UCR (**Figure R-9B**). However, when succinate plus rotenone were used as substrates the enrichment in cholesterol did not affect succinate-driven OCR and hence RCR and UCR remained unchanged (**Figure R-9C,D**).

Since the interaction of cholesterol with membrane proteins is enantioselective but the interaction with membrane lipids is not (Li et al., 2004; Westover and Covey, 2004; Xu et al., 2005), we next enriched mitochondria with enantiomer cholesterol (Ent-CBSAC), the mirror image of natural cholesterol, as an approach to assess the contribution of the interactions between cholesterol with lipids and/or proteins in the disrupting effect of cholesterol in pyruvate and malate-driven respiration. Mitochondria enriched in Ent-CBSAC exhibited an increase in cholesterol levels similar to those found with natural CBSAC (2.5-fold compared to BSA). As CBSAC failed to alter complex II-driven respiration, we tested the role of Ent-CBSAC on complex I-induced OCR. Interestingly, Ent-CBSAC decreased pyruvate and malate-driven state 3 and state 3u respiration, which resulted in lower RCR and UCR (**Figure R-9A,B**). These *in vitro* findings suggest

that cholesterol-lipid interactions could mediate the decrease in complex I-driven state 3 and state 3u respiration.

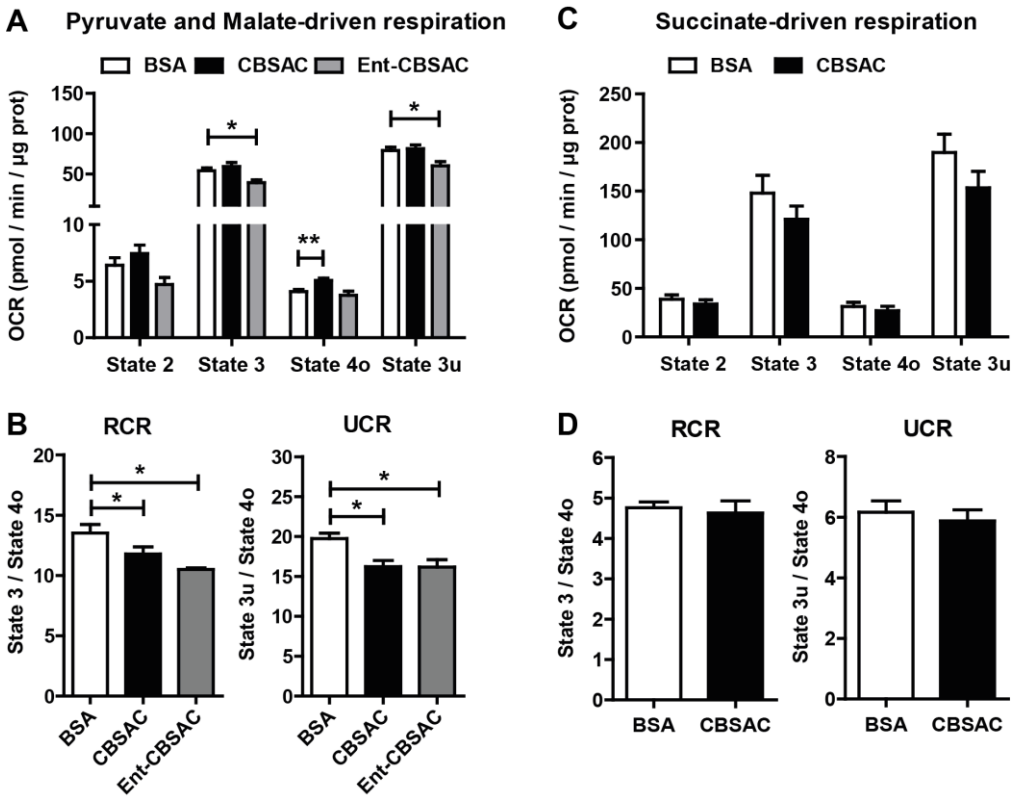

Figure R-9. Impact of *in vitro* cholesterol enrichment in mitochondrial respiration. Mitochondria from WT C57BL/6J mice fed a CTRL diet were isolated and incubated with natural cholesterol or its enantiomer complexed with BSA (CBSAC and Ent-CBSAC respectively). (A) Pyruvate and Malate-driven mitochondrial respiration. State 2: pyruvate and malate (10mM), State 3: ADP (4mM), State 4o: Oligomycin (2.5µg/ml), State 3u: FCCP (4µM), Non-mitochondrial respiration: AA (4µM). (B) Respiratory control ratios (RCR: state 3/state 4o, and UCR: state 3u/state 4o). Values are the mean ± SEM of N > 3 per group. *P < 0.05. One-way ANOVA followed by Tukey's Multiple Comparison test. (C) Succinate and Rotenone-driven mitochondrial respiration. State 2: succinate (10mM) and rotenone (2µM), State 3: ADP (4mM), State 4o: Oligomycin (2.5µg/ml), State 3u: FCCP (4µM), Non-mitochondrial respiration: AA (4µM). (D) Respiratory control ratios (RCR: state 3/state 4o, and UCR: state 3u/state 4o). Data are presented as means ± SEM (N > 3, *P < 0.05, Unpaired Student's t-test (two tailed)).

1.5. mCHOLESTEROL ENRICHMENT DISRUPTS THE ASSEMBLY OF RESPIRATORY SUPERCOMPLEXES

In view of the preceding findings, we hypothesized that mCholesterol loading *in vivo* by HC feeding may impact negatively the expression of respiratory complexes. Therefore, we first performed SDS electrophoresis to determine the expression of specific subunits of respiratory complexes. As seen, the expression of specific subunits from complex I (C-I-20), complex II (C-II-30), complex III (C-III-Core 2), complex IV (C-IV-I) and complex V (C-V-α) were unaffected by mCholesterol loading by HC feeding (**Figure R-10A,B**).

Since the structural organization of the mitochondrial respiratory complexes as independent entities connected by mobile carriers such as CoQ and cytochrome c (Cyt C) has been challenged (Acín-Pérez et al., 2008), we next hypothesized that cholesterol-mediated changes in membrane physical properties may impact the organization and assembly of supercomplexes structures, responsible for carrying out cellular respiration. Blue native electrophoresis of mitochondria after digitonin solubilization was carried out with subsequent antibody incubation against specific subunits of each respiratory complex sequentially. mCholesterol accumulation did not change the levels of respiratory complexes CI, CIV and CV but caused a significant downregulation of respiratory complex III_2 (**Figure R-10C,D**). This outcome mirrored the downregulation of supercomplexes I_1+III_2+IV and I_1+III_2 in cholesterol-enriched mitochondria (**Figure R-10C,D**). These data indicating a negative impact of cholesterol on the assembly of respiratory supercomplexes can account for the observed alterations in mitochondrial respiration and emerge as a potential molecular mechanism by which cholesterol accumulation in liver alters mitochondrial function.

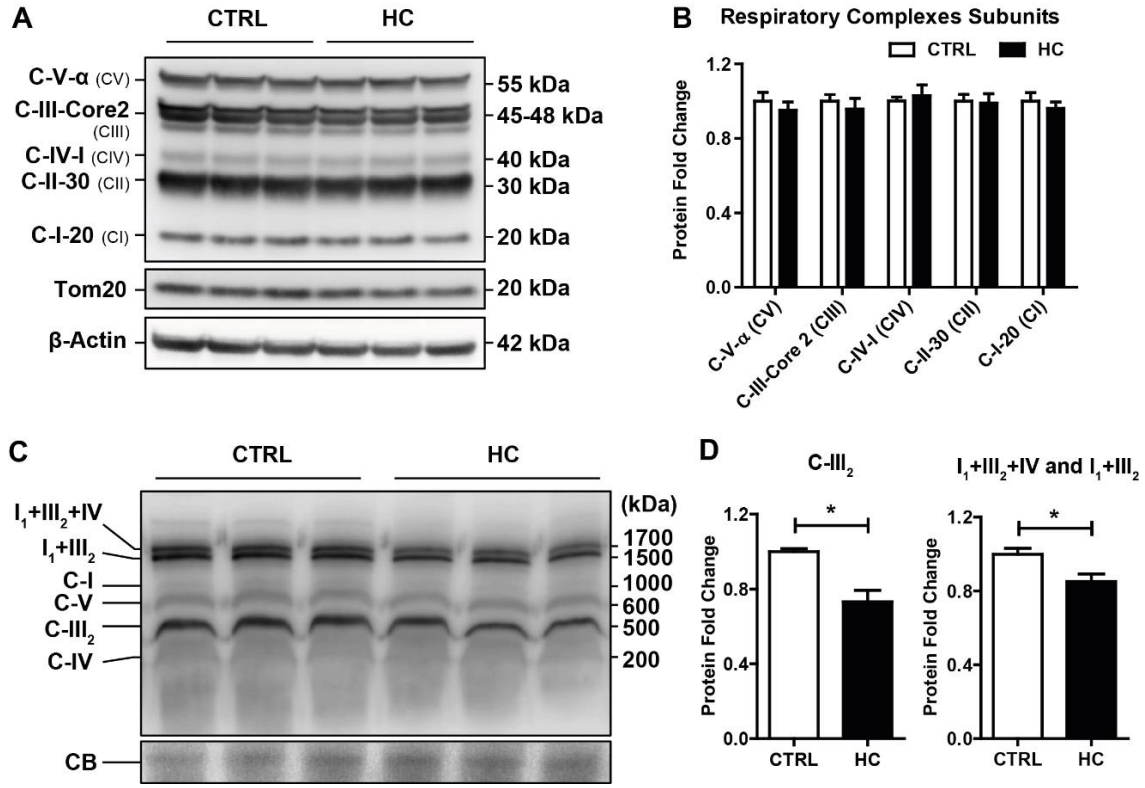

Figure R-10. Impairment of mitochondrial supercomplexes assembly by cholesterol enrichment. (A) Protein expression of mitochondrial respiratory complexes subunits from livers of WT C57BL/6J mice fed a CTRL or HC diet for 2 days. Images are representative of at least three independent experiments. (B) Protein Expression quantification of (A) by ImageJ software. Values are the mean ± SEM of >5 animals per group. *P<0.05 vs. CTRL samples. (C) Blue Native Page electrophoresis of livers from CTRL and HC mice to detect OXPHOS complexes and Supercomplexes expression. Coomassie Blue (CB) staining was used as loading control. Images are representatives of 9 replicates per group. (D) Protein Expression quantification of (C) by ImageJ software. Values are the mean ± SEM of >5 animals per group. *P<0.05. Unpaired Student's t-test (two tailed).

1.6. GSH ETHYL ESTER PROTECTS AGAINST HC-INDUCED OXIDATIVE STRESS AND LIVER INJURY

As mitochondria are the main consumers of oxygen and a major source of ROS, we next determined whether HC-induced mitochondrial dysfunction results in increased oxidative stress. As seen, staining of liver sections from HC-fed mice with DHE indicated increased generation of ROS compared to control mice (**Figure R-11A,B**). This outcome paralleled the depletion of cellular GSH levels (**Figure R-11C**) as well as the mGSH pool (**Figure R-11D**), which is primarily due to the defective transport of GSH into mitochondrial matrix (Colell et al., 1997; Fernández et al., 2009a; García-Ruiz et al., 1994). Consistent with these findings, HC feeding resulted in increased oxidative stress as shown by enhanced carbonylated proteins (**Figure R-11E**).

HC diet also induced a macroscopic change in liver color when compared to control diet. HC livers displayed a steatotic pale appearance compared to control livers (**Figure R-12A**) that paralleled oil-red staining (**Figure R-12B**). In addition, H&E staining revealed a significant dilation of liver perisinusoidal spaces after 2 days of HC feeding (**Figure R-12C**). These changes were accompanied by the release of AST and ALT in serum indicating that HC-diet induces liver injury (**Figure R-12D**).

We next explored the potential impact of total GSH and mGSH restoration by GSH ethyl ester (GSHee) in HC-fed mice. GSHee is a cell-permeable derivative of GSH that freely crosses membrane bilayers and diffuses into mitochondria resulting in mGSH replenishment. GSHee treatment of HC-fed mice restored both total and mGSH pools (**Figure R-11C,D**). Moreover, GSHee treatment decreased HC-induced DHE increase (**Figure R-11A,B**), reduced protein carbonylation (**Figure R-11E**), restored the HC-mediated dilation of liver perisinusoidal spaces (**Figure R-12C**), and decreased ALT/AST release (**Figure R-12D**), indicating that GSHee protected HC-fed mice from liver injury when compared to HC untreated mice. To assess whether the outcome of GSHee administration was accompanied by improved mitochondrial function, we examined the impact of *in vivo* GSHee administration in mitochondrial performance from pyruvate plus malate-induced OCR. Consistent with previous findings, HC feeding decreased OCR and RCR from complex I that was improved upon GSHee treatment (**Figure R-13A,B**). Moreover, GSHee restored the levels of respiratory complex III_2, although it did not affect the assembly of respiratory supercomplexes $I+III_2+IV$ and $I+III_2$ (**Figure R-13C,D**). Thus, these findings indicate that GSHee administration protects mice from HC-induced liver injury and oxidative stress in part by improving mitochondrial respiration.

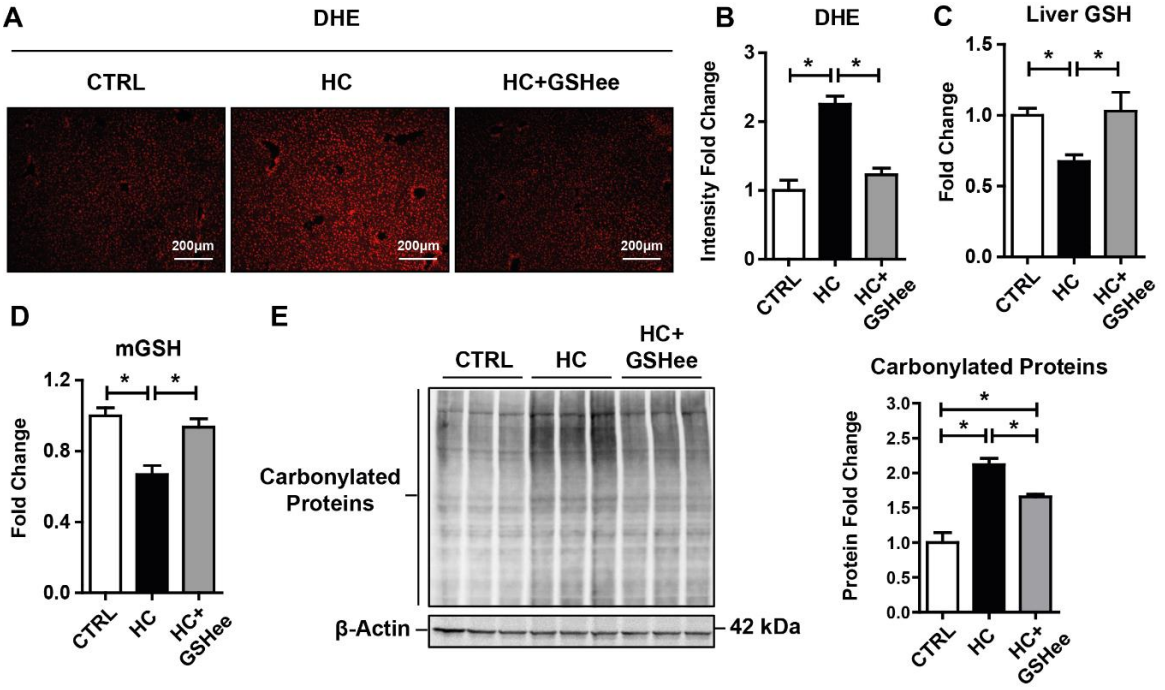

Figure R-11. Effects of GSHee treatment on HC-induced oxidative stress. (A) Reactive oxygen species content in liver tissue by DHE staining. Representative images obtained by fluorescence microscopy. (B) Fluorescence quantification of DHE intensity using ImageJ software. (C,D) GSH levels in liver and mitochondria. Values are the mean ± SEM of >5 animals per group. *P<0.05. One-way ANOVA followed by Tukey's Multiple Comparison test. (E) Carbonylated proteins from liver sections of CTRL or HC-fed mice with or without GSHee administration *in vivo*. Results are the mean ± SEM of 3 animals per group. *P<0.05. One-way ANOVA followed by Tukey's Multiple Comparison test.

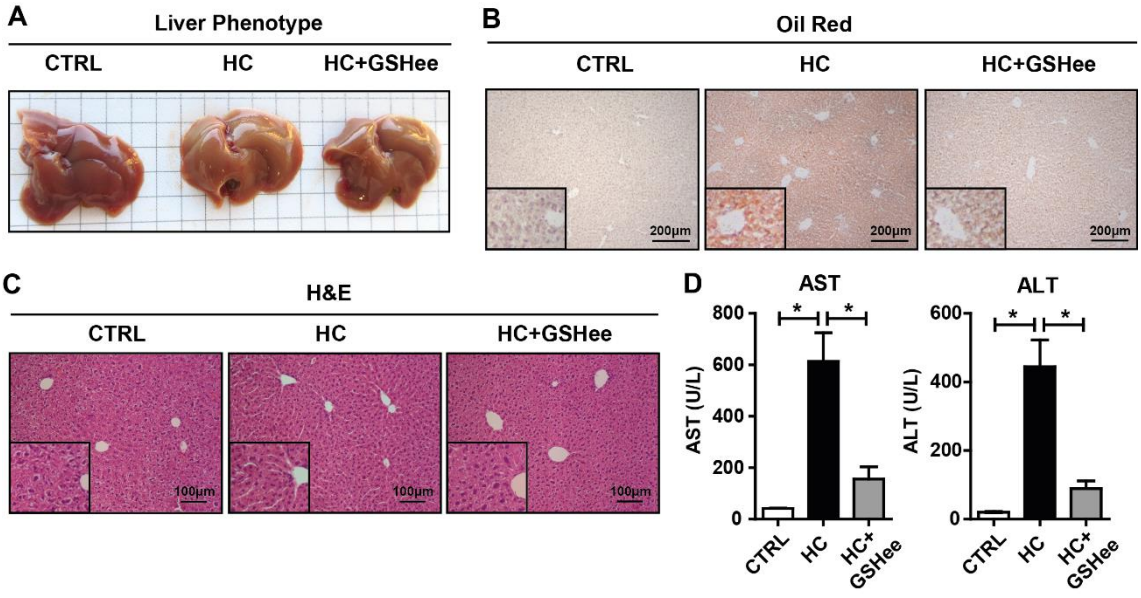

Figure R-12. Effects of GSHee treatment on HC-induced neutral lipid accumulation and liver damage. (A) Macroscopic view of liver after CTRL or HC feeding with or without GSHee treatment. Representative images of >5 replicates is shown. (B) Liver sections of CTRL, HC and HC+GSHee mice analyzed by Oil-Red staining. Representative images of >4 animals per group are shown. (C) Liver sections of CTRL, HC and HC+GSHee mice analyzed by H&E. (D) Serum AST and ALT levels from CTRL, HC and HC+GSHee mice. Data are presented as means ± SEM (N>5, *P<0.05, One-way ANOVA followed by Tukey's Multiple Comparison test).

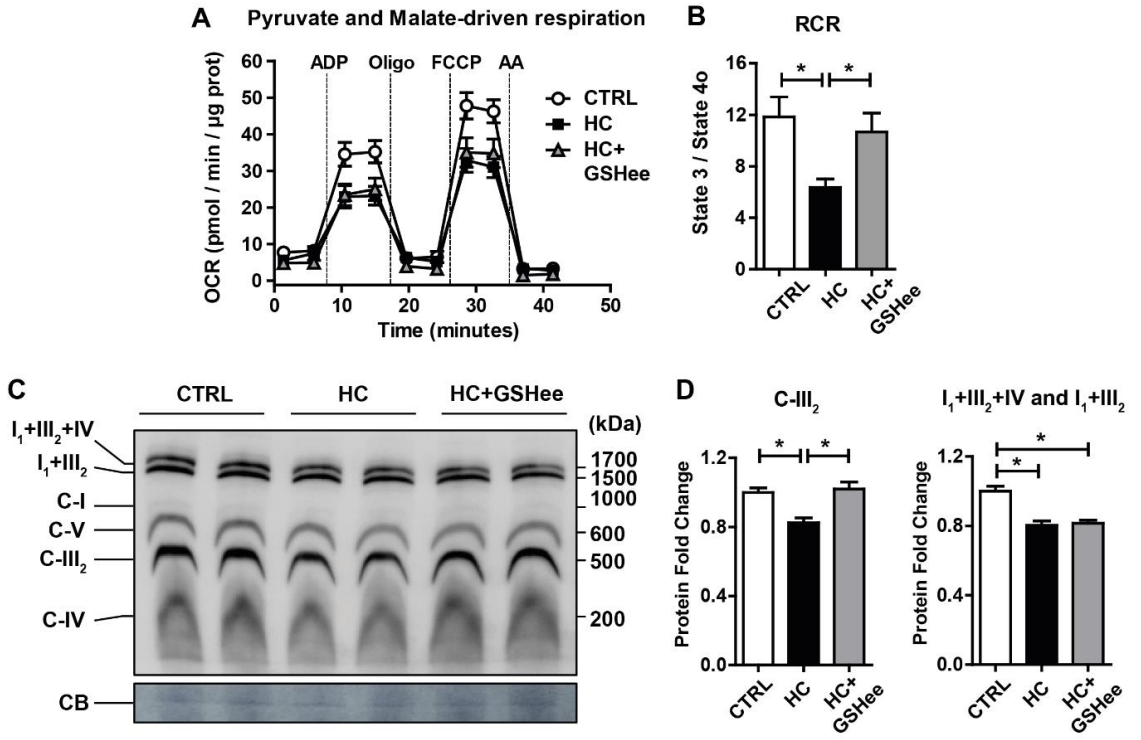

Figure R-13. Effects of GSHee treatment on HC-induced mitochondrial dysfunction. (A) Pyruvate and Malate-driven mitochondrial respiration. State 2: pyruvate and malate (10mM), State 3: ADP (4mM), State 4o: Oligomycin (2.5µg/ml), State 3u: FCCP (4µM), Non-mitochondrial respiration: AA (4µM). (B) Respiratory control ratio (RCR: state 3/state 4o) determined from OCR analyzed in I. (C) Blue Native Page electrophoresis of livers from CTRL and HC-fed mice with or without GSHee treatment to detect OXPHOS complexes and Supercomplexes expression. Coomassie Blue (CB) staining was used as loading control. Images are representatives of >5 replicates per group. (D) Protein expression quantification of (C) by ImageJ software. Values are the mean ± SEM of 8 animals per group. *P<0.05. One-way ANOVA followed by Tukey's Multiple Comparison test.

To sum up, findings from this study deeply describe the impact of mCholesterol accumulation on the function of liver mitochondria. We have shown that HC-fed mice exhibit increased expression of StARD1 and MLN64 and enhanced mitochondrial free cholesterol levels, leading to decreased membrane fluidity. Mitochondria from HC-fed mice display increased cholesterol loading in both outer and inner mitochondrial membranes. Cholesterol loading decreases complex I and complex II-driven state 3 respiration and mitochondrial membrane potential. Decreased respiratory and uncoupling control ratio from complex I is also observed after *in situ* enrichment of mouse liver mitochondria with cholesterol or enantiomer cholesterol, the mirror image of natural cholesterol. Moreover, *in vivo* cholesterol loading decreases the level of complex III_2 and the assembly of respiratory supercomplexes I_1+III_2+IV and I_1+III_2. HC feeding also causes oxidative stress and mGSH depletion, which translates in hepatic steatosis and liver injury, effects that are rescued by replenishing mGSH with GSHee. Overall, our results indicate that mCholesterol accumulation disrupts mitochondrial functional performance and the organization of respiratory supercomplexes assembly, which can contribute to oxidative stress and liver injury.

2. STUDY II. HEPATOCYTE-SPECIFIC STARD1 ABLATION PROTECTS FROM LIVER DAMAGE IN ALCOHOLIC LIVER DISEASE BY PREVENTING INCREASED MITOCHONDRIAL CHOLESTEROL AND OXIDATIVE STRESS PARTICULARY IN HEPATIC PERIVENOUS AREA

2.1. STARD1 LEVELS INCREASE UPON ETOH CONSUMPTION PREFERENTIALLY IN PV AREA

As explained in this thesis introduction, key players contributing to ALD pathogenesis include selectively impairment of antioxidant defense by glutathione depletion through mCholesterol loading. However, the mechanism through which alcohol-induced cholesterol accumulates in mitochondria remains unknown. One of the main mCholesterol transporters is StARD1, which has been reported to be increased in ALD but has never been related to the pathological mCholesterol levels in this disease (Fernández et al., 2013). Thus, we first aimed to examine liver zonation in relation to alcohol consumption and StARD1 in an experimental animal model of EtOH-induced liver injury.

For this purpose, 8 week male old WT C57BL/6J mice were exposed to a Lieber DeCarli diet with maltodextrin (CTRL) or 5% ethanol (EtOH) for 10 days. EtOH increased CYP2E1 expression in whole liver, as expected, as well as StARD1 levels (**Figure R-14A,B**). Interestingly, we observed that StARD1 was induced by EtOH in a zonal manner, preferentially in PV areas as seen by immunohistochemistry (**Figure R-14C**). Immunohistofluorescence using Glutamine synthase (GLUL) as a PV marker also revealed increased StARD1 expression in this area upon EtOH consumption (**Figure R-14D**).

To further confirm the observed StARD1 induction in PV hepatocytes in contrast to PP population, we selectively isolated PP and PV hepatocytes by using a dual digitonin-collagenase liver perfusion (**Figure R-15A**). Selective destruction of PP or PV mouse hepatocytes was achieved obtaining four hepatocyte populations: CTRL PP, EtOH PP, CTRL PV and EtOH PV. Population enrichment was confirmed by WB analysis of PP and PV markers: E-Cadherin, CYP2E1 and GLUL (**Figure R-15B,C**).

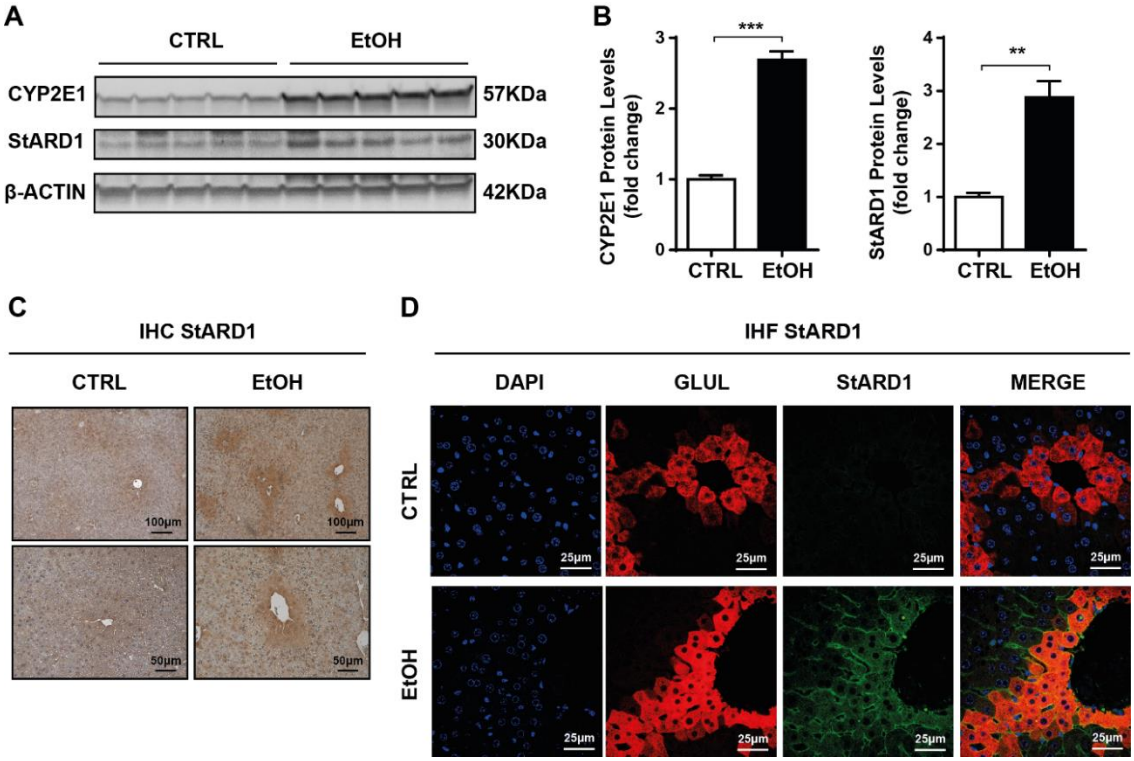

Figure R-14. Effects of EtOH consumption on hepatic StARD1 levels. WT C57BL/6J mice were exposed to Lieber DeCarli diet with maltodextrin (CTRL) or 5% ethanol (EtOH) for 10 days. (A) Protein expression of CYP2E1 and StARD1 in liver homogenates. Images are representative of at least three independent experiments. (B) Protein expression quantification of (A) by ImageJ software. Values are the mean ± SEM of >5 animals per group. P<0.05. Unpaired Student's t-test (two tailed). StARD1 levels in liver by (C) Immunohistochemistry and (D) Immunohistofluorescence. Images are representative of at least 3 replicates per group.

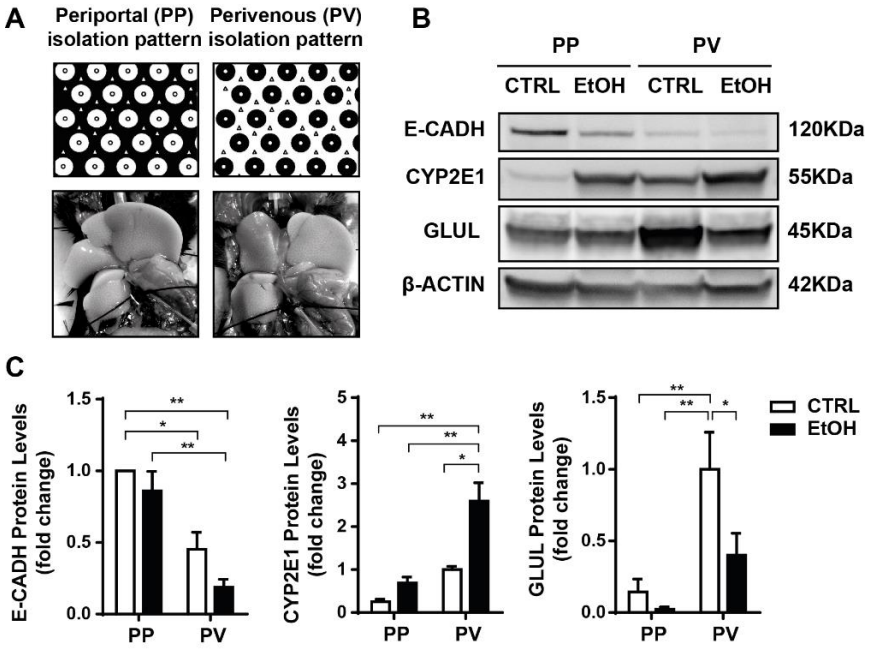

Figure R-15. PP and PV hepatocytes isolation by a dual digitonin-collagenase liver perfusion. (A) Periportal (PP) and perivenous (PV) isolation pattern. (B) Protein levels of population enrichment markers (PP: E-CADH; PV: CYP2E1 and GLUL). (C) Protein expression quantification of (B) by ImageJ software. Values are the mean ± SEM of >10 animals per group. P<0.05. Two-way ANOVA followed by Tukey's Multiple Comparison test.

Separation of both hepatocytes populations confirmed the previously observed StARD1 induction by EtOH mainly in PV hepatocytes. The increased expression of this particular mCholesterol transporter was unique since we could not observe changes in MLN64, another well-known transporter of cholesterol into mitochondria (**Figure R-16A,B**). Overall, these data confirm the previously described EtOH-induced StARD1 expression in liver and reveal new findings by specifically localizing this StARD1 upregulation in PV areas.

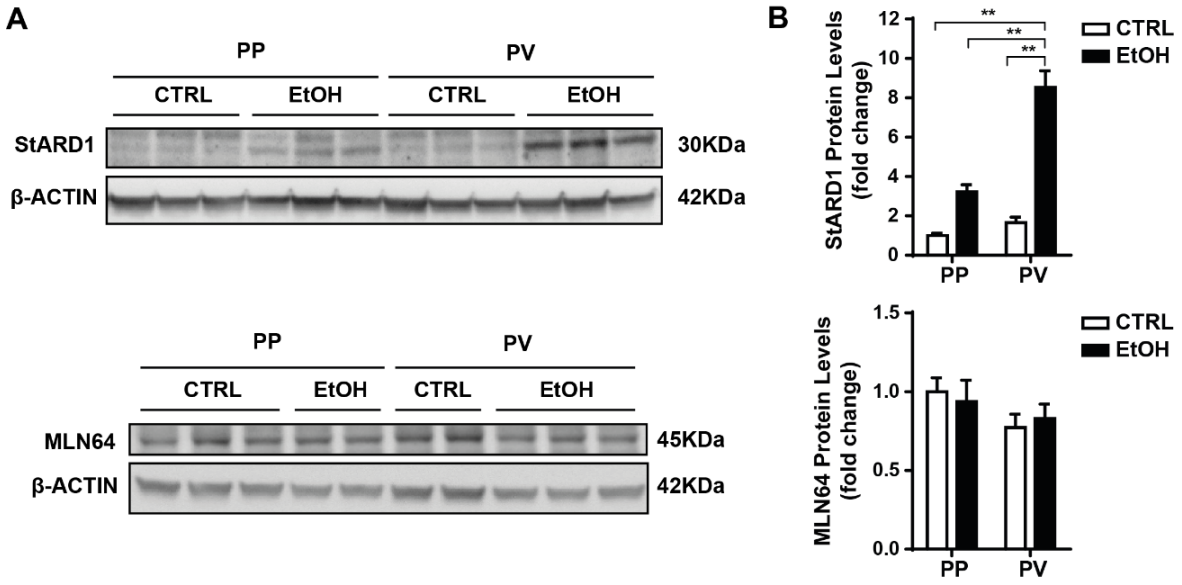

Figure R-16. Changes in StARD1 levels in PP and PV hepatocytes upon EtOH consumption. WT C57BL/6J mice were exposed to Lieber DeCarli diet with maltodextrin (CTRL) or 5% ethanol (EtOH) for 10 days. (A) StARD1 and MLN64 protein levels in CTRL or EtOH PP and PV hepatocytes. (B) Protein expression quantification of (A) by ImageJ software. Values are the mean ± SEM of >6 animals per group. P<0.05. Two-way ANOVA followed by Tukey's Multiple Comparison test.

2.2. LOWER OXYGEN TENSION IN PV POPULATION COMPARED TO PP AREA CONTRIBUTES TO ETOH-INDUCED STARD1 UPREGULATION

EtOH is mainly metabolized in PV hepatocytes since they exhibit more CYP2E1 expression compared to PP population (Bühler et al., 1992; Johansson et al., 1990). However, other factors determining metabolic zonation in liver could be also involved in the differences observed in EtOH-induced StARD1 expression between PP and PV populations. Among them, oxygen tension, which decreases in PV areas compared to PP areas (Jungermann and Kietzmann, 2000; Kietzmann, 2017). Hypoxia inducible factor HIF is a known transcriptional factor that promotes StARD1 expression in reproductive cells (Kowalewski et al., 2015). StARD1 promoter has indeed a hypoxia response element. Taking this into account, we wondered whether the increased StARD1

expression observed in PV areas could be due to not only higher EtOH metabolism in this zone but also lower oxygen levels through HIF regulation. To do so, we isolated PMH and treated them with or without 100µM $CoCl_2$ to induce a chemical hypoxia and simulate PV and PP areas respectively, and exposed them to 100mM EtOH. Interestingly, StARD1 levels increased in hypoxic conditions at the same extend as with EtOH treatment while the combination of both factors triggered the highest levels of StARD1 expression (**Figure R-17A,B**). Mimicking PV environment *in vitro* helped to prove StARD1 upregulation by both EtOH and hypoxia, and helped to better explain the significant differences seen in StARD1 expression between the hypoxic PV area and the PP population after EtOH consumption.

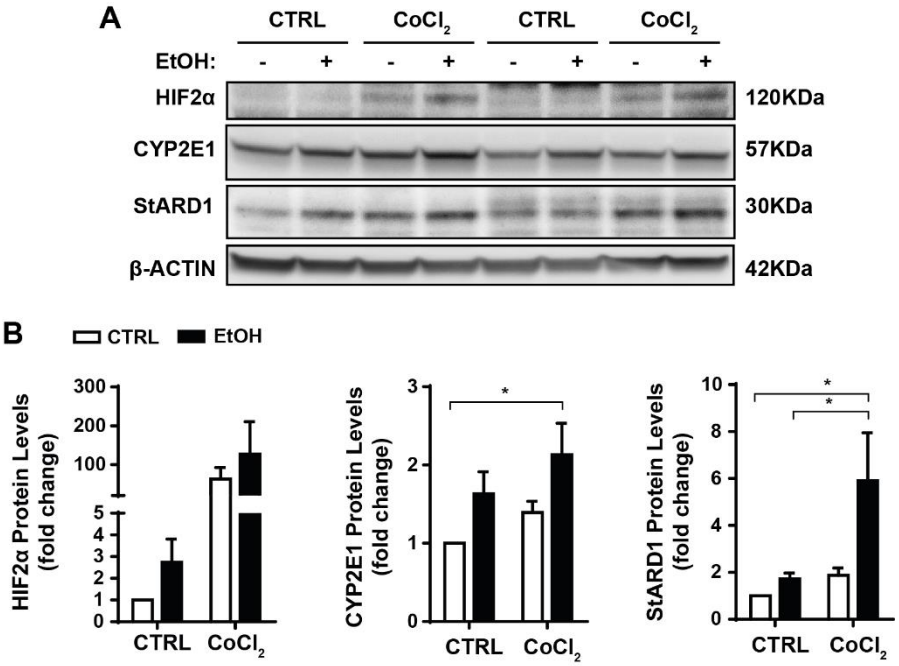

Figure R-17. Effects of EtOH and hypoxia on StARD1 expression in PMH. (A) Protein expression levels of HIF2α, CYP2E1 and StARD1 in PMH treated for 24 hours with 100µM $CoCl_2$ and/or 100mM EtOH. (B) Protein expression quantification of (A) by ImageJ software. Values are the mean ± SEM (N>3, P<0.05, Two-way ANOVA followed by Tukey's Multiple Comparison test).

2.3. ETOH INTAKE CAUSES AN INCREMENT OF mCHOLESTEROL SPECIFICALLY IN PV HEPATOCYTES

Since EtOH consumption has been shown to increase StARD1 levels mainly in PV area, we next examined hepatic cholesterol levels. Staining of liver sections with filipin showed no differences in global hepatic free cholesterol between CTRL and EtOH-fed mice (**Figure R-18A,B**). However, deeply analysis of the same liver sections taking into account PP and PV areas separately allowed us to unravel differences in cholesterol between both populations. GLUL and CYP2F2 images were used to create a contour area around central and portal veins respectively. Cholesterol content of the selected PV and PP areas was then measured in these contours based on the filipin fluorescence intensity (**Figure R-19**). This specific analysis showed increased free cholesterol content in PV population compared to PP after EtOH intake (**Figure R-18C,D**).

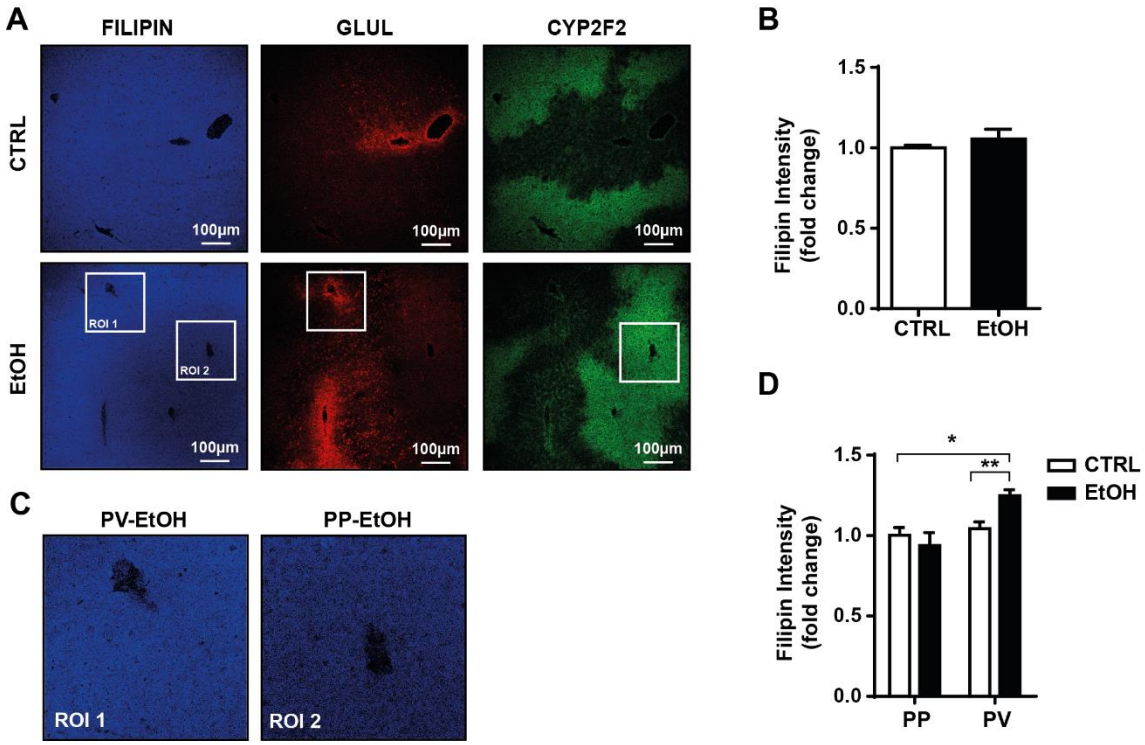

Figure R-18. Alteration of hepatic free cholesterol levels by EtOH feeding. (A) Cholesterol levels in liver by Immunohistofluorescence using Filipin as a cholesterol marker and GLUL and CYP2F2 as PV and PP markers respectively. (B) Filipin intensity of (A) analyzed using ImageJ software. Data are presented as means ± SEM (N>3, P<0.05, Unpaired Student's t-test (two tailed)). (C) Filipin staining of selected central and portal vein areas. (D) Filipin intensity of the selected PP and PV areas using ImageJ software. Values are the mean ± SEM of >3 animals per group. P<0.05. Two-way ANOVA followed by Tukey's Multiple Comparison test.

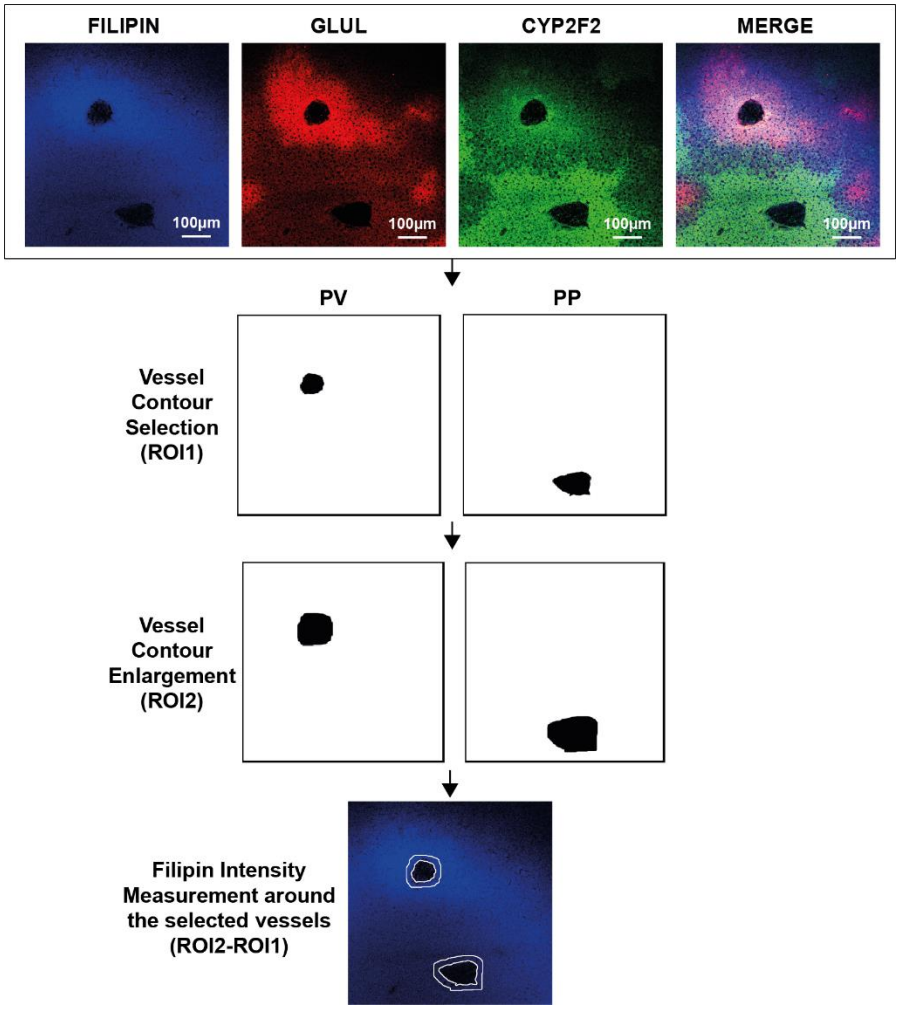

Figure R-19. Methodology conducted by ImageJ to measure cholesterol in PP and PV areas separately from EtOH-fed mice livers. Confocal microscope images were analyzed using ImageJ software. GLUL and CYP2F2 images were thresholded and binarized to generate a mask containing the central or portal vein contours, respectively. Masks were applied a median filter to reduce noise and get a better vessel contour. For each mask, everything but the contour of the vessel of interest was manually deleted. The original vessel contour was defined as ROI1, while a new contour generated by dilating ROI1 by 18µm-thick was defined as ROI2. A third ROI, ROI3, was generated by subtracting ROI1 from ROI2 to get an 18µm-thick region surrounding the vessel. ROI3 was used to extract the cholesterol content of the PV or PP areas based on the filipin fluorescence intensity.

Since StARD1 is a mCholesterol transporter, we next determined free cholesterol levels in mitochondria. In line with total liver free cholesterol, confocal imaging of PP and PV hepatocytes upon staining with filipin and Cyt C (mitochondrial marker) revealed increased mCholesterol levels in PV hepatocytes after EtOH feeding (**Figure R-20A,B**). Thus, these findings demonstrate the strong effects of EtOH on mCholesterol enrichment in the PV area.

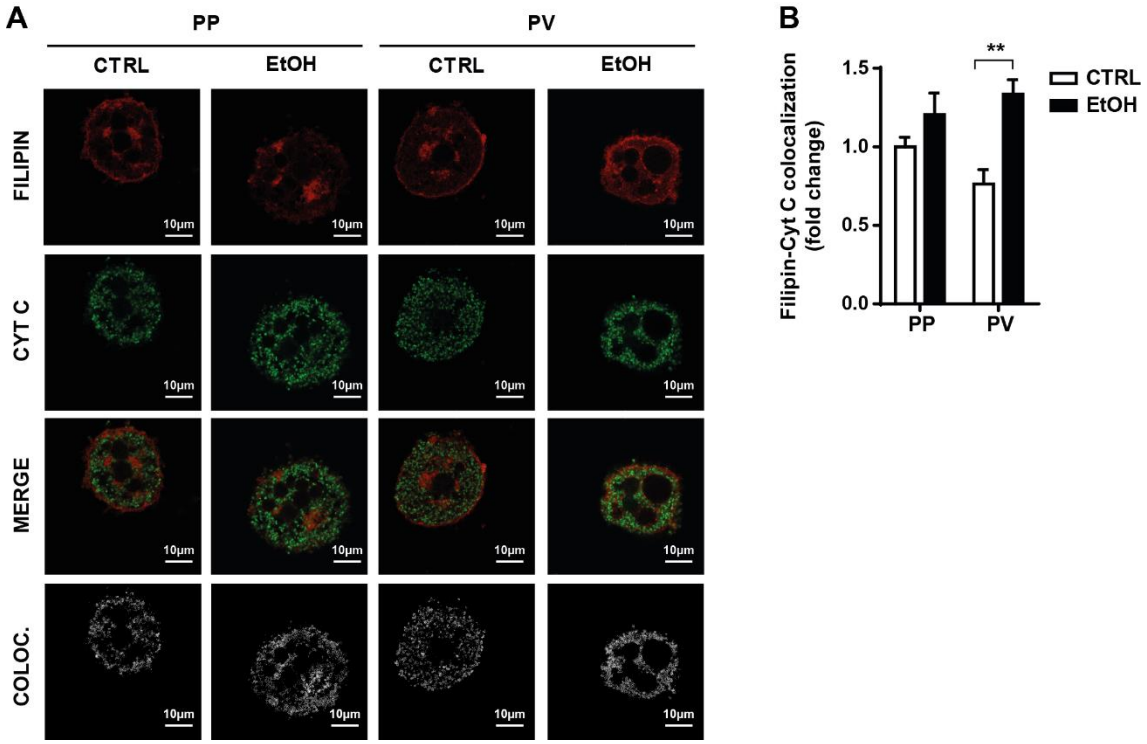

Figure R-20. Alteration of mCholesterol levels by EtOH feeding in PP and PV populations. (A) mCholesterol levels by Immunocytochemistry using Cyt C and Filipin. (B) Staining markers colocalization of (A) analyzed using ImageJ software. Data are presented as means ± SEM (N>5, P<0.05, Two-way ANOVA followed by Tukey's Multiple Comparison test).

2.4. ETOH-FED MICE PRESENT GSH DEPLETION AND INCREASED OXIDATIVE STRESS IN PV HEPATOCYTES WITH SUBSEQUENT LIVER DAMAGE

As mCholesterol loading has been described to result in antioxidant defense alteration by glutathione depletion (Ribas et al., 2014; Solsona-Vilarrasa et al., 2019), we next determined GSH levels in our model. Interestingly, we observed that in CTRL diet both total and mGSH levels are higher in PV hepatocytes compared to PP, which suggests that PV area has a higher antioxidant system in basal conditions. After EtOH consumption, GSH levels of both populations decreased to the same level being PV population the most affected one due to a higher drop in the antioxidant levels (**Figure R-21A**). These results were accompanied by an alteration of the mitochondrial dicarboxylate carrier (DIC) expression, protein that transports glutathione across the inner mitochondrial membrane. Although DIC levels were mainly increased in PV hepatocytes after EtOH consumption, this increment was insufficient to maintain basal glutathione levels (**Figure R-21B,C**). This outcome also paralleled the increased oxidative stress specifically observed in PV-EtOH hepatocytes by incremented 4-HNE presence and DCF intensity (**Figure R-21D-F**).

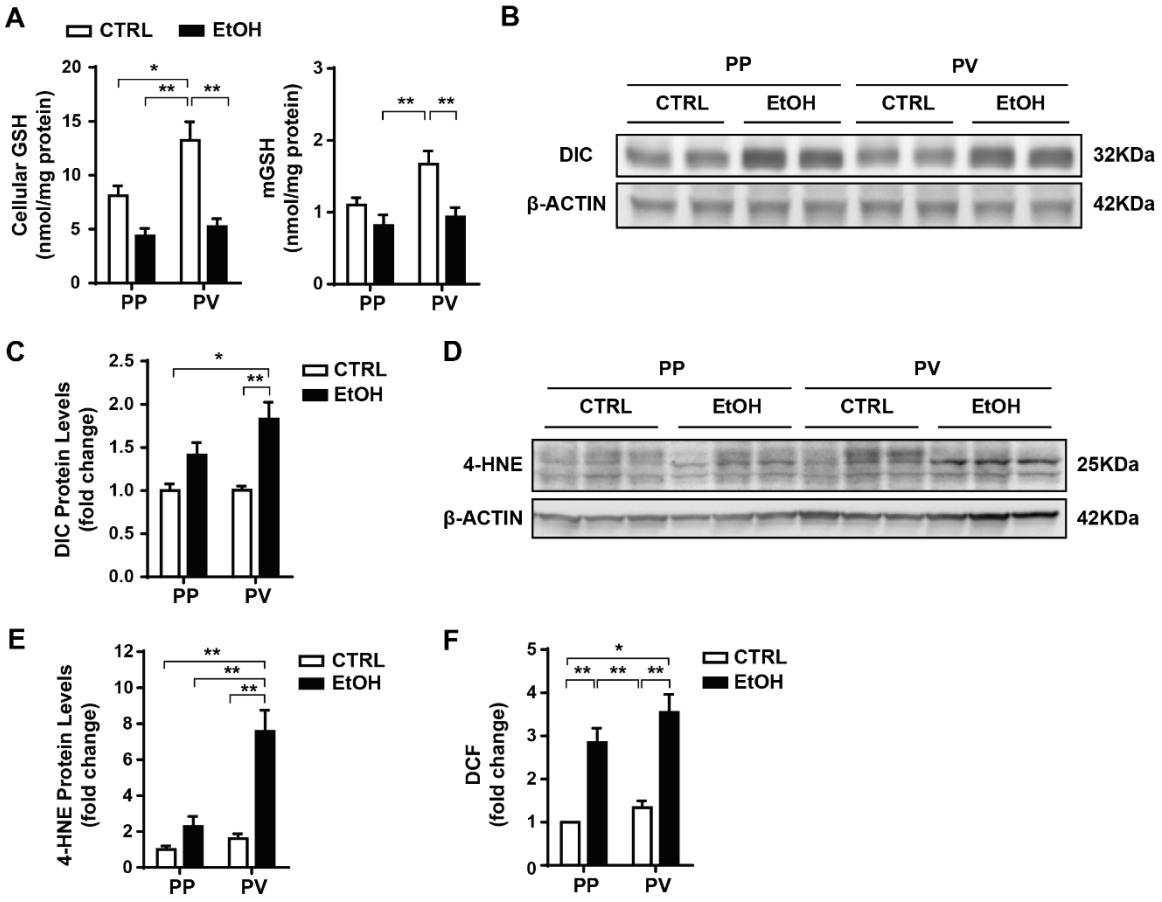

Figure R-21. Consequences of EtOH intake on GSH levels and oxidative stress. (A) GSH levels in total hepatocytes and mitochondria. Values are the mean ± SEM of >6 animals per group. P<0.05. Two-way ANOVA followed by Tukey's Multiple Comparison test. (B,D) DIC and 4-HNE-modified protein levels in CTRL or EtOH PP and PV hepatocytes. (C,E) Protein expression quantification of (B,D) by ImageJ software. Values are the mean ± SEM of >4 animals per group. P<0.05. Two-way ANOVA followed by Tukey's Multiple Comparison test. (F) Reactive oxygen species content in hepatocytes by DCF. Data are presented as means ± SEM (N>4, P<0.05, Two-way ANOVA followed by Tukey's Multiple Comparison test).

Based on these findings, we then examined whether the increase in ROS specifically in the PV area translated in an increase in liver damage in the PV zone. Staining of liver sections with H&E revealed mild but clear hepatic injury mainly around central veins in EtOH-fed mice in comparison with PP areas (**Figure R-22A**), results that correlated with increased levels of serum transaminases (**Figure R-22B**). Overall, these data indicate that EtOH induces GSH depletion and oxidative stress specifically in PV areas, which finally leads to liver damage.

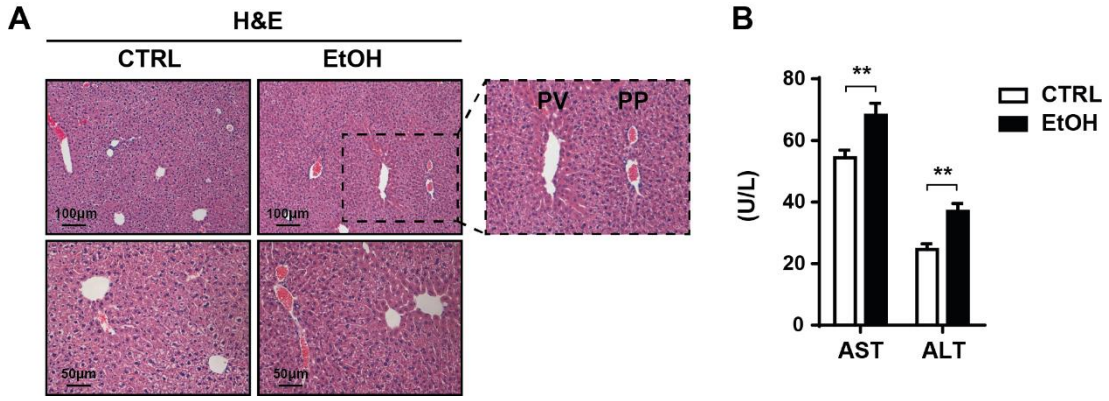

Figure R-22. Consequences of EtOH intake on liver damage. (A) Liver sections of CTRL and EtOH-fed mice analyzed by H&E. (B) Serum AST and ALT levels from CTRL and EtOH mice. Data are presented as means ± SEM (N>10, P<0.05, Unpaired Student's t-test (two tailed)).

2.5. ETOH CONSUMPTION ALTERS THE MORPHOLOGY OF PP AND PV HEPATOCYTES AS WELL AS THEIR MITOCHONDRIA

Alcohol-induced liver injury is characterized by the formation of lipid droplets containing triglyceride and esterified cholesterol in the cytosol of hepatocytes, because of ethanol-induced alteration of hepatic lipid metabolism (Crabb and Liangpunsakul, 2006; Nakajima et al., 2004; Ohashi et al., 2018; You et al., 2008). Also changes at subcellular level have been described as alterations in mitochondria which are enlarged after EtOH consumption (Bruguera et al., 1977). However, these features are regularly investigated in a general manner, without taking liver zonation into account. As we have observed that PV area is the most affected one in ALD, we then aimed to characterize the structural changes induced by EtOH in PP and PV hepatocytes separately using transmission electron microscopy. For this purpose, 8 week-old WT C57BL/6J male mice were fed a CTRL or EtOH diet for 30 days. Liver semifine sections of these mice were observed with light microscopy to define PP and PV areas and images from ultrathin sections containing both areas were taken using a TEM JEOL JEM-1010 (**Figure R-23A**).

In CTRL diet both areas presented high glycogen content and few small lipid droplets (LD). EtOH intake induced a strong decrease in glycogen content in both areas, especially in the PV zone (**Figure R-23A,B**). Regarding to LD, EtOH increased their number in both populations (**Figure R-23C**). However, while PP LD sizes ranged from small to very large, PV LD remained small (**Figure R-23D**).

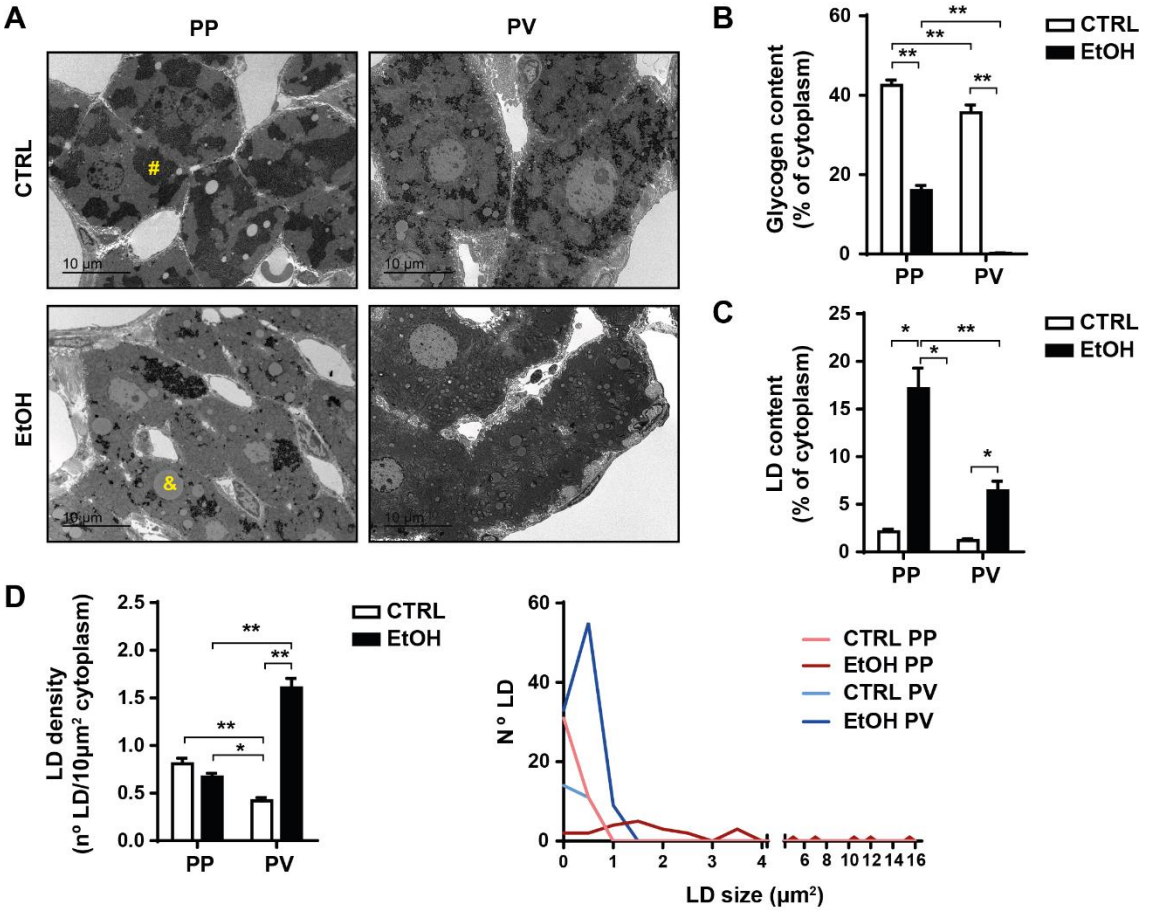

Figure R-23. Alteration of hepatic morphology from PP and PV areas by EtOH consumption. WT C57BL/6J mice were fed a CTRL or EtOH diet for 30 days. Liver semifine sections of these mice were observed with light microscopy to define PP and PV areas. (A) Representative images from ultrathin sections containing CTRL or EtOH PP and PV areas taken using a TEM JEOL JEM-1010. (B) Hepatocyte glycogen content. (C) Hepatocyte LD content. (D) Hepatocyte LD density and LD size distribution among the different populations. N=3 animals/diet and n≥35 hepatocytes/group. Data are presented as means ± SEM (P<0.05, Two-way ANOVA followed by Tukey's Multiple Comparison test). #, glycogen. &, lipid droplet.

EtOH also induced changes at subcellular levels, mainly in mitochondria (**Figure R-24A**). In CTRL conditions, PV mitochondria appeared to be smaller compared to PP mitochondria. This feature paralleled the observed increased expression of FIS1, a mitochondrial fission protein, in PV areas in contrast to PP (**Figure R-24B,C**). After EtOH consumption, mitochondrial number and length increased in PP hepatocytes with the largest mitochondria surrounding LDs, findings that correlated with increased OPA1 expression (mitochondrial fusion marker) (**Figure R-24B,C**). In contrast, EtOH did not affect mitochondrial size in PV areas but induced a dramatic change in mitochondrial shape: concave forms with thick edges and a thin matrix in the center, and donut-like forms with bent shapes shrinking into a ring with a lumen containing cytoplasm. Some of these mitochondria presented unusual parallel cristae. Furthermore, there were also changes in

endoplasmic reticulum. In CTRL diet PV hepatocytes contained more RER than PP hepatocytes. Interestingly, EtOH caused a shift from RER to SER in PV areas (**Figure R-24A**).

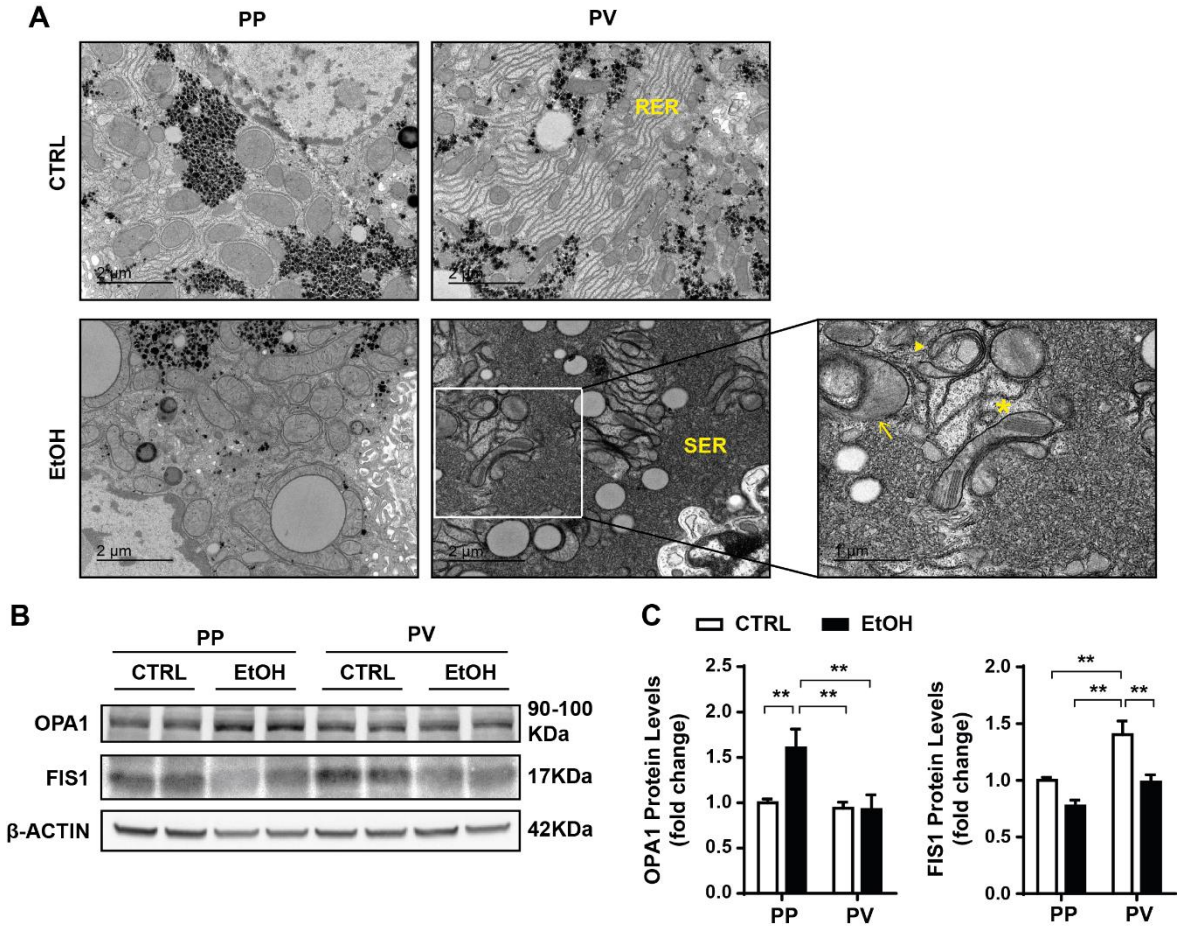

Figure R-24. Alteration of mitochondrial morphology from PP and PV areas by EtOH consumption. WT C57BL/6J mice were fed a CTRL or EtOH diet for 30 days. Liver semifine sections of these mice were observed with light microscopy to define PP and PV areas. (A) Representative images of CTRL or EtOH PP and PV hepatocyte mitochondria. ➔ donut-like forms. ► concave forms with thick edges and a thin matrix in the center. * Parallel cristae. RER, rough endoplasmatic reticulum (ER). SER, smooth ER. (B) OPA1 and FIS1 protein levels in CTRL or EtOH PP and PV hepatocytes. (C) Protein expression quantification of (B) by ImageJ software. Data are presented as means ± SEM (N>3, P<0.05, Two-way ANOVA followed by Tukey's Multiple Comparison test).

These data reveal that PP and PV areas are different in basal states and that EtOH induces differential changes in both populations, pooling them further apart. EtOH predominantly induces substantial structural changes in mitochondria from PV area, which correlates with our previous findings and may account for the prevailing injury seen in this area in ALD.

2.6. KNOCKING-OUT STARD1 PROTECTS ETOH-FED MICE FROM mCHOLESTEROL INCREASE, GSH REDUCTION AND INCREASED OXIDATIVE STRESS IN PV AREA AS WELL AS LIVER DAMAGE

In view of the preceding findings, we hypothesized that EtOH-induced StARD1 levels may be involved in the observed hepatic damage by increasing mCholesterol levels and oxidative stress in the PV area. Therefore, we decided to determine the effects of StARD1 absence in our ALD model by using PV hepatocytes from liver-specific StARD1-deficient mice (StARD1$^{\Delta Hep}$).

As expected, EtOH induced the expression of StARD1 in PV hepatocytes from StARD1$^{f/f}$ mice, alteration not observed in StARD1$^{\Delta Hep}$ mice (**Figure R-25A,B**). EtOH also increased mCholesterol levels in StARD1$^{f/f}$ but not StARD1$^{\Delta Hep}$ mice as determined by filipin and Cyt C colocalization (**Figure R-25C,D**).

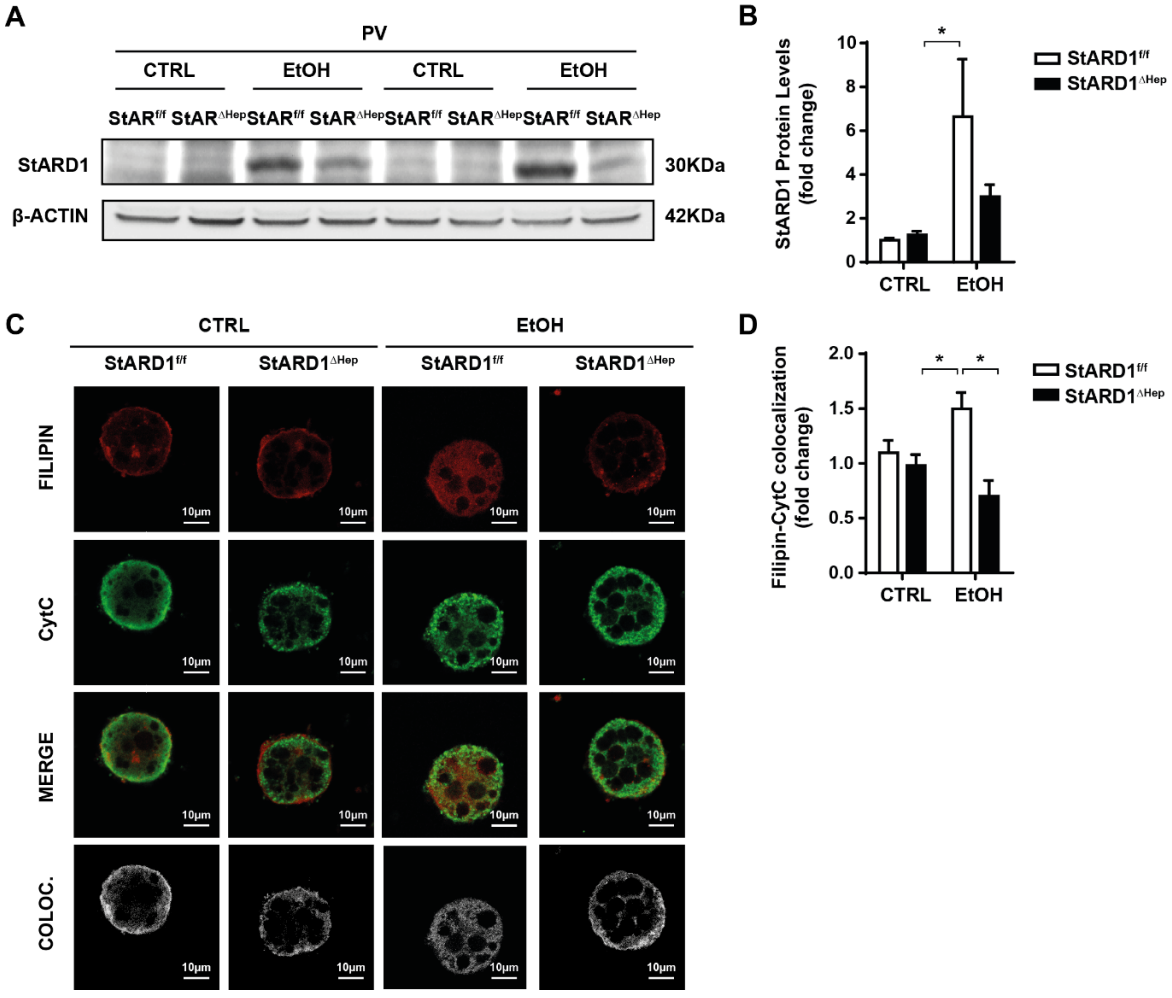

Figure R-25. Effects of EtOH intake in StARD1 and mCholesterol levels of PV hepatocytes from StARD1-deficient mice. (A) StARD1 protein levels in CTRL or EtOH PV hepatocytes from StARD1$^{f/f}$ and StARD1$^{\Delta Hep}$ mice. (B) Protein expression quantification of (A) by ImageJ software. Data are presented as means ± SEM (N>5, P < 0.05, Two-way ANOVA followed by Tukey's Multiple Comparison test). (C) mCholesterol levels by Immunocytochemistry using Cyt C and Filipin. (D) Staining markers colocalization of (C) analyzed using ImageJ software. Data are presented as means ± SEM (N>5, P<0.05, Two-way ANOVA followed by Tukey's Multiple Comparison test).

In line with this findings, while PV hepatocytes of StARD1$^{f/f}$ mice presented total and mGSH depletion upon EtOH intake, StARD1$^{\Delta Hep}$ hepatocytes exhibited higher antioxidant levels upon EtOH exposure (**Figure R-26A**). The differences in GSH levels were independent of DIC levels, since both groups showed increased DIC expression after EtOH consumption (**Figure R-26B,C**). Besides GSH, StARD1 deletion also protected hepatocytes from oxidative stress and ultimately protected mice from liver damage as observed by a decrease in 4-HNE modified proteins in hepatocytes and AST levels in StARD1$^{\Delta Hep}$ mice (**Figure R-26D-F**).

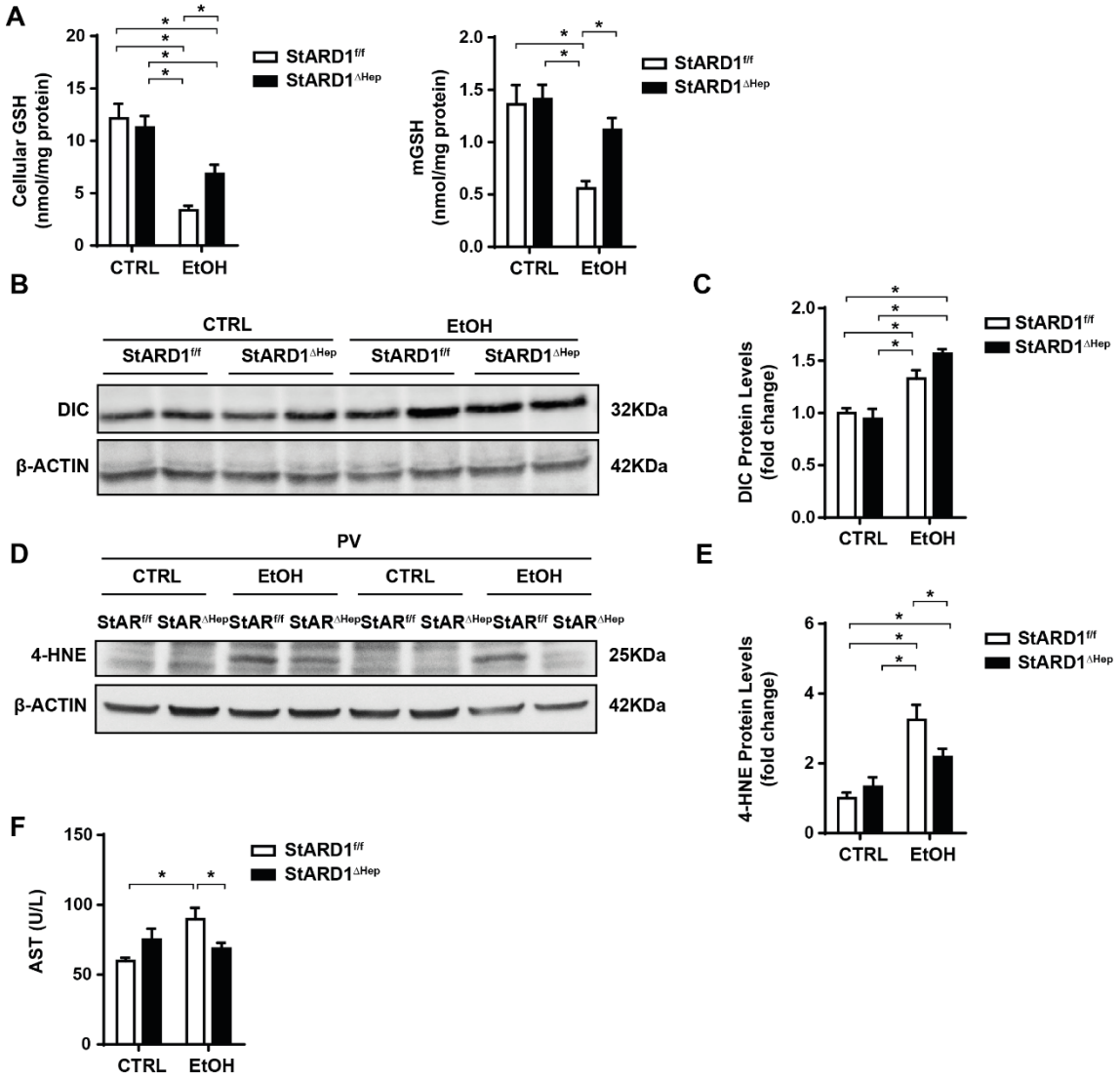

Figure R-26. Consequences of knocking-out StARD1 in EtOH-altered GSH levels, oxidative stress and hepatic damage. (A) GSH levels in CTRL or EtOH PV hepatocytes from StARD1$^{f/f}$ and StARD1$^{\Delta Hep}$ mice. Data are presented as means ± SEM (N>8, P<0.05, Two-way ANOVA followed by Tukey's Multiple Comparison and Unpaired Student's t-test (two-tailed) between EtOH groups). (B,D) DIC and 4-HNE modified proteins levels from StARD1$^{f/f}$ and StARD1$^{\Delta Hep}$ CTRL or EtOH PV hepatocytes. (C,E) Protein expression quantification of (B,D) by ImageJ software. Values are the mean ± SEM of >4 animals per group. P<0.05. Two-way ANOVA followed by Tukey's Multiple Comparison and Unpaired Student's t-test (two-tailed) between EtOH groups. (F) Serum AST levels from CTRL and EtOH StARD1$^{f/f}$ and StARD1$^{\Delta Hep}$ mice. Data are presented as means ± SEM (N>8, P<0.05, Two-way ANOVA followed by Tukey's Multiple Comparison test).

To summarize, this study contributes on expanding ALD molecular mechanisms by highlighting StARD1 as a new key player in ALD progression. By using a Lieber-DeCarli liquid diet model with mice we have shown that EtOH intake increases StARD1 expression specifically in the hepatic PV area compared to the PP zone. Interestingly, StARD1 upregulation in PV area depends of not only higher alcohol metabolism in PV zone but also lower oxygen levels since hypoxia also induces StARD1 increment. In line with StARD1 upregulation, EtOH-fed mice also exhibit increased mCholesterol levels and oxidative stress preferentially in PV hepatocytes compared to PP. Besides, we have observed a dramatically change in shape of mitochondria from PV hepatocytes after EtOH intake. Interestingly, these alterations in PV zone translating into significant liver injury are interrupted by StARD1 deletion. Liver-specific StARD1-deficient mice are protected from EtOH-induced liver injury since StARD1 deficiency prevents from increased mCholesterol levels and oxidative stress ensuring proper hepatic function.

3. STUDY III. ACID CERAMIDASE IMPROVES MITOCHONDRIAL FUNCTION IN NIEMANN-PICK TYPE C DISEASE BY REPRESSING STARD1-DEPENDENT MITOCHONDRIAL CHOLESTEROL ACCUMULATION

3.1. NPC1$^{-/-}$ MICE PRESENT HEPATIC mCHOLESTEROL ACCUMULATION AND STARD1 UPREGULATION

Accumulation of cholesterol in lysosomes caused by mutations in NPC1 is a hallmark of NPC disease (Beltroy et al., 2005; Patterson et al., 2012; Schultz et al., 2016; Vanier, 2015). Besides this event, accumulation of cholesterol in mitochondria of Npc1$^{-/-}$ mice has also been reported as well as its biological and clinical consequences (Marí et al., 2006; Torres et al., 2017b; Yu et al., 2005). However, the underlying mechanism involved has not been addressed yet.

Before exploring potential mechanisms of mCholesterol accumulation in NPC disease, we further analyzed hepatic mCholesterol homeostasis in Npc1$^{-/-}$ mice. Staining of liver sections with filipin revealed increased cholesterol levels in liver from Npc1$^{-/-}$ mice compared to Npc1$^{+/+}$ mice (**Figure R-27A**). These results were further confirmed by HPLC analyses of liver homogenates and isolated mitochondrial fraction from Npc1$^{+/+}$ and Npc1$^{-/-}$ mice (**Figure R-27B,C**). Consistent with the increase in mCholesterol loading, fluorescence anisotropy analysis of liver mitochondria labeled with the fluorescent probe DPH revealed an increase in mitochondrial membrane order in Npc1$^{-/-}$ mice compared to Npc1$^{+/+}$ mice (**Figure R-27D**). In addition, confocal microscopy analyses of PMH from Npc1$^{-/-}$ mice indicated increased filipin staining and colocalization with Cyt C-labeled mitochondria (**Figure R-27E,F**), indicating the increase in mCholesterol levels.

As a potential mechanism accounting for the increase in mCholesterol content, we examined the expression of StARD1, which plays a crucial role in cholesterol trafficking from the outer to inner mitochondrial membrane (Caron et al., 1997; Charman et al., 2010; Kishida et al., 2004; Miller, 2007b; Torres et al., 2019). Remarkably, StARD1 protein expression levels increased in liver of Npc1$^{-/-}$ mice (**Figure R-28A,B**). Moreover, levels of MLN64 also increased in liver of Npc1$^{-/-}$ mice compared to Npc1$^{+/+}$ mice (**Figure R-28A,B**). These findings establish the increase in hepatic mCholesterol levels that correlate with expression of StARD1 and MLN64.

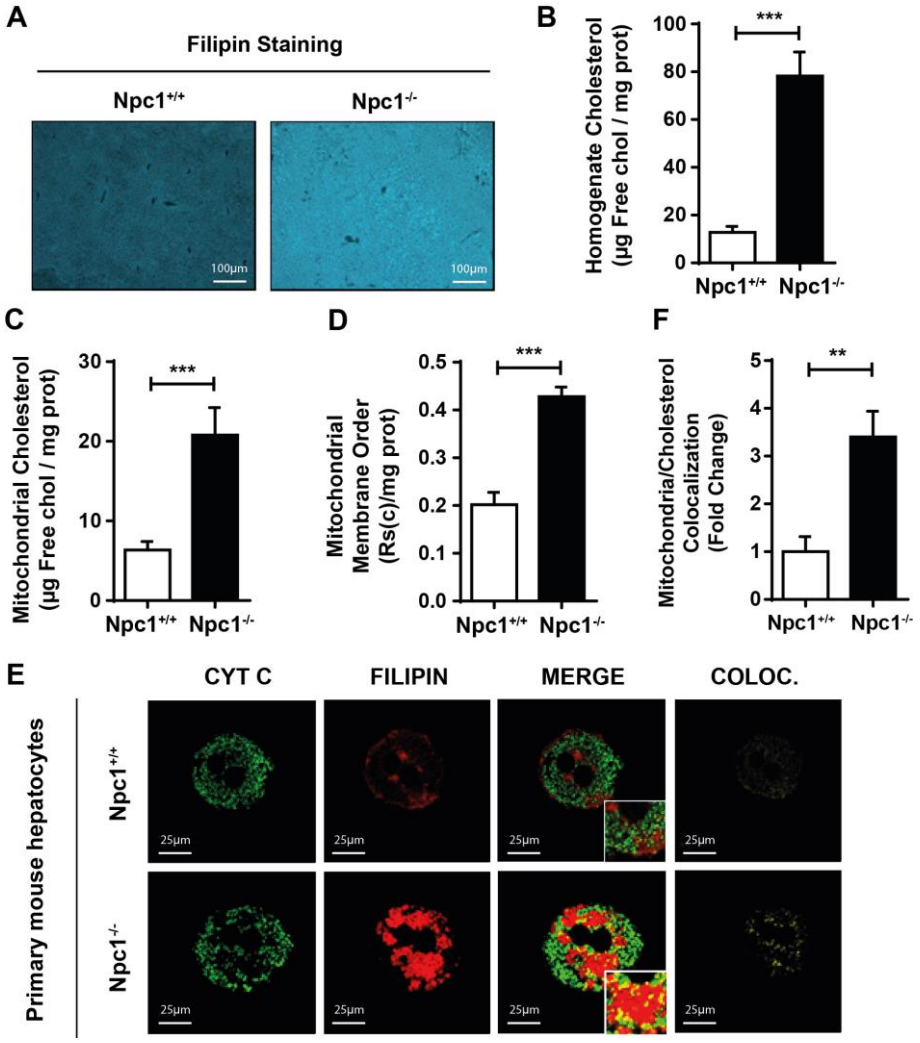

Figure R-27. mCholesterol content in livers of Npc1$^{+/+}$ and Npc1$^{-/-}$ mice. Npc1$^{+/+}$ and Npc1$^{-/-}$ mice were sacrificed at 6 weeks of age to isolate mitochondria from liver. (A) Filipin staining. (B) Homogenate and (C) mCholesterol levels by HPLC analyses. (D) Mitochondrial membrane order measured by DPH fluorescence anisotropy. (E) Cyt C and Filipin co-staining for confocal microscopy analyses of Npc1$^{+/+}$ and Npc1$^{-/-}$ PMH. (F) Staining markers colocalization analysis using Image J software. Data are presented as means ± SEM (n>4, P<0.05, Unpaired Student's t-test (two-tailed)).

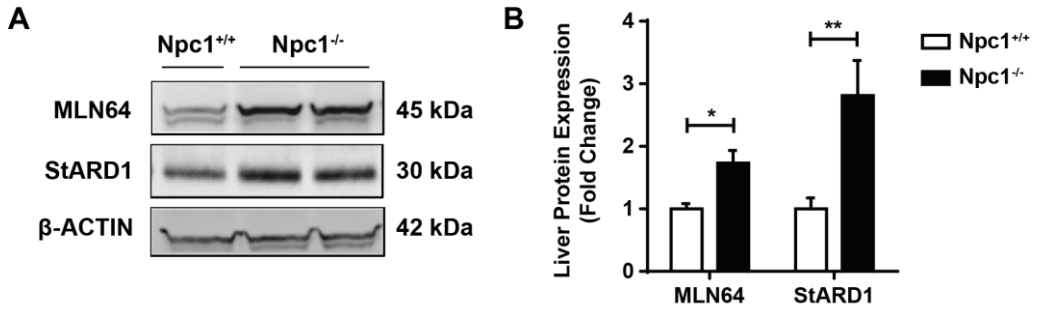

Figure R-28. StARD1 and MLN64 expression in livers of Npc1$^{+/+}$ and Npc1$^{-/-}$ mice. (A) StARD1 and MLN64 protein levels in livers of 6-weeks old Npc1$^{+/+}$ and Npc1$^{-/-}$ mice. (B) Protein expression quantification of (A) by ImageJ software. Values are the mean ± SEM of >4 animals per group. P<0.05. Unpaired Student's t-test (two-tailed).

3.2. FIBROBLASTS FROM PATIENTS WITH NPC DISEASE EXHIBIT INCREASED mCHOLESTEROL LEVELS AND STARD1 EXPRESSION

To validate the relevance of the preceding findings to human disease, we examined mCholesterol homeostasis in fibroblasts from patients with NPC disease ($Npc1^{-/-}$). In line with findings in liver, $Npc1^{-/-}$ fibroblasts exhibited increased free cholesterol levels determined by HPLC analysis in homogenate and mitochondria compared to fibroblasts from control subjects ($Npc1^{+/+}$) (**Figure R-29A,B**). Furthermore, confocal microscopy analyses of $Npc1^{-/-}$ fibroblasts revealed mCholesterol accumulation with respect to $Npc1^{+/+}$ fibroblasts, as indicated by the colocalization of filipin and Cyt C staining (**Figure R-29C,D**). StARD1 and MLN64 expression also increased in $Npc1^{-/-}$ fibroblasts compared to $Npc1^{+/+}$ fibroblasts (**Figure R-29E,F**). Thus, these findings confirm the outcome observed in liver from $Npc1^{-/-}$ mice and reveal mCholesterol accumulation in human NPC disease.

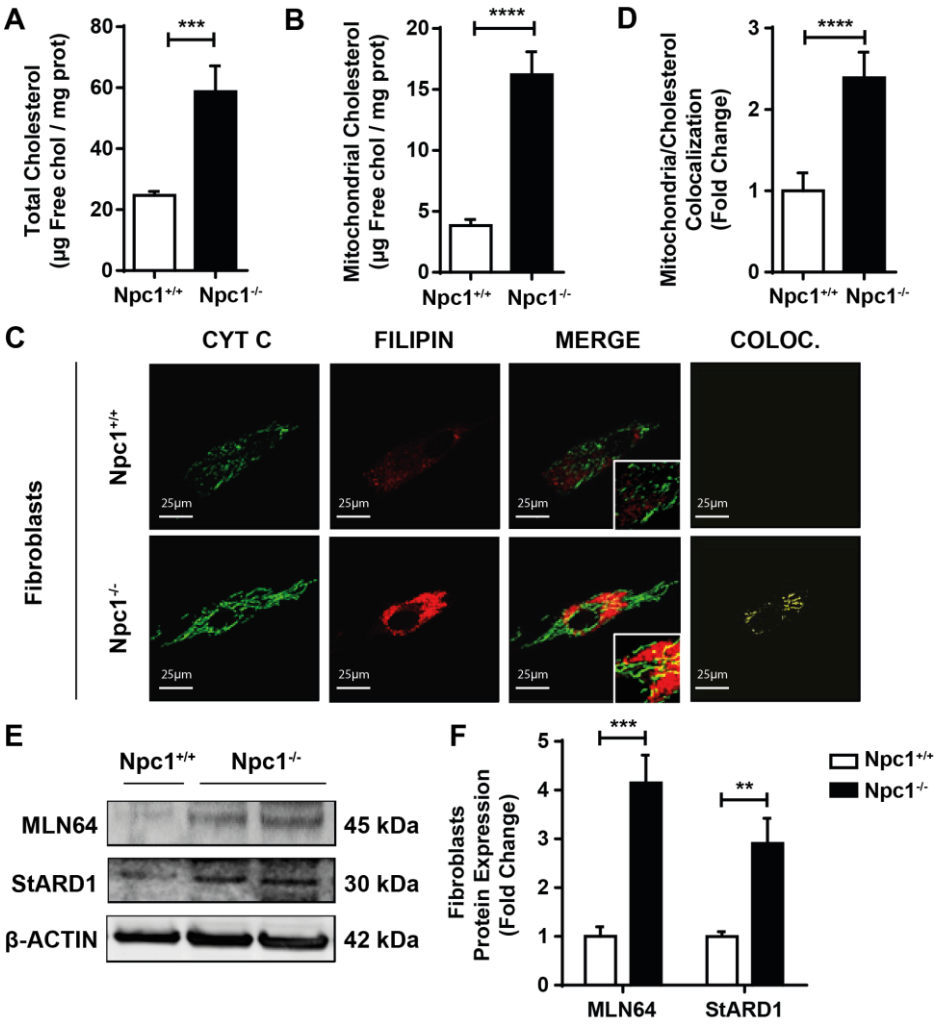

Figure R-29. mCholesterol trafficking and StARD1 expression in human skin fibroblasts from control subjects or patients with NPC disease. (A) Homogenate and (B) mCholesterol levels by HPLC analyses. (C) Cyt C and Filipin co-staining for confocal microscopy analyses. (D) Staining markers colocalization analysis using Image J software. (E) StARD1 and MLN64 protein levels in fibroblasts. (F) Protein expression quantification of (E) by ImageJ software. Data are presented as means ± SEM (n>5, Unpaired Student's t-test (two-tailed)).

3.3. LIVERS FROM NPC1$^{-/-}$ MICE AND FIBROBLASTS FROM NPC PATIENTS EXHIBIT DECREASED ACDASE EXPRESSION WITHOUT EVIDENCE OF ER STRESS

Given the relevance of StARD1 in the trafficking of cholesterol to mitochondrial inner membrane, we next examined potential mechanisms involved in the upregulation of StARD1 in NPC disease. ER stress has been shown to stimulate the transcriptional upregulation of StARD1 independently of SREBP activation (Fernández et al., 2013; Torres et al., 2019), and hence we analyzed the expression of ER stress markers in liver from Npc1$^{-/-}$ mice and Npc1$^{-/-}$ fibroblasts from patients with NPC disease. Protein levels of ER stress markers BIP, PDI, CHOP, p-EIF2α and s-XBP1 in liver fractions from Npc1$^{-/-}$ mice or Npc1$^{-/-}$ fibroblasts from patients with NPC disease were similar to those seen in Npc1$^{+/+}$ mice or control Npc1$^{+/+}$ fibroblasts (**Figure R-30A,B**). These findings are in line with previous reports indicating that ER stress appears to play a minor role in lysosomal storage disorders, including NPC disease (Klein et al., 2011).

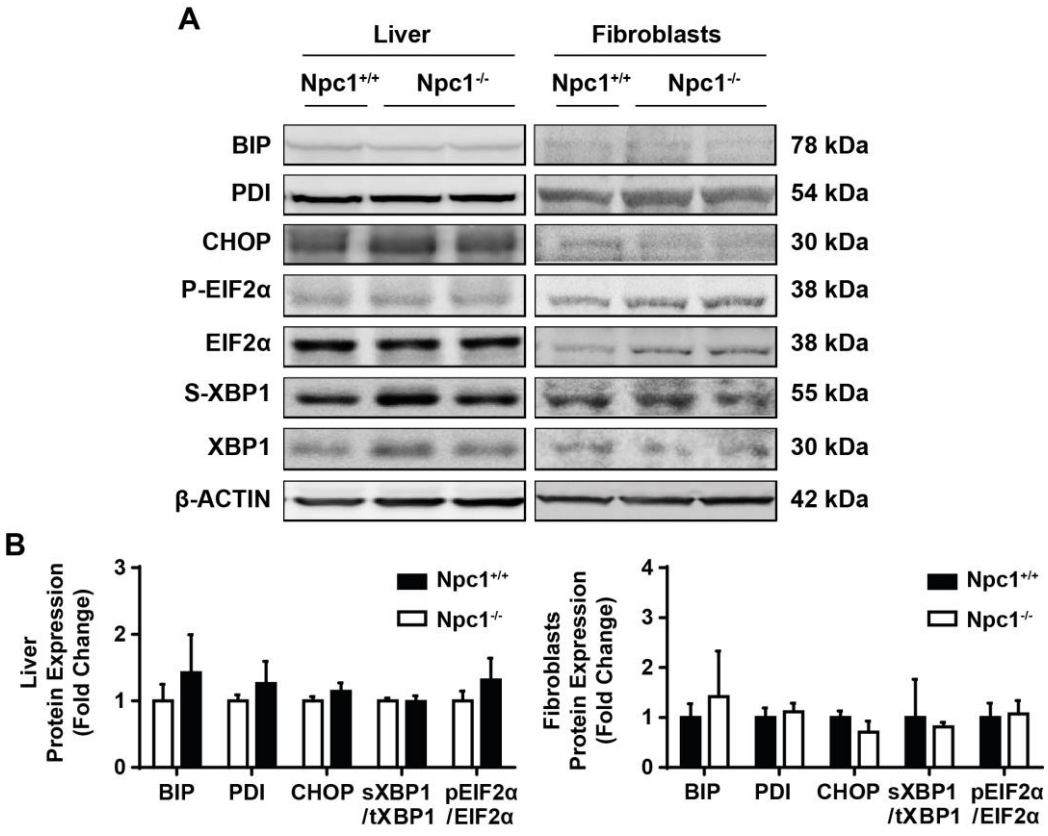

Figure R-30. ER stress markers protein expression in livers from Npc1$^{-/-}$ mice and fibroblasts from NPC patients. (A) ER stress markers protein levels. (B) Protein expression quantification of (A) by ImageJ software. Data are presented as means ± SEM (n>3, P<0.05. Unpaired Student's t-test (two-tailed)).

Next, we searched for alternative mechanisms involved in StARD1 regulation. As StARD1 is also regulated by steroidogenic factor 1 (SF-1), a member of the nuclear receptor family, and acid ceramidase (ACDase) has been shown to repress SF-1 and subsequently StARD1 upregulation (Lucki et al., 2012), we next examined ACDase expression in livers from Npc1$^{-/-}$ mice and Npc1$^{-/-}$ fibroblasts from patients with NPC disease. Interestingly, the expression of ACDase decreased in livers from Npc1$^{-/-}$ mice and Npc1$^{-/-}$ fibroblasts from NPC patients (**Figure R-31A,B**). These findings were confirmed by confocal microscopy analyses of PMH and fibroblasts stained with ACDase (**Figure R-31C-F**). Thus, these data reveal for the first time a potential inverse correlation between ACDase and StARD1 expression in NPC disease.

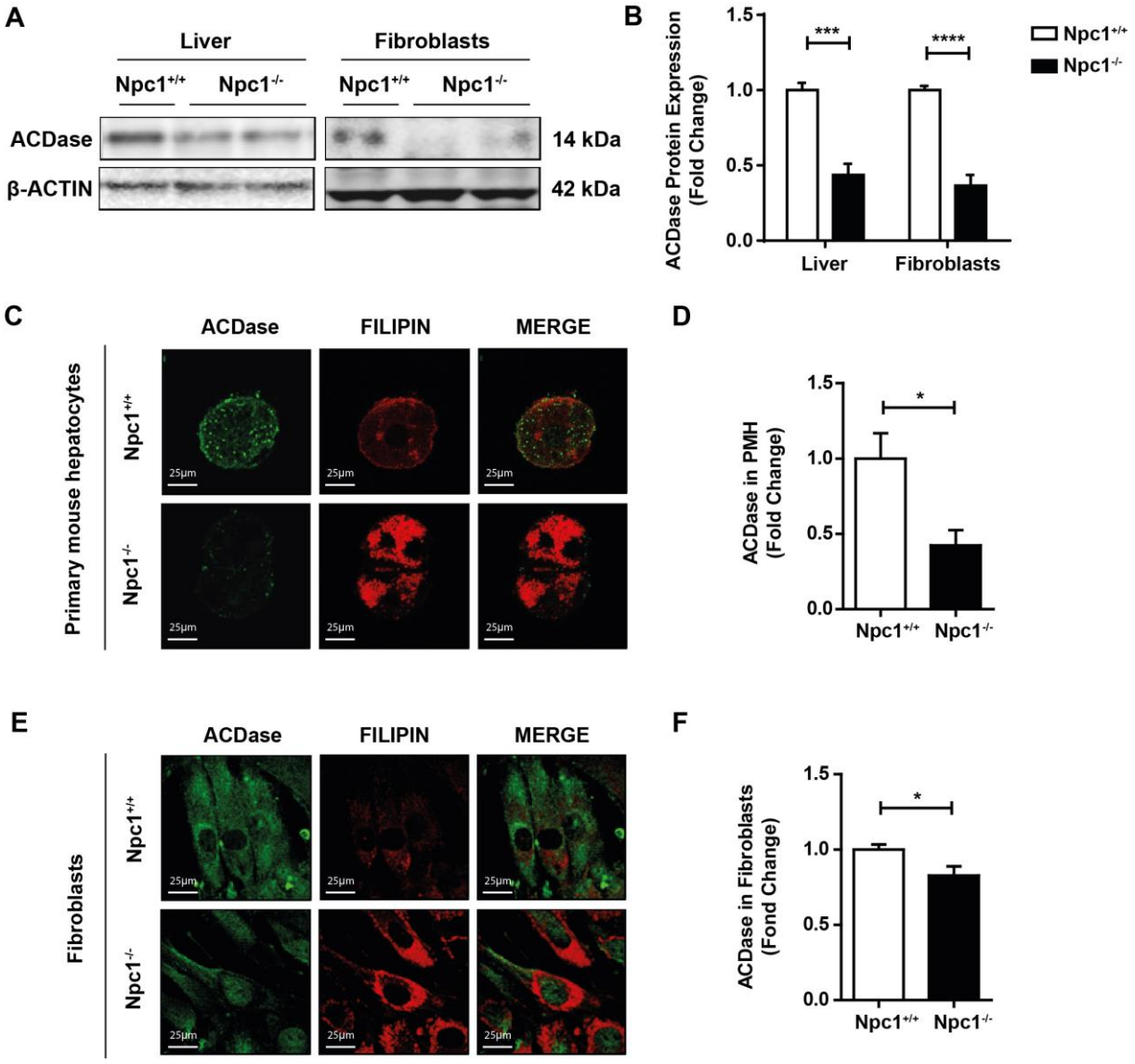

Figure R-31. ACDase expression in livers from Npc1$^{-/-}$ mice and fibroblasts from NPC patients. (A) ACDase protein levels. (B) Protein expression quantification of (A) by ImageJ software. (C,E) ACDase and Filipin co-staining in Npc1$^{+/+}$ and Npc1$^{-/-}$ PMH and in fibroblasts from control and NPC patients. (D,F) ACDase staining marker quantification of (C,E) by ImageJ software. Data are presented as means ± SEM (n>3, P<0.05. Unpaired Student's t-test (two-tailed)).

3.4. THE AMPHIPHILIC CATIONIC STEROL U18666A REPRODUCES THE INVERSE CORRELATION BETWEEN STARD1 AND ACDASE IN NPC1$^{+/+}$ PMH AND FIBROBLASTS

We next further characterized the relationship between StARD1 and ACDase. Since ACDase is a lysosomal enzyme, we first addressed whether the decrease in ACDase expression in NPC cells could be a consequence of the accumulation of cellular cholesterol. Hence, we used the amphiphilic aminosteroid U186661, which antagonizes NPC1 and increases intracellular cholesterol accumulation. Confocal imaging analysis of PMH from Npc1$^{+/+}$ mice stained with Filipin and Cyt C revealed that U18666A significantly increased mCholesterol accumulation (**Figure R-32A,B**). Similar accumulation of mCholesterol was observed in Npc1$^{+/+}$ fibroblasts upon U18666A treatment (**Figure R-32C,D**).

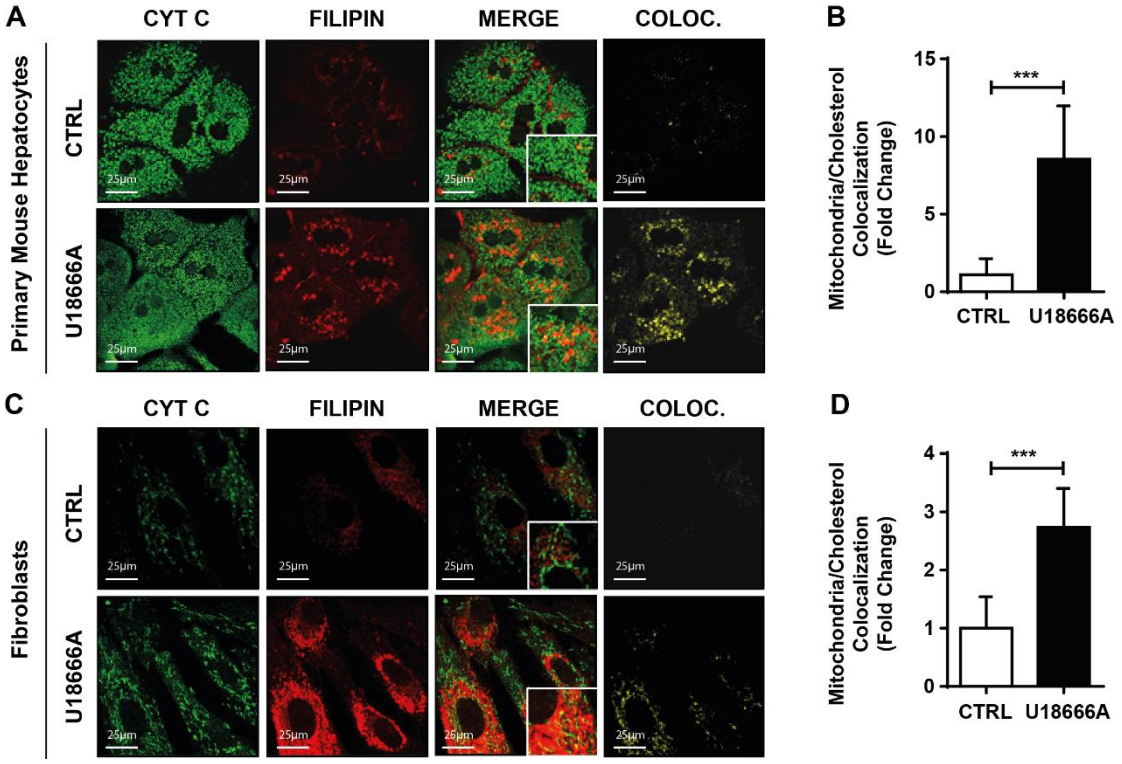

Figure R-32. Effects of U18666A treatment on liver and human fibroblasts mCholesterol levels. PMH from Npc1$^{+/+}$ mice and fibroblasts from control patients were treated with U18666A 2µg/µl for 16h. (A) Cyt C and Filipin co-staining in NPC$^{+/+}$ PMH. (B) Staining markers colocalization of analysis of (A) using Image J software. (C) Cyt C and Filipin co-staining in fibroblasts from control patients. (D) Staining markers colocalization of analysis of (C) using Image J software. Values are presented as means ± SEM (n>5, Unpaired Student's t-test (two-tailed)).

Interestingly, U18666A treatment also significantly increased StARD1 expression in both PMH from Npc1$^{+/+}$ mice and Npc1$^{+/+}$ fibroblasts (**Figure R-33A,B**). Similar findings were observed in the expression of MNL64 although to a lower extent than that of StARD1 (**Figure R-33A,B**). Moreover,

in line with preceding findings, U18666A treatment decreased the expression of ACDase in PMH from Npc1$^{+/+}$ mice and control Npc1$^{+/+}$ fibroblasts (**Figure R-33A,B**).

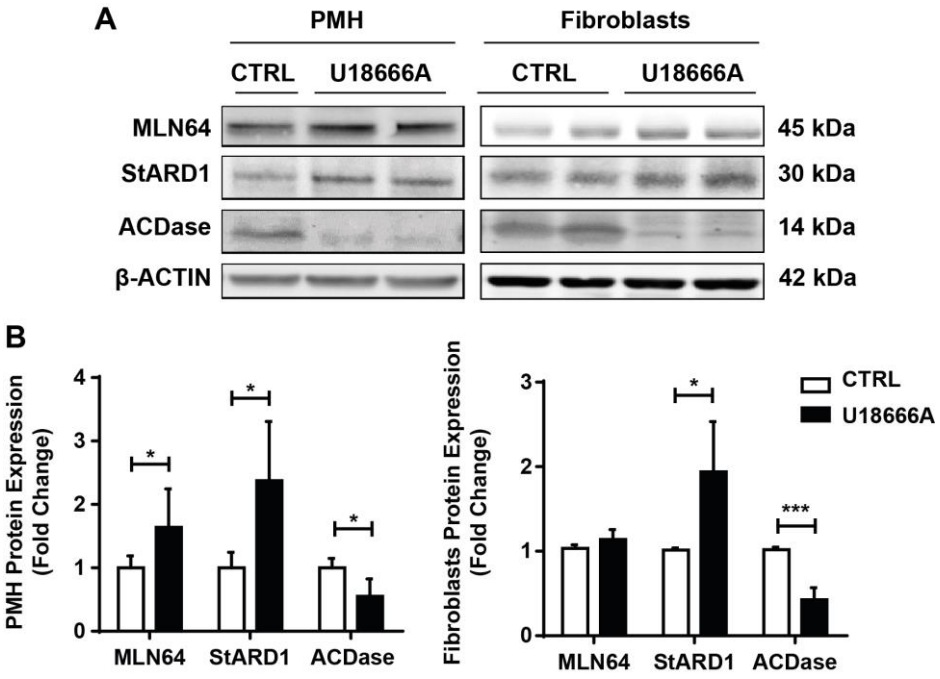

Figure R-33. Effects of U18666A treatment on liver and human fibroblasts StARD1 and ACDase expression levels. PMH from Npc1$^{+/+}$ mice and fibroblasts from control patients were treated with U18666A 2µg/µl for 16h. (A) StARD1, MLN64 and ACDase protein levels. (B) Protein expression quantification of (A) by ImageJ software. Data are presented as means ± SEM (n>5, P<0.05. Unpaired Student's t-test (two-tailed)).

3.5. ACDASE OVEREXPRESSION IN FIBROBLASTS FROM NPC PATIENTS PREVENTS STARD1 UPREGULATION AND mCHOLESTEROL ACCUMULATION WITHOUT ALTERATIONS IN MLN64 EXPRESSION

To examine the cause-and-effect relationship between the decreased expression of ACDase and the induction of StARD1, we analyzed whether ACDase overexpression has a specific impact in the regulation of StARD1. For this purpose, Npc$^{-/-}$ fibroblasts from NPC patients were transfected with cDNA encoding ACDase (MGC Human ASAH1 Sequence-Verified cDNA Accession: BC016481). Compared to transfection with scrambled control green fluorescence protein (GFP) vector, ACDase transfection resulted in a 30-fold increase in ACDase expression (**Figure R-34A**), which translated in significantly higher ACDase protein levels (**Figure R-34B,C**). While this event barely affected MLN64 expression, ACDase overexpression markedly downregulated the expression of StARD1 in Npc1$^{-/-}$ fibroblasts (**Figure R-34B,C**).

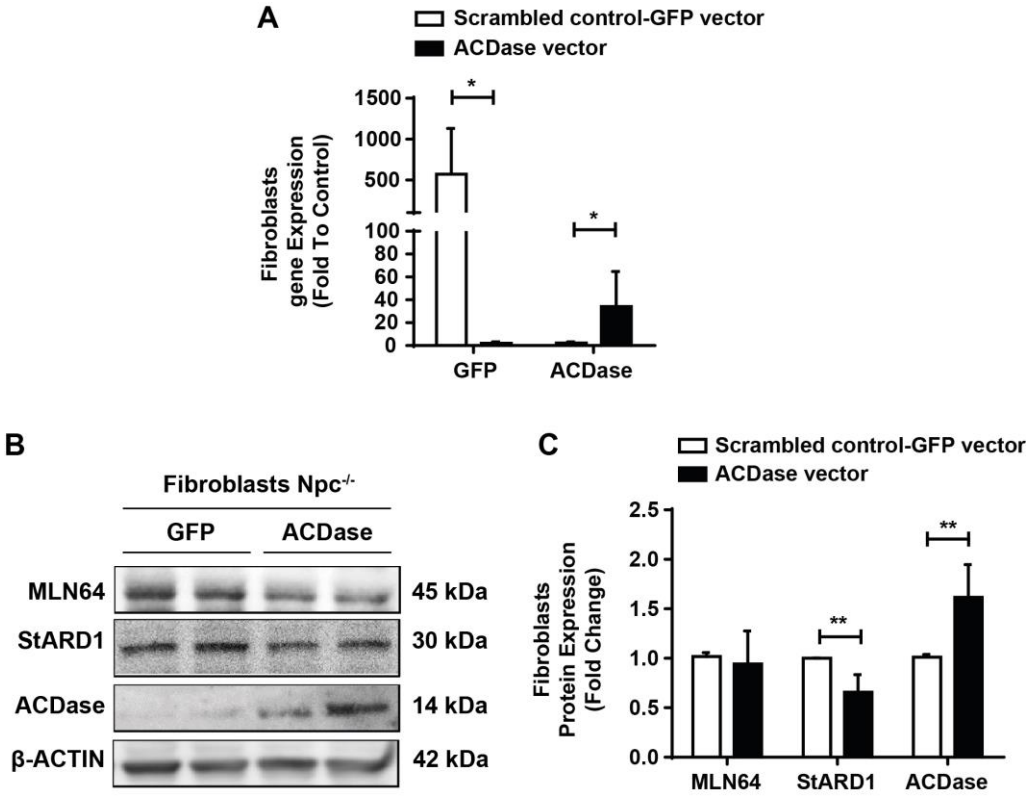

Figure R-34. Effects of ACDase overexpression in fibroblasts from NPC patients on StARD1 levels. Fibroblasts from NPC patients were transfected with a sobrexpression ACDase vector or the scrambled control-GFP vector. (A) GFP and ACDase mRNA expression levels. (B) StARD1, MLN64 and ACDase protein expression levels. (C) Protein expression quantification of (B) by ImageJ software. Data are presented as means ± SEM (n>5, P<0.05. Unpaired Student's t-test (two-tailed)).

To determine the impact of ACDase overexpression on the trafficking and accumulation of cholesterol in mitochondria, we performed confocal microscopy analyses of Npc1$^{-/-}$ fibroblasts transfected with ACDase. Npc1$^{-/-}$ fibroblasts from patients with NPC disease overexpressing ACDase exhibited lower mitochondrial free cholesterol levels as indicated by the colocalization of filipin with Cyt C staining, compared to scrambled control-GFP transfected fibroblasts (**Figure R-35A,B**). These findings indicate that ACDase expression represses StARD1 upregulation and decreases mCholesterol accumulation in human NPC disease.

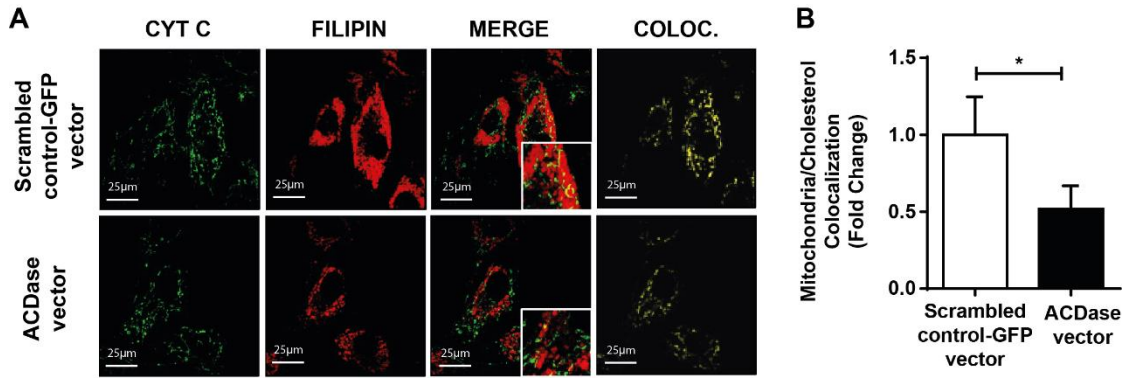

Figure R-35. Effects of ACDase overexpression in fibroblasts from NPC patients on mCholesterol levels. Fibroblasts from NPC patients were transfected with a sobrexpression ACDase vector or the scrambled control-GFP vector. (A) Mitochondria and Filipin co-staining for confocal microscopy analyses. (B) Staining markers colocalization analysis using Image J software. Data are presented as means ± SEM (n>5, Unpaired Student's t-test (two-tailed)).

3.6. ACDASE OVEREXPRESSION IN FIBROBLASTS FROM NPC PATIENTS INCREASES mGSH, IMPROVES MITOCHONDRIAL FUNCTION AND PROTECTS AGAINST OXIDATIVE STRESS AND CELL DEATH

We next examined the functional impact of ACDase overexpression in fibroblasts from NPC patients. Consistent with the ability of ACDase to decrease StARD1 expression and mCholesterol accumulation (**Figure R34,35**), Npc1$^{-/-}$ fibroblasts from patients with NPC transfected with ACDase exhibited increased mGSH levels compared to fibroblasts transfected with control GFP vector (**Figure R-36A**). Moreover, ACDase expression increased real-time oxygen consumption rates determined by a Seahorse extracellular flux analyzer compared to Npc1$^{-/-}$ fibroblasts from NPC patients transfected with control GFP control vector (**Figure R-36B**), leading to enhanced rates of basal respiration, ATP production and maximal respiration (**Figure R-36C**). Furthermore, ACDase transfection also resulted in decreased oxidative stress in response to H_2O_2 challenge as revealed by lower CellROX Deep Red fluorescence compared to Npc1$^{-/-}$ fibroblasts from NPC patients transfected with control GFP vector (**Figure R-36D**). In line with these observations, Npc1$^{-/-}$ fibroblasts from NPC patients transfected with control GFP vector were sensitive to H_2O_2-induced oxidative cell death and this outcome was ameliorated by ACDase transfection (**Figure R-36E**), consistent with the replenishment of mGSH levels and attenuation of CellROX Deep Red fluorescence. Overall, these findings indicate that expression of ACDase has important functional consequences in fibroblasts from NPC patients.

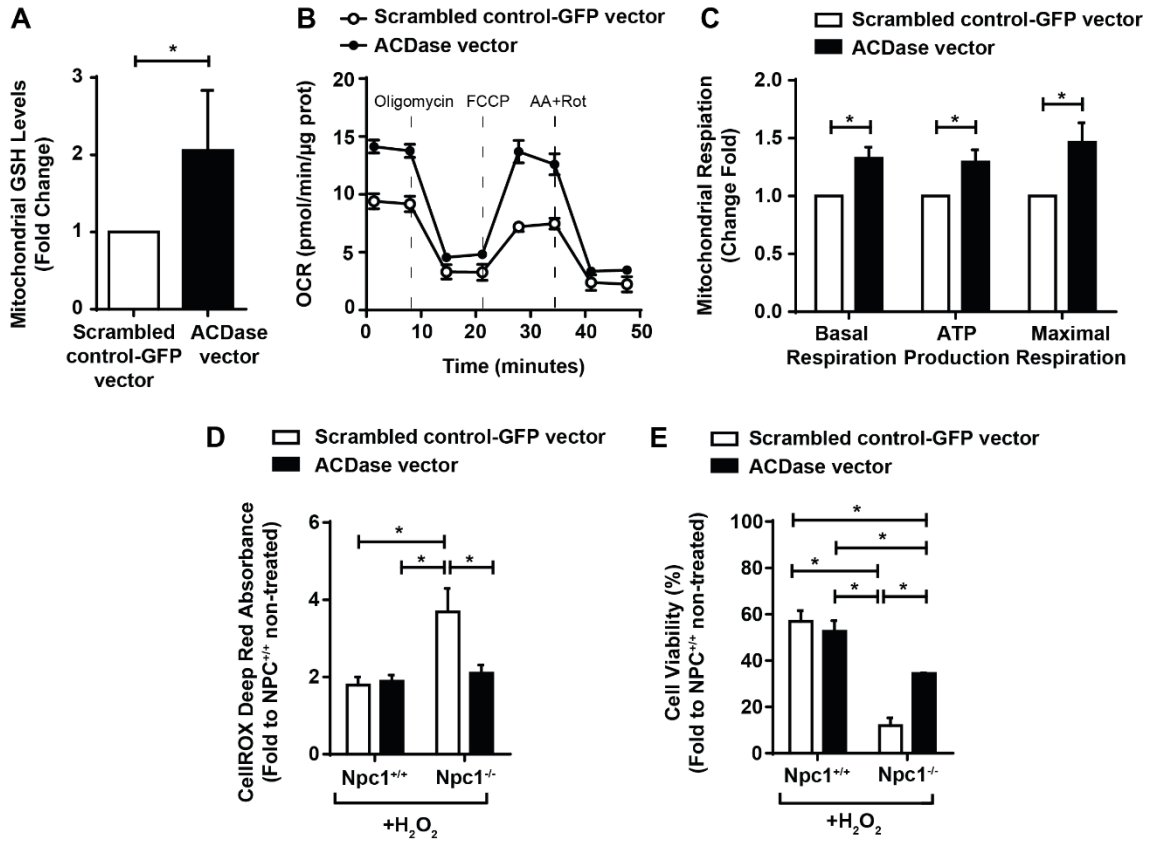

Figure R-36. Effects of ACDase overexpression on fibroblasts from NPC patients. Fibroblasts from NPC patients were transfected with a sobrexpression ACDase vector or the scrambled control-GFP vector. (A) Mitochondrial GSH levels. (B-C) Oxygen consumption rates by Seahorse XF analyzer. (D-E) Fibroblasts ROS production and cell viability after treatment with H_2O_2 1mM for 24h followed by CellROX Deep Red absorbance and MTT assay respectively. Data are presented as means ± SEM (N=3, P<0.05, Unpaired Student's t-tailed) or Two-way ANOVA test).

On the whole, in this study we have explored new molecular mechanisms of NPC disease involving mCholesterol accumulation and its regulation by StARD1. We have observed that livers of $Npc1^{-/-}$ mice and fibroblasts from NPC patients present a significant increase in mCholesterol levels and StARD1 expression. Interestingly, we have dissociated the induction of StARD1 expression from ER stress and established an inverse relationship between ACDase and StARD1 expression. Findings with PMH from $Npc1^{+/+}$ mice and fibroblasts from control patients treated with U18666A have also exhibited increased mCholesterol accumulation, StARD1 upregulation and ACDase repression. Moreover, transfection of fibroblasts from NPC patients with ACDase have led to decreased StARD1 expression and subsequent mCholesterol accumulation, resulting in the replenishment of mGSH levels, improvement of mitochondrial functional performance and protection against oxidative stress-mediated cell death.

DISCUSSION

Growing focus has been given to mCholesterol homeostasis and regulation over recent years as it has become evident that mCholesterol levels are altered in a wide range of pathological conditions. Although mCholesterol is essential to fulfil vital physiological functions, such as the synthesis of bile acids and steroid hormones, evidence reveals that mCholesterol accumulation may be a key step in disease progression. Accumulation of cholesterol in mitochondria has emerged as a key player in different liver diseases such as Alcoholic liver disease and Niemann-Pick Type C disease.

Given the critical structural role of cholesterol in membrane bilayers, it is known that mCholesterol enrichment contributes to disease pathogenesis in part through its effects in the perturbation of membrane physical properties (Baggetto et al., 1992; Colell et al., 2003; Montero et al., 2008; Paradis et al., 2013). This event also causes impaired mGSH import and alterations in mitochondrial permeability transition and apoptosis (Barbero-Camps et al., 2014, 2013; Bosch et al., 2011; Caballero et al., 2009; Colell et al., 2003; Fernández et al., 2013, 2009a; Llacuna et al., 2011; Lluis et al., 2003; Marí et al., 2006; Montero et al., 2010, 2008). Despite the great amount of studies describing mechanisms of cholesterol-mediated mitochondrial dysfunction, some aspects still require further clarification. Several studies have reported consequences of mCholesterol enrichment on bioenergetics, however, there is controversy among the scientific community as some groups have found decreases in ATP synthesis and mitochondrial respiration (Baggetto et al., 1992; Campbell and Chan, 2007; Echegoyen et al., 1993; Yu et al., 2005) while others have reported no effects at all (Colell et al., 2003; Dietzen and Davis, 1994). The different experimental conditions and the localization of cholesterol in the OMM or in both mitochondrial membranes may explain the differences reported, which deserved further consideration. To address the impact of mCholesterol accumulation on liver mitochondria functionality, we used models specifically involving targeted manipulations of mCholesterol import and content.

The *in vivo* approach to rapidly increase liver cholesterol levels consisted on feeding mice a cholesterol-enriched diet supplemented with sodium cholate, which has been used in other studies as it sustains liver cholesterol levels (Domínguez-Pérez et al., 2019; Marí et al., 2006). Findings in this thesis indicate that the presence of sodium cholate in the diet downregulates the expression of key enzymes involved in the synthesis of bile acids such as Cyp7a1 and Cyp8b1, without effect in the alternate pathway of bile acid synthesis in mitochondria. Thus, sodium cholate is an important component of the HC diet since it contributes to the maintenance of hepatic free cholesterol levels by preventing the metabolism of dietary cholesterol into bile acids.

The *in vivo* loading of hepatic cholesterol levels by HC feeding also affected the endogenous cholesterol synthesis as reflected by the attenuated expression of Srebp2 and Hmgcr.

Focusing on mitochondria, we observed an increased expression of StARD1 and MLN64, which play critical roles in the regulation of mitochondrial trafficking (Caron et al., 1997; Elustondo et al., 2017; Miller, 2007b). Importantly, mitochondrial fractionation into mitoplasts revealed that cholesterol accumulation occurs in both the outer and inner mitochondrial membranes, consistent with a concerted action between MLN64 and StARD1, which move cholesterol from extramitochondrial sources to the outer mitochondrial membrane and from here to the inner mitochondrial membrane, respectively (Caron et al., 1997; Elustondo et al., 2017; Miller, 2007b, p. 2). Of relevance, by using fluorescence anisotropy we confirmed the data from previous studies reporting increased mitochondrial membrane rigidity upon mCholesterol accumulation (Baggetto et al., 1992; Colell et al., 2003; Montero et al., 2008; Paradis et al., 2013). Such changes in the membrane physical properties could be linked with the alterations observed in mitochondrial morphology. Mitochondria after HC feeding presented abnormal cristae and appeared rounded, as observed by a decrease in mitochondrial length. These results were in line with a previous study also reporting mitochondrial loss of cristae and rarefied matrix upon HC feeding (Domínguez-Pérez et al., 2019). A feature we could not observe was the presence of vesicles lying between the inner and outer mitochondrial space as reported by Echegoyen et al. in rat liver mitochondria enriched with different amounts of cholesterol (Echegoyen et al., 1993). However, while this group performed transmission electron microscopy analysis on isolated mitochondria enriched in cholesterol *in situ*, we and Domínguez-Pérez et al. used preserved hepatic tissue of mice subjected to HC diet. Thus, the different experimental conditions could be the key point in the differences observed.

Aside from these findings, this thesis reports for the first time the specific role of mCholesterol accumulation on oxidative phosphorylation. We show that *in vivo* cholesterol accumulation impairs mitochondrial oxidative phosphorylation, reflected in decreased ADP-stimulated OCR from complex I, which translated in decreased RCR and UCR. A potential explanation for these results is that cholesterol could be altering either the expression of specific subunits of complex I-V or their assembly into supercomplexes. It is well established that the vast majority of the subunits of the mitochondrial respiratory complexes are encoded by nuclear DNA, which then traffic to mitochondria by the presence of intramitochondrial sorting signals to undergo a highly-regulated mechanism of import and insertion into mitochondrial membranes (Horvath et al., 2015). Once in the IMM, these subunits can remain as independent entities or associate with each

other into supercomplexes (Acín-Pérez et al., 2008; Acín-Perez and Enriquez, 2014). Cholesterol could thus be interfering in the gene expression of these subunits or in its aggregation. We observed that cholesterol loading does not affect the expression of mitochondrial respiratory chain subunits, but it disrupts the assembly of respiratory supercomplexes I_1+III_2+IV and I_1+III_2. These findings are consistent with the current concept that mitochondrial supercomplexes structures are responsible for carrying out cellular respiration (Acín-Pérez et al., 2008; Acín-Perez and Enriquez, 2014), as opposed to the long-held view of mitochondrial respiratory complexes as independent entities connected by mobile carriers CoQ and cytochrome c.

The effect of mCholesterol in the assembly of the mitochondrial supercomplexes may reflect the defects at the mitochondrial membrane level likely due to changes in membrane physical properties (Budin et al., 2018; Maranzana et al., 2013). Indeed, reconstitution of complex I and complex III in proteoliposomes with different lipid composition revealed that the ratio of phospholipid to protein determines the assembly of supercomplex I_1+III_2 (Maranzana et al., 2013). Moreover, studies in bacteria engineered to display increased levels of unsaturated fatty acids unraveled that membrane viscosity determined by lipid composition controlled the rate of respiration coupled to ADP phosphorylation (Budin et al., 2018). Whether the deleterious effect of cholesterol enrichment in mitochondrial function is reversible upon cholesterol extraction or membrane fluidization remains to be further investigated. In line with this possibility, Yu et al. showed that the defective ATPase function from brain mitochondria from NPC knockout mice, which exhibit an increased mCholesterol loading, was restored by cholesterol extraction with cyclodextrin (Yu et al., 2005).

While mCholesterol loading *in vivo* by feeding the HC diet reflects the combined effect of cholesterol on established and newly assembled respiratory supercomplexes by membrane mediated changes, we decided to also address the direct impact of cholesterol enrichment in the already existing respiratory complexes by using isolated mitochondria. In line with this, we wondered whether this event involves interactions of cholesterol with bilayer's proteins and/or lipids, fact that we tackled by using enantiomer cholesterol, the mirror image of natural cholesterol that specifically interacts with lipids but not proteins due to enantioselective restriction (Kristiana et al., 2012; Li et al., 2004; Westover and Covey, 2004; Xu et al., 2005). Enrichment of liver mitochondria in enantiomer cholesterol resulted in decreased complex I-driven state 3/state 3u respiration, suggesting that cholesterol-lipid interactions in mitochondrial membranes accounts for the impaired ADP-stimulated OCR driven by complex I. Intriguingly, *in vitro* cholesterol loading also increased complex I-driven state 4o respiration, an outcome not

observed with the *in vivo* mCholesterol loading by HC feeding. Whether cholesterol-lipid interactions is a predominant effect over the interaction of cholesterol with proteins to account for the decreased complex I-driven state 3/3u respiration remains to be further investigated. Another differential feature of our findings with the *in vivo* model with respect to the *in situ* mCholesterol enrichment is that the latest did not affect complex II-driven OCR. This differential effect suggests that the impact of cholesterol in impairing complex II-mediated OCR reflects the effects of cholesterol in the assembly of respiratory supercomplexes rather than a direct effect of the changes in membrane physical properties. A caveat from the *in vivo* enrichment of mitochondria in cholesterol on mitochondrial respiration by feeding a HC enriched diet is whether the effects truly reflect the actions of cholesterol per se or are determined by cholesterol-derived metabolites. As cholesterol is the precursor of bile acids, it is conceivable that part of the observed effects of cholesterol enrichment in mitochondrial performance could be mediated by the action of bile acids generated from dietary cholesterol. This potential contribution, however, seems unlikely in light of the fact that the presence of sodium cholate in the HC-enriched diet impaired the classical pathway of bile acid synthesis due to decreased the expression of cyp7a1 and cyp8b1, consistent with the lack of increased bile acid pool from HC-fed mice.

As one of the reported consequences of the disruption of the association between complex I and complex III and the impaired assembly of subsequent supercomplexes I_1+III_2+IV and I_1+III_2 is the enhanced generation of superoxide anion (Maranzana et al., 2013), we analyzed the impact of mCholesterol enrichment in oxidative stress and liver injury. HC feeding caused increased ROS formation, mitochondrial ROS generation and mGSH depletion that was accompanied by steatosis and liver injury. Considering these findings, we decided to explore the potential impact of mGSH restoration upon mitochondrial performance and liver function. While glutathione is not effectively transported into cells, the ethyl ester of glutathione known as GSHee, in which the carboxyl group of the glycine residue is esterified, can easily penetrate cells and reach mitochondria. Once inside, it undergoes hydrolysis by intracellular esterases overall releasing GSH. This compound has been found to protect cells against a wide range of damages such as radiation and oxidants (Wellner et al., 1984), and it has also been found to rescue mitochondrial defects in cystic fibrosis and NPC disease animal models (Kelly-Aubert et al., 2011; Torres et al., 2017b). Findings in these thesis showed that GSHee treatment in HC-fed mice recovered both total and mGSH levels at the same time that reduced mitochondrial ROS production, oxidative stress and liver injury. Interestingly, the effect of mGSH restoration by GSHee also translated in replenishing mitochondrial respiration and RCR, in line with previous findings in cerebellar mitochondrial function in NPC disease (Torres et al., 2017b). Restoration of mGSH levels by GSHee

rescued the content of complex III_2, although it failed to normalize the assembly of supercomplexes I+III_2+IV and I+III_2, which likely reflects the effect of remaining cholesterol-mediated effect on membrane dynamics that are not reversed by mGSH restoration. However, quite intriguingly, the restoration of complex III_2 by GSHee seems to compensate the function of mitochondrial respiration. Further work will be required to determine the mechanisms whereby mGSH depletion by mCholesterol loading impact the redox-dependent assembly of supercomplexes and whether the reversible loss of complex III_2 by cholesterol is redox dependent in view of its restoration by mGSH with GSHee.

All together these findings reveal that mCholesterol accumulation disrupts mitochondrial functional performance and the organization of respiratory supercomplexes assembly, which contributes to oxidative stress and liver injury (**Figure D-1**).

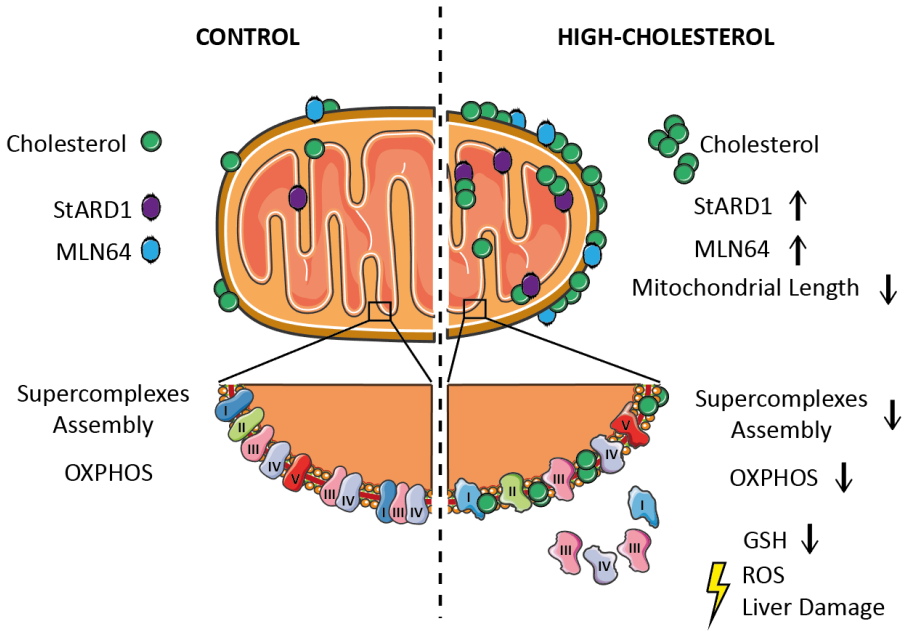

Figure D-1. Schematic representation of the new findings on cholesterol-induced mitochondrial and liver damage.

mCholesterol accumulation has been shown to play a key role in alcoholic liver injury. ALD presents as a broad spectrum of disorders, ranging from simple fatty liver to more severe forms of liver injury, including cirrhosis. Hepatocellular injury in ALD is mainly found in the PV zone in line with the pericentral zonation of fatty acid synthesis and alcohol metabolism pathways. To date, most information on the role of zonation in ALD have revealed that this disease progresses from PV areas to the PP zones by a gradual accumulation of lipid droplets and a different zonal expression of ADH and CYP2E1 (Chalasani et al., 2008; Jauhonen et al., 1982; Keegan et al., 1995;

MacSween and Burt, 1986; Nakano et al., 1982). However, an important and still not completely resolved issue is why ALD originates and occurs in the PV zone. Although the zonated expression of CYP2E1 seems to play a key role in the zonal progression of ALD, other mechanisms may be involved. As described in this thesis introduction, there is a great amount of studies that have characterized many molecular mechanisms of alcohol-induced liver injury such as abnormal methionine metabolism, impaired antioxidant defense and mitochondrial dysfunction. However, to the best of our knowledge the majority of these studies have described ALD related molecular mechanisms without taking liver heterogeneity into account. Not focusing on specific liver areas when studying ALD can completely obscure existing differences in the organ and may be a limitation for increasing the disease knowledge. Extending previous work describing specific mGSH depletion in PV hepatocytes after chronic alcohol feeding (García-Ruiz et al., 1994), in this thesis we have described the hepatic zonal effects of alcohol-induced StARD1 and its regulation of mCholesterol levels.

To study liver zonation in ALD we used the Lieber-De Carli Liquid diet model and we combined histological techniques with specific isolation of murine PV and PP hepatocytes. Despite being technically challenging, the separation of PV and PP hepatocytes by liver perfusion was highly efficient leading to enriched and intact PP and PV subfractions. The markers used to check the quality of hepatocytes separation were decided upon their abundance in the different hepatic areas and the previous work by others in the field (Ben-Moshe and Itzkovitz, 2019; Braeuning et al., 2006). Hepatic zonation was also studied through transmission electron microscopy. Following a similar approach to Elsayed and colleagues (Elsayed et al., 2019), we developed a methodology that allowed us to distinguish between PP and PV hepatocytes in the electron microscope and to analyze the structural effects of alcohol consumption on both hepatocytes populations.

Our findings revealed that StARD1 is upregulated in liver tissue upon alcohol feeding and that its expression is mainly increased in PV areas. Interestingly, we showed that alcohol is not the only factor that increases PV StARD1 expression as low levels of oxygen, a typical feature of the PV zone, also trigger StARD1 upregulation. Hypoxia has been long studied in ALD as ethanol elimination depends on the rate of oxygen utilization by the liver (French, 2004; Morris and Yeligar, 2018). Among the different hypoxia models cobalt chloride ($CoCl_2$) is one of the most commonly used. This compound chemically stabilizes hypoxia inducible factors 1α and 2α under normoxic conditions and overcomes the limitation of many researchers in accessing to a hypoxia chamber or a CO_2 incubator with regulated oxygen levels (Muñoz-Sánchez and Chánez-Cárdenas,

2019). In this thesis we show for the first time the synergic effect of alcohol and hypoxia on the upregulation of StARD1.

In line with the preceding findings, we observed that alcohol consumption increases both total and mCholesterol levels specifically in PV hepatocytes. StARD1 is thus presented as the master regulator of mCholesterol accumulation in ALD as we did not observe MLN64 upregulation upon alcohol consumption. It is important to mention that cholesterol analysis in the whole liver tissue unmasked the differences between PV and PP areas and that we had to develop a quantification method by ImageJ to measure cholesterol in different hepatic areas separately. This limitation highlights the importance of taking liver zonation into account when studying ALD.

As previously reported and also shown in this thesis with the *in vivo* HC feeding model, mCholesterol accumulation results in oxidative stress and mGSH depletion. Thus, we determined the effects of alcohol consumption on such parameters in PV and PP hepatocytes separately. PV hepatocytes, in contrast to PP population, presented a bigger drop in total and mGSH levels despite their effort in increasing the expression of the mGSH transporter DIC. This specific GSH decrease in PV hepatocytes correlated with increased lipid peroxidation and ROS generation in the same hepatocytes population and, overall, it resulted in liver injury. Interestingly, the drop in GSH content was bigger in PV hepatocytes as this population presented higher total and mGSH levels in basal conditions compared to PP fraction. These findings notably contrast with previous observations reporting higher glutathione peroxidase and GSH levels in the PP zone (Harisch and Meyer, 1985; Smith et al., 1979). These contradictory results may be explained by the different techniques and models used for studying hepatocyte heterogeneity as conclusions drawn from the different zonal hepatic studies largely depend on the methodology used. Harisch et al. studied GSH distribution in the liver lobule of rats by using histochemical techniques, a similar approach used by Smith and colleagues. In our case, we specifically analyzed GSH levels in fractionated PP and PV hepatocytes from mice. These differences regarding the basal levels of GSH along the hepatic acinus should be further investigated. In any event, our findings support previous evidence reporting the PV area as the most affected one by alcohol intake and reveal for the first time an upregulation of StARD1 and mCholesterol levels by alcohol consumption specifically in PV hepatocytes.

In view of the preceding findings, we studied the impact of StARD1 deletion on alcohol-induced liver injury. We used liver-specific StARD1-deficient mice as they do not express StARD1 in hepatocytes. The absence of StARD1 expression in this animal model has been shown to protect against acetaminophen hepatotoxicity elicited by valproic acid or fasting in mice (Torres et al.,

2019). In our case, knocking-out StARD1 protected alcohol-fed mice from mCholesterol increase, GSH reduction and increased oxidative stress in PV area. StARD1 deletion also protected mice from alcohol-induced elevation of serum levels of AST. Overall, our study defines a previously unrecognized role of StARD1 in ALD disease as the deletion of StARD1 protects from alcohol-induced mCholesterol accumulation and its detrimental effects. Most importantly, these events take place specifically in the PV area and may account for the pericentral hepatocellular injury observed in ALD.

Findings in this thesis clearly indicate that taking liver zonation into account is highly important when studying ALD. To further investigate the effects of alcohol consumption along the hepatic acinus, we conducted transmission electron microscopy analysis in PV and PP hepatocytes separately. In the past decades, interesting studies have been made to analyze the structural changes in hepatocytes by alcohol consumption. However, as far as we are aware, any of these studies have taken liver zonation into consideration. We observed significant differences between PP and PV areas in glycogen and lipid droplet content as well as mitochondrial morphology.

Decreased glycogen levels after alcohol intake have already been reported, which could be explained by either a decreased rate of glycogen synthesis or an increased rate of breakdown. Winston and Reitz conducted several studies on the effects of ethanol on glycogenolysis and concluded that increased glycogen breakdown did not occur and could not account for lowered glycogen levels (Winston and Reitz, 1984, 1981, 1980). Regarding to glycogenesis, Van horn et al. reported alterations in glucose transport and glycogen synthase activity after alcohol consumption, which may contribute to the lowered glycogen levels (Van Horn et al., 2001). Whether this decrease in glycogen synthesis is enough to account for the magnitude of the decreases in glycogen levels observed remains to be determined. In any event, glycogen metabolism seems to be closely linked to alcohol-induced liver injury as the stimulation of glycogenesis in alcohol-fed mice reversed glycogen levels decrease and abrogated alcohol-induced liver injury as well as hepatic lipid deposition (Gu et al., 2015). Although we also observed a decrease in glycogen content in both PP and PV areas, the major decrease was found in PV hepatocytes. Whether the differences in glucose and glycogen metabolism between these two areas are responsible for these observations remains to be further investigated. Focusing on lipid metabolism, ALD is characterized by the accumulation of lipid droplets in the cytosol of hepatocytes, a distinguishing characteristic of steatosis (Crabb and Liangpunsakul, 2006; Groebner et al., 2019, 2019; McNiven and Casey, 2011; Nakajima et al., 2004; Ohashi et al., 2018; You et al., 2008). We examined lipid droplet content in PV and PP hepatocytes from our ethanol-

fed mice and we found that ethanol dramatically increased lipid droplet numbers in both areas. Interestingly, lipid droplets from PP area were highly different in sizes while in PV hepatocytes they were mainly small. The mobilization and storage of hepatic lipids is a highly complex and regulated mechanism that is affected by physiological, hormonal and nutrient signals. As with glycogen, the differential metabolic gene expression and functionality between PP and PV hepatocytes as well as the signals they are subjected to could explain the differences observed in lipid droplets sizes.

Mitochondrial morphology is also another aspect highly studied in ALD as mitochondria are known to be challenged by alcohol consumption. Different studies have reported the appearance of misshapen and enlarged mitochondria (megamitochondria) upon alcohol consumption (Bruguera et al., 1977; Chedid et al., 1986; Das et al., 2012; Han et al., 2012). We observed such changes in PP hepatocytes with the largest mitochondria surrounding lipid droplets. However, alcohol in PV areas did not trigger mitochondria enlargement but a dramatic change in their shape. The same structures we observed in PV hepatocytes after alcohol intake have been previously observed as a consequence of mitochondrial membrane potential loss. Miyazono et al. reported that CCCP administration induces a mitochondrial structural transformation into distinct U-, C-, and ring-shaped mitochondria (the latest also called doughnut mitochondria) (Miyazono et al., 2018). These mitochondrial spheroid formation has also been reported to occur in the murine liver by acetaminophen overdose (Ding et al., 2012). These two models share with ours the presence of a severe oxidative mitochondrial stress. Thus, alcohol consumption could be triggering mitochondrial structural collapse in PV hepatocytes through the increase oxidative stress observed in this population.

In summary these data reveal a preferential damage after alcohol consumption in liver zone 3 or perivenous, inducing structural changes in mitochondria from PV area, which may account for the prevailing injury seen in this area in ALD (**Figure D-2**). Basal differences in PP and PV areas should be thus taken in consideration when approaching ALD studies.

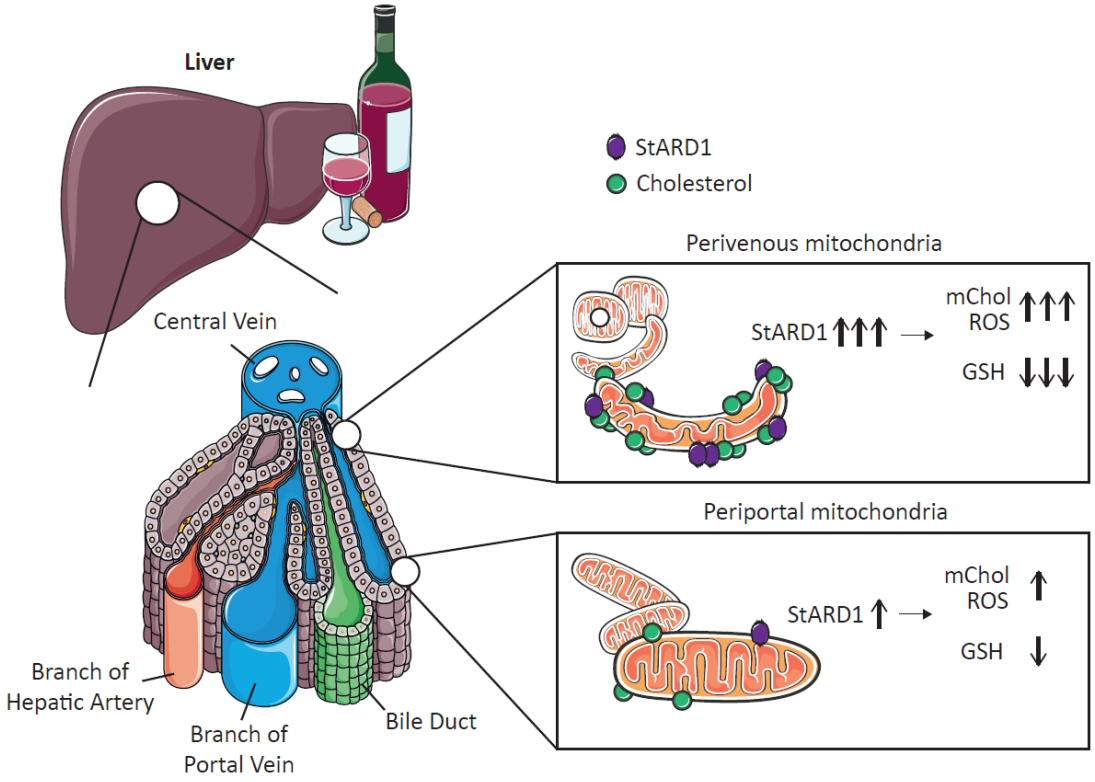

Figure D-2. Diagram depicting the new findings of this thesis on alcohol-induced mitochondrial and liver damage.

Niemann-Pick Type C disease is another pathology also characterized by a defect in intracellular trafficking of cholesterol. While the accumulation of cholesterol in lysosomes is a primary event in NPC disease and believed to promote disease progression, the disturbance of intracellular cholesterol trafficking is more extensive and affects other intracellular organelles. The trafficking of mCholesterol in NPC disease is not well understood and may involve different intracellular sources and different molecular players. MLN64 overexpression has been shown to increase mCholesterol levels in NPC cells (Balboa et al., 2017). However, targeted mutation of the MLN64 STAR domain results in modest alterations in cellular sterol metabolism (Kishida et al., 2004). Another potential key molecule involved in NPC is StARD1. Although this protein is key in the intramitochondrial trafficking of cholesterol, the regulation of StARD1 in NPC disease has not been explored yet. In this thesis we have further characterized the accumulation of cholesterol in mitochondria and provided evidence for a previously unrecognized inverse relationship between ACDase and StARD1.

Previous work have revealed that mCholesterol accumulation and subsequent impairment of mitochondrial function and GSH depletion contribute to NPC disease. Following on the role of mGSH depletion in NPC disease (Torres et al., 2017b), we analyzed mCholesterol levels using *in vivo* and *in vitro* models of NPC disease: 1) livers from NPC1$^{-/-}$ mice, 2) fibroblasts from NPC

patients, and 3) *in vitro* treatment of healthy primary mouse hepatocytes and fibroblasts with U18666A, a compound that promotes the accumulation of intracellular cholesterol mimicking NPC disease (Cenedella, 2009; Lu et al., 2015). We showed increased mCholesterol levels in the three NPC models and its correlation with increased mitochondrial membrane rigidity specifically in livers from NPC1$^{-/-}$ mice. These data also correlated with increased expression of MLN64 and StARD1. Although forced MLN64 overexpression results in mCholesterol accumulation (Balboa et al., 2017), global deletion of StARD1 in mice results in lethal congenital lipoid hyperplasia (Caron et al., 1997), arguing that in the absence of StARD1 other members of the family cannot compensate for the trafficking of cholesterol to mitochondrial inner membrane for metabolism and generation of steroid hormones. Thus, while the mechanism involved in the trafficking of cholesterol to the mitochondrial inner membrane, which is the rate-limiting step in steroidogenesis, is not fully characterized likely involving a coordinated action among STAR family members, StARD1 plays a crucial role in this event and hence understanding the regulation of StARD1 in NPC disease may be of relevance to prevent mitochondrial dysfunction and mGSH depletion (Torres et al., 2017b).

ER stress has been shown to stimulate the transcriptional upregulation of StARD1 independently of SREBP activation (Fernández et al., 2013; Torres et al., 2019). However, we confirmed that the onset of ER stress is not a characteristic feature of NPC disease (Klein et al., 2011; Platt et al., 2012), and hence we searched for alternative mechanisms involved in StARD1 uregulation. Another potential mechanism involved in StARD1 regulation is through ACDase, a lysosomal enzyme responsible for the degradation of ceramide into sphingosine and free fatty acids that regulates sphingomyelin homeostasis. Built on previous findings in adrenocortical cells showing that ACDase antagonizes SF-1 and represses target genes, including StARD1 (Lucki et al., 2012), we showed that the increased expression of StARD1 correlates with lower levels of ACDase in liver from Npc1$^{-/-}$ mice and in fibroblast from NPC patients. Importantly, we also showed that increased intracellular cholesterol induced by U18666A reproduces the outcome seen in Npc1$^{-/-}$ mice in regards to the inverse relationship between ACDase and StARD1 expression. Although further work will be required to understand the basis for the ACDase repression in NPC disease, it is conceivable that cholesterol accumulation in lysosomes may affect membrane physical properties, secondarily modulating ACDase expression. Whether fluidization of lysosomes reverses the ACDase repression in NPC disease remains to be established.

An interesting point that deserves further consideration is the relationship between the basal levels of ACDase and its enzymatic product sphingosine in NPC disease. Sphingosine is one of the

glycosphingolipids whose levels have been shown to be increased in NPC disease (Lloyd-Evans et al., 2008; Torres et al., 2017b). As ACDase catalyzes the deacylation of ceramide to sphingosine, its lower expression would not account of the observed higher sphingosine levels in NPC disease. How can it be that sphingosine levels increased despite lower ACDase expression? Although the status of other CDases in NPC disease remains to be investigated, recent findings have reported lower expression of sphingosine kinase 1 in NPC disease (Newton et al., 2020). As sphingosine is the substrate of sphingosine kinase 1, its downregulation may contribute to the higher levels of sphingosine in NPC disease.

To further establish a specific relationship between ACDase with StARD1 expression but not MLN64 regulation, we overexpressed ACDase in fibroblasts from patients with NPC. This approach, which increased ACDase levels, resulted in decreased mCholesterol levels and downregulation of StARD1 with minimal effect in MLN64 expression, thus dissociating ACDase from MLN64 regulation. Of interest, while our findings suggest that StARD1 upregulation contributes to mCholesterol accumulation, this event could be an additional consequence of impaired mCholesterol metabolism. For instance, consistent with this possibility, reduced levels of CYP450scc (also known as CYP11A1) have been described in cerebellum of $Npc1^{-/-}$ mice, reflecting the disruption in neurosteroidogenesis and decreased levels of pregnenolone, the first steroid produced from mCholesterol, in brain of $Npc1^{-/-}$ mice (Griffin et al., 2004). ACDase overexpression in fibroblasts from NPC patients also translated in improved mitochondrial performance with higher basal respiration, ATP production and maximal respiration and protection against oxidative stress-mediated cell death. These relevant *in vitro* findings reveal the potential effect of ACDase overexpression in ameliorating mitochondrial dysfunction in NPC disease and will need to be further characterized *in vivo* by using NPC animal models.

Overall, the present study has examined the molecular players that contribute to the mCholesterol accumulation in NPC disease, and revealed a key link between ACDase and StARD1 in this event (**Figure D-3**). Given the relevance of mCholesterol accumulation in NPC disease progression through mGSH depletion (Torres et al., 2017b), these findings may provide novel opportunities for treatment to prevent mCholesterol loading and its known consequences on mitochondrial function and antioxidant defense, which are of potential relevance in NPC disease.

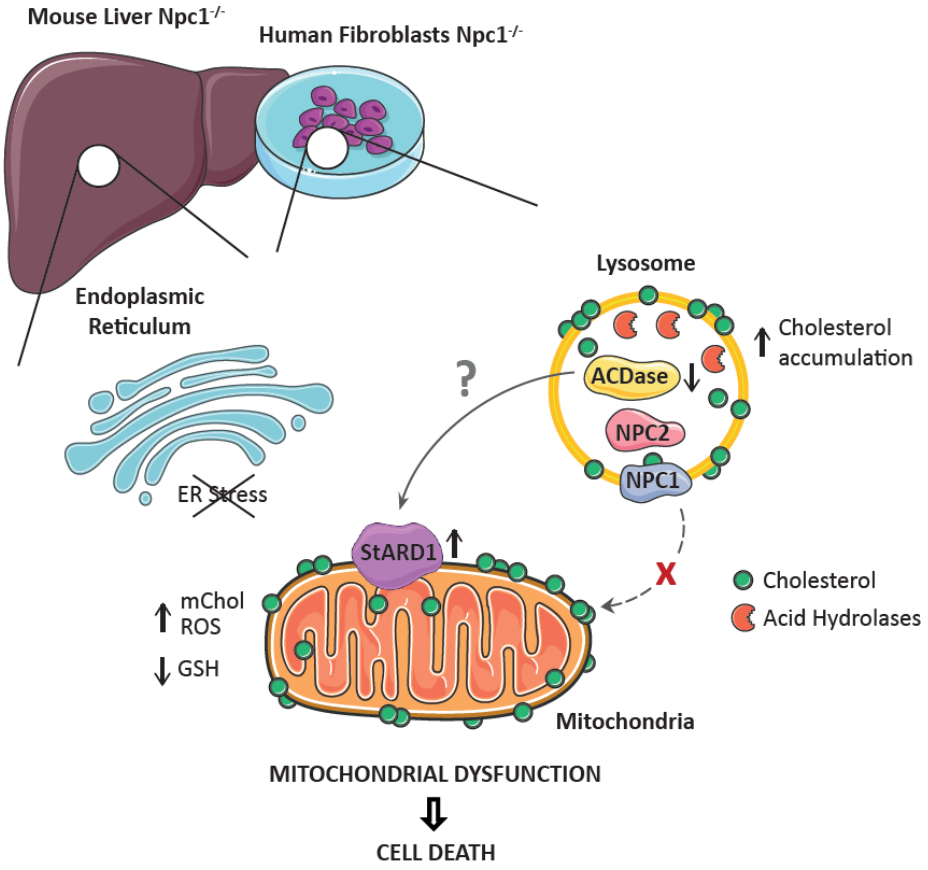

Figure D-3. Schematic illustration of the putative mechanisms of mCholesterol accumulation in NPC disease based on the present thesis findings.

In summary, although the trigger and etiology of NPC disease and ALD are certainly different, we have observed that they share a common pathological mechanism that involves mCholesterol and StARD1. Specifically, StARD1 is induced in both diseases, which triggers mCholesterol enrichment and mGSH depletion. These alterations are responsible for the observed mitochondrial dysfunction and oxidative stress that underlie the phenotype of both diseases and could be explored for development of potential therapeutics for these pathologies.

CONCLUSIONS

STUDY I. CHOLESTEROL ENRICHMENT IN LIVER MITOCHONDRIA ALTERS MITOCHONDRIAL MORPHOLOGY, IMPAIRS OXIDATIVE PHOSPHORYLATION AND DISRUPTS THE ASSEMBLY OF RESPIRATORY SUPERCOMPLEXES.

- Mitochondrial cholesterol accumulation perturbs mitochondrial membrane physical properties and morphology.
- Hepatic mitochondrial cholesterol enrichment impairs oxidative phosphorylation.
- Cholesterol loading in liver mitochondria disrupts the assembly of mitochondrial respiratory supercomplexes.
- *In vivo* mitochondrial cholesterol accumulation induces liver injury, which is prevented by GSH ethyl ester administration.

STUDY II. HEPATOCYTE-SPECIFIC STARD1 ABLATION PROTECTS FROM LIVER DAMAGE IN ALCOHOLIC LIVER DISEASE BY PREVENTING INCREASED MITOCHONDRIAL CHOLESTEROL AND OXIDATIVE STRESS PARTICULARY IN HEPATIC PERIVENOUS AREA

- Alcohol intake preferentially induces StARD1 in hepatic perivenous areas in contrast to periportal zones.
- Alcohol consumption predominantly triggers mitochondrial cholesterol levels increase and consequent oxidative stress in perivenous hepatocytes.
- Consumption of alcohol alters morphology of mitochondria from perivenous areas.
- Liver-specific StARD1 ablation protects from alcohol-induced mitochondrial cholesterol accumulation and oxidative stress overall preventing liver damage.

STUDY III. ACID CERAMIDASE IMPROVES MITOCHONDRIAL FUNCTION IN NIEMANN-PICK TYPE C DISEASE BY REPRESSING STARD1-DEPENDENT MITOCHONDRIAL CHOLESTEROL ACCUMULATION

- Cholesterol accumulates in liver mitochondria from $Npc1^{-/-}$ mice and in fibroblasts from NPC patients.
- Livers of $Npc1^{-/-}$ mice and fibroblasts from NPC patients exhibit increased StARD1 expression.
- Healthy primary mouse hepatocytes and fibroblasts treated with U18666A also exhibit increased mitochondrial cholesterol and StARD1 levels.
- Decreased expression of ACDase is found in livers of $Npc1^{-/-}$ mice, in fibroblasts from NPC patients and in healthy primary mouse hepatocytes and fibroblasts treated with U18666A.
- ACDase overexpression represses StARD1 expression, mitochondrial cholesterol accumulation and improves mitochondrial function and oxidative stress in fibroblasts from NPC patients.

BIBLIOGRAPHY

Abdelmegeed, M.A., Banerjee, A., Jang, S., Yoo, S.-H., Yun, J.-W., Gonzalez, F.J., Keshavarzian, A., Song, B.-J., 2013. CYP2E1 potentiates binge alcohol-induced gut leakiness, steatohepatitis, and apoptosis. Free Radic. Biol. Med. 65, 1238–1245. https://doi.org/10.1016/j.freeradbiomed.2013.09.009

Acín-Perez, R., Enriquez, J.A., 2014. The function of the respiratory supercomplexes: the plasticity model. Biochim Biophys Acta 1837, 444–450. https://doi.org/10.1016/j.bbabio.2013.12.009

Acín-Pérez, R., Fernández-Silva, P., Peleato, M.L., Pérez-Martos, A., Enriquez, J.A., 2008. Respiratory Active Mitochondrial Supercomplexes. Molecular Cell 32, 529–539. https://doi.org/10.1016/j.molcel.2008.10.021

Adams, D.H., Eksteen, B., 2006. Aberrant homing of mucosal T cells and extra-intestinal manifestations of inflammatory bowel disease. Nature Reviews Immunology 6, 244–251. https://doi.org/10.1038/nri1784

Aerts, J.M.F.G., Hollak, C.E.M., Boot, R.G., Groener, J.E.M., Maas, M., 2006. Substrate reduction therapy of glycosphingolipid storage disorders. J Inherit Metab Dis 29, 449–456. https://doi.org/10.1007/s10545-006-0272-5

Afonso, M.S., Machado, R.M., Lavrador, M.S., Quintao, E.C.R., Moore, K.J., Lottenberg, A.M., 2018. Molecular Pathways Underlying Cholesterol Homeostasis. Nutrients 10, 760. https://doi.org/10.3390/nu10060760

Alpy, F., Tomasetto, C., 2005. Give lipids a START: the StAR-related lipid transfer (START) domain in mammals. Journal of Cell Science 118, 2791–2801. https://doi.org/10.1242/jcs.02485

Altamirano, J., Bataller, R., 2011. Alcoholic liver disease: pathogenesis and new targets for therapy. Nature Reviews Gastroenterology & Hepatology 8, 491–501. https://doi.org/10.1038/nrgastro.2011.134

Amritraj, A., Wang, Y., Revett, T.J., Vergote, D., Westaway, D., Kar, S., 2013. Role of cathepsin D in U18666A-induced neuronal cell death: potential implication in Niemann-Pick type C disease pathogenesis. J Biol Chem 288, 3136–3152. https://doi.org/10.1074/jbc.M112.412460

Amsel, S., 2005. Liver Structures and Functions - A Closer Look (Advanced) [WWW Document]. URL https://www.exploringnature.org/db/view/Liver-Structures-and-Functions-A-Closer-Look-Advanced (accessed 4.23.20).

Arenas, F., Castro, F., Nuñez, S., Gay, G., Garcia-Ruiz, C., Fernandez-Checa, J.C., 2020. STARD1 and NPC1 expression as pathological markers associated with astrogliosis in post-mortem brains from patients with Alzheimer's disease and Down syndrome. Aging (Albany NY) 12, 571–592. https://doi.org/10.18632/aging.102641

Arias, I.M., Wolkoff, A.W., Boyer, J.L., Shafritz, D.A., Fausto, N., Alter, H.J., Cohen, D.E., 2011. The Liver: Biology and Pathobiology. John Wiley & Sons.

Arnold, D.R., Kwiterovich, P.O., 2003. CHOLESTEROL | Absorption, Function, and Metabolism, in: Caballero, B. (Ed.), Encyclopedia of Food Sciences and Nutrition (Second Edition).

Academic Press, Oxford, pp. 1226–1237. https://doi.org/10.1016/B0-12-227055-X/00225-X

Artemenko, I.P., Zhao, D., Hales, D.B., Hales, K.H., Jefcoate, C.R., 2001. Mitochondrial processing of newly synthesized steroidogenic acute regulatory protein (StAR), but not total StAR, mediates cholesterol transfer to cytochrome P450 side chain cleavage enzyme in adrenal cells. J Biol Chem 276, 46583–46596. https://doi.org/10.1074/jbc.M107815200

Asrani, S.K., Devarbhavi, H., Eaton, J., Kamath, P.S., 2019. Burden of liver diseases in the world. J Hepatol 70, 151–171. https://doi.org/10.1016/j.jhep.2018.09.014

Bach, D., Pich, S., Soriano, F.X., Vega, N., Baumgartner, B., Oriola, J., Daugaard, J.R., Lloberas, J., Camps, M., Zierath, J.R., Rabasa-Lhoret, R., Wallberg-Henriksson, H., Laville, M., Palacín, M., Vidal, H., Rivera, F., Brand, M., Zorzano, A., 2003. Mitofusin-2 determines mitochondrial network architecture and mitochondrial metabolism. A novel regulatory mechanism altered in obesity. J Biol Chem 278, 17190–17197. https://doi.org/10.1074/jbc.M212754200

Baggetto, L.G., Clottes, E., Vial, C., 1992. Low Mitochondrial Proton Leak Due to High Membrane Cholesterol Content and Cytosolic Creatine Kinase as Two Features of the Deviant Bioenergetics of Ehrlich and AS30-D Tumor Cells. Cancer Res 52, 4935–4941.

Baggetto, L.G., Testa-Parussini, R., 1990. Role of acetoin on the regulation of intermediate metabolism of ehrlich ascites tumor mitochondria: Its contribution to membrane cholesterol enrichment modifying passive proton permeability. Archives of Biochemistry and Biophysics 283, 241–248. https://doi.org/10.1016/0003-9861(90)90638-F

Bailey, S.M., Cunningham, C.C., 2002. Contribution of mitochondria to oxidative stress associated with alcoholic liver disease1 1This article is part of a series of reviews on “Alcohol, Oxidative Stress and Cell Injury”. The full list of papers may be found on the homepage of the journal. Free Radical Biology and Medicine 32, 11–16. https://doi.org/10.1016/S0891-5849(01)00769-9

Bailey, S.M., Robinson, G., Pinner, A., Chamlee, L., Ulasova, E., Pompilius, M., Page, G.P., Chhieng, D., Jhala, N., Landar, A., Kharbanda, K.K., Ballinger, S., Darley-Usmar, V., 2006. S-adenosylmethionine prevents chronic alcohol-induced mitochondrial dysfunction in the rat liver. American Journal of Physiology-Gastrointestinal and Liver Physiology 291, G857–G867. https://doi.org/10.1152/ajpgi.00044.2006

Bajwa, H., Azhar, W., 2020. Niemann-Pick Disease, in: StatPearls. StatPearls Publishing, Treasure Island (FL).

Balboa, E., Castro, J., Pinochet, M.-J., Cancino, G.I., Matías, N., Sáez, P.J., Martínez, A., Álvarez, A.R., Garcia-Ruiz, C., Fernandez-Checa, J.C., Zanlungo, S., 2017. MLN64 induces mitochondrial dysfunction associated with increased mitochondrial cholesterol content. Redox Biol 12, 274–284. https://doi.org/10.1016/j.redox.2017.02.024

Ballinger, S.W., 2005. Mitochondrial dysfunction in cardiovascular disease. Free Radical Biology and Medicine 38, 1278–1295. https://doi.org/10.1016/j.freeradbiomed.2005.02.014

Baraona, E., Lieber, C.S., 1979. Effects of ethanol on lipid metabolism. J. Lipid Res. 20, 289–315.

Baraona, E., Zeballos, G.A., Shoichet, L., Mak, K.M., Lieber, C.S., 2002. Ethanol Consumption Increases Nitric Oxide Production in Rats, and Its Peroxynitrite-Mediated Toxicity Is Attenuated by Polyenylphosphatidylcholine. Alcoholism: Clinical and Experimental Research 26, 883–889. https://doi.org/10.1111/j.1530-0277.2002.tb02618.x

Barbero-Camps, E., Fernández, A., Baulies, A., Martinez, L., Fernández-Checa, J.C., Colell, A., 2014. Endoplasmic Reticulum Stress Mediates Amyloid β Neurotoxicity via Mitochondrial Cholesterol Trafficking. The American Journal of Pathology 184, 2066–2081. https://doi.org/10.1016/j.ajpath.2014.03.014

Barbero-Camps, E., Fernández, A., Martínez, L., Fernández-Checa, J.C., Colell, A., 2013. APP/PS1 mice overexpressing SREBP-2 exhibit combined Aβ accumulation and tau pathology underlying Alzheimer's disease. Hum Mol Genet 22, 3460–3476. https://doi.org/10.1093/hmg/ddt201

Barrientos, A., Ugalde, C., 2013. I Function, Therefore I Am: Overcoming Skepticism about Mitochondrial Supercomplexes. Cell Metabolism 18, 147–149. https://doi.org/10.1016/j.cmet.2013.07.010

Beale, L., 1856. The minute anatomy of the liver. Medical Times and Gazette 13, 82–85.

Beltroy, E.P., Richardson, J.A., Horton, J.D., Turley, S.D., Dietschy, J.M., 2005. Cholesterol accumulation and liver cell death in mice with Niemann-Pick type C disease. Hepatology 42, 886–893. https://doi.org/10.1002/hep.20868

Ben-Moshe, S., Itzkovitz, S., 2019. Spatial heterogeneity in the mammalian liver. Nature Reviews Gastroenterology & Hepatology 16, 395–410. https://doi.org/10.1038/s41575-019-0134-x

Bernstein, J.D., Penniall, R., 1978. Effects of chronic ethanol treatment upon rat liver mitochondria. Biochemical Pharmacology 27, 2337–2342. https://doi.org/10.1016/0006-2952(78)90141-7

Bhuvaneswaran, C., Morris, M.D., Shio, H., Fowler, S., 1982. Lysosome lipid storage disorder in NCTR-BALB/c mice. III. Isolation and analysis of storage inclusions from liver. Am J Pathol 108, 160–170.

Boccuto, L., Abenavoli, L., 2017. Genetic and Epigenetic Profile of Patients With Alcoholic Liver Disease. Ann Hepatol 16, 490–500. https://doi.org/10.5604/01.3001.0010.0274

Bosch, M., Marí, M., Herms, A., Fernández, A., Fajardo, A., Kassan, A., Giralt, A., Colell, A., Balgoma, D., Barbero, E., González-Moreno, E., Matias, N., Tebar, F., Balsinde, J., Camps, M., Enrich, C., Gross, S.P., García-Ruiz, C., Pérez-Navarro, E., Fernández-Checa, J.C., Pol, A., 2011. Caveolin-1 Deficiency Causes Cholesterol-Dependent Mitochondrial Dysfunction and Apoptotic Susceptibility. Current Biology 21, 681–686. https://doi.org/10.1016/j.cub.2011.03.030

Braeuning, A., Ittrich, C., Köhle, C., Hailfinger, S., Bonin, M., Buchmann, A., Schwarz, M., 2006. Differential gene expression in periportal and perivenous mouse hepatocytes. FEBS J 273, 5051–5061. https://doi.org/10.1111/j.1742-4658.2006.05503.x

Bruguera, M., Bertran, A., Bombi, J.A., Rodes, J., 1977. Giant mitochondria in hepatocytes: a diagnostic hint for alcoholic liver disease. Gastroenterology 73, 1383–1387.

Budin, I., de Rond, T., Chen, Y., Chan, L.J.G., Petzold, C.J., Keasling, J.D., 2018. Viscous control of cellular respiration by membrane lipid composition. Science 362, 1186–1189. https://doi.org/10.1126/science.aat7925

Buhaescu, I., Izzedine, H., 2007. Mevalonate pathway: A review of clinical and therapeutical implications. Clinical Biochemistry 40, 575–584. https://doi.org/10.1016/j.clinbiochem.2007.03.016

Bühler, R., Lindros, K.O., Nordling, Å., Johansson, I., Ingelman-Sundberg, M., 1992. Zonation of cytochrome P450 isozyme expression and induction in rat liver. European Journal of Biochemistry 204, 407–412. https://doi.org/10.1111/j.1432-1033.1992.tb16650.x

Caballero, F., Fernández, A., Lacy, A.M.D., Fernández-Checa, J.C., Caballería, J., García-Ruiz, C., 2009. Enhanced free cholesterol, SREBP-2 and StAR expression in human NASH. Journal of Hepatology 50, 789–796. https://doi.org/10.1016/j.jhep.2008.12.016

Cahill, A., Cunningham, C.C., 2000. Effects of chronic ethanol feeding on the protein composition of mitochondrial ribosomes. Electrophoresis 21, 3420–3426. https://doi.org/10.1002/1522-2683(20001001)21:16<3420::AID-ELPS3420>3.0.CO;2-Q

Campbell, A.M., Chan, S.H.P., 2007. The voltage dependent anion channel affects mitochondrial cholesterol distribution and function. Archives of Biochemistry and Biophysics 466, 203–210. https://doi.org/10.1016/j.abb.2007.06.012

Caron, K.M., Soo, S.C., Wetsel, W.C., Stocco, D.M., Clark, B.J., Parker, K.L., 1997. Targeted disruption of the mouse gene encoding steroidogenic acute regulatory protein provides insights into congenital lipoid adrenal hyperplasia. Proc Natl Acad Sci U S A 94, 11540–11545. https://doi.org/10.1073/pnas.94.21.11540

Case, A.J., 2017. On the Origin of Superoxide Dismutase: An Evolutionary Perspective of Superoxide-Mediated Redox Signaling. Antioxidants 6, 82. https://doi.org/10.3390/antiox6040082

Cederbaum, A.I., 2012. Alcohol Metabolism. Clinics in Liver Disease, A Practical Approach to the Spectrum of Alcoholic Liver Disease 16, 667–685. https://doi.org/10.1016/j.cld.2012.08.002

Cederbaum, A.I., 2006. Cytochrome P450 2E1-dependent oxidant stress and upregulation of anti-oxidant defense in liver cells. Journal of Gastroenterology and Hepatology 21, S22–S25. https://doi.org/10.1111/j.1440-1746.2006.04595.x

Cenedella, R.J., 2009. Cholesterol synthesis inhibitor U18666A and the role of sterol metabolism and trafficking in numerous pathophysiological processes. Lipids 44, 477–487. https://doi.org/10.1007/s11745-009-3305-7

Ceni, E., Mello, T., Galli, A., 2014. Pathogenesis of alcoholic liver disease: Role of oxidative metabolism. World Journal of Gastroenterology 20, 17756–17772. https://doi.org/10.3748/wjg.v20.i47.17756

Cerqueira, N.M.F.S.A., Oliveira, E.F., Gesto, D.S., Santos-Martins, D., Moreira, C., Moorthy, H.N., Ramos, M.J., Fernandes, P.A., 2016. Cholesterol Biosynthesis: A Mechanistic Overview. Biochemistry 55, 5483–5506. https://doi.org/10.1021/acs.biochem.6b00342

Chaban, Y., Boekema, E.J., Dudkina, N.V., 2014. Structures of mitochondrial oxidative phosphorylation supercomplexes and mechanisms for their stabilisation. Biochimica et Biophysica Acta (BBA) - Bioenergetics, Dynamic and ultrastructure of bioenergetic membranes and their components 1837, 418–426. https://doi.org/10.1016/j.bbabio.2013.10.004

Chalasani, N., Wilson, L., Kleiner, D.E., Cummings, O.W., Brunt, E.M., Ünalp, A., 2008. Relationship of steatosis grade and zonal location to histological features of steatohepatitis in adult patients with non-alcoholic fatty liver disease. Journal of Hepatology 48, 829–834. https://doi.org/10.1016/j.jhep.2008.01.016

Chan, D.C., 2020. Mitochondrial Dynamics and Its Involvement in Disease. Annual Review of Pathology: Mechanisms of Disease 15, 235–259. https://doi.org/10.1146/annurev-pathmechdis-012419-032711

Chance, B., Williams, G.R., 1955. A method for the localization of sites for oxidative phosphorylation. Nature 176, 250–254. https://doi.org/10.1038/176250a0

Chang, T.-S., Cho, C.-S., Park, S., Yu, S., Kang, S.W., Rhee, S.G., 2004. Peroxiredoxin III, a Mitochondrion-specific Peroxidase, Regulates Apoptotic Signaling by Mitochondria. J. Biol. Chem. 279, 41975–41984. https://doi.org/10.1074/jbc.M407707200

Chao, X., Wang, S., Zhao, K., Li, Y., Williams, J.A., Li, T., Chavan, H., Krishnamurthy, P., He, X.C., Li, L., Ballabio, A., Ni, H.-M., Ding, W.-X., 2018. Impaired TFEB-Mediated Lysosome Biogenesis and Autophagy Promote Chronic Ethanol-Induced Liver Injury and Steatosis in Mice. Gastroenterology 155, 865-879.e12. https://doi.org/10.1053/j.gastro.2018.05.027

Charman, M., Kennedy, B.E., Osborne, N., Karten, B., 2010. MLN64 mediates egress of cholesterol from endosomes to mitochondria in the absence of functional Niemann-Pick Type C1 protein. J Lipid Res 51, 1023–1034. https://doi.org/10.1194/jlr.M002345

Chedid, A., Mendenhall, C.L., Tosch, T., Chen, T., Rabin, L., Garcia-Pont, P., Goldberg, S.J., Kiernan, T., Seeff, L.B., Sorrell, M., 1986. Significance of megamitochondria in alcoholic liver disease. Gastroenterology 90, 1858–1864. https://doi.org/10.1016/0016-5085(86)90253-2

Chiang, J., 2014. Liver Physiology: Metabolism and Detoxification, in: McManus, L.M., Mitchell, R.N. (Eds.), Pathobiology of Human Disease. Academic Press, San Diego, pp. 1770–1782. https://doi.org/10.1016/B978-0-12-386456-7.04202-7

Chiquoine, A.D., 1953. The distribution of glucose-6-phosphate in the liver and kidney of the mouse. J Histochem Cytochem. 1, 429–435. https://doi.org/10.1177/1.6.429

Cirman, T., Oresić, K., Mazovec, G.D., Turk, V., Reed, J.C., Myers, R.M., Salvesen, G.S., Turk, B., 2004. Selective disruption of lysosomes in HeLa cells triggers apoptosis mediated by cleavage of Bid by multiple papain-like lysosomal cathepsins. J Biol Chem 279, 3578–3587. https://doi.org/10.1074/jbc.M308347200

Cogliati, S., Frezza, C., Soriano, M.E., Varanita, T., Quintana-Cabrera, R., Corrado, M., Cipolat, S., Costa, V., Casarin, A., Gomes, L.C., Perales-Clemente, E., Salviati, L., Fernandez-Silva, P., Enriquez, J.A., Scorrano, L., 2013. Mitochondrial Cristae Shape Determines Respiratory Chain Supercomplexes Assembly and Respiratory Efficiency. Cell 155, 160–171. https://doi.org/10.1016/j.cell.2013.08.032

Colell, A., Coll, O., García-Ruiz, C., París, R., Tiribelli, C., Kaplowitz, N., Fernández-Checa, J.C., 2001. Tauroursodeoxycholic acid protects hepatocytes from ethanol-fed rats against tumor necrosis factor-induced cell death by replenishing mitochondrial glutathione. Hepatology 34, 964–971. https://doi.org/10.1053/jhep.2001.28510

Colell, A., García-Ruiz, C., Lluis, J.M., Coll, O., Mari, M., Fernández-Checa, J.C., 2003. Cholesterol Impairs the Adenine Nucleotide Translocator-mediated Mitochondrial Permeability Transition through Altered Membrane Fluidity. J. Biol. Chem. 278, 33928–33935. https://doi.org/10.1074/jbc.M210943200

Colell, A., Garcia-Ruiz, C., Morales, A., Ballesta, A., Ookhtens, M., Rodes, J., Kaplowitz, N., Fernandez-Checa, J.C., 1997. Transport of reduced glutathione in hepatic mitochondria and mitoplasts from ethanol-treated rats: Effect of membrane physical properties and S-adenosyl-L-methionine. Hepatology 26, 699–708. https://doi.org/10.1002/hep.510260323

Coll, O., Colell, A., García-Ruiz, C., Kaplowitz, N., Fernández-Checa, J.C., 2003. Sensitivity of the 2-oxoglutarate carrier to alcohol intake contributes to mitochondrial glutathione depletion. Hepatology 38, 692–702. https://doi.org/10.1053/jhep.2003.50351

Colletti, M., Cicchini, C., Conigliaro, A., Santangelo, L., Alonzi, T., Pasquini, E., Tripodi, M., Amicone, L., 2009. Convergence of Wnt Signaling on the HNF4α-Driven Transcription in Controlling Liver Zonation. Gastroenterology 137, 660–672. https://doi.org/10.1053/j.gastro.2009.05.038

Cox, A.G., Winterbourn, C.C., Hampton, M.B., 2010. Mitochondrial peroxiredoxin involvement in antioxidant defence and redox signalling. Biochem J 425, 313–325. https://doi.org/10.1042/BJ20091541

Crabb, D.W., Liangpunsakul, S., 2006. Alcohol and lipid metabolism. Journal of Gastroenterology and Hepatology 21, S56–S60. https://doi.org/10.1111/j.1440-1746.2006.04582.x

Crain, R.C., Clark, R.W., Harvey, B.E., 1983. Role of Lipid Transfer Proteins in the Abnormal Lipid Content of Morris Hepatoma Mitochondria and Microsomes. Cancer Res 43, 3197–3202.

Cunningham, C.C., Bottenus, R.E., Spach, P.I., Rudel, L.L., 1983. Ethanol-Related Changes in Liver Microsomes and Mitochondria from the Monkey, Macaca fascicularis. Alcoholism: Clinical and Experimental Research 7, 424–430. https://doi.org/10.1111/j.1530-0277.1983.tb05500.x

Cunningham, C.C., Coleman, W.B., Spach, P.I., 1990. The effects of chronic ethanol consumption on hepatic mitochondrial energy metabolism. Alcohol Alcohol. 25, 127–136. https://doi.org/10.1093/oxfordjournals.alcalc.a044987

Dai, W., Jiang, L., 2019. Dysregulated Mitochondrial Dynamics and Metabolism in Obesity, Diabetes, and Cancer. Front Endocrinol (Lausanne) 10, 570. https://doi.org/10.3389/fendo.2019.00570

Dam, H., 1958. Historical introduction to cholesterol, in: Cook, R.P. (Ed.), Cholesterol: Chemistry, Biochemistry, and Pathology. Academic Press, New York, pp. 1–14.

Das, S., Hajnóczky, N., Antony, A.N., Csordás, G., Gaspers, L.D., Clemens, D.L., Hoek, J.B., Hajnóczky, G., 2012. Mitochondrial morphology and dynamics in hepatocytes from normal and ethanol-fed rats. Pflugers Arch 464, 101–109. https://doi.org/10.1007/s00424-012-1100-4

Davidson, C.D., Ali, N.F., Micsenyi, M.C., Stephney, G., Renault, S., Dobrenis, K., Ory, D.S., Vanier, M.T., Walkley, S.U., 2009. Chronic cyclodextrin treatment of murine Niemann-Pick C disease ameliorates neuronal cholesterol and glycosphingolipid storage and disease progression. PLoS One 4, e6951. https://doi.org/10.1371/journal.pone.0006951

De Windt, A., Rai, M., Kytömäki, L., Thelen, K.M., Lütjohann, D., Bernier, L., Davignon, J., Soini, J., Pandolfo, M., Laaksonen, R., 2007. Gene set enrichment analyses revealed several affected pathways in Niemann-pick disease type C fibroblasts. DNA Cell Biol 26, 665–671. https://doi.org/10.1089/dna.2006.0570

Deane, H.W., 1944. A cytological study of the diurnal cycle of the liver of the mouse in relation to storage and secretion. The Anatomical Record 88, 39–65. https://doi.org/10.1002/ar.1090880104

DeBose-Boyd, R.A., 2008. Feedback regulation of cholesterol synthesis: sterol-accelerated ubiquitination and degradation of HMG CoA reductase. Cell Research 18, 609–621. https://doi.org/10.1038/cr.2008.61

DeCarli, L.M., Lieber, C.S., 1967. Fatty Liver in the Rat after Prolonged Intake of Ethanol with a Nutritionally Adequate New Liquid Diet. J Nutr 91, 331–336. https://doi.org/10.1093/jn/91.3_Suppl.331

Devlin, C., Pipalia, N.H., Liao, X., Schuchman, E.H., Maxfield, F.R., Tabas, I., 2010. Improvement in lipid and protein trafficking in Niemann-Pick C1 cells by correction of a secondary enzyme defect. Traffic 11, 601–615. https://doi.org/10.1111/j.1600-0854.2010.01046.x

Dietschy, J.M., Turley, S.D., Spady, D.K., 1993. Role of liver in the maintenance of cholesterol and low density lipoprotein homeostasis in different animal species, including humans. J. Lipid Res. 34, 1637–1659.

Dietzen, D.J., Davis, E.J., 1994. Excess Membrane Cholesterol Is Not Responsible for Metabolic and Bioenergetic Changes in AS-30D Hepatoma Mitochondria. Archives of Biochemistry and Biophysics 309, 341–347. https://doi.org/10.1006/abbi.1994.1122

Dikic, I., Elazar, Z., 2018. Mechanism and medical implications of mammalian autophagy. Nat Rev Mol Cell Biol 19, 349–364. https://doi.org/10.1038/s41580-018-0003-4

Ding, W.-X., Guo, F., Ni, H.-M., Bockus, A., Manley, S., Stolz, D.B., Eskelinen, E.-L., Jaeschke, H., Yin, X.-M., 2012. Parkin and mitofusins reciprocally regulate mitophagy and mitochondrial

spheroid formation. J Biol Chem 287, 42379–42388. https://doi.org/10.1074/jbc.M112.413682

Domínguez-Pérez, M., Simoni-Nieves, A., Rosales, P., Nuño-Lámbarri, N., Rosas-Lemus, M., Souza, V., Miranda, R.U., Bucio, L., Carvajal, S.U., Marquardt, J.U., Seo, D., Gomez-Quiroz, L.E., Gutiérrez-Ruiz, M.C., 2019. Cholesterol burden in the liver induces mitochondrial dynamic changes and resistance to apoptosis. Journal of Cellular Physiology 234, 7213–7223. https://doi.org/10.1002/jcp.27474

Dong, J., Du, X., Wang, H., Wang, J., Lu, C., Chen, X., Zhu, Z., Luo, Z., Yu, L., Brown, A.J., Yang, H., Wu, J.-W., 2019. Allosteric enhancement of ORP1-mediated cholesterol transport by PI(4,5)P 2 /PI(3,4)P 2. Nature Communications 10, 1–16. https://doi.org/10.1038/s41467-019-08791-0

Dorn, G.W., 2019. Evolving Concepts of Mitochondrial Dynamics. Annual Review of Physiology 81, 1–17. https://doi.org/10.1146/annurev-physiol-020518-114358

Du, X., Kumar, J., Ferguson, C., Schulz, T.A., Ong, Y.S., Hong, W., Prinz, W.A., Parton, R.G., Brown, A.J., Yang, H., 2011. A role for oxysterol-binding protein–related protein 5 in endosomal cholesterol trafficking. J Cell Biol 192, 121–135. https://doi.org/10.1083/jcb.201004142

Echegoyen, S., Oliva, E.B., Sepulveda, J., Díaz-Zagoya, J.C., Espinosa-García, M.T., Pardo, J.P., Martínez, F., 1993. Cholesterol increase in mitochondria: its effect on inner-membrane functions, submitochondrial localization and ultrastructural morphology. Biochem J 289, 703–708. https://doi.org/10.1042/bj2890703

Ellingson, J.S., Taraschi, T.F., Wu, A., Zimmerman, R., Rubin, E., 1988. Cardiolipin from ethanol-fed rats confers tolerance to ethanol in liver mitochondrial membranes. PNAS 85, 3353–3357. https://doi.org/10.1073/pnas.85.10.3353

Elrick, M.J., Lieberman, A.P., 2013. Autophagic dysfunction in a lysosomal storage disorder due to impaired proteolysis. Autophagy 9, 234–235. https://doi.org/10.4161/auto.22501

Elsayed, H.R.H., El Nashar, E.M., Abd-Elmonem, M.M., 2019. Is the hepatocyte ultrastructural zonal heterogeneity changed by overnight (16 h) fasting? Morphometric study. Ultrastruct Pathol 43, 290–300. https://doi.org/10.1080/01913123.2019.1696906

Elustondo, P., Martin, L.A., Karten, B., 2017. Mitochondrial cholesterol import. Biochimica et Biophysica Acta (BBA) - Molecular and Cell Biology of Lipids, Lipids of Mitochondria 1862, 90–101. https://doi.org/10.1016/j.bbalip.2016.08.012

Enrich, C., Rentero, C., Hierro, A., Grewal, T., 2015. Role of cholesterol in SNARE-mediated trafficking on intracellular membranes. J Cell Sci 128, 1071–1081. https://doi.org/10.1242/jcs.164459

Ernster, L., Schatz, G., 1981. Mitochondria: a historical review. J Cell Biol 91, 227s–255s. https://doi.org/10.1083/jcb.91.3.227s

Fan, J., Campioli, E., Midzak, A., Culty, M., Papadopoulos, V., 2015. Conditional steroidogenic cell-targeted deletion of TSPO unveils a crucial role in viability and hormone-dependent steroid formation. Proc Natl Acad Sci U S A 112, 7261–7266. https://doi.org/10.1073/pnas.1502670112

Feingold, K.R., Grunfeld, C., 2000. Introduction to Lipids and Lipoproteins, in: Feingold, K.R., Anawalt, B., Boyce, A., Chrousos, G., Dungan, K., Grossman, A., Hershman, J.M., Kaltsas, G., Koch, C., Kopp, P., Korbonits, M., McLachlan, R., Morley, J.E., New, M., Perreault, L., Purnell, J., Rebar, R., Singer, F., Trence, D.L., Vinik, A., Wilson, D.P. (Eds.), Endotext. MDText.com, Inc., South Dartmouth (MA).

Feo, F., Canuto, R.A., Garcea, R.A., Gabriel, L., 1975. Effect of cholesterol content on some physical and functional properties of mitochondria isolated from adult rat liver, fetal liver, cholesterol-enriched liver and hepatomas AH-130, 3924A and 5123. Biochimica et Biophysica Acta (BBA) - Biomembranes 413, 116–134. https://doi.org/10.1016/0005-2736(75)90063-2

Fernández, A., Colell, A., Caballero, F., Matías, N., García-Ruiz, C., Fernández-Checa, J.C., 2009a. Mitochondrial S-Adenosyl-l-Methionine Transport is Insensitive to Alcohol-Mediated Changes in Membrane Dynamics. Alcoholism: Clinical and Experimental Research 33, 1169–1180. https://doi.org/10.1111/j.1530-0277.2009.00940.x

Fernández, A., Llacuna, L., Fernández-Checa, J.C., Colell, A., 2009b. Mitochondrial Cholesterol Loading Exacerbates Amyloid β Peptide-Induced Inflammation and Neurotoxicity. J. Neurosci. 29, 6394–6405. https://doi.org/10.1523/JNEUROSCI.4909-08.2009

Fernández, A., Matias, N., Fucho, R., Ribas, V., Montfort, C.V., Nuño, N., Baulies, A., Martinez, L., Tarrats, N., Mari, M., Colell, A., Morales, A., Dubuquoy, L., Mathurin, P., Bataller, R., Caballeria, J., Elena, M., Balsinde, J., Kaplowitz, N., Garcia-Ruiz, C., Fernandez-Checa, J.C., 2013. ASMase is required for chronic alcohol induced hepatic endoplasmic reticulum stress and mitochondrial cholesterol loading. Journal of Hepatology 59, 805–813. https://doi.org/10.1016/j.jhep.2013.05.023

Fernández-Checa, J.C., García-Ruiz, C., Ookhtens, M., Kaplowitz, N., 1991. Impaired uptake of glutathione by hepatic mitochondria from chronic ethanol-fed rats. Tracer kinetic studies in vitro and in vivo and susceptibility to oxidant stress. J Clin Invest 87, 397–405. https://doi.org/10.1172/JCI115010

Fernández-Checa, J.C., Kaplowitz, N., 2005. Hepatic mitochondrial glutathione: transport and role in disease and toxicity. Toxicology and Applied Pharmacology, Membrane Transporters in Toxicology 204, 263–273. https://doi.org/10.1016/j.taap.2004.10.001

Fernández-Checa, J.C., Kaplowitz, N., García-Ruiz, C., Colell, A., 1998. Mitochondrial Glutathione: Importance and Transport. Semin Liver Dis 18, 389–401. https://doi.org/10.1055/s-2007-1007172

Fernández-Checa, J.C., Kaplowitz, N., Garcia-Ruiz, C., Colell, A., Miranda, M., Mari, M., Ardite, E., Morales, A., 1997. GSH transport in mitochondria: defense against TNF-induced oxidative stress and alcohol-induced defect. American Journal of Physiology-Gastrointestinal and Liver Physiology 273, G7–G17. https://doi.org/10.1152/ajpgi.1997.273.1.G7

Ferri, D., Moro, L., Mastrodonato, M., Capuano, F., Marra, E., Liquori, G.E., Greco, M., 2005. Ultrastructural zonal heterogeneity of hepatocytes and mitochondria within the hepatic

acinus during liver regeneration after partial hepatectomy. Biol Cell 97, 277–288. https://doi.org/10.1042/BC20040154

Fischer, M., You, M., Matsumoto, M., Crabb, D.W., 2003. Peroxisome Proliferator-activated Receptor α (PPARα) Agonist Treatment Reverses PPARα Dysfunction and Abnormalities in Hepatic Lipid Metabolism in Ethanol-fed Mice. J. Biol. Chem. 278, 27997–28004. https://doi.org/10.1074/jbc.M302140200

Fog, C.K., Kirkegaard, T., 2019. Animal models for Niemann-Pick type C: implications for drug discovery & development. Expert Opin Drug Discov 14, 499–509. https://doi.org/10.1080/17460441.2019.1588882

French, S.W., 2004. The role of hypoxia in the pathogenesis of alcoholic liver disease. Hepatol Res 29, 69–74. https://doi.org/10.1016/j.hepres.2004.02.006

Fritz, K.S., Galligan, J.J., Smathers, R.L., Roede, J.R., Shearn, C.T., Reigan, P., Petersen, D.R., 2011. 4-Hydroxynonenal Inhibits SIRT3 via Thiol-Specific Modification. Chem. Res. Toxicol. 24, 651–662. https://doi.org/10.1021/tx100355a

Frolov, A., Zielinski, S.E., Crowley, J.R., Dudley-Rucker, N., Schaffer, J.E., Ory, D.S., 2003. NPC1 and NPC2 regulate cellular cholesterol homeostasis through generation of low density lipoprotein cholesterol-derived oxysterols. J Biol Chem 278, 25517–25525. https://doi.org/10.1074/jbc.M302588200

Fu, R., Wassif, C.A., Yanjanin, N.M., Watkins-Chow, D.E., Baxter, L.L., Incao, A., Liscum, L., Sidhu, R., Firnkes, S., Graham, M., Ory, D.S., Porter, F.D., Pavan, W.J., 2013. Efficacy of N-acetylcysteine in phenotypic suppression of mouse models of Niemann-Pick disease, type C1. Hum Mol Genet 22, 3508–3523. https://doi.org/10.1093/hmg/ddt206

Fu, R., Yanjanin, N.M., Bianconi, S., Pavan, W.J., Porter, F.D., 2010. Oxidative stress in Niemann-Pick disease, type C. Mol Genet Metab 101, 214–218. https://doi.org/10.1016/j.ymgme.2010.06.018

Fu, X., Sluka, J.P., Clendenon, S.G., Dunn, K.W., Wang, Z., Klaunig, J.E., Glazier, J.A., 2018. Modeling of xenobiotic transport and metabolism in virtual hepatic lobule models. PLOS ONE 13, e0198060. https://doi.org/10.1371/journal.pone.0198060

Gao, B., Bataller, R., 2011. Alcoholic Liver Disease: Pathogenesis and New Therapeutic Targets. Gastroenterology 141, 1572–1585. https://doi.org/10.1053/j.gastro.2011.09.002

García-Ruiz, C., Fernández-Checa, J.C., 2018. Mitochondrial Oxidative Stress and Antioxidants Balance in Fatty Liver Disease. Hepatology Communications 2, 1425–1439. https://doi.org/10.1002/hep4.1271

García-Ruiz, C., Kaplowitz, N., Fernandez-Checa, J.C., 2013. Role of Mitochondria in Alcoholic Liver Disease. Curr Pathobiol Rep 1, 159–168. https://doi.org/10.1007/s40139-013-0021-z

García-Ruiz, C., Marí, M., Colell Riera, A., Morales, A., Caballero, F., Montero, J., Terrones, O., Basañez, G., Fernández-Checa, J.C., 2009. Mitochondrial cholesterol in health and disease.

García-Ruiz, C., Morales, A., Ballesta, A., Rodés, J., Kaplowitz, N., Fernández-Checa, J.C., 1994. Effect of chronic ethanol feeding on glutathione and functional integrity of mitochondria

in periportal and perivenous rat hepatocytes. J Clin Invest 94, 193–201. https://doi.org/10.1172/JCI117306

García-Ruiz, C., Morales, A., Colell, A., Ballesta, A., Rodés, J., Kaplowitz, N., Fernández-Checa, J.C., 1995. Feeding S-adenosyl-l-methionine attenuates both ethanol-induced depletion of mitochondrial glutathione and mitochondrial dysfunction in periportal and perivenous rat hepatocytes. Hepatology 21, 207–214. https://doi.org/10.1002/hep.1840210133

García-Ruiz, C., Ribas, V., Baulies, A., Fernández-Checa, J.C., 2017. Mitochondrial Cholesterol and the Paradox in Cell Death, in: Singh, H., Sheu, S.-S. (Eds.), Pharmacology of Mitochondria, Handbook of Experimental Pharmacology. Springer International Publishing, Cham, pp. 189–210. https://doi.org/10.1007/164_2016_110

García-Villafranca, J., Guillén, A., Castro, J., 2008. Ethanol consumption impairs regulation of fatty acid metabolism by decreasing the activity of AMP-activated protein kinase in rat liver. Biochimie 90, 460–466. https://doi.org/10.1016/j.biochi.2007.09.019

Garver, W.S., Heidenreich, R.A., 2002. The Niemann-Pick C proteins and trafficking of cholesterol through the late endosomal/lysosomal system. Curr Mol Med 2, 485–505. https://doi.org/10.2174/1566524023362375

Geberhiwot, T., Moro, A., Dardis, A., Ramaswami, U., Sirrs, S., Marfa, M.P., Vanier, M.T., Walterfang, M., Bolton, S., Dawson, C., Héron, B., Stampfer, M., Imrie, J., Hendriksz, C., Gissen, P., Crushell, E., Coll, M.J., Nadjar, Y., Klünemann, H., Mengel, E., Hrebicek, M., Jones, S.A., Ory, D., Bembi, B., Patterson, M., International Niemann-Pick Disease Registry (INPDR), 2018. Consensus clinical management guidelines for Niemann-Pick disease type C. Orphanet J Rare Dis 13, 50. https://doi.org/10.1186/s13023-018-0785-7

Gebhardt, R., 1992. Metabolic zonation of the liver: Regulation and implications for liver function. Pharmacology & Therapeutics 53, 275–354. https://doi.org/10.1016/0163-7258(92)90055-5

Gebhardt, R., Matz-Soja, M., 2014. Liver zonation: Novel aspects of its regulation and its impact on homeostasis. World Journal of Gastroenterology 20, 8491–8504. https://doi.org/10.3748/wjg.v20.i26.8491

Genova, M.L., Lenaz, G., 2014. Functional role of mitochondrial respiratory supercomplexes. Biochimica et Biophysica Acta (BBA) - Bioenergetics, Dynamic and ultrastructure of bioenergetic membranes and their components 1837, 427–443. https://doi.org/10.1016/j.bbabio.2013.11.002

Giacomello, M., Pyakurel, A., Glytsou, C., Scorrano, L., 2020. The cell biology of mitochondrial membrane dynamics. Nature Reviews Molecular Cell Biology 21, 204–224. https://doi.org/10.1038/s41580-020-0210-7

Giustarini, D., Dalle-Donne, I., Milzani, A., Fanti, P., Rossi, R., 2013. Analysis of GSH and GSSG after derivatization with N-ethylmaleimide. Nat Protoc 8, 1660–1669. https://doi.org/10.1038/nprot.2013.095

Godoy, P., Hewitt, N.J., Albrecht, U., Andersen, M.E., Ansari, N., Bhattacharya, S., Bode, J.G., Bolleyn, J., Borner, C., Böttger, J., Braeuning, A., Budinsky, R.A., Burkhardt, B., Cameron,

N.R., Camussi, G., Cho, C.-S., Choi, Y.-J., Craig Rowlands, J., Dahmen, U., Damm, G., Dirsch, O., Donato, M.T., Dong, J., Dooley, S., Drasdo, D., Eakins, R., Ferreira, K.S., Fonsato, V., Fraczek, J., Gebhardt, R., Gibson, A., Glanemann, M., Goldring, C.E.P., Gómez-Lechón, M.J., Groothuis, G.M.M., Gustavsson, L., Guyot, C., Hallifax, D., Hammad, S., Hayward, A., Häussinger, D., Hellerbrand, C., Hewitt, P., Hoehme, S., Holzhütter, H.-G., Houston, J.B., Hrach, J., Ito, K., Jaeschke, H., Keitel, V., Kelm, J.M., Kevin Park, B., Kordes, C., Kullak-Ublick, G.A., LeCluyse, E.L., Lu, P., Luebke-Wheeler, J., Lutz, A., Maltman, D.J., Matz-Soja, M., McMullen, P., Merfort, I., Messner, S., Meyer, C., Mwinyi, J., Naisbitt, D.J., Nussler, A.K., Olinga, P., Pampaloni, F., Pi, J., Pluta, L., Przyborski, S.A., Ramachandran, A., Rogiers, V., Rowe, C., Schelcher, C., Schmich, K., Schwarz, M., Singh, B., Stelzer, E.H.K., Stieger, B., Stöber, R., Sugiyama, Y., Tetta, C., Thasler, W.E., Vanhaecke, T., Vinken, M., Weiss, T.S., Widera, A., Woods, C.G., Xu, J.J., Yarborough, K.M., Hengstler, J.G., 2013. Recent advances in 2D and 3D in vitro systems using primary hepatocytes, alternative hepatocyte sources and non-parenchymal liver cells and their use in investigating mechanisms of hepatotoxicity, cell signaling and ADME. Arch Toxicol 87, 1315–1530. https://doi.org/10.1007/s00204-013-1078-5

Goldstein, J.L., Brown, M.S., 1990. Regulation of the mevalonate pathway. Nature 343, 425–430. https://doi.org/10.1038/343425a0

Gougelet, A., Torre, C., Veber, P., Sartor, C., Bachelot, L., Denechaud, P.-D., Godard, C., Moldes, M., Burnol, A.-F., Dubuquoy, C., Terris, B., Guillonneau, F., Ye, T., Schwarz, M., Braeuning, A., Perret, C., Colnot, S., 2014. T-cell factor 4 and β-catenin chromatin occupancies pattern zonal liver metabolism in mice. Hepatology 59, 2344–2357. https://doi.org/10.1002/hep.26924

Griffin, L.D., Gong, W., Verot, L., Mellon, S.H., 2004. Niemann-Pick type C disease involves disrupted neurosteroidogenesis and responds to allopregnanolone. Nat Med 10, 704–711. https://doi.org/10.1038/nm1073

Groebner, J.L., Girón-Bravo, M.T., Rothberg, M.L., Adhikari, R., Tuma, D.J., Tuma, P.L., 2019. Alcohol-induced microtubule acetylation leads to the accumulation of large, immobile lipid droplets. Am J Physiol Gastrointest Liver Physiol 317, G373–G386. https://doi.org/10.1152/ajpgi.00026.2019

Groen, A.K., Bloks, V.W., Verkade, H., Kuipers, F., 2014. Cross-talk between liver and intestine in control of cholesterol and energy homeostasis. Molecular Aspects of Medicine, Molecular pathogenesis of chronic cholestatic liver disease: Impact on novel therapeutic approaches 37, 77–88. https://doi.org/10.1016/j.mam.2014.02.001

Grundy, S.M., 1983. Absorption and Metabolism of Dietary Cholesterol. Annual Review of Nutrition 3, 71–96. https://doi.org/10.1146/annurev.nu.03.070183.000443

Gu, J., Zhang, Yongxian, Xu, D., Zhao, Z., Zhang, Yuxue, Pan, Y., Cao, P., Wang, Z., Chen, Y., 2015. Ethanol-induced hepatic steatosis is modulated by glycogen level in the liver. J Lipid Res 56, 1329–1339. https://doi.org/10.1194/jlr.M056978

Guo, F., Zheng, K., Benedé-Ubieto, R., Cubero, F.J., Nevzorova, Y.A., 2018. The Lieber-DeCarli Diet—A Flagship Model for Experimental Alcoholic Liver Disease. Alcoholism: Clinical and Experimental Research 42, 1828–1840. https://doi.org/10.1111/acer.13840

Guo, R., Gu, J., Zong, S., Wu, M., Yang, M., 2018. Structure and mechanism of mitochondrial electron transport chain. Biomedical Journal 41, 9–20. https://doi.org/10.1016/j.bj.2017.12.001

Ha, S.-D., Park, S., Han, C.Y., Nguyen, M.L., Kim, S.O., 2012. Cellular Adaptation to Anthrax Lethal Toxin-Induced Mitochondrial Cholesterol Enrichment, Hyperpolarization, and Reactive Oxygen Species Generation through Downregulating MLN64 in Macrophages. Molecular and Cellular Biology 32, 4846–4860. https://doi.org/10.1128/MCB.00494-12

Hadjiivanova, C., 2009. Peripheral Benzodiazepine Receptors in Health and Disease. Biotechnology & Biotechnological Equipment 23, 502–506. https://doi.org/10.1080/13102818.2009.10818473

Halpern, K.B., Shenhav, R., Matcovitch-Natan, O., Tóth, B., Lemze, D., Golan, M., Massasa, E.E., Baydatch, S., Landen, S., Moor, A.E., Brandis, A., Giladi, A., Stokar-Avihail, A., David, E., Amit, I., Itzkovitz, S., 2017. Single-cell spatial reconstruction reveals global division of labour in the mammalian liver. Nature 542, 352–356. https://doi.org/10.1038/nature21065

Han, D., Ybanez, M.D., Johnson, H.S., McDonald, J.N., Mesropyan, L., Sancheti, H., Martin, G., Martin, A., Lim, A.M., Dara, L., Cadenas, E., Tsukamoto, H., Kaplowitz, N., 2012. Dynamic Adaptation of Liver Mitochondria to Chronic Alcohol Feeding in Mice BIOGENESIS, REMODELING, AND FUNCTIONAL ALTERATIONS. J. Biol. Chem. 287, 42165–42179. https://doi.org/10.1074/jbc.M112.377374

Han, K.-H., Hashimoto, N., Fukushima, M., 2016. Relationships among alcoholic liver disease, antioxidants, and antioxidant enzymes. World Journal of Gastroenterology 22, 37–49. https://doi.org/10.3748/wjg.v22.i1.37

Harisch, G., Meyer, W., 1985. Studies on tissue distribution of glutathione and on activities of glutathione-related enzymes after carbon tetrachloride-induced liver injury. Res Commun Chem Pathol Pharmacol 47, 399–314.

Hauet, T., Yao, Z.-X., Bose, H.S., Wall, C.T., Han, Z., Li, W., Hales, D.B., Miller, W.L., Culty, M., Papadopoulos, V., 2005. Peripheral-Type Benzodiazepine Receptor-Mediated Action of Steroidogenic Acute Regulatory Protein on Cholesterol Entry into Leydig Cell Mitochondria. Mol Endocrinol 19, 540–554. https://doi.org/10.1210/me.2004-0307

Hernández-Alvarez, M.I., Sebastián, D., Vives, S., Ivanova, S., Bartoccioni, P., Kakimoto, P., Plana, N., Veiga, S.R., Hernández, V., Vasconcelos, N., Peddinti, G., Adrover, A., Jové, M., Pamplona, R., Gordaliza-Alaguero, I., Calvo, E., Cabré, N., Castro, R., Kuzmanic, A., Boutant, M., Sala, D., Hyotylainen, T., Orešič, M., Fort, J., Errasti-Murugarren, E., Rodrígues, C.M.P., Orozco, M., Joven, J., Cantó, C., Palacin, M., Fernández-Veledo, S., Vendrell, J., Zorzano, A., 2019. Deficient Endoplasmic Reticulum-Mitochondrial

Phosphatidylserine Transfer Causes Liver Disease. Cell 177, 881-895.e17. https://doi.org/10.1016/j.cell.2019.04.010

Hirano, A., Kaplowitz, N., Tsukamoto, H., Kamimura, S., Fernandez-Checa, J.C., 1992. Hepatic mitochondrial glutathione depletion and progression of experimental alcoholic liver disease in rats. Hepatology 16, 1423–1427. https://doi.org/10.1002/hep.1840160619

Hirst, J., 2018. Open questions: respiratory chain supercomplexes—why are they there and what do they do? BMC Biology 16, 111. https://doi.org/10.1186/s12915-018-0577-5

Hofsäss, C., Lindahl, E., Edholm, O., 2003. Molecular dynamics simulations of phospholipid bilayers with cholesterol. Biophys. J. 84, 2192–2206. https://doi.org/10.1016/S0006-3495(03)75025-5

Höglinger, D., Burgoyne, T., Sanchez-Heras, E., Hartwig, P., Colaco, A., Newton, J., Futter, C.E., Spiegel, S., Platt, F.M., Eden, E.R., 2019. NPC1 regulates ER contacts with endocytic organelles to mediate cholesterol egress. Nature Communications 10, 1–14. https://doi.org/10.1038/s41467-019-12152-2

Holley, A.K., Bakthavatchalu, V., Velez-Roman, J.M., St. Clair, D.K., 2011. Manganese Superoxide Dismutase: Guardian of the Powerhouse. Int J Mol Sci 12, 7114–7162. https://doi.org/10.3390/ijms12107114

Holmes, R.S., Duley, J.A., Algar, E.M., Mather, P.B., Rout, U.K., 1986. Biochemical and genetic studies on enzymes of alcohol metabolism: the mouse as a model organism for human studies. Alcohol Alcohol. 21, 41–56.

Horton, J.D., Goldstein, J.L., Brown, M.S., 2002. SREBPs: activators of the complete program of cholesterol and fatty acid synthesis in the liver. J Clin Invest 109, 1125–1131. https://doi.org/10.1172/JCI15593

Horvath, S.E., Rampelt, H., Oeljeklaus, S., Warscheid, B., van der Laan, M., Pfanner, N., 2015. Role of membrane contact sites in protein import into mitochondria. Protein Sci 24, 277–297. https://doi.org/10.1002/pro.2625

Hunt, J.L., Finkelstein, S.D., 2004. Microdissection Techniques for Molecular Testing in Surgical Pathology. Archives of Pathology & Laboratory Medicine 128, 1372–1378. https://doi.org/10.1043/1543-2165(2004)128<1372:MTFMTI>2.0.CO;2

Ighodaro, O.M., Akinloye, O.A., 2018. First line defence antioxidants-superoxide dismutase (SOD), catalase (CAT) and glutathione peroxidase (GPX): Their fundamental role in the entire antioxidant defence grid. Alexandria Journal of Medicine 54, 287–293. https://doi.org/10.1016/j.ajme.2017.09.001

Ikonen, E., 2008. Cellular cholesterol trafficking and compartmentalization. Nature Reviews Molecular Cell Biology 9, 125–138. https://doi.org/10.1038/nrm2336

Infante, R.E., Radhakrishnan, A., Abi-Mosleh, L., Kinch, L.N., Wang, M.L., Grishin, N.V., Goldstein, J.L., Brown, M.S., 2008. Purified NPC1 protein: II. Localization of sterol binding to a 240-amino acid soluble luminal loop. J Biol Chem 283, 1064–1075. https://doi.org/10.1074/jbc.M707944200

Iseri, O.A., Lieber, C.S., Gottlieb, L.S., 1966. The ultrastructure of fatty liver induced by prolonged ethanol ingestion. Am J Pathol 48, 535–555.

Issop, L., Rone, M.B., Papadopoulos, V., 2013. Organelle plasticity and interactions in cholesterol transport and steroid biosynthesis. Molecular and Cellular Endocrinology, Fifteenth Conference on the Adrenal Cortex (Adrenal 2012) League City, Texas June 19 – 22, 2012 371, 34–46. https://doi.org/10.1016/j.mce.2012.12.003

Istvan, E.S., 2002. Structural mechanism for statin inhibition of 3-hydroxy-3-methylglutaryl coenzyme A reductase. American Heart Journal 144, S27–S32. https://doi.org/10.1067/mhj.2002.130300

Istvan, E.S., Deisenhofer, J., 2000. The structure of the catalytic portion of human HMG-CoA reductase. Biochimica et Biophysica Acta (BBA) - Molecular and Cell Biology of Lipids, Cholesterol in the year 2000 1529, 9–18. https://doi.org/10.1016/S1388-1981(00)00134-7

Jamin, N., Neumann, J.-M., Ostuni, M.A., Vu, T.K.N., Yao, Z.-X., Murail, S., Robert, J.-C., Giatzakis, C., Papadopoulos, V., Lacapère, J.-J., 2005. Characterization of the Cholesterol Recognition Amino Acid Consensus Sequence of the Peripheral-Type Benzodiazepine Receptor. Mol Endocrinol 19, 588–594. https://doi.org/10.1210/me.2004-0308

Jauhonen, P., Baraona, E., Miyakawa, H., Lieber, C.S., 1982. Mechanism for selective perivenular hepatotoxicity of ethanol. Alcohol Clin Exp Res 6, 350–357. https://doi.org/10.1111/j.1530-0277.1982.tb04990.x

Jefcoate, C., 2002. High-flux mitochondrial cholesterol trafficking, a specialized function of the adrenal cortex. J Clin Invest 110, 881–890. https://doi.org/10.1172/JCI16771

Jeon, S., Carr, R., 2020. Alcohol effects on hepatic lipid metabolism. J. Lipid Res. 61, 470–479. https://doi.org/10.1194/jlr.R119000547

Ji, C., 2008. Dissection of endoplasmic reticulum stress signaling in alcoholic and non-alcoholic liver injury. Journal of Gastroenterology and Hepatology 23, S16–S24. https://doi.org/10.1111/j.1440-1746.2007.05276.x

Ji, C., Kaplowitz, N., 2003. Betaine decreases hyperhomocysteinemia, endoplasmic reticulum stress, and liver injury in alcohol-fed mice. Gastroenterology 124, 1488–1499. https://doi.org/10.1016/S0016-5085(03)00276-2

Jin, S., Chen, J., Chen, L., Histen, G., Lin, Z., Gross, S., Hixon, J., Chen, Yue, Kung, C., Chen, Yiwei, Fu, Y., Lu, Y., Lin, H., Cai, X., Yang, H., Cairns, R.A., Dorsch, M., Su, S.M., Biller, S., Mak, T.W., Cang, Y., 2015. ALDH2(E487K) mutation increases protein turnover and promotes murine hepatocarcinogenesis. PNAS 112, 9088–9093. https://doi.org/10.1073/pnas.1510757112

Johansson, I., Lindros, K.O., Eriksson, H., Ingelman-Sundberg, M., 1990. Transcriptional control of CYP2E1 in the perivenous liver region and during starvation. Biochem Biophys Res Commun 173, 331–338. https://doi.org/10.1016/s0006-291x(05)81061-7

Josekutty, J., Iqbal, J., Iwawaki, T., Kohno, K., Hussain, M.M., 2013. Microsomal Triglyceride Transfer Protein Inhibition Induces Endoplasmic Reticulum Stress and Increases Gene

Transcription via Ire1α/cJun to Enhance Plasma ALT/AST. J. Biol. Chem. 288, 14372–14383. https://doi.org/10.1074/jbc.M113.459602

Jungermann, K., Katz, N., 1982. Functional hepatocellular heterogeneity. Hepatology 2, 385–395. https://doi.org/10.1002/hep.1840020316

Jungermann, K., Keitzmann, T., 1996. Zonation of Parenchymal and Nonparenchymal Metabolism in Liver. Annual Review of Nutrition 16, 179–203. https://doi.org/10.1146/annurev.nu.16.070196.001143

Jungermann, K., Kietzmann, T., 2000. Oxygen: modulator of metabolic zonation and disease of the liver. Hepatology 31, 255–260. https://doi.org/10.1002/hep.510310201

Junqueira's Basic Histology: Text and Atlas, 15e | AccessMedicine | McGraw-Hill Medical [WWW Document], 2013. URL https://accessmedicine.mhmedical.com/book.aspx?bookID=2430 (accessed 4.23.20).

Kalra, A., Tuma, F., 2020. Physiology, Liver, in: StatPearls. StatPearls Publishing, Treasure Island (FL).

Kaplowitz, N., Ji, C., 2006. Unfolding new mechanisms of alcoholic liver disease in the endoplasmic reticulum. Journal of Gastroenterology and Hepatology 21, S7–S9. https://doi.org/10.1111/j.1440-1746.2006.04581.x

Kapourchali, F.R., Surendiran, G., Goulet, A., Moghadasian, M.H., 2016. The Role of Dietary Cholesterol in Lipoprotein Metabolism and Related Metabolic Abnormalities: A Mini-review. Critical Reviews in Food Science and Nutrition 56, 2408–2415. https://doi.org/10.1080/10408398.2013.842887

Kater, J.McA., 1933. Comparative and experimental studies on the cytology of the liver. Z.Zellforsch 17, 217–246. https://doi.org/10.1007/BF00374042

Keegan, A., Martini, R., Batey, R., 1995. Ethanol-related liver injury in the rat: a model of steatosis, inflammation and pericentral fibrosis. Journal of Hepatology 23, 591–600. https://doi.org/10.1016/0168-8278(95)80067-0

Kelly-Aubert, M., Trudel, S., Fritsch, J., Nguyen-Khoa, T., Baudouin-Legros, M., Moriceau, S., Jeanson, L., Djouadi, F., Matar, C., Conti, M., Ollero, M., Brouillard, F., Edelman, A., 2011. GSH monoethyl ester rescues mitochondrial defects in cystic fibrosis models. Hum Mol Genet 20, 2745–2759. https://doi.org/10.1093/hmg/ddr173

Kietzmann, T., 2017. Metabolic zonation of the liver: The oxygen gradient revisited. Redox Biol 11, 622–630. https://doi.org/10.1016/j.redox.2017.01.012

King, A.L., Swain, T.M., Dickinson, D.A., Lesort, M.J., Bailey, S.M., 2010. Chronic ethanol consumption enhances sensitivity to Ca2+-mediated opening of the mitochondrial permeability transition pore and increases cyclophilin D in liver. American Journal of Physiology-Gastrointestinal and Liver Physiology 299, G954–G966. https://doi.org/10.1152/ajpgi.00246.2010

Kiriyama, Y., Nochi, H., 2019. The Biosynthesis, Signaling, and Neurological Functions of Bile Acids. Biomolecules 9, 232. https://doi.org/10.3390/biom9060232

Kishida, T., Kostetskii, I., Zhang, Z., Martinez, F., Liu, P., Walkley, S.U., Dwyer, N.K., Blanchette-Mackie, E.J., Radice, G.L., Strauss, J.F., 2004. Targeted mutation of the MLN64 START domain causes only modest alterations in cellular sterol metabolism. J Biol Chem 279, 19276–19285. https://doi.org/10.1074/jbc.M400717200

Klein, A., Mosqueira, M., Martínez, G., Robledo, F., González, M., Caballero, B., Cancino, G.I., Alvarez, A.R., Hetz, C., Zanlungo, S., 2011. Lack of activation of the unfolded protein response in mouse and cellular models of Niemann-Pick type C disease. Neurodegener Dis 8, 124–128. https://doi.org/10.1159/000316540

Kmiec, Z., 2001. Cooperation of Liver Cells in Health and Disease: With 18 Tables. Springer Science & Business Media.

Knockaert, L., Fromenty, B., Robin, M.-A., 2011. Mechanisms of mitochondrial targeting of cytochrome P450 2E1: physiopathological role in liver injury and obesity. The FEBS Journal 278, 4252–4260. https://doi.org/10.1111/j.1742-4658.2011.08357.x

Ko, D.C., Milenkovic, L., Beier, S.M., Manuel, H., Buchanan, J., Scott, M.P., 2005. Cell-autonomous death of cerebellar purkinje neurons with autophagy in Niemann-Pick type C disease. PLoS Genet 1, 81–95. https://doi.org/10.1371/journal.pgen.0010007

Kobayashi, T., Beuchat, M.H., Lindsay, M., Frias, S., Palmiter, R.D., Sakuraba, H., Parton, R.G., Gruenberg, J., 1999. Late endosomal membranes rich in lysobisphosphatidic acid regulate cholesterol transport. Nat Cell Biol 1, 113–118. https://doi.org/10.1038/10084

Kong, L.-Z., Chandimali, N., Han, Y.-H., Lee, D.-H., Kim, J.-S., Kim, S.-U., Kim, T.-D., Jeong, D.K., Sun, H.-N., Lee, D.S., Kwon, T., 2019. Pathogenesis, Early Diagnosis, and Therapeutic Management of Alcoholic Liver Disease. International Journal of Molecular Sciences 20, 2712. https://doi.org/10.3390/ijms20112712

Kosicek, M., Gudelj, I., Horvatic, A., Jovic, T., Vuckovic, F., Lauc, G., Hecimovic, S., 2018. N-glycome of the Lysosomal Glycocalyx is Altered in Niemann-Pick Type C Disease (NPC) Model Cells. Mol Cell Proteomics 17, 631–642. https://doi.org/10.1074/mcp.RA117.000129

Kowalewski, M.P., Gram, A., Boos, A., 2015. The role of hypoxia and HIF1α in the regulation of STAR-mediated steroidogenesis in granulosa cells. Mol Cell Endocrinol 401, 35–44. https://doi.org/10.1016/j.mce.2014.11.023

Kristiana, I., Luu, W., Stevenson, J., Cartland, S., Jessup, W., Belani, J.D., Rychnovsky, S.D., Brown, A.J., 2012. Cholesterol through the looking glass: ability of its enantiomer also to elicit homeostatic responses. J Biol Chem 287, 33897–33904. https://doi.org/10.1074/jbc.M112.360537

Kubista, M., Andrade, J.M., Bengtsson, M., Forootan, A., Jonák, J., Lind, K., Sindelka, R., Sjöback, R., Sjögreen, B., Strömbom, L., Ståhlberg, A., Zoric, N., 2006. The real-time polymerase chain reaction. Mol Aspects Med 27, 95–125. https://doi.org/10.1016/j.mam.2005.12.007

Kumar, K.K., Devi, B.U., Neeraja, P., 2018. Molecular activities and ligand-binding specificities of StAR-related lipid transfer domains: exploring integrated in silico methods and ensemble-

docking approaches. SAR QSAR Environ Res 29, 483–501. https://doi.org/10.1080/1062936X.2018.1462847

Kurutas, E.B., 2016. The importance of antioxidants which play the role in cellular response against oxidative/nitrosative stress: current state. Nutrition Journal 15, 71. https://doi.org/10.1186/s12937-016-0186-5

Kusminski, C.M., Scherer, P.E., 2018. New zoning laws enforced by glucagon. Proc Natl Acad Sci U S A 115, 4308–4310. https://doi.org/10.1073/pnas.1804203115

Kwon, H.J., Abi-Mosleh, L., Wang, M.L., Deisenhofer, J., Goldstein, J.L., Brown, M.S., Infante, R.E., 2009. Structure of N-terminal domain of NPC1 reveals distinct subdomains for binding and transfer of cholesterol. Cell 137, 1213–1224. https://doi.org/10.1016/j.cell.2009.03.049

Lacapère, J.-J., Papadopoulos, V., 2003. Peripheral-type benzodiazepine receptor: structure and function of a cholesterol-binding protein in steroid and bile acid biosynthesis. Steroids 68, 569–585. https://doi.org/10.1016/S0039-128X(03)00101-6

Lamas-Paz, A., Hao, F., Nelson, L.J., Vázquez, M.T., Canals, S., Moral, M.G. del, Martínez-Naves, E., Nevzorova, Y.A., Cubero, F.J., 2018. Alcoholic liver disease: Utility of animal models. World Journal of Gastroenterology 24, 5063–5075. https://doi.org/10.3748/wjg.v24.i45.5063

Lange, Y., 1991. Disposition of intracellular cholesterol in human fibroblasts. J. Lipid Res. 32, 329–339.

Lapuente-Brun, E., Moreno-Loshuertos, R., Acín-Pérez, R., Latorre-Pellicer, A., Colás, C., Balsa, E., Perales-Clemente, E., Quirós, P.M., Calvo, E., Rodríguez-Hernández, M.A., Navas, P., Cruz, R., Carracedo, Á., López-Otín, C., Pérez-Martos, A., Fernández-Silva, P., Fernández-Vizarra, E., Enríquez, J.A., 2013. Supercomplex Assembly Determines Electron Flux in the Mitochondrial Electron Transport Chain. Science 340, 1567–1570. https://doi.org/10.1126/science.1230381

Lautt, W.W., 2009. Hepatic Circulation: Physiology and Pathophysiology, Colloquium Series on Integrated Systems Physiology: From Molecule to Function to Disease. Morgan & Claypool Life Sciences, San Rafael (CA).

Lavoie, H.A., King, S.R., 2009. Transcriptional regulation of steroidogenic genes: STARD1, CYP11A1 and HSD3B. Exp Biol Med (Maywood) 234, 880–907. https://doi.org/10.3181/0903-MR-97

Lee, J.H., Yang, E.S., Park, J.-W., 2003. Inactivation of NADP+-dependent Isocitrate Dehydrogenase by Peroxynitrite IMPLICATIONS FOR CYTOTOXICITY AND ALCOHOL-INDUCED LIVER INJURY. J. Biol. Chem. 278, 51360–51371. https://doi.org/10.1074/jbc.M302332200

Lejay, A., Charles, A.L., Zoll, J., Bouitbir, J., Thaveau, F., Piquard, F., Geny, B., 2012. Skeletal Muscle Mitochondrial Function in Peripheral Arterial Disease: Usefulness of Muscle Biopsy. Muscle Biopsy. https://doi.org/10.5772/31674

Letts, J.A., Fiedorczuk, K., Sazanov, L.A., 2016. The architecture of respiratory supercomplexes. Nature 537, 644–648. https://doi.org/10.1038/nature19774

Li, S., Rousseau, D., 2012. ATAD3, a vital membrane bound mitochondrial ATPase involved in tumor progression. J Bioenerg Biomembr 44, 189–197. https://doi.org/10.1007/s10863-012-9424-5

Li, X., Saha, P., Li, J., Blobel, G., Pfeffer, S.R., 2016. Clues to the mechanism of cholesterol transfer from the structure of NPC1 middle lumenal domain bound to NPC2. PNAS 113, 10079–10084. https://doi.org/10.1073/pnas.1611956113

Li, Y., Ge, M., Ciani, L., Kuriakose, G., Westover, E.J., Dura, M., Covey, D.F., Freed, J.H., Maxfield, F.R., Lytton, J., Tabas, I., 2004. Enrichment of endoplasmic reticulum with cholesterol inhibits sarcoplasmic-endoplasmic reticulum calcium ATPase-2b activity in parallel with increased order of membrane lipids: implications for depletion of endoplasmic reticulum calcium stores and apoptosis in cholesterol-loaded macrophages. J Biol Chem 279, 37030–37039. https://doi.org/10.1074/jbc.M405195200

Liao, G., Yao, Y., Liu, J., Yu, Z., Cheung, S., Xie, A., Liang, X., Bi, X., 2007. Cholesterol accumulation is associated with lysosomal dysfunction and autophagic stress in Npc1 -/- mouse brain. Am J Pathol 171, 962–975. https://doi.org/10.2353/ajpath.2007.070052

Lieber, C.S., 2005. Metabolism of Alcohol. Clinics in Liver Disease, Alcoholic Liver Disease 9, 1–35. https://doi.org/10.1016/j.cld.2004.10.005

Lieber, C.S., DeCarli, L.M., 1989. Liquid diet technique of ethanol administration: 1989 update. Alcohol Alcohol. 24, 197–211.

Lieber, C.S., DeCarli, L.M., 1982. The Feeding of Alcohol in Liquid Diets: Two Decades of Applications and 1982 Update. Alcoholism: Clinical and Experimental Research 6, 523–531. https://doi.org/10.1111/j.1530-0277.1982.tb05017.x

Lieber, C.S., Jones, D.P., DeCarli, L.M., 1965. Effects of Prolonged Ethanol Intake: Production of Fatty Liver Despite Adequate Diets. J Clin Invest 44, 1009–1021. https://doi.org/10.1172/JCI105200

Lieber, C.S., Jones, D.P., Medelson, J., DeCarli, L.M., 1963. Fatty liver, hyperlipemia and hyperuricemia produced by prolonged alcohol consumption, despite adequate dietary intake. Trans Assoc Am Physicians 76, 289–300.

Liesa, M., Palacín, M., Zorzano, A., 2009. Mitochondrial Dynamics in Mammalian Health and Disease. Physiological Reviews 89, 799–845. https://doi.org/10.1152/physrev.00030.2008

Lindros, K.O., Penttilä, K.E., 1985. Digitonin-collagenase perfusion for efficient separation of periportal or perivenous hepatocytes. Biochem J 228, 757–760. https://doi.org/10.1042/bj2280757

Liscum, L., Ruggiero, R.M., Faust, J.R., 1989. The intracellular transport of low density lipoprotein-derived cholesterol is defective in Niemann-Pick type C fibroblasts. J Cell Biol 108, 1625–1636. https://doi.org/10.1083/jcb.108.5.1625

Liu, B., Li, H., Repa, J.J., Turley, S.D., Dietschy, J.M., 2008. Genetic variations and treatments that affect the lifespan of the NPC1 mouse. J Lipid Res 49, 663–669. https://doi.org/10.1194/jlr.M700525-JLR200

Llacuna, L., Fernández, A., Montfort, C.V., Matías, N., Martínez, L., Caballero, F., Rimola, A., Elena, M., Morales, A., Fernández-Checa, J.C., García-Ruiz, C., 2011. Targeting cholesterol at different levels in the mevalonate pathway protects fatty liver against ischemia–reperfusion injury. Journal of Hepatology 54, 1002–1010. https://doi.org/10.1016/j.jhep.2010.08.031

Lloyd-Evans, E., Morgan, A.J., He, X., Smith, D.A., Elliot-Smith, E., Sillence, D.J., Churchill, G.C., Schuchman, E.H., Galione, A., Platt, F.M., 2008. Niemann-Pick disease type C1 is a sphingosine storage disease that causes deregulation of lysosomal calcium. Nat Med 14, 1247–1255. https://doi.org/10.1038/nm.1876

Lloyd-Evans, E., Waller-Evans, H., Peterneva, K., Platt, F.M., 2010. Endolysosomal calcium regulation and disease. Biochem Soc Trans 38, 1458–1464. https://doi.org/10.1042/BST0381458

Lluis, J.M., Colell, A., García–Ruiz, C., Kaplowitz, N., Fernández–Checa, J.C., 2003. Acetaldehyde impairs mitochondrial glutathione transport in HepG2 cells through endoplasmic reticulum stress. Gastroenterology 124, 708–724. https://doi.org/10.1053/gast.2003.50089

Loftus, S.K., Morris, J.A., Carstea, E.D., Gu, J.Z., Cummings, C., Brown, A., Ellison, J., Ohno, K., Rosenfeld, M.A., Tagle, D.A., Pentchev, P.G., Pavan, W.J., 1997. Murine model of Niemann-Pick C disease: mutation in a cholesterol homeostasis gene. Science 277, 232–235. https://doi.org/10.1126/science.277.5323.232

Loomba, R., Bettencourt, R., Barrett-Connor, E., 2009. Synergistic association between alcohol intake and body mass index with serum alanine and aspartate aminotransferase levels in older adults: the Rancho Bernardo Study. Alimentary Pharmacology & Therapeutics 30, 1137–1149. https://doi.org/10.1111/j.1365-2036.2009.04141.x

Lopez, M.E., Scott, M.P., 2013. Genetic dissection of a cell-autonomous neurodegenerative disorder: lessons learned from mouse models of Niemann-Pick disease type C. Dis Model Mech 6, 1089–1100. https://doi.org/10.1242/dmm.012385

Louvet, A., Mathurin, P., 2015. Alcoholic liver disease: mechanisms of injury and targeted treatment. Nature Reviews Gastroenterology & Hepatology 12, 231–242. https://doi.org/10.1038/nrgastro.2015.35

Lu, F., Liang, Q., Abi-Mosleh, L., Das, A., De Brabander, J.K., Goldstein, J.L., Brown, M.S., 2015. Identification of NPC1 as the target of U18666A, an inhibitor of lysosomal cholesterol export and Ebola infection. Elife 4. https://doi.org/10.7554/eLife.12177

Lu, Y., Zhuge, J., Wang, X., Bai, J., Cederbaum, A.I., 2008. Cytochrome P450 2E1 contributes to ethanol-induced fatty liver in mice. Hepatology 47, 1483–1494. https://doi.org/10.1002/hep.22222

Lucki, N.C., Li, D., Bandyopadhyay, S., Wang, E., Merrill, A.H., Sewer, M.B., 2012. Acid ceramidase (ASAH1) represses steroidogenic factor 1-dependent gene transcription in H295R human adrenocortical cells by binding to the receptor. Mol Cell Biol 32, 4419–4431. https://doi.org/10.1128/MCB.00378-12

Luo, J., Jiang, L.-Y., Yang, H., Song, B.-L., 2019. Intracellular Cholesterol Transport by Sterol Transfer Proteins at Membrane Contact Sites. Trends in Biochemical Sciences 44, 273–292. https://doi.org/10.1016/j.tibs.2018.10.001

Luo, J., Yang, H., Song, B.-L., 2020. Mechanisms and regulation of cholesterol homeostasis. Nat Rev Mol Cell Biol 21, 225–245. https://doi.org/10.1038/s41580-019-0190-7

Lusis, A.J., Pajukanta, P., 2008. A treasure trove for lipoprotein biology. Nature Genetics 40, 129–130. https://doi.org/10.1038/ng0208-129

Lyu, J., Yang, E.J., Shim, J.S., 2019. Cholesterol Trafficking: An Emerging Therapeutic Target for Angiogenesis and Cancer. Cells 8, 389. https://doi.org/10.3390/cells8050389

Ma, H.-Y., Xu, J., Liu, X., Zhu, Y., Gao, B., Karin, M., Tsukamoto, H., Jeste, D.V., Grant, I., Roberts, A.J., Contet, C., Geoffroy, C., Zheng, B., Brenner, D., Kisseleva, T., 2016. The role of IL-17 signaling in regulation of the liver-brain axis and intestinal permeability in Alcoholic Liver Disease. Curr Pathobiol Rep 4, 27–35. https://doi.org/10.1007/s40139-016-0097-3

MacSween, R.N.M., Burt, A.D., 1986. Histologic Spectrum of Alcoholic Liver Disease. Semin Liver Dis 6, 221–232. https://doi.org/10.1055/s-2008-1040605

Mailloux, R.J., 2018. Mitochondrial Antioxidants and the Maintenance of Cellular Hydrogen Peroxide Levels [WWW Document]. Oxidative Medicine and Cellular Longevity. https://doi.org/10.1155/2018/7857251

Manzo-Avalos, S., Saavedra-Molina, A., 2010. Cellular and Mitochondrial Effects of Alcohol Consumption. International Journal of Environmental Research and Public Health 7, 4281–4304. https://doi.org/10.3390/ijerph7124281

Maranzana, E., Barbero, G., Falasca, A.I., Lenaz, G., Genova, M.L., 2013. Mitochondrial Respiratory Supercomplex Association Limits Production of Reactive Oxygen Species from Complex I. Antioxidants & Redox Signaling 19, 1469–1480. https://doi.org/10.1089/ars.2012.4845

Marcellin, P., Kutala, B.K., 2018. Liver diseases: A major, neglected global public health problem requiring urgent actions and large-scale screening. Liver International 38, 2–6. https://doi.org/10.1111/liv.13682

Marí, M., Caballero, F., Colell, A., Morales, A., Caballeria, J., Fernandez, A., Enrich, C., Fernandez-Checa, J.C., García-Ruiz, C., 2006. Mitochondrial free cholesterol loading sensitizes to TNF- and Fas-mediated steatohepatitis. Cell Metab. 4, 185–198. https://doi.org/10.1016/j.cmet.2006.07.006

Marí, M., Morales, A., Colell, A., García-Ruiz, C., Fernández-Checa, J.C., 2014. Mitochondrial cholesterol accumulation in alcoholic liver disease: Role of ASMase and endoplasmic reticulum stress. Redox Biology 3, 100–108. https://doi.org/10.1016/j.redox.2014.09.005

Marín, T., Contreras, P., Castro, J.F., Chamorro, D., Balboa, E., Bosch-Morató, M., Muñoz, F.J., Alvarez, A.R., Zanlungo, S., 2014. Vitamin E dietary supplementation improves neurological symptoms and decreases c-Abl/p73 activation in Niemann-Pick C mice. Nutrients 6, 3000–3017. https://doi.org/10.3390/nu6083000

Marques, L.R., Diniz, T.A., Antunes, B.M., Rossi, F.E., Caperuto, E.C., Lira, F.S., Gonçalves, D.C., 2018. Reverse Cholesterol Transport: Molecular Mechanisms and the Non-medical

Approach to Enhance HDL Cholesterol. Front. Physiol. 9. https://doi.org/10.3389/fphys.2018.00526

Martin, L.A., Kennedy, B.E., Karten, B., 2016. Mitochondrial cholesterol: mechanisms of import and effects on mitochondrial function. J Bioenerg Biomembr 48, 137–151. https://doi.org/10.1007/s10863-014-9592-6

Mato, J.M., Lu, S.C., 2007. Role of S-adenosyl-L-methionine in liver health and injury. Hepatology 45, 1306–1312. https://doi.org/10.1002/hep.21650

Matsuhashi, T., Karbowski, M., Liu, X., Usukura, J., Wozniak, M., Wakabayashi, T., 1998. Complete Suppression of Ethanol-Induced Formation of Megamitochondria By 4-Hydroxy-2,2,6,6-Tetramethyl-Piperidine-1-Oxyl (4-OH-Tempo). Free Radical Biology and Medicine 24, 139–147. https://doi.org/10.1016/S0891-5849(97)00210-4

Matsuo, M., Togawa, M., Hirabaru, K., Mochinaga, S., Narita, A., Adachi, M., Egashira, M., Irie, T., Ohno, K., 2013. Effects of cyclodextrin in two patients with Niemann-Pick Type C disease. Mol Genet Metab 108, 76–81. https://doi.org/10.1016/j.ymgme.2012.11.005

Maxfield, F.R., Tabas, I., 2005. Role of cholesterol and lipid organization in disease. Nature 438, 612–621. https://doi.org/10.1038/nature04399

Maxfield, F.R., Wüstner, D., 2002. Intracellular cholesterol transport. J Clin Invest 110, 891–898. https://doi.org/10.1172/JCI16500

McClain, C., Vatsalya, V., Cave, M., 2017. Role of Zinc in the Development/Progression of Alcoholic Liver Disease. Curr Treat Options Gastro 15, 285–295. https://doi.org/10.1007/s11938-017-0132-4

McClain, C.J., Hill, D.B., Song, Z., Chawla, R., Watson, W.H., Chen, T., Barve, S., 2002. S-Adenosylmethionine, cytokines, and alcoholic liver disease. Alcohol 27, 185–192. https://doi.org/10.1016/s0741-8329(02)00224-0

McNiven, M.A., Casey, C.A., 2011. Alcohol and lipid traffic don't mix. Hepatology 53, 1073–1075. https://doi.org/10.1002/hep.24277

Mei, S., Gu, H., Yang, X., Guo, H., Liu, Z., Cao, W., 2012. Prolonged Exposure to Insulin Induces Mitochondrion-Derived Oxidative Stress through Increasing Mitochondrial Cholesterol Content in Hepatocytes. Endocrinology 153, 2120–2129. https://doi.org/10.1210/en.2011-2119

Meister, A., 1988a. On the discovery of glutathione. Trends in Biochemical Sciences 13, 185–188. https://doi.org/10.1016/0968-0004(88)90148-X

Meister, A., 1988b. Glutathione metabolism and its selective modification. J. Biol. Chem. 263, 17205–17208.

Melkov, A., Abdu, U., 2018. Regulation of long-distance transport of mitochondria along microtubules. Cell. Mol. Life Sci. 75, 163–176. https://doi.org/10.1007/s00018-017-2590-1

Melov, S., Coskun, P., Patel, M., Tuinstra, R., Cottrell, B., Jun, A.S., Zastawny, T.H., Dizdaroglu, M., Goodman, S.I., Huang, T.-T., Miziorko, H., Epstein, C.J., Wallace, D.C., 1999. Mitochondrial

disease in superoxide dismutase 2 mutant mice. PNAS 96, 846–851. https://doi.org/10.1073/pnas.96.3.846

Meng, Y., Heybrock, S., Neculai, D., Saftig, P., 2020. Cholesterol Handling in Lysosomes and Beyond. Trends in Cell Biology 0. https://doi.org/10.1016/j.tcb.2020.02.007

Mesquita, E.T., Marchese, L. de D., Dias, D.W., Barbeito, A.B., Gomes, J.C., Muradas, M.C.S., Lanzieri, P.G., Gismondi, R.A., 2015. Nobel Prizes: Contributions to Cardiology. Arq Bras Cardiol 105, 188–196. https://doi.org/10.5935/abc.20150041

Mestas, J., Hughes, C.C.W., 2004. Of Mice and Not Men: Differences between Mouse and Human Immunology. The Journal of Immunology 172, 2731–2738. https://doi.org/10.4049/jimmunol.172.5.2731

Michalopoulos, G.K., 2007. Liver regeneration. Journal of Cellular Physiology 213, 286–300. https://doi.org/10.1002/jcp.21172

Milenkovic, D., Blaza, J.N., Larsson, N.-G., Hirst, J., 2017. The Enigma of the Respiratory Chain Supercomplex. Cell Metabolism 25, 765–776. https://doi.org/10.1016/j.cmet.2017.03.009

Miller, W.L., 2013. Steroid hormone synthesis in mitochondria. Molecular and Cellular Endocrinology, Mitochondrial endocrinology – Mitochondria as key to hormones and metabolism 379, 62–73. https://doi.org/10.1016/j.mce.2013.04.014

Miller, W.L., 2007a. Mechanism of StAR's regulation of mitochondrial cholesterol import. Mol. Cell. Endocrinol. 265–266, 46–50. https://doi.org/10.1016/j.mce.2006.12.002

Miller, W.L., 2007b. Steroidogenic acute regulatory protein (StAR), a novel mitochondrial cholesterol transporter. Biochim Biophys Acta 1771, 663–676. https://doi.org/10.1016/j.bbalip.2007.02.012

Miller, W.L., Auchus, R.J., 2011. The Molecular Biology, Biochemistry, and Physiology of Human Steroidogenesis and Its Disorders. Endocr Rev 32, 81–151. https://doi.org/10.1210/er.2010-0013

Misra, U.K., Yamanaka, H., Kizaki, Z., Kauffman, F.C., Thurman, R.G., 1988. A new method for the isolation of fresh hepatocytes from periportal and pericentral regions of the liver lobule. Biochemical and Biophysical Research Communications 155, 455–462. https://doi.org/10.1016/S0006-291X(88)81108-2

Miyazono, Y., Hirashima, S., Ishihara, N., Kusukawa, J., Nakamura, K.-I., Ohta, K., 2018. Uncoupled mitochondria quickly shorten along their long axis to form indented spheroids, instead of rings, in a fission-independent manner. Sci Rep 8, 350. https://doi.org/10.1038/s41598-017-18582-6

Montero, J., Mari, M., Colell, A., Morales, A., Basañez, G., Garcia-Ruiz, C., Fernández-Checa, J.C., 2010. Cholesterol and peroxidized cardiolipin in mitochondrial membrane properties, permeabilization and cell death. Biochimica et Biophysica Acta (BBA) - Bioenergetics, 16th European Bioenergetics Conference 2010 1797, 1217–1224. https://doi.org/10.1016/j.bbabio.2010.02.010

Montero, J., Morales, A., Llacuna, L., Lluis, J.M., Terrones, O., Basañez, G., Antonsson, B., Prieto, J., García-Ruiz, C., Colell, A., Fernández-Checa, J.C., 2008. Mitochondrial Cholesterol Contributes to Chemotherapy Resistance in Hepatocellular Carcinoma. Cancer Res 68, 5246–5256. https://doi.org/10.1158/0008-5472.CAN-07-6161

Morohaku, K., Pelton, S.H., Daugherty, D.J., Butler, W.R., Deng, W., Selvaraj, V., 2014. Translocator Protein/Peripheral Benzodiazepine Receptor Is Not Required for Steroid Hormone Biosynthesis. Endocrinology 155, 89–97. https://doi.org/10.1210/en.2013-1556

Morris, M.D., Bhuvaneswaran, C., Shio, H., Fowler, S., 1982. Lysosome lipid storage disorder in NCTR-BALB/c mice. I. Description of the disease and genetics. Am J Pathol 108, 140–149.

Morris, N.L., Yeligar, S.M., 2018. Role of HIF-1α in Alcohol-Mediated Multiple Organ Dysfunction. Biomolecules 8. https://doi.org/10.3390/biom8040170

Mukherjee, S., Zha, X., Tabas, I., Maxfield, F.R., 1998. Cholesterol Distribution in Living Cells: Fluorescence Imaging Using Dehydroergosterol as a Fluorescent Cholesterol Analog. Biophysical Journal 75, 1915–1925. https://doi.org/10.1016/S0006-3495(98)77632-5

Muñoz-Sánchez, J., Chánez-Cárdenas, M.E., 2019. The use of cobalt chloride as a chemical hypoxia model. J Appl Toxicol 39, 556–570. https://doi.org/10.1002/jat.3749

Murphy, M.P., 2011. Mitochondrial Thiols in Antioxidant Protection and Redox Signaling: Distinct Roles for Glutathionylation and Other Thiol Modifications. Antioxidants & Redox Signaling 16, 476–495. https://doi.org/10.1089/ars.2011.4289

Nakajima, T., Kamijo, Y., Tanaka, N., Sugiyama, E., Tanaka, E., Kiyosawa, K., Fukushima, Y., Peters, J.M., Gonzalez, F.J., Aoyama, T., 2004. Peroxisome proliferator-activated receptor alpha protects against alcohol-induced liver damage. Hepatology 40, 972–980. https://doi.org/10.1002/hep.20399

Nakano, M., Worner, T.M., Lieber, C.S., 1982. Perivenular fibrosis in alcoholic liver injury: ultrastructure and histologic progression. Gastroenterology 83, 777–785.

Nanji, A.A., Dannenberg, A.J., Jokelainen, K., Bass, N.M., 2004. Alcoholic Liver Injury in the Rat Is Associated with Reduced Expression of Peroxisome Proliferator-α (PPARα)-Regulated Genes and Is Ameliorated by PPARα Activation. J Pharmacol Exp Ther 310, 417–424. https://doi.org/10.1124/jpet.103.064717

Newton, J., Hait, N.C., Maceyka, M., Colaco, A., Maczis, M., Wassif, C.A., Cougnoux, A., Porter, F.D., Milstien, S., Platt, N., Platt, F.M., Spiegel, S., 2017. FTY720/fingolimod increases NPC1 and NPC2 expression and reduces cholesterol and sphingolipid accumulation in Niemann-Pick type C mutant fibroblasts. FASEB J 31, 1719–1730. https://doi.org/10.1096/fj.201601041R

Newton, J., Palladino, E.N.D., Weigel, C., Maceyka, M., Gräler, M.H., Senkal, C.E., Enriz, R.D., Marvanova, P., Jampilek, J., Lima, S., Milstien, S., Spiegel, S., 2020. Targeting defective sphingosine kinase 1 in Niemann-Pick type C disease with an activator mitigates cholesterol accumulation. J Biol Chem 295, 9121–9133. https://doi.org/10.1074/jbc.RA120.012659

Nguyen, A.D., McDonald, J.G., Bruick, R.K., DeBose-Boyd, R.A., 2007. Hypoxia Stimulates Degradation of 3-Hydroxy-3-methylglutaryl-coenzyme A Reductase through Accumulation of Lanosterol and Hypoxia-Inducible Factor-mediated Induction of Insigs. J. Biol. Chem. 282, 27436–27446. https://doi.org/10.1074/jbc.M704976200

Ohashi, K., Pimienta, M., Seki, E., 2018. Alcoholic liver disease: A current molecular and clinical perspective. Liver Res 2, 161–172. https://doi.org/10.1016/j.livres.2018.11.002

Osellame, L.D., Blacker, T.S., Duchen, M.R., 2012. Cellular and molecular mechanisms of mitochondrial function. Best Practice & Research Clinical Endocrinology & Metabolism, Mitochondria in Endocrinology 26, 711–723. https://doi.org/10.1016/j.beem.2012.05.003

Osellame, L.D., Duchen, M.R., 2014. Quality control gone wrong: mitochondria, lysosomal storage disorders and neurodegeneration. Br J Pharmacol 171, 1958–1972. https://doi.org/10.1111/bph.12453

Owen, J.B., Butterfield, D.A., 2010. Measurement of Oxidized/Reduced Glutathione Ratio, in: Bross, P., Gregersen, N. (Eds.), Protein Misfolding and Cellular Stress in Disease and Aging: Concepts and Protocols, Methods in Molecular Biology. Humana Press, Totowa, NJ, pp. 269–277. https://doi.org/10.1007/978-1-60761-756-3_18

Pacheco, C.D., Kunkel, R., Lieberman, A.P., 2007. Autophagy in Niemann-Pick C disease is dependent upon Beclin-1 and responsive to lipid trafficking defects. Hum Mol Genet 16, 1495–1503. https://doi.org/10.1093/hmg/ddm100

Pacheco, C.D., Lieberman, A.P., 2008. The pathogenesis of Niemann-Pick type C disease: a role for autophagy? Expert Rev Mol Med 10, e26. https://doi.org/10.1017/S146239940800080X

Pandak, W.M., Kakiyama, G., 2019. The acidic pathway of bile acid synthesis: Not just an alternative pathway. Liver Research 3, 88–98. https://doi.org/10.1016/j.livres.2019.05.001

Pandak, W.M., Ren, S., Marques, D., Hall, E., Redford, K., Mallonee, D., Bohdan, P., Heuman, D., Gil, G., Hylemon, P., 2002. Transport of Cholesterol into Mitochondria Is Rate-limiting for Bile Acid Synthesis via the Alternative Pathway in Primary Rat Hepatocytes. J. Biol. Chem. 277, 48158–48164. https://doi.org/10.1074/jbc.M205244200

Papadopoulos, V., 2003. Peripheral benzodiazepine receptor: structure and function in health and disease. Ann Pharm Fr 61, 30–50.

Papadopoulos, V., Miller, W.L., 2012. Role of mitochondria in steroidogenesis. Best Practice & Research Clinical Endocrinology & Metabolism, Mitochondria in Endocrinology 26, 771–790. https://doi.org/10.1016/j.beem.2012.05.002

Paradis, S., Leoni, V., Caccia, C., Berdeaux, A., Morin, D., 2013. Cardioprotection by the TSPO ligand 4'-chlorodiazepam is associated with inhibition of mitochondrial accumulation of cholesterol at reperfusion. Cardiovasc Res 98, 420–427. https://doi.org/10.1093/cvr/cvt079

Pastorino, J.G., Marcineviciute, A., Cahill, A., Hoek, J.B., 1999. Potentiation by Chronic Ethanol Treatment of the Mitochondrial Permeability Transition. Biochemical and Biophysical Research Communications 265, 405–409. https://doi.org/10.1006/bbrc.1999.1696

Patterson, M., 1993. Niemann-Pick Disease Type C, in: Adam, M.P., Ardinger, H.H., Pagon, R.A., Wallace, S.E., Bean, L.J., Stephens, K., Amemiya, A. (Eds.), GeneReviews®. University of Washington, Seattle, Seattle (WA).

Patterson, M.C., Di Bisceglie, A.M., Higgins, J.J., Abel, R.B., Schiffmann, R., Parker, C.C., Argoff, C.E., Grewal, R.P., Yu, K., Pentchev, P.G., 1993. The effect of cholesterol-lowering agents on hepatic and plasma cholesterol in Niemann-Pick disease type C. Neurology 43, 61–64. https://doi.org/10.1212/wnl.43.1_part_1.61

Patterson, M.C., Hendriksz, C.J., Walterfang, M., Sedel, F., Vanier, M.T., Wijburg, F., NP-C Guidelines Working Group, 2012. Recommendations for the diagnosis and management of Niemann-Pick disease type C: an update. Mol Genet Metab 106, 330–344. https://doi.org/10.1016/j.ymgme.2012.03.012

Patterson, M.C., Mengel, E., Vanier, M.T., Schwierin, B., Muller, A., Cornelisse, P., Pineda, M., NPC Registry investigators, 2015. Stable or improved neurological manifestations during miglustat therapy in patients from the international disease registry for Niemann-Pick disease type C: an observational cohort study. Orphanet J Rare Dis 10, 65. https://doi.org/10.1186/s13023-015-0284-z

Peet, D.J., Janowski, B.A., Mangelsdorf, D.J., 1998. The LXRs: a new class of oxysterol receptors. Current Opinion in Genetics & Development 8, 571–575. https://doi.org/10.1016/S0959-437X(98)80013-0

Pentchev, P.G., Gal, A.E., Booth, A.D., Omodeo-Sale, F., Fouks, J., Neumeyer, B.A., Quirk, J.M., Dawson, G., Brady, R.O., 1980. A lysosomal storage disorder in mice characterized by a dual deficiency of sphingomyelinase and glucocerebrosidase. Biochim Biophys Acta 619, 669–679. https://doi.org/10.1016/0005-2760(80)90116-2

Perkins, A., Nelson, K.J., Parsonage, D., Poole, L.B., Karplus, P.A., 2015. Peroxiredoxins: guardians against oxidative stress and modulators of peroxide signaling. Trends in Biochemical Sciences 40, 435–445. https://doi.org/10.1016/j.tibs.2015.05.001

Phaniendra, A., Jestadi, D.B., Periyasamy, L., 2015. Free Radicals: Properties, Sources, Targets, and Their Implication in Various Diseases. Indian J Clin Biochem 30, 11–26. https://doi.org/10.1007/s12291-014-0446-0

Picklo, M.J., 2008. Ethanol intoxication increases hepatic N-lysyl protein acetylation. Biochemical and Biophysical Research Communications 376, 615–619. https://doi.org/10.1016/j.bbrc.2008.09.039

Pineda, M., Juríčková, K., Karimzadeh, P., Kolnikova, M., Malinova, V., Insua, J.L., Velten, C., Kolb, S.A., 2019. Disease characteristics, prognosis and miglustat treatment effects on disease progression in patients with Niemann-Pick disease Type C: an international, multicenter, retrospective chart review. Orphanet J Rare Dis 14, 32. https://doi.org/10.1186/s13023-019-0996-6

Platt, F.M., 2018. Emptying the stores: lysosomal diseases and therapeutic strategies. Nat Rev Drug Discov 17, 133–150. https://doi.org/10.1038/nrd.2017.214

Platt, F.M., Boland, B., van der Spoel, A.C., 2012. The cell biology of disease: lysosomal storage disorders: the cellular impact of lysosomal dysfunction. J Cell Biol 199, 723–734. https://doi.org/10.1083/jcb.201208152

Porter, F.D., Scherrer, D.E., Lanier, M.H., Langmade, S.J., Molugu, V., Gale, S.E., Olzeski, D., Sidhu, R., Dietzen, D.J., Fu, R., Wassif, C.A., Yanjanin, N.M., Marso, S.P., House, J., Vite, C., Schaffer, J.E., Ory, D.S., 2010. Cholesterol oxidation products are sensitive and specific blood-based biomarkers for Niemann-Pick C1 disease. Sci Transl Med 2, 56ra81. https://doi.org/10.1126/scitranslmed.3001417

Praggastis, M., Tortelli, B., Zhang, J., Fujiwara, H., Sidhu, R., Chacko, A., Chen, Z., Chung, C., Lieberman, A.P., Sikora, J., Davidson, C., Walkley, S.U., Pipalia, N.H., Maxfield, F.R., Schaffer, J.E., Ory, D.S., 2015. A murine Niemann-Pick C1 I1061T knock-in model recapitulates the pathological features of the most prevalent human disease allele. J Neurosci 35, 8091–8106. https://doi.org/10.1523/JNEUROSCI.4173-14.2015

Prinz, W.A., 2007. Non-vesicular sterol transport in cells. Progress in Lipid Research 46, 297–314. https://doi.org/10.1016/j.plipres.2007.06.002

Purohit, V., Bode, J.C., Bode, C., Brenner, D.A., Choudhry, M.A., Hamilton, F., Kang, Y.J., Keshavarzian, A., Rao, R., Sartor, R.B., Swanson, C., Turner, J.R., 2008. Alcohol, intestinal bacterial growth, intestinal permeability to endotoxin, and medical consequences: Summary of a symposium. Alcohol 42, 349–361. https://doi.org/10.1016/j.alcohol.2008.03.131

Purohit, V., Russo, D., 2002. Cellular and molecular mechanisms of alcoholic hepatitis: introduction and summary of the symposium. Alcohol 27, 3–6. https://doi.org/10.1016/S0741-8329(02)00211-2

Quistorff, B., Grunnet, N., 1987. Dual-digitonin-pulse perfusion. Concurrent sampling of periportal and perivenous cytosol of rat liver for determination of metabolites and enzyme activities. Biochem J 243, 87–95. https://doi.org/10.1042/bj2430087

Quistorff, B., Grunnet, N., Cornell, N.W., 1985. Digitonin perfusion of rat liver. A new approach in the study of intra-acinar and intracellular compartmentation in the liver. Biochem J 226, 289–297. https://doi.org/10.1042/bj2260289

Rambaldi, A., Gluud, C., 2006. S-adenosyl-L-methionine for alcoholic liver diseases. Cochrane Database Syst Rev CD002235. https://doi.org/10.1002/14651858.CD002235.pub2

Reddy, J.V., Ganley, I.G., Pfeffer, S.R., 2006. Clues to neuro-degeneration in Niemann-Pick type C disease from global gene expression profiling. PLoS One 1, e19. https://doi.org/10.1371/journal.pone.0000019

Rehm, J., Kanteres, F., Lachenmeier, D.W., 2010. Unrecorded consumption, quality of alcohol and health consequences. Drug and Alcohol Review 29, 426–436. https://doi.org/10.1111/j.1465-3362.2009.00140.x

Ren, S., Hylemon, P., Marques, D., Hall, E., Redford, K., Gil, G., Pandak, W.M., 2004. Effect of increasing the expression of cholesterol transporters (StAR, MLN64, and SCP-2) on bile acid synthesis. J. Lipid Res. 45, 2123–2131. https://doi.org/10.1194/jlr.M400233-JLR200

Ribas, V., García-Ruiz, C., Fernández-Checa, J.C., 2016. Mitochondria, cholesterol and cancer cell metabolism. Clinical and Translational Medicine 5, 22. https://doi.org/10.1186/s40169-016-0106-5

Ribas, V., García-Ruiz, C., Fernández-Checa, J.C., 2014. Glutathione and mitochondria. Front. Pharmacol. 5. https://doi.org/10.3389/fphar.2014.00151

Rimkunas, V.M., Graham, M.J., Crooke, R.M., Liscum, L., 2008. In vivo antisense oligonucleotide reduction of NPC1 expression as a novel mouse model for Niemann Pick type C- associated liver disease. Hepatology 47, 1504–1512. https://doi.org/10.1002/hep.22327

Riscal, R., Skuli, N., Simon, M.C., 2019. Even Cancer Cells Watch Their Cholesterol! Molecular Cell 76, 220–231. https://doi.org/10.1016/j.molcel.2019.09.008

Robin, M.-A., Sauvage, I., Grandperret, T., Descatoire, V., Pessayre, D., Fromenty, B., 2005. Ethanol increases mitochondrial cytochrome P450 2E1 in mouse liver and rat hepatocytes. FEBS Letters 579, 6895–6902. https://doi.org/10.1016/j.febslet.2005.11.029

Rone, M.B., Midzak, A.S., Issop, L., Rammouz, G., Jagannathan, S., Fan, J., Ye, X., Blonder, J., Veenstra, T., Papadopoulos, V., 2012. Identification of a Dynamic Mitochondrial Protein Complex Driving Cholesterol Import, Trafficking, and Metabolism to Steroid Hormones. Mol Endocrinol 26, 1868–1882. https://doi.org/10.1210/me.2012-1159

Rosenbaum, A.I., Maxfield, F.R., 2011. Niemann-Pick type C disease: molecular mechanisms and potential therapeutic approaches. J Neurochem 116, 789–795. https://doi.org/10.1111/j.1471-4159.2010.06976.x

Rovira-Llopis, S., Bañuls, C., Diaz-Morales, N., Hernandez-Mijares, A., Rocha, M., Victor, V.M., 2017. Mitochondrial dynamics in type 2 diabetes: Pathophysiological implications. Redox Biol 11, 637–645. https://doi.org/10.1016/j.redox.2017.01.013

Rubin, E., Beattie, D.S., Lieber, C.S., 1970. Effects of ethanol on the biogenesis of mitochondrial membranes and associated mitochondrial functions. Lab. Invest. 23, 620–627.

Rusiñol, A.E., Cui, Z., Chen, M.H., Vance, J.E., 1994. A unique mitochondria-associated membrane fraction from rat liver has a high capacity for lipid synthesis and contains pre-Golgi secretory proteins including nascent lipoproteins. J. Biol. Chem. 269, 27494–27502.

Saito, K., Negishi, M., James Squires, E., 2013. Sexual dimorphisms in zonal gene expression in mouse liver. Biochemical and Biophysical Research Communications 436, 730–735. https://doi.org/10.1016/j.bbrc.2013.06.025

Santos-Lozano, A., Villamandos García, D., Sanchis-Gomar, F., Fiuza-Luces, C., Pareja-Galeano, H., Garatachea, N., Nogales Gadea, G., Lucia, A., 2015. Niemann-Pick disease treatment: a systematic review of clinical trials. Ann Transl Med 3, 360. https://doi.org/10.3978/j.issn.2305-5839.2015.12.04

Šarenac, T.M., Mikov, M., 2018. Bile Acid Synthesis: From Nature to the Chemical Modification and Synthesis and Their Applications as Drugs and Nutrients. Front Pharmacol 9. https://doi.org/10.3389/fphar.2018.00939

Sarkar, S., Carroll, B., Buganim, Y., Maetzel, D., Ng, A.H.M., Cassady, J.P., Cohen, M.A., Chakraborty, S., Wang, H., Spooner, E., Ploegh, H., Gsponer, J., Korolchuk, V.I., Jaenisch, R., 2013. Impaired autophagy in the lipid-storage disorder Niemann-Pick type C1 disease. Cell Rep 5, 1302–1315. https://doi.org/10.1016/j.celrep.2013.10.042

Schägger, H., Pfeiffer, K., 2000. Supercomplexes in the respiratory chains of yeast and mammalian mitochondria. The EMBO Journal 19, 1777–1783. https://doi.org/10.1093/emboj/19.8.1777

Scharwey, M., Tatsuta, T., Langer, T., 2013. Mitochondrial lipid transport at a glance. J Cell Sci 126, 5317–5323. https://doi.org/10.1242/jcs.134130

Schieber, M., Chandel, N.S., 2014. ROS Function in Redox Signaling and Oxidative Stress. Current Biology 24, R453–R462. https://doi.org/10.1016/j.cub.2014.03.034

Schiff, E.R., Maddrey, W.C., Sorrell, M.F., 2011. Schiff's Diseases of the Liver. Wiley-Blackwell. https://doi.org/10.1002/9781119950509

Schroeder, F., Atshaves, B.P., McIntosh, A.L., Gallegos, A.M., Storey, S.M., Parr, R.D., Jefferson, J.R., Ball, J.M., Kier, A.B., 2007. Sterol carrier protein-2: New roles in regulating lipid rafts and signaling. Biochimica et Biophysica Acta (BBA) - Molecular and Cell Biology of Lipids, Lipid Transporters in Cell Biology 1771, 700–718. https://doi.org/10.1016/j.bbalip.2007.04.005

Schroeder, F., Huang, H., McIntosh, A.L., Atshaves, B.P., Martin, G.G., Kier, A.B., 2010. Caveolin, Sterol Carrier Protein-2, Membrane Cholesterol-Rich Microdomains and Intracellular Cholesterol Trafficking, in: Harris, J.R. (Ed.), Cholesterol Binding and Cholesterol Transport Proteins: Structure and Function in Health and Disease, Subcellular Biochemistry. Springer Netherlands, Dordrecht, pp. 279–318. https://doi.org/10.1007/978-90-481-8622-8_10

Schultz, M.L., Krus, K.L., Lieberman, A.P., 2016. Lysosome and endoplasmic reticulum quality control pathways in Niemann-Pick type C disease. Brain Res 1649, 181–188. https://doi.org/10.1016/j.brainres.2016.03.035

Seker Yilmaz, B., Baruteau, J., Rahim, A.A., Gissen, P., 2020. Clinical and Molecular Features of Early Infantile Niemann Pick Type C Disease. Int J Mol Sci 21. https://doi.org/10.3390/ijms21145059

Selvaraj, V., Stocco, D.M., Tu, L.N., 2015. Minireview: Translocator Protein (TSPO) and Steroidogenesis: A Reappraisal. Mol Endocrinol 29, 490–501. https://doi.org/10.1210/me.2015-1033

Setshedi, M., Wands, J.R., de la Monte, S.M., 2010. Acetaldehyde adducts in alcoholic liver disease. Oxid Med Cell Longev 3, 178–185. https://doi.org/10.4161/oxim.3.3.3

Sever, N., Yang, T., Brown, M.S., Goldstein, J.L., DeBose-Boyd, R.A., 2003. Accelerated Degradation of HMG CoA Reductase Mediated by Binding of Insig-1 to Its Sterol-Sensing Domain. Molecular Cell 11, 25–33. https://doi.org/10.1016/S1097-2765(02)00822-5

Shio, H., Fowler, S., Bhuvaneswaran, C., Morris, M.D., 1982. Lysosome lipid storage disorder in NCTR-BALB/c mice. II. Morphologic and cytochemical studies. Am J Pathol 108, 150–159.

Siri-Tarino, P.W., Krauss, R.M., 2016. The early years of lipoprotein research: from discovery to clinical application. J. Lipid Res. 57, 1771–1777. https://doi.org/10.1194/jlr.R069575

Sirtori, C.R., 2014. The pharmacology of statins. Pharmacological Research, Statin: New Life for an Old Drug 88, 3–11. https://doi.org/10.1016/j.phrs.2014.03.002

Sluchanko, N.N., Tugaeva, K.V., Maksimov, E.G., 2017. Solution structure of human steroidogenic acute regulatory protein STARD1 studied by small-angle X-ray scattering. Biochem Biophys Res Commun 489, 445–450. https://doi.org/10.1016/j.bbrc.2017.05.167

Smith, D., Wallom, K.-L., Williams, I.M., Jeyakumar, M., Platt, F.M., 2009. Beneficial effects of anti-inflammatory therapy in a mouse model of Niemann-Pick disease type C1. Neurobiol Dis 36, 242–251. https://doi.org/10.1016/j.nbd.2009.07.010

Smith, M.T., Loveridge, N., Wills, E.D., Chayen, J., 1979. The distribution of glutathione in the rat liver lobule. Biochem J 182, 103–108. https://doi.org/10.1042/bj1820103

Soccio Raymond E., Breslow Jan L., 2004. Intracellular Cholesterol Transport. Arteriosclerosis, Thrombosis, and Vascular Biology 24, 1150–1160. https://doi.org/10.1161/01.ATV.0000131264.66417.d5

Sokol, J., Blanchette-Mackie, J., Kruth, H.S., Dwyer, N.K., Amende, L.M., Butler, J.D., Robinson, E., Patel, S., Brady, R.O., Comly, M.E., 1988. Type C Niemann-Pick disease. Lysosomal accumulation and defective intracellular mobilization of low density lipoprotein cholesterol. J Biol Chem 263, 3411–3417.

Solsona-Vilarrasa, E., Fucho, R., Torres, S., Nuñez, S., Nuño-Lámbarri, N., Enrich, C., García-Ruiz, C., Fernández-Checa, J.C., 2019. Cholesterol enrichment in liver mitochondria impairs oxidative phosphorylation and disrupts the assembly of respiratory supercomplexes. Redox Biol 24, 101214. https://doi.org/10.1016/j.redox.2019.101214

Song, B.-J., Akbar, M., Abdelmegeed, M.A., Byun, K., Lee, B., Yoon, S.K., Hardwick, J.P., 2014. Mitochondrial dysfunction and tissue injury by alcohol, high fat, nonalcoholic substances and pathological conditions through post-translational protein modifications. Redox Biology 3, 109–123. https://doi.org/10.1016/j.redox.2014.10.004

Spinelli, J.B., Haigis, M.C., 2018. The multifaceted contributions of mitochondria to cellular metabolism. Nat Cell Biol 20, 745–754. https://doi.org/10.1038/s41556-018-0124-1

Stancu, C., Sima, A., 2001. Statins: mechanism of action and effects. Journal of Cellular and Molecular Medicine 5, 378–387. https://doi.org/10.1111/j.1582-4934.2001.tb00172.x

Stanulović, V.S., Kyrmizi, I., Julio, M.K., Hoogenkamp, M., Vermeulen, J.L.M., Ruijter, J.M., Talianidis, I., Hakvoort, T.B.M., Lamers, W.H., 2007. Hepatic HNF4α deficiency induces periportal expression of glutamine synthetase and other pericentral enzymes. Hepatology 45, 433–444. https://doi.org/10.1002/hep.21456

Stein, V.M., Crooks, A., Ding, W., Prociuk, M., O'Donnell, P., Bryan, C., Sikora, T., Dingemanse, J., Vanier, M.T., Walkley, S.U., Vite, C.H., 2012. Miglustat Improves Purkinje Cell Survival and

Alters Microglial Phenotype in Feline Niemann-Pick Disease Type C. J Neuropathol Exp Neurol 71, 434–448. https://doi.org/10.1097/NEN.0b013e31825414a6

Stewart, S.F., Vidali, M., Day, C.P., Albano, E., Jones, D.E.J., 2004. Oxidative stress as a trigger for cellular immune responses in patients with alcoholic liver disease. Hepatology 39, 197–203. https://doi.org/10.1002/hep.20021

Stocco, D.M., 2014. The Role of PBR/TSPO in Steroid Biosynthesis Challenged. Endocrinology 155, 6–9. https://doi.org/10.1210/en.2013-2041

Stocco, D.M., 2001. StAR protein and the regulation of steroid hormone biosynthesis. Annu Rev Physiol 63, 193–213. https://doi.org/10.1146/annurev.physiol.63.1.193

Stocco, D.M., 2000. Intramitochondrial cholesterol transfer. Biochim Biophys Acta 1486, 184–197. https://doi.org/10.1016/s1388-1981(00)00056-1

Stocco, D.M., 1999. The steroidogenic acute regulatory (StAR) protein. Medicina (B Aires) 59, 538–539.

Sugii, S., Reid, P.C., Ohgami, N., Du, H., Chang, T.-Y., 2003. Distinct Endosomal Compartments in Early Trafficking of Low Density Lipoprotein-derived Cholesterol. J. Biol. Chem. 278, 27180–27189. https://doi.org/10.1074/jbc.M300542200

Sun, L.-P., Seemann, J., Goldstein, J.L., Brown, M.S., 2007. Sterol-regulated transport of SREBPs from endoplasmic reticulum to Golgi: Insig renders sorting signal in Scap inaccessible to COPII proteins. Proc Natl Acad Sci U S A 104, 6519–6526. https://doi.org/10.1073/pnas.0700907104

Systemic Veins. Structure of the Veins. Functions of the Veins [WWW Document], n.d. URL http://encyclopedia.lubopitko-bg.com/Systemic_Veins.html (accessed 10.28.20).

Tabas, I., 2002. Cholesterol in health and disease. J Clin Invest 110, 583–590. https://doi.org/10.1172/JCI16381

Taraschi, T.F., Rubin, E., 1985. Effects of ethanol on the chemical and structural properties of biologic membranes. Lab. Invest. 52, 120–131.

Tilokani, L., Nagashima, S., Paupe, V., Prudent, J., 2018. Mitochondrial dynamics: overview of molecular mechanisms. Essays Biochem 62, 341–360. https://doi.org/10.1042/EBC20170104

Tomita, K., Tamiya, G., Ando, S., Kitamura, N., Koizumi, H., Kato, S., Horie, Y., Kaneko, T., Azuma, T., Nagata, H., Ishii, H., Hibi, T., 2005. AICAR, an AMPK activator, has protective effects on alcohol-induced fatty liver in rats. Alcohol. Clin. Exp. Res. 29, 240S–5S. https://doi.org/10.1097/01.alc.0000191126.11479.69

Töröcsik, D., Szanto, A., Nagy, L., 2009. Oxysterol signaling links cholesterol metabolism and inflammation via the liver X receptor in macrophages. Molecular Aspects of Medicine, Oxysterols in Human Pathophysiology 30, 134–152. https://doi.org/10.1016/j.mam.2009.02.002

Torres, S., Balboa, E., Zanlungo, S., Enrich, C., Garcia-Ruiz, C., Fernandez-Checa, J.C., 2017a. Lysosomal and Mitochondrial Liaisons in Niemann-Pick Disease. Front Physiol 8, 982. https://doi.org/10.3389/fphys.2017.00982

Torres, S., Baulies, A., Insausti-Urkia, N., Alarcón-Vila, C., Fucho, R., Solsona-Vilarrasa, E., Núñez, S., Robles, D., Ribas, V., Wakefield, L., Grompe, M., Lucena, M.I., Andrade, R.J., Win, S., Aung, T.A., Kaplowitz, N., García-Ruiz, C., Fernández-Checa, J.C., 2019. Endoplasmic Reticulum Stress-Induced Upregulation of STARD1 Promotes Acetaminophen-Induced Acute Liver Failure. Gastroenterology 157, 552–568. https://doi.org/10.1053/j.gastro.2019.04.023

Torres, S., Matías, N., Baulies, A., Nuñez, S., Alarcon-Vila, C., Martinez, L., Nuño, N., Fernandez, A., Caballeria, J., Levade, T., Gonzalez-Franquesa, A., Garcia-Rovés, P., Balboa, E., Zanlungo, S., Fabrías, G., Casas, J., Enrich, C., Garcia-Ruiz, C., Fernández-Checa, J.C., 2017b. Mitochondrial GSH replenishment as a potential therapeutic approach for Niemann Pick type C disease. Redox Biol 11, 60–72. https://doi.org/10.1016/j.redox.2016.11.010

Traverso, N., Ricciarelli, R., Nitti, M., Marengo, B., Furfaro, A.L., Pronzato, M.A., Marinari, U.M., Domenicotti, C., 2013. Role of Glutathione in Cancer Progression and Chemoresistance [WWW Document]. Oxidative Medicine and Cellular Longevity. https://doi.org/10.1155/2013/972913

Trefts, E., Gannon, M., Wasserman, D.H., 2017. The liver. Current Biology 27, R1147–R1151. https://doi.org/10.1016/j.cub.2017.09.019

Tsujishita, Y., Hurley, J.H., 2000. Structure and lipid transport mechanism of a StAR-related domain. Nature Structural Biology 7, 408–414. https://doi.org/10.1038/75192

Tugaeva, K.V., Sluchanko, N.N., 2019. Steroidogenic Acute Regulatory Protein: Structure, Functioning, and Regulation. Biochemistry Moscow 84, 233–253. https://doi.org/10.1134/S0006297919140141

Tugaeva, K.V., Titterington, J., Sotnikov, D.V., Maksimov, E.G., Antson, A.A., Sluchanko, N.N., 2020. Molecular basis for the recognition of steroidogenic acute regulatory protein by the 14-3-3 protein family. FEBS J 287, 3944–3966. https://doi.org/10.1111/febs.15474

Van Horn, C.G., Ivester, P., Cunningham, C.C., 2001. Chronic Ethanol Consumption and Liver Glycogen Synthesis. Archives of Biochemistry and Biophysics 392, 145–152. https://doi.org/10.1006/abbi.2001.2433

Van Meer, G., Voelker, D.R., Feigenson, G.W., 2008. Membrane lipids: where they are and how they behave. Nature Reviews Molecular Cell Biology 9, 112–124. https://doi.org/10.1038/nrm2330

Vance, J.E., 2014. MAM (mitochondria-associated membranes) in mammalian cells: Lipids and beyond. Biochimica et Biophysica Acta (BBA) - Molecular and Cell Biology of Lipids 1841, 595–609. https://doi.org/10.1016/j.bbalip.2013.11.014

Vanier, M.T., 2015. Complex lipid trafficking in Niemann-Pick disease type C. J Inherit Metab Dis 38, 187–199. https://doi.org/10.1007/s10545-014-9794-4

Vanier, M.T., 2010. Niemann-Pick disease type C. Orphanet J Rare Dis 5, 16. https://doi.org/10.1186/1750-1172-5-16

Vartak, R., Porras, C.A.-M., Bai, Y., 2013. Respiratory supercomplexes: structure, function and assembly. Protein Cell 4, 582–590. https://doi.org/10.1007/s13238-013-3032-y

Vázquez, M.C., Balboa, E., Alvarez, A.R., Zanlungo, S., 2012. Oxidative stress: a pathogenic mechanism for Niemann-Pick type C disease. Oxid Med Cell Longev 2012, 205713. https://doi.org/10.1155/2012/205713

Vázquez, M.C., del Pozo, T., Robledo, F.A., Carrasco, G., Pavez, L., Olivares, F., González, M., Zanlungo, S., 2011. Alteration of gene expression profile in Niemann-Pick type C mice correlates with tissue damage and oxidative stress. PLoS One 6, e28777. https://doi.org/10.1371/journal.pone.0028777

Venkatraman, A., Landar, A., Davis, A.J., Chamlee, L., Sanderson, T., Kim, H., Page, G., Pompilius, M., Ballinger, S., Darley-Usmar, V., Bailey, S.M., 2004a. Modification of the Mitochondrial Proteome in Response to the Stress of Ethanol-dependent Hepatotoxicity. J. Biol. Chem. 279, 22092–22101. https://doi.org/10.1074/jbc.M402245200

Venkatraman, A., Shiva, S., Wigley, A., Ulasova, E., Chhieng, D., Bailey, S.M., Darley-Usmar, V.M., 2004b. The role of iNOS in alcohol-dependent hepatotoxicity and mitochondrial dysfunction in mice. Hepatology 40, 565–573. https://doi.org/10.1002/hep.20326

Visentin, S., De Nuccio, C., Bernardo, A., Pepponi, R., Ferrante, A., Minghetti, L., Popoli, P., 2013. The stimulation of adenosine A2A receptors ameliorates the pathological phenotype of fibroblasts from Niemann-Pick type C patients. J Neurosci 33, 15388–15393. https://doi.org/10.1523/JNEUROSCI.0558-13.2013

Vonck, J., Schäfer, E., 2009. Supramolecular organization of protein complexes in the mitochondrial inner membrane. Biochimica et Biophysica Acta (BBA) - Molecular Cell Research, Assembly of the Mitochondrial Respiratory Chain 1793, 117–124. https://doi.org/10.1016/j.bbamcr.2008.05.019

Wellner, V.P., Anderson, M.E., Puri, R.N., Jensen, G.L., Meister, A., 1984. Radioprotection by glutathione ester: transport of glutathione ester into human lymphoid cells and fibroblasts. Proc Natl Acad Sci U S A 81, 4732–4735. https://doi.org/10.1073/pnas.81.15.4732

Westover, E.J., Covey, D.F., 2004. The enantiomer of cholesterol. J Membr Biol 202, 61–72. https://doi.org/10.1007/s00232-004-0714-7

Wheeler, S., Sillence, D.J., 2020. Niemann-Pick type C disease: cellular pathology and pharmacotherapy. J Neurochem 153, 674–692. https://doi.org/10.1111/jnc.14895

Wilhelm, L.P., Wendling, C., Védie, B., Kobayashi, T., Chenard, M.-P., Tomasetto, C., Drin, G., Alpy, F., 2017. STARD3 mediates endoplasmic reticulum-to-endosome cholesterol transport at membrane contact sites. The EMBO Journal 36, 1412–1433. https://doi.org/10.15252/embj.201695917

Winston, G.W., Reitz, R.C., 1984. Effects of chronic ethanol ingestion on male and female rat liver glycogen phosphorylase phosphatase. Alcohol Clin Exp Res 8, 277–282. https://doi.org/10.1111/j.1530-0277.1984.tb05511.x

Winston, G.W., Reitz, R.C., 1981. Effects of chronic ethanol ingestion on liver glycogen phosphorylase in male and female rats. Am J Clin Nutr 34, 2499–2507. https://doi.org/10.1093/ajcn/34.11.2499

Winston, G.W., Reitz, R.C., 1980. Chronic ethanol ingestion and glycogen metabolism in male and female rats. Adv Exp Med Biol 132, 569–577. https://doi.org/10.1007/978-1-4757-1419-7_59

World Health Organization, 2018. Alcohol [WWW Document]. URL https://www.who.int/news-room/fact-sheets/detail/alcohol (accessed 12.15.20).

Wu, D., Cederbaum, A.I., 2009. Oxidative Stress and Alcoholic Liver Disease. Semin Liver Dis 29, 141–154. https://doi.org/10.1055/s-0029-1214370

Wu, M., Gu, J., Zong, S., Guo, R., Liu, T., Yang, M., 2020. Research journey of respirasome. Protein Cell. https://doi.org/10.1007/s13238-019-00681-x

Xie, X., Brown, M.S., Shelton, J.M., Richardson, J.A., Goldstein, J.L., Liang, G., 2011. Amino acid substitution in NPC1 that abolishes cholesterol binding reproduces phenotype of complete NPC1 deficiency in mice. Proc Natl Acad Sci U S A 108, 15330–15335. https://doi.org/10.1073/pnas.1112751108

Xu, F., Rychnovsky, S.D., Belani, J.D., Hobbs, H.H., Cohen, J.C., Rawson, R.B., 2005. Dual roles for cholesterol in mammalian cells. Proc Natl Acad Sci U S A 102, 14551–14556. https://doi.org/10.1073/pnas.0503590102

Yeagle, P.L., 1985. Cholesterol and the cell membrane. Biochim. Biophys. Acta 822, 267–287. https://doi.org/10.1016/0304-4157(85)90011-5

You, M., Fischer, M., Deeg, M.A., Crabb, D.W., 2002. Ethanol Induces Fatty Acid Synthesis Pathways by Activation of Sterol Regulatory Element-binding Protein (SREBP). J. Biol. Chem. 277, 29342–29347. https://doi.org/10.1074/jbc.M202411200

You, M., Liang, X., Ajmo, J.M., Ness, G.C., 2008. Involvement of mammalian sirtuin 1 in the action of ethanol in the liver. Am J Physiol Gastrointest Liver Physiol 294, G892-898. https://doi.org/10.1152/ajpgi.00575.2007

You, M., Matsumoto, M., Pacold, C.M., Cho, W.K., Crabb, D.W., 2004. The role of AMP-activated protein kinase in the action of ethanol in the liver. Gastroenterology 127, 1798–1808. https://doi.org/10.1053/j.gastro.2004.09.049

Youle, R.J., Bliek, A.M. van der, 2012. Mitochondrial Fission, Fusion, and Stress. Science 337, 1062–1065. https://doi.org/10.1126/science.1219855

Yu, W., Gong, J.-S., Ko, M., Garver, W.S., Yanagisawa, K., Michikawa, M., 2005. Altered Cholesterol Metabolism in Niemann-Pick Type C1 Mouse Brains Affects Mitochondrial Function. J. Biol. Chem. 280, 11731–11739. https://doi.org/10.1074/jbc.M412898200

Zakhari, S., 2013. Alcohol Metabolism and Epigenetics Changes. Alcohol Res 35, 6–16.

Zampieri, S., Mellon, S.H., Butters, T.D., Nevyjel, M., Covey, D.F., Bembi, B., Dardis, A., 2009. Oxidative stress in NPC1 deficient cells: protective effect of allopregnanolone. J Cell Mol Med 13, 3786–3796. https://doi.org/10.1111/j.1582-4934.2008.00493.x

Zhang, M., Liu, P., Dwyer, N.K., Christenson, L.K., Fujimoto, T., Martinez, F., Comly, M., Hanover, J.A., Blanchette-Mackie, E.J., Strauss, J.F., 2002. MLN64 Mediates Mobilization of Lysosomal Cholesterol to Steroidogenic Mitochondria. J. Biol. Chem. 277, 33300–33310. https://doi.org/10.1074/jbc.M200003200

Zhang, X., Tachibana, S., Wang, H., Hisada, M., Williams, G.M., Gao, B., Sun, Z., 2010. Interleukin-6 is an important mediator for mitochondrial DNA repair after alcoholic liver injury in mice. Hepatology 52, 2137–2147. https://doi.org/10.1002/hep.23909

Zhao, C., Dahlman-Wright, K., 2010. Liver X receptor in cholesterol metabolism. Journal of Endocrinology 204, 233–240. https://doi.org/10.1677/JOE-09-0271

Zhao, H., Lappalainen, P., 2012. A simple guide to biochemical approaches for analyzing protein-lipid interactions. Mol Biol Cell 23, 2823–2830. https://doi.org/10.1091/mbc.E11-07-0645

Zhao, N., Guo, F.-F., Xie, K.-Q., Zeng, T., 2018. Targeting Nrf-2 is a promising intervention approach for the prevention of ethanol-induced liver disease. Cell. Mol. Life Sci. 75, 3143–3157. https://doi.org/10.1007/s00018-018-2852-6

Zhao, R.-Z., Jiang, S., Zhang, L., Yu, Z.-B., 2019. Mitochondrial electron transport chain, ROS generation and uncoupling (Review). International Journal of Molecular Medicine 44, 3–15. https://doi.org/10.3892/ijmm.2019.4188

Ziolkowski, W., Szkatula, M., Nurczyk, A., Wakabayashi, T., Kaczor, J.J., Olek, R.A., Knap, N., Antosiewicz, J., Wieckowski, M.R., Wozniak, M., 2010. Methyl-beta-cyclodextrin induces mitochondrial cholesterol depletion and alters the mitochondrial structure and bioenergetics. FEBS Letters 584, 4606–4610. https://doi.org/10.1016/j.febslet.2010.10.023

Zorova, L.D., Popkov, V.A., Plotnikov, E.Y., Silachev, D.N., Pevzner, I.B., Jankauskas, S.S., Babenko, V.A., Zorov, S.D., Balakireva, A.V., Juhaszova, M., Sollott, S.J., Zorov, D.B., 2018. Mitochondrial membrane potential. Analytical Biochemistry, Mitochondrial Biochemistry and Bioenergenetics 552, 50–59. https://doi.org/10.1016/j.ab.2017.07.009

APPENDIX

Redox Biology 24 (2019) 101214

Contents lists available at ScienceDirect

Redox Biology

journal homepage: www.elsevier.com/locate/redox

Research Paper

Cholesterol enrichment in liver mitochondria impairs oxidative phosphorylation and disrupts the assembly of respiratory supercomplexes

Estel Solsona-Vilarrasa[a,b,c,d,1], Raquel Fucho[a,b,c,1], Sandra Torres[a,b,c], Susana Nuñez[c], Natalia Nuño-Lámbarri[a,b,f], Carlos Enrich[b,d], Carmen García-Ruiz[a,b,c,e,*], José C. Fernández-Checa[a,b,c,e,*]

[a] Department of Cell Death and Proliferation, Institute of Biomedical Research of Barcelona (IIBB), CSIC, Barcelona, Spain
[b] Liver Unit, Hospital Clinic I Provincial de Barcelona, Instituto de Investigaciones Biomédicas August Pi i Sunyer (IDIBAPS), Barcelona, Spain
[c] Centro de Investigación Biomédica en Red (CIBEREHD), Barcelona, Spain
[d] Department of Biomedical Sciences, Medicine Faculty, Universitat de Barcelona (UB), Spain
[e] Research Center for ALPD, Keck School of Medicine, University of Southern California, Los Angeles, CA, United States
[f] Traslational Research Unit, Medica Sur Clinic & Foundation, Mexico City, Mexico

ARTICLE INFO

Keywords:
Mitochondria
Cholesterol
Liver
Hepatic diseases
Respiration
Oxidative stress

ABSTRACT

Mitochondrial cholesterol accumulation is a hallmark of alcoholic and non-alcoholic fatty liver diseases and impairs the function of specific solute carriers through changes in membrane physical properties. However, its impact on mitochondrial respiration and organization of respiratory supercomplexes has not been determined so far. Here we fed mice a cholesterol-enriched diet (HC) supplemented with sodium cholate to examine the effect of cholesterol in mitochondrial function. HC feeding increased liver cholesterol content, which downregulated *Srebp2* and *Hmgcr* expression, while sodium cholate administration decreased *Cyp7a1* and *Cyp8b1* mRNA levels, suggesting the downregulation of bile acid synthesis through the classical pathway. HC-fed mice exhibited increased expression of *Stard1* and *Mln64* and enhanced mitochondrial free cholesterol levels (2–3 fold), leading to decreased membrane fluidity. Mitochondria from HC-fed mice displayed increased cholesterol loading in both outer and inner mitochondrial membranes. Cholesterol loading decreased complex I and complex II-driven state 3 respiration and mitochondrial membrane potential. Decreased respiratory and uncoupling control ratio from complex I was also observed after *in situ* enrichment of mouse liver mitochondria with cholesterol or enantiomer cholesterol, the mirror image of natural cholesterol. Moreover, *in vivo* cholesterol loading decreased the level of complex III_2 and the assembly of respiratory supercomplexes I_1+III_2+IV and I_1+III_2. Moreover, HC feeding caused oxidative stress and mitochondrial GSH (mGSH) depletion, which translated in hepatic steatosis and liver injury, effects that were rescued by replenishing mGSH with GSH ethyl ester. Overall, mitochondrial cholesterol accumulation disrupts mitochondrial functional performance and the organization of respiratory supercomplexes assembly, which can contribute to oxidative stress and liver injury.

1. Introduction

Cholesterol is an integral component of cellular membranes that not only plays an essential role in determining membrane physical properties, but also regulates multiple signaling pathways [1–3]. Due to this key role in modulating membrane structure and function, cholesterol levels in cell membranes are tightly regulated. Cells satisfy their need for cholesterol either through the uptake from nutrients and cholesterol-rich low-density lipoproteins, or by *de novo* synthesis from acetyl-CoA in the mevalonate pathway controlled by HMG-CoA reductase (HMGCR), the rate-limiting step in cholesterol synthesis. The endoplasmic reticulum (ER)-based transcription factor SREBP-2 is a master regulator of cholesterol synthesis by controlling the expression of HMGCR [3,4].

Abbreviations: ALD, Alcoholic Liver Disease; DHE, Dihydroethidium; FFA, Free Fatty Acids; HC, High-Cholesterol diet; HMGCoA R, HydroxyMethylGlutaryl CoA Reductase; StARD1, Steroidogenic Acute Regulatory protein; TMRM, Tetramethylrhodamine Methyl ester; HPLC, High-Performance Liquid Chromatography; PMH, primary mouse hepatocytes

* Corresponding authors. Department of Cell Death and Proliferation, Institute of Biomedical Research of Barcelona (IIBB), CSIC, Barcelona, Spain.
E-mail addresses: cgrbam@iibb.csic.es (C. García-Ruiz), checa229@yahoo.com (J.C. Fernández-Checa).
[1] Both authors contributed equally to the work.

https://doi.org/10.1016/j.redox.2019.101214
Received 11 February 2019; Received in revised form 24 April 2019; Accepted 6 May 2019
Available online 09 May 2019

Cholesterol is distributed from the plasma membrane and ER to different membrane bilayers, including mitochondria, where it plays key functional and structural roles. Mitochondria are essential organelles with numerous functions in cellular metabolism and homeostasis. They have long been considered as crucial organelles acting as the source of energy in the form of ATP synthesis. Besides this key function, mitochondria are also crucial for other cellular processes, including autophagy, apoptosis, fatty acid synthesis, Ca^{2+} homeostasis and cell signaling [5]. In addition, mitochondrial function extends beyond the boundaries of the cell and influence the physiology of the organism by regulating communication between cells and tissues [6]. Given this plethora of functions, it is not surprising that mitochondrial dysfunction has emerged as a key factor in a myriad of diseases [7–10]. Furthermore, mitochondria are the main consumers of molecular oxygen in the cell in the respiratory chain, which can result in the collateral generation of reactive oxygen species (ROS) [11–13].

Mitochondria are cholesterol-poor organelles compared to plasma membranes. The levels of cholesterol in mitochondrial membranes are under tight control, particularly in specialized organs, such as steroidogenic tissues or liver, where mitochondrial cholesterol is metabolized into steroid hormones or bile acids, respectively. The rate-limiting step in this metabolic process is determined by the cholesterol availability in mitochondria and therefore its mitochondrial trafficking regulates mitochondrial cholesterol homeostasis under physiological conditions. Mitochondrial cholesterol trafficking is controlled largely by STAR family members, including STARD1 and MLN64 (also known as StARD3) [14–16], and the unbalance between cholesterol trafficking and its metabolism can result in mitochondrial cholesterol accumulation, which can impact mitochondrial membrane physical properties and fluidity [17]. Indeed, mitochondrial cholesterol loading has been shown to perturb the function of specific membrane carriers, such as SLC25A11, which results in mitochondrial GSH (mGSH) depletion through impaired transport of cytosolic GSH into mitochondria, leading to increased oxidative stress [18–20].

Mitochondrial cholesterol accumulation is a hallmark of chronic diseases, including cardiovascular disorders, cancer and Alzheimer's disease [21–28]. In addition, previous studies have shown an association between increased mitochondrial cholesterol levels and liver injury in alcoholic and nonalcoholic liver disease [29–34]. However, the specific role of mitochondrial cholesterol accumulation in mitochondrial respiration and organization of functional respiratory complexes has not been previously examined. Therefore, our aim was to use *in vivo* and *in vitro* models of mitochondrial cholesterol enrichment to examine the impact of this event on oxygen consumption rates and the assembly of mitochondrial respiratory supercomplexes.

2. Material and methods

2.1. Animals and treatments

Wild type C57BL/6J male mice were obtained from Charles River Laboratories. All procedures involving animals and their care were approved by the Ethics Committee of the University of Barcelona and were conducted in accordance with institutional guidelines in compliance with national and international laws and policies. Mice were randomly separated in two groups that were fed with a regular chow diet (CTRL) or a high cholesterol diet (HC, 2% cholesterol and 0.5% sodium cholate, custom made Research Diets, Brogaarden Denmark, C18021901) for up to two days, as described previously [19]. In some cases, mice were fed with a diet enriched in 0.5% sodium cholate (SC) (Research Diet) alone. To test the role of mGSH replenishment, mice were fed HC diet and treated with 1.25 mmol/kg of GSH ethyl ester (GSHee), as described previously [35].

2.2. Mitochondria isolation and ROS determination

Livers were minced in 10 vol of cold Buffer A (225 mM mannitol, 75 mM sucrose, 0.1 mM EGTA, 10 mM HEPES and 1 mg/ml fatty acid-free BSA, pH 7.4) supplemented with protease and phosphatase inhibitors (Roche). Tissue was then disrupted with a drill-driven Teflon dounce homogenizer (4 strokes at 1500 rpms). Mitochondria were isolated by differential centrifugation, 15 min at 700 ×g followed by 15 min at 10000 ×g at 4 °C. Pellets containing mitochondria were resuspended in Buffer B (395 mM sucrose, 0.1 mM EGTA and 10 mM HEPES, pH 7.4).

ROS generation was determined in isolated mitochondria using MitoSox and Amplex Red Hydrogen peroxide/Peroxidase Assay Kit under basal conditions as described previously [36] and detailed in Supplemental Materials.

2.3. Mitoplasts preparation

Mitoplasts were prepared by permeabilization of intact mitochondria by digitonin. Briefly, to a mitochondrial protein suspension of 8 μg/μl in Buffer B (395 mM sucrose, 0.1 mM EGTA and 10 mM HEPES, pH 7.4) an equal volume of digitonin (7.68μg/μl) was added (960 μg digitonin/mg mitochondria). After incubation for 30 min at 4 °C, the sample was centrifuged for 10 min at 10000×*g* at 4 °C, and the pellet was resuspended in Buffer B and centrifuged again for washing. Mitoplasts purity was assessed by the presence of Porin or COX IV.

2.4. In vitro cholesterol increase in mouse liver mitochondria

In vitro cholesterol enrichment was performed by incubation of mitochondria with a cholesterol-BSA Complex (CBSAC) or enantiomer cholesterol (Ent-CBSAC) as described previously [32]. Enantiomer cholesterol was described before and generously provided by Scott Rychnovsky (Department of Chemistry, University of California Irvine) [37]. CBSAC and Ent-CBSAC were prepared by dissolving 50 mg of cholesterol or enantiomer cholesterol in 5 ml of absolute ethanol and then diluted with 5 ml of double distilled water. The milk-like solution was then centrifuged at 2000×*g* for 10min. The supernatant was discarded, and the pellet was resuspended in 5 ml of Buffer CHS (0.25 M sucrose, 1 mM EDTA, pH 7.3). The white solution was stirred gently and 2 g of Free-Fatty Acid BSA were slowly added at room temperature. Once BSA was completely dissolved, the pH of the solution was adjusted to 7.3, and then centrifuged in the cold at 12000×*g* for 10min. The supernatant was collected and used for cholesterol incorporation into mitochondria. CBSAC or ent-CBSAC was added to mouse liver mitochondria (0.2 mg/mg mitochondria) at 4 °C for 1min. Mitochondria were subsequently diluted about 20 times with cold Buffer CHS, and spun down immediately at 12000×*g* for 10min to eliminate the unbound cholesterol. Parallel control experiments were performed using only BSA.

2.5. Electron microscopy

Mice were perfused through the portal vein to wash the liver with cold saline and then fixed by perfusion with 2.5% glutaraldehyde in phosphate buffer. Liver tissue fragments were extracted and fixed with glutaraldehyde 2.5% and paraformaldehyde 2% in buffer phosphate (0.1 M, pH 7.4), post-fixed in 1% osmium tetroxide and 0.8% potassium ferrocyanide, dehydrated with acetone, and embedded in epoxy resin. Sections were cut and stained with methylene blue for light microscopy. Ultrathin sections for transmission electron microscopy were cut and stained with 2% uranyl acetate for 10min and with a lead-staining solution for 2min. Images from stained ultrathin sections were acquired by moving randomly across the EM grid using a transmission electron microscope JEOL JEM-1010 fitted with a Gatan Orius SC1000 (model 832) digital camera. ImageJ software was used to quantify the number

and length of mitochondria.

2.6. Measurement of fluorescence anisotropy

Fluidity of mitochondrial membranes was evaluated by fluorescence anisotropy of mitochondria-bound dye DPH. DPH (20 mM in tetrahydrofuran) was first diluted 100 times with 10 mM Tris-HCl, 150 mM KCl, 1 mM EDTA, pH 7.4. Subsequently, DPH was injected into stirred mitochondrial suspensions (0.5 mg/ml) and the mixture was incubated for 30 min at 37 °C. Fluorescence polarization was measured in a Hitachi spectrofluorometer at wavelengths of 366 nm for excitation and 425 nm for emission. The results are expressed as anisotropy units (r), where $r = (I_0/I_{90})/(I_0 + 2I_{90})$. I_0 and I_{90} represent the intensities of light when polarizers were in parallel or perpendicular orientation, respectively. Light scattering and intrinsic fluorescence were routinely corrected by subtracting the signal obtained from unlabeled samples and the fluorescence of the buffer plus label alone.

2.7. Blue-Native PAGE

Blue-Native PAGE was performed as described previously [38,39]. Briefly, 200 µg of mitochondria were isolated and solubilized using solubilization buffer A (50 mM Sodium Chloride, 50 mM Imidazole, 2 mM 6-aminohexanoic acid, EDTA 1 mM, pH 7) with digitonin (6 mg digitonin/mg mitochondria). Mitochondrial complexes were subsequently separated using a Criterion™ TGX™ Precast 4–15% gel (Biorad) and Running Buffer 10x Tris/Gly (Biorad), and transferred to a PVDF membrane using the Trans Blot Turbo (Biorad). To detect OXPHOS (super)complexes, the membrane was incubated overnight with the following primary antibodies: COXIV (Cell Signaling, #4844), UQCRC2 (G-10) (Santa Cruz, sc-390378) and MitoProfile® Total OXPHOS Rodent WB Antibody Cocktail (Abcam, ab110413). Membranes were thoroughly washed with TBS-Tween and incubated for 45min with HRP-conjugated secondary antibody. Pierce ECL Western Blotting Substrate (ThermoScientific) was used to develop the membranes. Images were digitally captured by LAS4000 (GE Healthcare) and optical density was analyzed with ImageJ software. Coomassie blue staining was used as loading control.

2.8. Real time PCR

Total RNA was isolated from mouse liver with Trizol reagent (ThermoScientific) and converted to cDNA using the High-Capacity cDNA Reverse Transcription Kit from ThermoFisher. Quantitative Reverse Transcription Polymerase Chain Reaction (qRT-PCR) was subsequently performed using the SensiFAST™ SYBR® No-ROX Kit (Bioline) following the manufacturer's instructions. Each reaction was run in triplicate to determine the threshold (CT) for each mRNA, and the amount of each cDNA relative to the β2-Microglobulin (B2M) endogenous control was determined using the 2-ΔΔCt method. The primer sequences (Invitrogen) for the expression of *Srebp2, Hmgcr, Stard1, Mln64, Cyp27a1, Cyp7a1, Cyp7b1, Cyp8b1* and *B2M* are described in Supplementary Table 1.

2.9. Extracellular flux analyses

0.2 µg protein/µl mitochondria stocks were prepared in cold MAS buffer (70 mM sucrose, 220 mM mannitol, 10 mM KH_2PO_4, 5 mM $MgCl_2$, 2 mM HEPES, 1.0 mM EGTA and 0.2% (w/v) fatty acid-free BSA, pH 7.2) with pyruvate and malate (10 mM) or succinate (10 mM) and rotenone (2 µM) as substrates for respiration. 50 µl of mitochondrial suspension (10 µg) were delivered per well of XFe24 Seahorse plate and plates were spun 15 min at 2000 × g at 4 °C. After centrifugation, 450 µl of warm (37 °C) MAS buffer with substrates were added. Plates were incubated 8–10 min at 37 °C in an incubator without CO_2 to allow the plate to warm and then loaded into the XFe24 Analyzer for mitochondrial respiration analysis. Mitochondria began in a coupled state with substrate present; pyruvate and malate (10 mM) or succinate (10 mM) and rotenone (2 µM) (state 2). State 3 was initiated with ADP (4 mM) addition, state 4 was induced with the injection of oligomycin (2.5 µg/ml) (state 4o), and FCCP (4 µM) induced maximal uncoupler-stimulated respiration (state 3u). Non-mitochondrial respiration was assessed by OCR measurement in the presence of antimycin (4 µM). All states were sequentially measured, allowing calculation of respiratory control ratios (RCR: state 3/state 4o, or UCR: state 3u/state 4o). 3–5 mitochondrial preparations per experimental group were analyzed always in triplicates in each plate. Measurement protocol for standard liver mitochondria: 2 cycles of 1min mix and 3min measure per state. Measurement protocol for liver mitochondria after incubation with CBSAC: 2 cycles of 1min mix and 4min measure (State 2); 1 cycle of 1min mix and 4min measure (other States).

2.10. Immunofluorescence and laser confocal imaging

Cultured mouse hepatocytes were fixed for 15min with 4% paraformaldehyde and permeabilized and blocked for 15min with 0.2% saponin dissolved in 1% BSA-fatty acid free (FAF) in PBS commercial buffer. Tom20 (Santa Cruz) primary antibody was incubated overnight in BSA 1% followed by a secondary antibody for 1 h at room temperature in BSA 0.1%. Filipin (Sigma) was added at 0.33 mg/ml during the secondary antibody incubation and the following steps were performed in the dark. Stained samples were embedded in fluoromount (Sigma) and digital images were taken in a Leica DM2500 confocal microscope.

2.11. Protein carbonylation

Protein carbonylation was assessed by measuring the levels of carbonyl groups using the OxyBlot Protein Oxidation Detection Kit (Millipore), following manufacturer's instruction. The DNPH derivatization was carried out on 10 µg of protein for 15min. One-dimensional electrophoresis was carried out after DNPH derivatization using 4–12% SDS-polyacrylamide gels (SDS-PAGE) (Bio-Rad, XT-Criterion). Proteins were transferred to nitrocellulose membranes (Bio Rad) which were then blocked with 1% BSA in TBS-Tween. Membranes were then incubated in the primary antibody solution (anti-DNP 1:150) followed by incubation with secondary antibody solution (1:300), both incubations during 1 h at room temperature. After every step, membranes were thoroughly washed with TBS-Tween. Immunoreactive bands were visualized by Pierce ECL Western Blotting Substrate (Thermo Scientific) and band signal intensity was quantified by ImageJ software.

2.12. Statistical analyses

Statistical analyses were performed using GraphPad Prism 6 (Graphpad Software Inc). Unpaired Student's t-test (two tailed) was performed between two groups and one or two-way ANOVA followed by Tukey's Multiple Comparison test were used for statistical comparisons between three or more groups. The corresponding number of experiments is indicated in the figure legends. Data in graphs are shown as mean ± s.e.m.

3. Results

3.1. HC diet alters hepatic cholesterol homeostasis while sodium cholate feeding represses bile acid synthesis

Although feeding a HC diet supplemented with sodium cholate has been previously used as a nutritional approach to steadily increase liver cholesterol content [19,34], the contribution of sodium cholate in the regulation of cholesterol homeostasis in relationship with bile acid synthesis has not been previously examined. Thus, we first

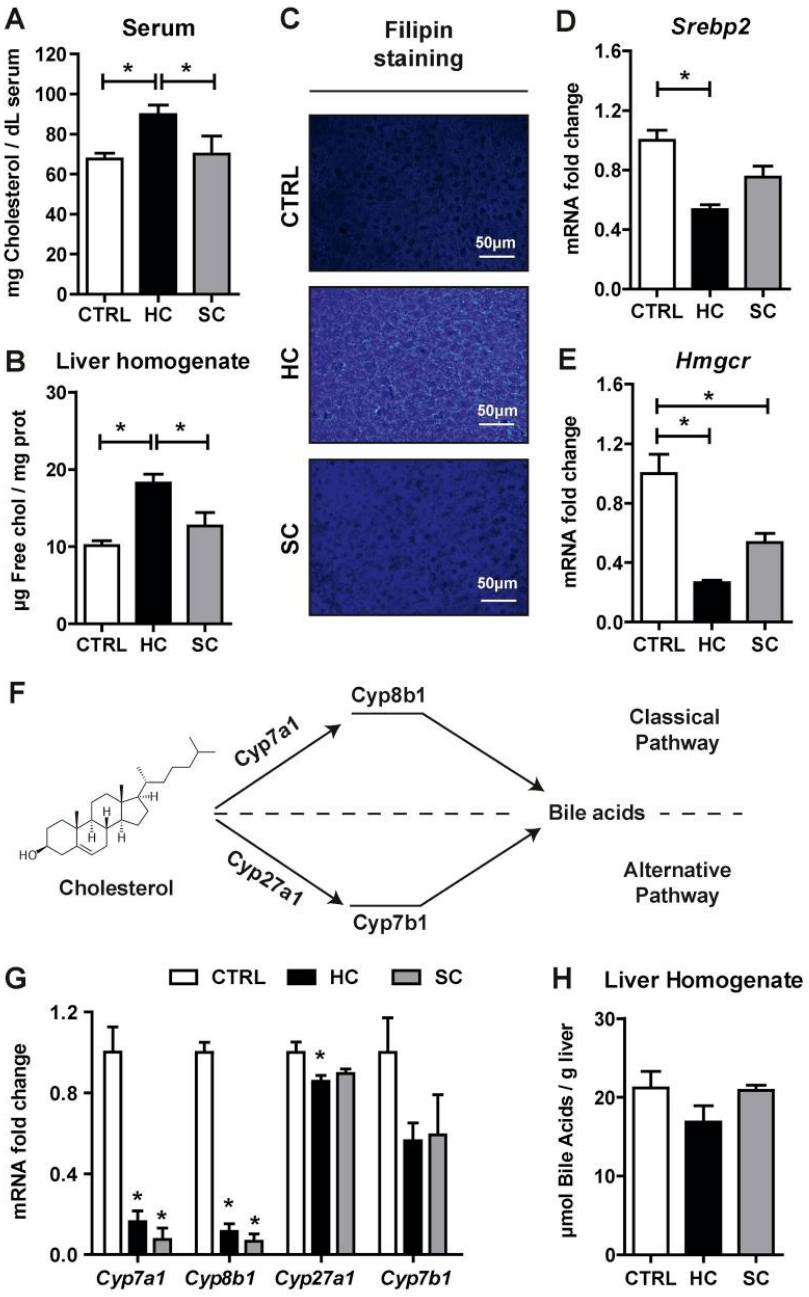

Fig. 1. Alteration of hepatic cholesterol homeostasis and bile acid synthesis by HC feeding. Cholesterol levels in (A) Serum and (B) Liver of WT C57BL/6J mice fed a CTRL, HC or SC (sodium cholate) diet for 2 days. Data are presented as means ± SEM (N > 10, *P < 0.05, One-way ANOVA followed by Tukey's Multiple Comparison test). (C) Cholesterol content in liver by Filipin staining in liver cryosections. Representative images obtained by fluorescence microscopy. (D–E) mRNA levels of *Srebp2* and *Hmgcr* in liver. Values are the mean ± SEM of > 10 animals per group. *P < 0.05. (F) Diagram of classical and alternative pathways of bile acid synthesis in liver. (G) mRNA levels of *Cyp7a1*, Cyp8b1, *Cyp27a1* and *Cyp7b1* in liver. Values are the mean ± SEM of > 10 animals per group. *P < 0.05 vs. CTRL samples. (H) Bile Acids levels in liver. Data are presented as means ± SEM (N > 5, *P < 0.05, One-way ANOVA followed by Tukey's Multiple Comparison test).

characterized the regulation of hepatic cholesterol homeostasis and whether dietary cholesterol feeding in the presence of sodium cholate was channeled for bile acids generation. Short-term HC feeding increased cholesterol levels in serum (Fig. 1A) and liver, as determined by HPLC analyses (Fig. 1B), or upon staining of liver sections with filipin to detect free cholesterol levels (Fig. 1C). However, feeding sodium cholate (0.5%) for two days did not significantly increase serum or liver cholesterol levels (Fig. 1A–C). Moreover, the increase of liver cholesterol levels following HC feeding translated in decreased expression of key steps involved in *de novo* cholesterol biosynthesis, such as *Srebp2* (Fig. 1D), a transcription factor that regulates cholesterol neosynthesis, and its target gene *Hmgcr* (Fig. 1E), which catalyzes the rate-limiting step in the mevalonate pathway. Moreover, as cholesterol is a precursor for bile acids synthesis, we next examined the expression of enzymes

involved in classical (Cyp7a1, Cyp8b1) and the alternative pathway of bile acid synthesis in mitochondria (Cyp27a1, Cyp7b1) (Fig. 1F). While HC feeding markedly decreased the expression of *cyp7a1* as well as *cyp8b1*, this effect was primarily due to the presence of sodium cholate in the diet (Fig. 1G). HC or sodium cholate feeding, however, exerted a modest effect in the expression of Cyp27a1 and Cyp7b1, indicating a minor impact in the alternate pathway of mitochondrial bile acid synthesis. Consistent with these findings, HC feeding did not stimulate the net increase in the total bile acid pool in the liver, likely reflecting the repression by sodium cholate of the enzymes involved in bile acid synthesis (Fig. 1H). Thus, these findings indicate that the presence of sodium cholate in the HC diet contributes to the maintenance of free cholesterol levels, in part, by suppressing its metabolism into bile acid.

3.2. HC-induced mitochondrial cholesterol loading distributes in both mitochondrial membranes and disrupts mitochondrial morphology

Since HC feeding has been shown to increase mitochondrial cholesterol content [19,34], we next examined the expression of putative mitochondrial cholesterol carriers and the distribution of cholesterol between the outer and inner mitochondrial membranes. Confirming previous findings in rat liver mitochondria [19], isolated mitochondria from HC-fed mice exhibited a significant increase in free cholesterol levels (> 2-fold) determined by HPLC analyses compared to mitochondria from control mice (Fig. 2A). Feeding a 0.5% sodium cholate without cholesterol failed to significantly increase mitochondrial cholesterol levels (5.7 ± 0.7 μg free cholesterol/mg protein). The increase in mitochondrial cholesterol was also observed by confocal imaging of primary mouse hepatocytes (PMH) isolated from HC-fed mice upon staining with filipin (free-cholesterol marker) and Tom20 (mitochondrial marker). As seen, HC feeding resulted in increased filipin staining, which co-localized with Tom20 indicating increased trafficking of free cholesterol into mitochondria (Fig. 2B). Since STARD1 and MLN64 are known to regulate mitochondrial cholesterol trafficking [14–16,40], we examined their expression in mice fed the HC diet. As shown, *Stard1* and *Mln64* expression increased after HC feeding (Fig. 2C). We next assessed the relative distribution of cholesterol enrichment within mitochondrial membranes. Mitoplasts were isolated from intact mitochondria after permeabilization of the outer membrane upon digitonin treatment. Mitoplasts purity was confirmed by the de-enrichment of porin and the increase in COX IV, compared to intact mitochondria, which was enriched in both markers (Fig. 2D). While cholesterol levels in mitoplasts were lower than in intact mitochondria, the cholesterol content of mitoplasts from cholesterol-enriched mitochondria was higher than in mitoplasts from control mitochondria, indicating the enrichment of cholesterol in both outer and inner mitochondrial membranes (Fig. 2E). The increase of cholesterol in mitochondrial membranes is known to change membrane physical properties [3,19,20]. Thus, we next confirmed whether the presence of cholesterol in mitochondrial membrane inserted into the lipid bilayers and altered membrane fluidity. Fluorescence anisotropy analysis of mitochondria labeled with the fluorescent probe DPH revealed an increase in membrane order of mitochondria from HC-fed animals compared to control mice (Fig. 2F). Moreover, we next addressed whether the loss of mitochondrial fluidity by cholesterol enrichment altered mitochondrial morphology. Electron microscopy analyses revealed that mitochondria from HC-fed mice appeared rounded and with abnormal cristae compared to mitochondria from control animals (Fig. 2G). Although mitochondrial number was not altered by cholesterol accumulation, a significant decrease in mitochondrial length was observed (Fig. 2H). These findings indicate that nutritional cholesterol feeding traffics to mitochondria and alters mitochondrial membrane fluidity and morphology.

3.3. Mitochondrial cholesterol enrichment impairs complex I and complex II-driven state 3 respiration

In view of the preceding findings indicating increased cholesterol in mitochondrial membranes, we next examined the impact of this event in mitochondrial respiration, determining real-time oxygen consumption rates (OCR) by a flux analyzer. Using pyruvate and malate as substrates of complex I, mitochondria from HC-fed mice showed a significant reduction in mitochondrial performance and respiratory states compared to mitochondria from mice-fed control diet (Fig. 3A). In particular, HC feeding impaired ADP-stimulated state 3 respiration as well as the FCCP-induced maximal uncoupler-stimulated respiration (state 3u) without significant change in state 4o respiration (Fig. 3B). These alterations were reflected in the respiratory control ratio (RCR) (state 3/state 4o) and uncoupling control ratio (UCR) (state 3u/state 4o), decreasing both in mitochondria from HC-fed mice (Fig. 3C). Similar analysis was performed using succinate plus rotenone to examine respiration through complex II. HC feeding impaired OCR from succinate plus rotenone with decreased state 3 and state 3u (Fig. 4A and B). In addition, HC feeding decreased succinate plus rotenone-driven state 4o respiration (Fig. 4B), which translated in unchanged RCR and UCR ratios (Fig. 4C). Thus, these findings indicate that *in vivo* mitochondrial cholesterol loading significantly impairs mitochondrial complex I and complex II-driven state 3 respiration. Since the protonmotive force generated from coupled respiration determines the mitochondrial membrane potential, we next assessed the impact of mitochondrial cholesterol loading in membrane potential. Incubation of PMH from HC-fed mice stained with TMRM revealed a decrease in mitochondrial membrane potential (Fig. 3D). Overall, these findings demonstrate the deleterious effects of cholesterol enrichment on mitochondrial respiration.

3.4. Cholesterol-lipid interactions contribute to decreased complex I-driven state 3 respiration

To determine whether the impairment of mitochondrial respiration by HC-induced mitochondrial cholesterol loading is a direct consequence of cholesterol enrichment in mitochondrial membranes, we used an *in situ* approach in which cholesterol complexed with BSA (CBSAC) results in the enrichment of cholesterol content in both membranes [32]. Compared to incubation with BSA alone, CBSAC resulted in the increase in cholesterol levels with a 4-fold increase. Real-time OCR driven by pyruvate plus malate revealed that cholesterol did not affect state 3 or state 3u respiration, although it uncoupled mitochondrial respiration as revealed by the increased state 4o respiration (Fig. 5A), which translated in decreased RCR and UCR (Fig. 5B). However, when succinate plus rotenone were used as substrates the enrichment in cholesterol did not affect succinate-driven OCR and hence RCR and UCR remained unchanged (Fig. 5C and D). Since the interaction of cholesterol with membrane proteins is enantioselective but the interaction with membrane lipids is not [41–43], we next enriched mitochondria with enantiomer cholesterol (Ent-CBSAC), the mirror image of natural cholesterol, as an approach to assess the contribution of the interactions between cholesterol with lipids and/or proteins in the disrupting effect of cholesterol in pyruvate and malate-driven respiration. Mitochondria enriched in Ent-CBSAC exhibited an increase in cholesterol levels similar to those found with natural CBSAC (2.5-fold compared to BSA). As CBSAC failed to alter complex II-driven respiration, we tested the role of Ent-CBSAC on complex I-induced OCR. Interestingly, Ent-CBSAC decreased pyruvate and malate-driven state 3 and state 3u respiration, which resulted in lower RCR and UCR (Fig. 5A and B). These *in vitro* findings suggest that cholesterol-lipid interactions could mediate the decrease in complex I-driven state 3 and state 3u respiration.

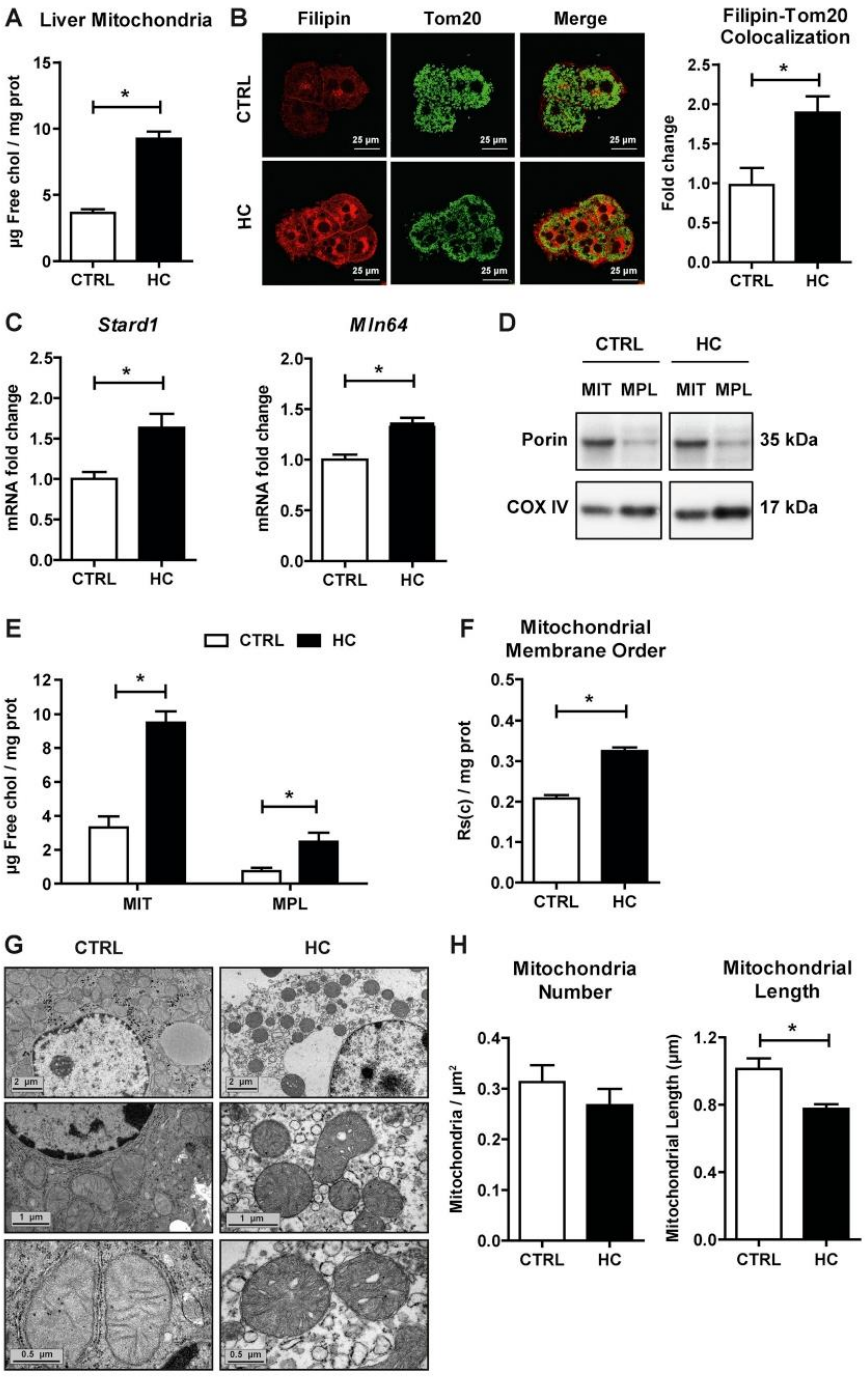

(caption on next page)

Fig. 2. Effects of HC feeding on liver mitochondrial cholesterol levels, membrane order and morphology. WT C57BL/6J mice were fed a CTRL or HC diet for 2 days. Cholesterol levels in Mitochondria by (A) HPLC and (B) Immunocytochemistry using Tom20 and Filipin. Staining markers colocalization analyzed using ImageJ software. Data are presented as means ± SEM (N > 10, *P < 0.05, Unpaired Student's t-test (two tailed)). (C) mRNA levels of *Stard1* and *Mln64* in liver. Values are the mean ± SEM of > 10 animals per group. *P < 0.05. (D) Purity of mitoplasts from CTRL and cholesterol-enriched mitochondria (Mitochondria = MIT, Mitoplast = MPL). (E) Levels of cholesterol in mitochondria and mitoplasts by HPLC. (F) Mitochondrial membrane order measured by DPH fluorescence anisotropy. (G) Electron microscopy analyses of livers from mice fed a CTRL or HC diet for 2 days. Images were acquired with a Gatan Orius digital camera by moving randomly across the EM grid and are representative of 3 replicates per group. (H) Mitochondrial number and length of liver samples quantified from images of ultrathin sections (G) and analyzed using ImageJ software. Data are presented as means ± SEM (N = 3, *P < 0.05, Unpaired Student's t-test (two tailed)).

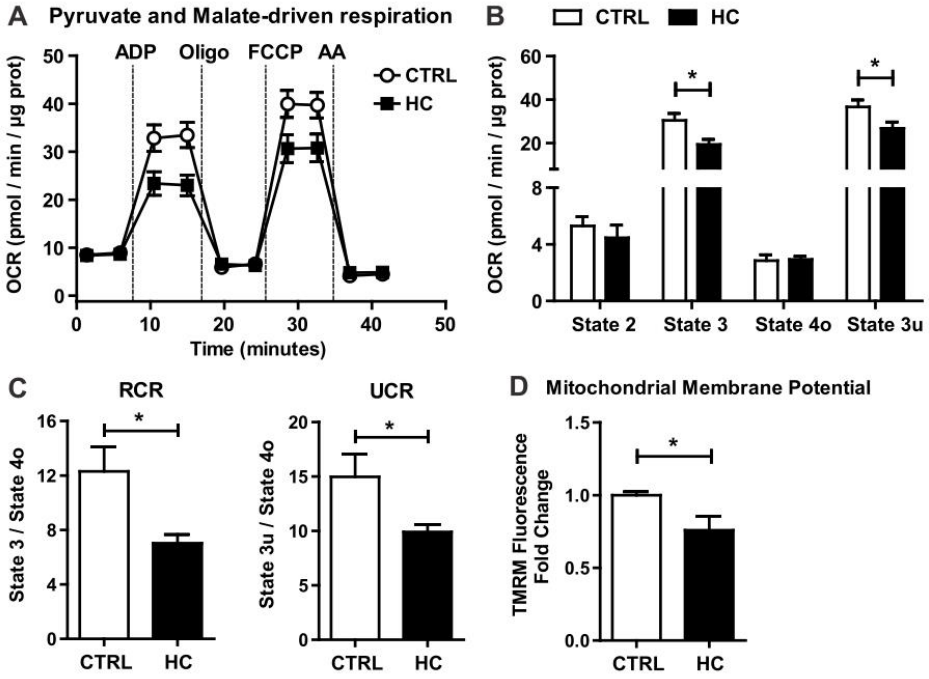

Fig. 3. Effect of cholesterol in mitochondrial OCR using pyruvate and malate as substrates and membrane potential. WT C57BL/6J mice were fed a CTRL or HC diet for 2 days. (A–B) Respiration of CTRL and cholesterol-enriched mitochondria using XFe24 Seahorse Analyzer. Mitochondria began in a coupled state with pyruvate and malate (10 mM) present (state 2). State 3 initiated with ADP (4 mM) addition, state 4 was induced with the injection of oligomycin (2.5 µg/ml) (state 4o), and FCCP (4 µM) induced maximal uncoupler-stimulated respiration (state 3u). Non-mitochondrial respiration was assessed by OCR measurement in the presence of antimycin (4 µM). (C) Respiratory control ratios (RCR: state 3/state 4o, and UCR: state 3u/state 4o). (D) Mitochondrial Membrane Potential measured by TMRM Fluorescence in a fluorescence spectroscope. Data are presented as means ± SEM (N = 7 or otherwise stated, *P < 0.05, Unpaired Student's t-test (two tailed)).

3.5. Mitochondrial cholesterol enrichment disrupts the assembly of respiratory supercomplexes

In view of the preceding findings, we hypothesized that mitochondrial cholesterol loading *in vivo* by HC feeding may impact negatively the expression of respiratory complexes. Therefore, we first performed SDS electrophoresis to determine the expression of specific subunits of respiratory complexes. As seen, the expression of specific subunits from complex I (C-I-20), complex II (C-II-30), complex III (C-III-Core 2), complex IV (C-IV-I) and complex V (C-V-α) were unaffected by mitochondrial cholesterol loading by HC feeding (Fig. 6A and B). Since the structural organization of the mitochondrial respiratory complexes as independent entities connected by mobile carriers such as CoQ and cytochrome *c* has been challenged [39], we next hypothesized that cholesterol-mediated changes in membrane physical properties may impact the organization and assembly of supercomplexes structures, responsible for carrying out cellular respiration. Blue native electrophoresis of mitochondria after digitonin solubilization was carried out with subsequent antibody incubation against specific subunits of each respiratory complex sequentially. Mitochondrial cholesterol accumulation did not change the levels of respiratory complexes CI, CIV and CV but caused a significant downregulation of respiratory complex III_2 (Fig. 6C and D). This outcome mirrored the downregulation of supercomplexes I_1+III_2+IV and I_1+III_2 in cholesterol-enriched mitochondria (Fig. 6C and D). These data indicating a negative impact of cholesterol on the assembly of respiratory supercomplexes can account for the observed alterations in mitochondrial respiration and emerge as a potential molecular mechanism by which cholesterol accumulation in liver alters mitochondrial function.

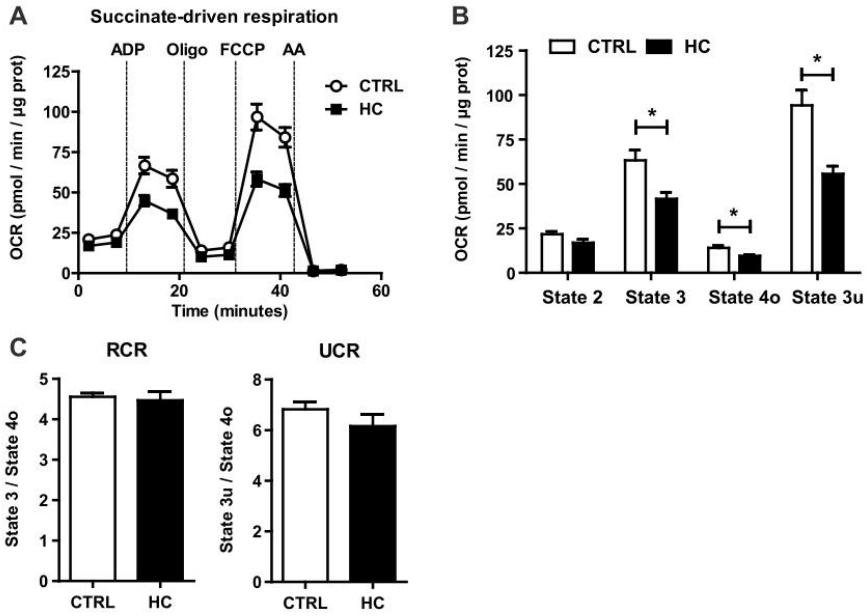

Fig. 4. Effect of cholesterol in mitochondrial respiration from succinate and rotenone. WT C57BL/6J mice were fed a CTRL or HC diet for 2 days. (A–B) Respiration of CTRL and cholesterol-enriched mitochondria using XFe24 Seahorse Analyzer. Mitochondria began in a coupled state with succinate (10 mM) and rotenone (2 µM) present (state 2). State 3: ADP (4 mM), State 4o: Oligomycin (2.5 µg/ml), State 3u: FCCP (4 µM), Non-mitochondrial respiration: Antimycin (4 µM). (C) Respiratory control ratios (RCR: state 3/state 4o, and UCR: state 3u/state 4o). Data are presented as means ± SEM (N > 10, *P < 0.05, Unpaired Student's t-test (two tailed)).

3.6. GSH ethyl ester protects against HC-induced oxidative stress and liver injury

As mitochondria are the main consumers of oxygen and a major source of ROS [11–13], we next determined whether HC-induced mitochondrial dysfunction results in increased oxidative stress. As seen, staining of liver sections from HC-fed mice with DHE indicated increased generation of ROS compared to control mice (Fig. 7A and B). This outcome paralleled the depletion of cellular GSH levels (Fig. 7C) as well as the mGSH pool (Fig. 7D), which is primarily due to the defective transport of GSH into mitochondrial matrix [20,29,30]. These findings were accompanied by the stimulation of superoxide anion and especially hydrogen peroxide in isolated mitochondria from HC-fed mice (Supplementary Fig. 1), with the latter effect reflecting the depletion of mGSH induced by mitochondrial cholesterol loading. Consistent with these findings, HC feeding resulted in the increased oxidative stress as shown by enhanced carbonylated proteins (Fig. 7E). HC diet induced a macroscopic change in liver color when compared to control diet. HC livers displayed a steatotic pale appearance compared to control livers (Fig. 7F) that paralleled oil-red staining (Supplementary Fig. 2). In addition, H&E staining revealed a significant dilation of liver perisinusoidal spaces after 2 days of HC feeding (Fig. 7G). These changes were accompanied by the release of AST and ALT in serum indicating that HC-diet induces liver injury (Fig. 7H). We next explored the potential impact of total GSH and mGSH restoration by GSHee in HC-fed mice. GSHee treatment of HC-fed mice restored both total and mGSH pools (Fig. 7C and D). Moreover, GSHee treatment decreased HC-induced DHE increase (Fig. 7A and B), reduced protein carbonylation (Fig. 7E), restored the HC-mediated dilation of liver perisinusoidal spaces (Fig. 7G), and decreased ALT/AST release, indicating that GSHee protected HC-fed mice from liver injury when compared to HC non-treated mice (Fig. 7H). To assess whether the outcome of GSHee administration was accompanied by improved mitochondrial function, we examined the impact of *in vivo* GSHee administration in mitochondrial performance from pyruvate plus malate-induced OCR. Consistent with previous findings, HC feeding decreased OCR and RCR from complex I that was improved upon GSHee treatment (Fig. 7 I, J). Moreover, GSHee restored the levels of respiratory complex III_2, although it did not affect the assembly of respiratory supercomplexes $I+III_2+IV$ and $I+III_2$ (Fig. 7K). Thus, these findings indicate that GSHee administration protects mice from HC-induced liver injury and oxidative stress in part by improving mitochondrial respiration.

4. Discussion

Cholesterol accumulation and, particularly its trafficking to mitochondria, has emerged as a key player in different chronic diseases, including fatty liver disease and hepatocellular carcinoma [12,19,24]. Given the critical structural role of cholesterol in membrane bilayers, the contribution of mitochondrial cholesterol enrichment in disease pathogenesis is exerted in part through its effects in the perturbation of membrane physical properties. However, the specific impact of cholesterol in mitochondrial function and routine performance has not been previously addressed. In order to rapidly increase liver cholesterol levels, we used an *in vivo* approach in which mice were fed a cholesterol-enriched diet supplemented with sodium cholate, which has been shown to sustain liver cholesterol levels [19,34]. Importantly, the presence of sodium cholate in the diet downregulated the expression of

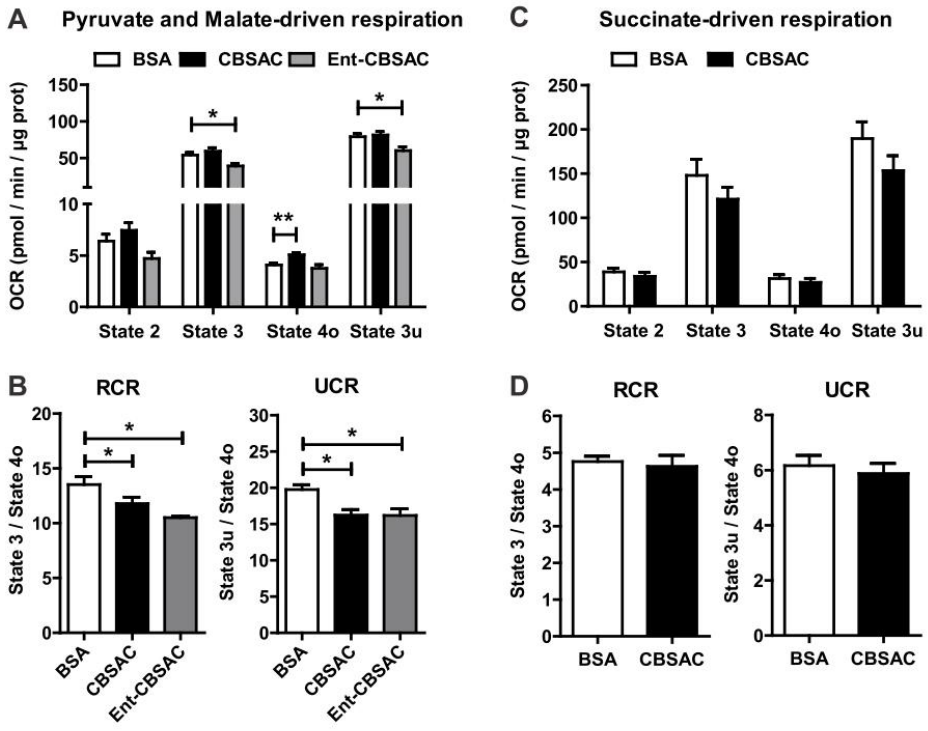

Fig. 5. Impact of *in vitro* cholesterol enrichment in mitochondrial respiration. Mitochondria from WT C57BL/6J mice fed a CTRL diet were isolated and incubated with natural cholesterol or its enantiomer complexed with BSA (CBSAC and Ent-CBSAC respectively). (A) Pyruvate and Malate-driven mitochondrial respiration. State 2: pyruvate and malate (10 mM), State 3: ADP (4 mM), State 4o: Oligomycin (2.5 µg/ml), State 3u: FCCP (4 µM), Non-mitochondrial respiration: Antimycin (4 µM). (B) Respiratory control ratios (RCR: state 3/state 4o, and UCR: state 3u/state 4o). Values are the mean ± SEM of N > 3 per group. *P < 0.05. One-way ANOVA followed by Tukey's Multiple Comparison test. (C) Succinate and Rotenone-driven mitochondrial respiration. State 2: succinate (10 mM) and rotenone (2 µM), State 3: ADP (4 mM), State 4o: Oligomycin (2.5 µg/ml), State 3u: FCCP (4 µM), Non-mitochondrial respiration: Antimycin (4 µM). (D) Respiratory control ratios (RCR: state 3/state 4o, and UCR: state 3u/state 4o). Data are presented as means ± SEM (N > 3, *P < 0.05, Unpaired Student's t-test (two tailed)).

key enzymes involved in the synthesis of bile acids such as Cyp7a1 and Cyp8b1, without effect in the alternate pathway of bile acid synthesis in mitochondria. This finding indicates that sodium cholate is an important component of the HC diet, which contributes to the maintenance of hepatic free cholesterol levels by preventing the metabolism of dietary cholesterol into bile acids.

The *in vivo* loading of hepatic cholesterol levels by HC feeding attenuated the expression of *Srebp2* and *Hmgcr*, which reflects the alterations in endogenous cholesterol homeostasis, an effect that was accompanied by its accumulation in mitochondria. This outcome paralleled the increased expression of *Stard1* and *Mln64*, which play critical roles in the regulation of mitochondrial trafficking [14–16]. Importantly, mitochondrial fractionation into mitoplasts revealed that cholesterol accumulation occurs in both the outer and inner mitochondrial membranes, consistent with a concerted action between MLN64 and StARD1, which move cholesterol from extramitochondrial sources to the outer mitochondrial membrane and from here to the inner mitochondrial membrane, respectively [14–16]. Of relevance, we show that *in vivo* cholesterol accumulation impairs mitochondrial oxidative phosphorylation, reflected in decreased ADP-stimulated OCR from complex I, which translated in decreased RCR and UCR. This outcome is accompanied by the defective assembly of respiratory supercomplexes I_1+III_2+IV and I_1+III_2. These findings are consistent with the current concept that mitochondrial supercomplexes structures are responsible for carrying out cellular respiration [39,44], as opposed to the long-held view of mitochondrial respiratory complexes as independent entities connected by mobile carriers CoQ and cytochrome c. The vast majority of the subunits of the mitochondrial respiratory complexes are encoded by nuclear DNA, which then traffic to mitochondria by the presence of intramitochondrial sorting signals to undergo a highly-regulated mechanism of import and insertion into mitochondrial membranes [45]. However, hepatic cholesterol loading does not affect the expression of specific subunits of complex I-V, suggesting that the effect of mitochondrial cholesterol in the assembly of the mitochondrial supercomplexes may reflect defects at the mitochondrial membrane level likely due to changes in membrane physical properties. This outcome is consistent with recent findings pointing that membrane lipid composition determines cellular respiration through changes in membrane fluidity and physical properties [46,47]. Indeed, reconstitution of complex I and complex III in proteoliposomes with different lipid composition revealed that the ratio of phospholipid to protein determines the assembly of supercomplex I_1-III_2 [46]. Moreover, studies in bacteria engineered to express increased levels of unsaturated fatty acids unraveled that membrane viscosity

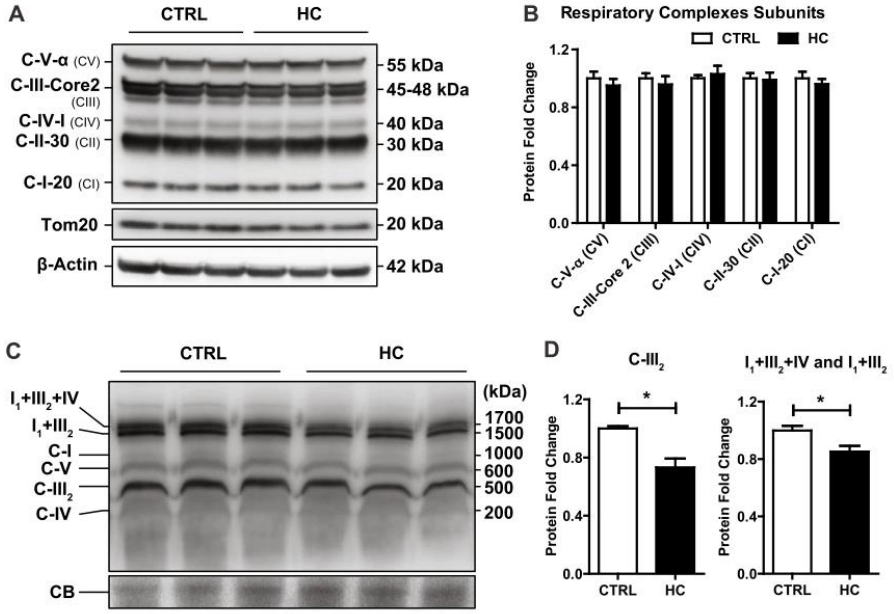

Fig. 6. Impairment of mitochondrial supercomplexes assembly by cholesterol enrichment. (A) Protein expression of mitochondrial respiratory complexes subunits from livers of WT C57BL/6J mice fed a CTRL or HC diet for 2 days. β-Actin was used as loading control. Images are representative of at least three independent experiments. (B) Protein Expression quantification of (A) by ImageJ software. Values are the mean ± SEM of > 5 animals per group. *P < 0.05 vs. CTRL samples. (C) Blue Native Page electrophoresis of livers from CTRL and HC mice to detect OXPHOS complexes and Supercomplexes expression. Coomassie Blue (CB) staining was used as loading control. Images are representatives of 9 replicates per group. (D) Protein Expression quantification of (C) by ImageJ software. Values are the mean ± SEM of N > 5 animals per group. *P < 0.05. Unpaired Student's t-test (two tailed).

determined by lipid composition controlled the rate of respiration coupled to ADP phosphorylation [47]. Whether the deleterious effect of cholesterol enrichment in mitochondrial function is reversible upon cholesterol extraction or membrane fluidization remains to be further investigated. In line with this possibility, Yu et al. showed that the defective ATPase function from brain mitochondria from NPC knockout mice, which exhibit an increased mitochondrial cholesterol loading, was restored by cholesterol extraction with cyclodextrin [48]. Thus, while mitochondrial cholesterol loading *in vivo* by feeding the HC diet may reflect the combined effect of cholesterol on established and newly assembled respiratory complexes by membrane mediated changes, we addressed the direct impact of cholesterol enrichment in the existing respiratory complexes in isolated mitochondria and whether this event involves interactions of cholesterol with bilayer's proteins and/or lipids using enantiomer cholesterol, the mirror image of natural cholesterol. Enrichment of liver mitochondria in enantiomer cholesterol, which specifically interacts with lipids but not proteins due to enantioselective restriction [37,41–43], resulted in decreased complex I-driven state 3/state 3u respiration, suggesting that cholesterol-lipid interactions in mitochondrial membranes accounts for the impaired ADP-stimulated OCR driven by complex I. Intriguingly, although *in vitro* cholesterol loading increased complex I-driven state 4o respiration, this outcome was not observed with the *in vivo* mitochondrial cholesterol loading by HC feeding. Whether cholesterol-lipid interactions is a predominant effect over the interaction of cholesterol with proteins to account for the decreased complex I-driven state 3/3u respiration remains to be further investigated. Interestingly, *in situ* cholesterol enrichment in mitochondria did not affect complex II-driven OCR although *in vivo* mitochondrial cholesterol loading did impair state 3 respiration. This differential effect suggests that the impact of cholesterol in impairing complex II-mediated OCR reflects the impact of cholesterol in the assembly of respiratory supercomplexes rather than a direct effect of the changes in membrane physical properties.

A caveat from the *in vivo* enrichment of mitochondria in cholesterol on mitochondrial respiration by feeding a HC enriched diet is whether the effects truly reflect the actions of cholesterol *per se* or are determined by cholesterol-derived metabolites. As cholesterol is the precursor of bile acids, it is conceivable that part of the observed effects of cholesterol enrichment in mitochondrial performance could be mediated by the action of bile acids generated from dietary cholesterol. This potential contribution, however, seems unlikely in light of the fact that the presence of sodium cholate in the HC-enriched diet impaired the classical pathway of bile acid synthesis due to decreased the expression of *cyp7a1* and *cyp8b1*, consistent with the lack of increased bile acid pool from HC-fed mice.

As one of the reported consequences of the disruption of the association between complex I and complex III and the impaired assembly of subsequent supercomplexes I_1+III_2+IV and I_1+III_2 is the enhanced generation of superoxide anion [46], we analyzed the impact of mitochondrial cholesterol enrichment in oxidative stress and liver injury. While HC feeding caused increased ROS formation, mitochondrial ROS generation and mGSH depletion that was accompanied by steatosis and liver injury, these events were recovered by GSHee administration. Interestingly, the effect of mGSH restoration by GSHee translated in

replenishing mitochondrial respiration and RCR, in line with previous findings in cerebellar mitochondrial function in NPC disease [35]. Restoration of mGSH levels by GSHee rescued the content of complex III_2, although it failed to normalize the assembly of supercomplexes I $+III_2+IV$ and $I+III_2$, which likely reflects the effect of remaining cholesterol-mediated effect on membrane dynamics that are not reversed by mGSH restoration. However, quite intriguingly, the restoration of complex III_2 by GSHee seems to compensate the function of mitochondrial respiration. Further work will be required to determine the mechanisms whereby mGSH depletion by mitochondrial cholesterol

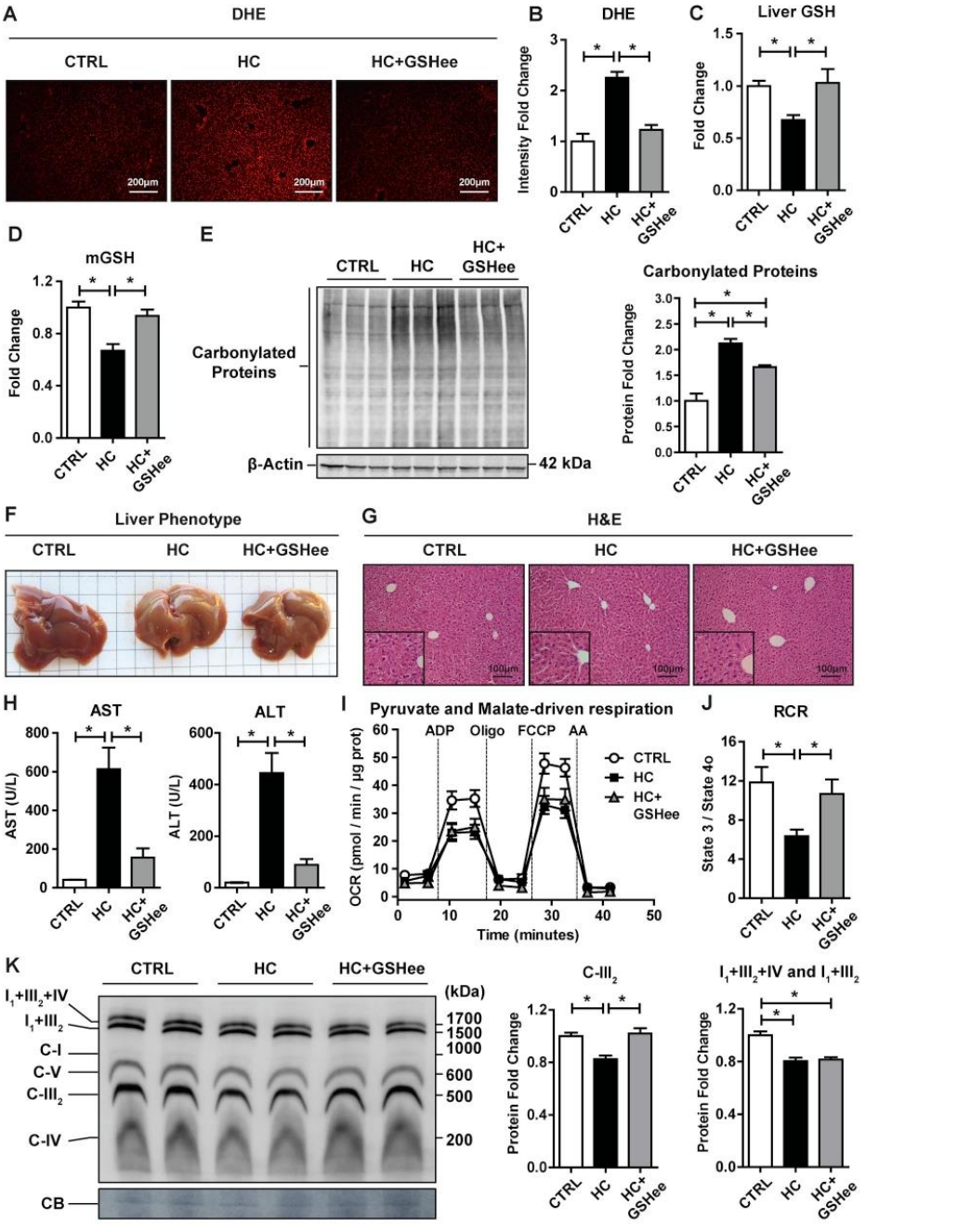

(caption on next page)

Fig. 7. Effects of GSHee treatment on HC-induced oxidative stress and liver damage. (A) Reactive oxygen species content in liver tissue by DHE staining. Representative images obtained by fluorescence microscopy. (B) Fluorescence quantification of DHE intensity using ImageJ software. (C–D) GSH levels in liver and mitochondria. Values are the mean ± SEM of > 5 animals per group. *P < 0.05. One-way ANOVA followed by Tukey's Multiple Comparison test. (E) Carbonylated proteins from liver sections of CTRL or HC-fed mice with or without GSHee administration *in vivo*. Results are the mean ± SEM of 3 animals per group. *P < 0.05. One-way ANOVA followed by Tukey's Multiple Comparison test. (F) Macroscopic view of liver after CTRL or HC feeding with or without GSHee treatment. Representative image of > 5 replicates is shown. (G) Liver sections of CTRL, HC and HC + GSHee mice analyzed by H&E. (H) Serum AST and ALT levels from CTRL, HC and HC + GSHee mice. Data are presented as means ± SEM (N > 5, *P < 0.05, One-way ANOVA followed by Tukey's Multiple Comparison test). (I) Pyruvate and Malate-driven mitochondrial respiration. State 2: pyruvate and malate (10 mM), State 3: ADP (4 mM), State 4o: Oligomycin (2.5 μg/ml), State 3u: FCCP (4 μM), Non-mitochondrial respiration: Antimycin (4 μM). (J) Respiratory control ratio (RCR: state 3/state 4o) determined from OCR analyzed in I. (K) Blue Native Page electrophoresis of livers from CTRL and HC-fed mice with or without GSHee treatment to detect OXPHOS complexes and Supercomplexes expression. Coomassie Blue (CB) staining was used as loading control. Results are the mean ± SEM of 8 animals per group. *P < 0.05. One-way ANOVA followed by Tukey's Multiple Comparison test. (For interpretation of the references to color in this figure legend, the reader is referred to the Web version of this article.)

loading impact the redox-dependent assembly of supercomplexes assembly and whether the reversible loss of complex III_2 by cholesterol is redox dependent in view of its restoration by mGSH with GSHee.

Acknowledgments

We want to thank Dr. José A. Enriquez and Sara Cogliati from the CNIC, Madrid, Spain for valuable suggestions and comments regarding the supercomplexes analysis. We want to acknowledge the Electronic microscopy (TEM/SEM) facility of the University of Barcelona (CCiT-UB) for the electron microscopy studies. We acknowledge the support from grants SAF2014-57674R, SAF-2015-69944R, and SAF2017-85877R from Plan Nacional de I+D, by the CIBEREHD from the Instituto de Salud Carlos III, by AGAUR of the Generalitat de Catalunya SGR-2017-1112, and by the Fundación BBVA, Spain. We also acknowledge support from the center grant P50AA011999 Southern California Research Center for ALPD and Cirrhosis funded by NIAAA/NIH and by the European Cooperation in Science and Technology (COST) ACTION CA17112 Prospective European Drug-Induced Liver Injury Network. We also acknowledge the gift of enantiomer cholesterol by Dr. Scott Rychnovsky (Department of Chemistry, University of California Irvine).

E.S.-V. was supported by a contract from the "Ministerio de Educación, Cultura y Deporte" (FPU15/04537) of the Spanish Government. R.F. was funded by "Juan de la Cierva Incorporación" from the National Programme for the Promotion of Talent and Its Employability of the "Ministerio de Ciencia, Innovación y Universidades" (IJCI-2015-23219) of the Spanish Government.. Mitochondria and protein images from graphical abstract were taken and adapted from Smart Servier Medical Art under Creative Commons Attribution 3.0 Unported License.

Appendix A. Supplementary data

Supplementary data to this article can be found online at https://doi.org/10.1016/j.redox.2019.101214.

References

[1] G. Gimpl, K. Burger, F. Fahrenholz, Cholesterol as modulator of receptor function, Biochemistry 36 (1997) 10959–10974.
[2] K. Simons, R. Ehehalt, Cholesterol, lipid rafts, and disease, J. Clin. Investig. 110 (2002) 597–603.
[3] F.R. Maxfield, I. Tabas, Role of cholesterol and lipid organization in disease, Nature 438 (2005) 612–621.
[4] J.D. Horton, J.L. Goldstein, M.S. Brown, SREBPs: activators of the complete program of cholesterol and fatty acid synthesis in the liver, J. Clin. Investig. 109 (2002) 1125–1131.
[5] S.W. Tait, D.R. Green, Mitochondria and cell signalling, J. Cell Sci. 125 (Pt 4) (2012) 807–815.
[6] J. Nunnari, A. Suomalainen, Mitochondria: in sickness and in health, Cell 148 (6) (2012 Mar 16) 1145–1159.
[7] B. Westermann, Mitochondrial fusion and fission in cell life and death, Nat. Rev. Mol. Cell Biol. 11 (12) (2010 Dec) 872–884.
[8] P. Mishra, D.C. Chan, Mitochondrial dynamics and inheritance during cell division, development and disease, Nat. Rev. Mol. Cell Biol. 15 (10) (2014 Oct) 634–646.
[9] T. Wai, T. Langer, Mitochondrial dynamics and metabolic regulation, Trends Endocrinol. Metabol. 27 (2) (2016 Feb) 105–117.
[10] A. Murley, J. Nunnari, The emerging network of mitochondria-organelle contacts, Mol. Cell 61 (5) (2016 Mar 3) 648–653.
[11] M.P. Murphy, Understanding and preventing mitochondrial oxidative damage, Biochem. Soc. Trans. 44 (5) (2016 Oct 15) 1219–1226.
[12] C. Garcia Ruiz, J.C. Fernandez-Checa, Mitochondrial oxidative stress and antioxidants balance in fatty liver disease, Hepatol. Commun. (2) (2018 Oct 30) 1425–1439.
[13] T. Finkel, Signal transduction by mitochondrial oxidants, J. Biol. Chem. 287 (7) (2012 Feb 10) 4434–4440.
[14] W.L. Miller, Steroidogenic acute regulatory protein (StAR), a novel mitochondrial cholesterol transporter, Biochim. Biophys. Acta 1771 (6) (2007 Jun) 663–676.
[15] K.M. Caron, S.C. Soo, W.C. Wetsel, D.M. Stocco, B.J. Clark, K.L. Parker, Targeted disruption of the mouse gene encoding steroidogenic acute regulatory protein provides insights into congenital lipoid adrenal hyperplasia, Proc. Natl. Acad. Sci. U. S. A. 94 (21) (1997 Oct 14) 11540–11545.
[16] P. Elustondo, L.A. Martin, B. Karten, Mitochondrial cholesterol import, Biochim. Biophys. Acta Mol. Cell Biol. Lipids 1862 (1) (2017 Jan) 90–101.
[17] G. van Meer, D.R. Voelker, G.W. Feigenson, Membrane lipids: where they are and how they behave, Nat. Rev. Mol. Cell Biol. 9 (2008) 112–124.
[18] A. Baulies, J. Montero, N. Matías, N. Insausti, O. Terrones, G. Basañez, C. Vallejo, L. Conde de La Rosa, L. Martinez, D. Robles, A. Morales, J. Abian, M. Carrascal, K. Machida, D.B.U. Kumar, H. Tsukamoto, N. Kaplowitz, C. Garcia-Ruiz, J.C. Fernández-Checa, The 2-oxoglutarate carrier promotes liver cancer by sustaining mitochondrial GSH despite cholesterol loading, Redox Biol. 14 (2018 Apr) 164–177.
[19] M. Marí, F. Caballero, A. Colell, A. Morales, J. Caballeria, A. Fernandez, C. Enrich, J.C. Fernandez-Checa, C. García-Ruiz, Mitochondrial free cholesterol loading sensitizes to TNF- and Fas-mediated steatohepatitis, Cell Metabol. 4 (3) (2006 Sep) 185–198.
[20] A. Fernández, A. Colell, F. Caballero, N. Matías, C. García-Ruiz, J.C. Fernández-Checa, Mitochondrial S-adenosyl-L-methionine transport is insensitive to alcohol-mediated changes in membrane dynamics, Alcohol Clin. Exp. Res. 33 (7) (2009 Jul) 1169–1180.
[21] L.G. Baggetto, R. Testa-Parussini, Role of acetoin on the regulation of intermediate metabolism of Ehrlich ascites tumor mitochondria: its contribution to membrane cholesterol enrichment modifying passive proton permeability, Arch. Biochem. Biophys. 283 (1990) 241–248.
[22] L.G. Baggetto, E. Clottes, C. Vial, Low mitochondrial proton leak due to high membrane cholesterol content and cytosolic creatine kinase as two features of the deviant bioenergetics of Ehrlich and AS30-D tumor cells, Cancer Res. 52 (1992) 4935–4941.
[23] S.W. Ballinger, Mitochondrial dysfunction in cardiovascular disease, Free Radic. Biol. Med. 38 (2005) 1278–1295.
[24] V. Ribas, C. García-Ruiz, J.C. Fernández-Checa, Mitochondria, cholesterol and cancer cell metabolism, Clin. Transl. Med. 5 (1) (2016 Dec) 22.
[25] J. Montero, A. Morales, L. Llacuna, J.M. Lluis, O. Terrones, G. Basañez, B. Antonsson, J. Prieto, C. García-Ruiz, A. Colell, J.C. Fernández-Checa, Mitochondrial cholesterol contributes to chemotherapy resistance in hepatocellular carcinoma, Cancer Res. 68 (13) (2008) 5246–5256.
[26] A. Fernández, L. Llacuna, J.C. Fernandez-Checa, A. Colell, Mitochondrial cholesterol loading exacerbates amyloid beta peptide-induced inflammation and neurotoxicity, J. Neurosci. 29 (20) (2009) 6394–6405.
[27] F. Feo, R.A. Canuto, R. Garcea, L. Gabriel, Effect of cholesterol content on some physical and functional properties of mitochondria isolated from adult rat liver, fetal liver, cholesterol-enriched liver and hepatomas AH-130, 3924A and 5123, Biochim. Biophys. Acta 413 (1975) 116–134.
[28] R.C. Crain, R.W. Clark, B.E. Harvey, Role of lipid transfer proteins in the abnormal lipid content of Morris hepatoma mitochondria and microsomes, Cancer Res. 43 (1983) 3197–3202.
[29] C. Garcia-Ruiz, A. Morales, A. Ballesta, J. Rodes, N. Kaplowitz, J.C. Fernandez-Checa, Effect of chronic ethanol feeding on glutathione and functional integrity of mitochondria in periportal and perivenous rat hepatocytes, J. Clin. Investig. 94 (1994) 193–201.
[30] A. Colell, C. Garcia-Ruiz, A. Morales, et al., Transport of reduced glutathione in hepatic mitochondria and mitoplasts from ethanol-treated rats: effect of membrane physical properties and S-adenosyl- L-methionine, Hepatology 26 (1997) 699–708.
[31] O. Coll, A. Colell, C. Garcia-Ruiz, N. Kaplowitz, J.C. Fernandez-Checa, Sensitivity of the 2-oxoglutarate carrier to alcohol intake contributes to mitochondrial

glutathione depletion, Hepatology 38 (2003) 692–702.
[32] A. Colell, C. Garcia-Ruiz, J.M. Lluis, O. Coll, M. Marí, J.C. Fernandez-Checa, Cholesterol impairs the adenine nucleotide translocator-mediated mitochondrial permeability transition through altered membrane fluidity, J. Biol. Chem. 278 (2003) 33928–33935.
[33] Shuang Mei, Haihua Gu, Xuefeng Yang, Huailan Guo, Zhenqi Liu, Wenhong Cao, Prolonged exposure to insulin induces mitochondrion-derived oxidative stress through increasing mitochondrial cholesterol content in hepatocytes, Endocrinology 153 (5) (2012) 2120–2129.
[34] M. Domínguez-Pérez, A. Simoni-Nieves, P. Rosales, N. Nuño-Lámbarri, M. Rosas-Lemus, V. Souza, R.U. Miranda, L. Bucio, S. Uribe Carvajal, J.U. Marquardt, D. Seo, L.E. Gomez-Quiroz, M.C. Gutiérrez-Ruiz, Cholesterol burden in the liver induces mitochondrial dynamic changes and resistance to apoptosis, J. Cell. Physiol. 234 (2019 May) 7213–7223.
[35] S. Torres, N. Matías, A. Baulies, S. Nuñez, C. Alarcon-Vila, L. Martinez, N. Nuño, A. Fernandez, J. Caballeria, T. Levade, A. Gonzalez-Franquesa, P. Garcia-Rovés, E. Balboa, S. Zanlungo, G. Fabrías, J. Casas, C. Enrich, C. Garcia-Ruiz, J.C. Fernández-Checa, Mitochondrial GSH replenishment as a potential therapeutic approach for Niemann Pick type C disease, Redox Biol. 11 (2017 Apr) 60–72.
[36] C. Von Montfort, N. Matias, A. Fernandez, R. Fucho, L. Conde de la Rosa, M.L. Martinez-Chantar, J.M. Mato, K. Machida, H. Tsukamoto, M.P. Murphy, A. Mansouri, N. Kaplowitz, C. Garcia-Ruiz, J.C. Fernandez-Checa, Mitochondrial GSH determines the toxic or therapeutic potential of superoxide scavenging in steatohepatitis, J. Hepatol. 57 (2012) 852–859.
[37] I. Kristiana, W. Luu, J. Stevenson, S. Cartland, W. Jessup, J.D. Belani, S.D. Rychnovsky, A.J. Brown, Cholesterol through the looking glass: ability of its enantiomer also to elicit homeostatic responses, J. Biol. Chem. 287 (40) (2012 Sep 28) 33897–33904.
[38] I. Wittig, H.P. Braun, H. Schägger, Blue native page, Nat. Protoc. 1 (1) (2006) 418–428.
[39] R. Acín-Pérez, P. Fernández-Silva, M.L. Peleato, A. Pérez-Martos, J.A. Enriquez, Respiratory active mitochondrial supercomplexes, Mol. Cell 32 (4) (2008 Nov 21) 529–539.
[40] E. Balboa, J. Castro, M.J. Pinochet, G.I. Cancino, N. Matías, P. José Sáez, A. Martínez, A.R. Álvarez, C. Garcia-Ruiz, J.C. Fernandez-Checa, S. Zanlungo, MLN64 induces mitochondrial dysfunction associated with increased mitochondrial cholesterol content, Redox Biol. 12 (2017 Aug) 274–284.
[41] F. Xu, S.D. Rychnovsky, J.D. Belani, H.H. Hobbs, J.C. Cohen, R.B. Rawson, Dual roles for cholesterol in mammalian cells, Proc. Natl. Acad. Sci. U. S. A. 102 (41) (2005 Oct 11) 14551–14556.
[42] E.J. Westover, D.F. Covey, The enantiomer of cholesterol, J. Membr. Biol. 202 (2) (2004 Nov) 61–72.
[43] Y. Li, M. Ge, L. Ciani, G. Kuriakose, E.J. Westover, M. Dura, D.F. Covey, J.H. Freed, F.R. Maxfield, J. Lytton, I. Tabas, Enrichment of endoplasmic reticulum with cholesterol inhibits sarcoplasmic-endoplasmic reticulum calcium ATPase-2b activity in parallel with increased order of membrane lipids: implications for depletion of endoplasmic reticulum calcium stores and apoptosis in cholesterol-loaded macrophages, J. Biol. Chem. 279 (35) (2004 Aug 27) 37030–37039.
[44] R. Acin-Perez, J.A. Enriquez, The function of the respiratory supercomplexes: the plasticity model, Biochim. Biophys. Acta 1837 (4) (2014 Apr) 444–450.
[45] S.E. Horvath, H. Rampelt, S. Oeljeklaus, B. Warscheid, M. van der Laan, N. Pfanner, Role of membrane contact sites in protein import into mitochondria, Protein Sci. 24 (3) (2015 Mar) 277–297.
[46] E. Maranzana, G. Barbero, A.I. Falasca, G. Lenaz, M.L. Genova, Mitochondrial respiratory supercomplex association limits production of reactive oxygen species from complex I, Antioxidants Redox Signal. 119 (2013) 1469–1480.
[47] I. Budin, R. de Rond, Y. Chen, L.J. Chan, C.J. Petzold, J.D. Keasling, Viscous control of cellular respiration by membrane lipid composition, Science 326 (2018 Dec 7) 1186–1189.
[48] W. Yu, J.S. Gong, M. Ko, W.S. Garver, K. Yanagisawa, M. Michikawa, Altered cholesterol metabolism in Niemann-Pick type C1 mouse brains affects mitochondrial function, J. Biol. Chem. 280 (12) (2005 Mar 25) 11731–11739.